Unconventional roles of the GABARAP subfamily of human ATG8 proteins in trafficking and degradation of cell surface proteins

Inaugural-Dissertation

Zur Erlangung des Doktorgrades der Mathematisch-Naturwissenschaftlichen Fakultät
der Heinrich-Heine-Universität Düsseldorf

vorgelegt von

Jochen Dobner

aus Landau in der Pfalz

Düsseldorf, 24. September 2020

aus dem Institut für Physikalische Biologie
der Heinrich-Heine-Universität Düsseldorf

Gedruckt mit der Genehmigung der
Mathematisch-Naturwissenschaftlichen Fakultät der
Heinrich-Heine-Universität Düsseldorf

Berichterstatter:

1. Prof. Dr. Dieter Willbold
2. Prof. Dr. Johannes G. Bode
3. Prof. Dr. Jörg Tatzelt

Tag der mündlichen Prüfung: 28.01.2021

Eidesstattliche Erklärung

Ich versichere an Eides statt, dass die Dissertation von mir selbstständig und ohne unzulässige fremde Hilfe unter Beachtung der Grundsätze zur Sicherung guter wissenschaftlicher Praxis an der Heinrich-Heine-Universität Düsseldorf erstellt worden ist.

Ferner erkläre ich, dass ich in keinem anderen Dissertationsverfahren mit oder ohne Erfolg versucht habe, diese Dissertation einzureichen.

Düsseldorf, den

_____

(Jochen Dobner)

Table of Contents

List of Figures and Tables

Acknowledgements

Mein Dank gebührt allen ehemaligen und vor allem aktuellen Weggefährten meines wissenschaftlichen Werdegangs, die das Gelingen der vorliegenden Promotionsarbeit überhaupt erst möglich gemacht haben.

Mein besonderer Dank geht an meinen Betreuer Prof. Dieter Willbold, der mir die Möglichkeit gab, dieses spannende Promotionsprojekt bearbeiten zu dürfen. Bei Prof. Johannes G. Bode möchte ich mich für die fruchtbare Kooperation und sicherlich ungewöhnlich intensive Zweitbetreuung meiner Arbeit bedanken. Im gleichen Atemzug geht der Dank natürlich an das gesamte Team der Experimentellen Hepatologie, das mich hervorragend aufgenommen hat. Da eine vollständige namentliche Nennung den Rahmen sprengen würde, ist hier exemplarisch Dr. Marianne Wammers zu nennen, mit der die Zusammenarbeit an der FACS „Diva“ stets sowohl unterhaltsam als auch produktiv war. Besten Dank auch an Prof. Heiner Schaal, meinen Mentor, für die Diskussionen meiner Ergebnisse bei den Follow-Up Meetings.

Ein riesiges Dankeschön geht an Dr. Silke Hoffmann für die hervorragende Zusammenarbeit, die nicht nur zahl- sondern auch hilfreichen Diskussionen, die perfekte Betreuung und den Spaß an der Arbeit. Zugleich bedanke ich mich bei allen Kollegen an der „GABARAP-Front“ (Dr. Thomas Gensch, Dr. Oliver H. Weiergräber, Dr. Melanie Schwarten, Dr. Iman Abdollazahdeh, Alina Üffing). Speziell hervorzuheben sind hier meine PhD-Mitstreiterinnen Julia L. Sanwald und Indra M. Simons, mit denen die Zusammenarbeit thematisch sehr eng und die vielen Verknüpfungspunkte immer angenehm zu diskutieren waren.

Für die Zeit in der Graduiertenschule *Molecules of Infection III* (MOI III) bin ich besonders dankbar. Zum einen natürlich für die Finanzierung dieses Projektes und zum anderen für die Zeit mit ihren Mitgliedern jeglicher Hierarchiestufe. Diese Jahre waren nicht nur äußerst unterhaltsam, sondern auch sehr lehrreich!

Danke natürlich auch an meine Frau Kerstin, die im Grunde Teil all dieser Teilbereiche war und ohne die die Zeit nicht halb so viel Spaß gemacht hätte. Außerdem ein dickes Dankeschön an meine Familie (ganz generell ohne wissenschaftlichen Kontext).

List of Abbreviations

AIM	Atg8-family interacting motif
AL	autophagosome-lysosome
AMBRA1	activating molecule in BECN1-regulated autophagy protein 1
AMP	adenosine monophosphate
AT_1R	angiotensin 1 receptor
Atg	autophagy-related
ATG16L	autophagy-related 16 like
BCL2	B-cell lymphoma 2
BECN1	Beclin-1
BIR	baculovirus inhibitor of apoptosis protein repeat
BRCA1	breast cancer type 1 susceptibility protein
BRUCE	BIR repeat-containing ubiquitin-conjugating enzyme
CIE	clathrin-independent endocytosis
CME	clathrin-mediated endocytosis
CORVET	class C core vacuole/endosome tethering
CRISPR	clustered interspaced short palindromic repeats
crRNA	CRISPRRNA
DKO	double knockout
DSB	double-strand break
E1L	E1-like
E2L	E2-like
E3L	E3-like
EEA1	early endosomal antigen 1
EGF	epidermal growth factor
EGFR	EGF receptor
ER	endoplasmic reticulum
ERK	extracellular-signal regulated kinase
ESCRT	endosomal sorting complex required for transport
FAK	focal adhesion kinase
FIP200	FAK family-interacting protein of 200 kDa
FP	fluorescent protein
FYCO1	FYVE and coiled-coil (CC) domain containing protein 1
$GABA_AR$	γ-aminobutyric acid type A receptor
GABARAP	$GABA_AR$-associated protein
GABARAPL1	GABARAP-like 1

GABARAPL2	GABARAP-like 2
GFP	green fluorescent protein
GIM	GABARAP interaction motif
GM130	130 kDa *cis*-Golgi matrix protein
HA	hemagglutinin
HAP1	haploid 1
HDR	homology-directed repair
HeLa	Henrietta Lacks
HEK	human embryonic kidney
HOPS	homeotypic fusion and protein sorting
Huh	human hepatoma
IB	immunoblot
IF	immunofluorescence
ILV	intraluminal vesicle
indel	insertion or deletion
IMM	inner mitochondrial membrane
KI	knock-in
KO	knockout
KOR	κ-opioid receptor
LANDO	LC3-associated endocytosis
LAP	LC3-associated phagocytosis
LE	late endosome
LIR	LC3-interacting region
MAP1LC3	microtubule-associated protein 1 light chain 3
MAPK	mitogen-activated protein kinase
mTORC1	mammalian target of rapamycin complex 1
MVB	multivesicular body
NHEJ	non-homologous end-joining
NSF	N-ethyl-maleimide-sensitive factor
nt	nucleotides
OMM	outer mitochondrial membrane
ORP1L	oxysterol-binding protein-related protein 1L
PAELR	parkin-associated endothelin receptor-like receptor
PAM	protospacer-adjacent motif
PE	phosphatidylethanolamine
PI	phosphatidylinositol

PI3	phosphatidylinositol 3
PI3K	phosphatidylinositol 3-kinase
PI3KC	phosphatidylinositol 3-kinase complex
PI3P	phosphatidylinositol-3-phosphate
PI4KIIα	phosphatidylinositol 4-kinase IIα
PI4P	phosphatidylinositol 4-phosphate
PIK3C3	phosphatidylinositol 3-kinase catalytic subunit type 3
PIK3R4	phosphatidylinositol 3-kinase regulatory subunit 4
PINK1	mitochondrial serine/threonine-protein kinase PINK1
PIP3	phosphatidylinositol-3,4,5-triphosphate
PKB	protein kinase B
PLEKHM1	pleckstrin homology domain-containing protein family member 1
PM	plasma membrane
PTB	protein tyrosine phosphatase
PX	phosphoinositide-binding
PTEN	phosphatase and tensin homolog
RAB	Ras-related in brain
RICS	Rho GTPase-activating protein
RILP	RAB7-interacting lysosomal protein
RUBICON	RUN domain Beclin-1-interacting and cysteine-rich domain-containing protein
RTK	receptor tyrosine kinase
SAR	selective autophagy receptor
sgRNA	short guide RNA
SKO	single knockout
SLC34A1	solute carrier family 34 member 1
SNAP	soluble NSF attachment protein
SNARE	SNAP receptor
SQSTM1	Sequestosome 1
STX	syntaxin
TFRC	transferrin receptor
TKO	triple knockout
TNFRSF12A	tumor necrosis factor receptor superfamily member 12 A
t-SNARE	target SNARE
UIM	ubiquitin-interacting motif
ULK1	UNC-51-like kinase 1

UNC51	serine/threonine-protein kinase unc-51
UVRAG	UV radiation resistance-associated gene
VAMP	vesicle-associated membrane protein
VMP1	vacuole membrane protein 1
v-SNARE	vesicular SNARE
WIPI	WD-40 repeat containing protein that Interacts with PtdIns
WT	wildtype
xLIR	extended LIR

List of publications and conference contributions

Publications

2019

Simons, I.M.; Mohrlüder, J.; Feederle, R.; Kremmer, E.; Zobel, T.; **Dobner, J.**; Bleffert, N.; Hoffmann, S.; Willbold, D. The highly GABARAP specific rat monoclonal antibody 8H5 visualizes GABARAP in immunofluorescence imaging at endogenous levels. *Sci. Rep.* **2019**, *9*, 526.

2020

Dobner, J.; Simons, I.M.; Rufinatscha, K.; Hänsch, S.; Schwarten, M.; Weiergräber, O.H.; Abdollahzadeh, I.; Gensch, T.; Bode, J.G.; Hoffmann, S.; et al. Deficiency of GABARAP but Not Its Paralogs Causes Enhanced EGF-Induced EGFR Degradation. *Cells* **2020**, *9*, 1296.

Sanwald, J.L. *; **Dobner, J.** *; Simons, I.M.; Poschmann, G.; Stühler, K.; Üffing, A.; Hoffmann, S.; Willbold, D. Lack of GABARAP-Type Proteins Is Accompanied by Altered Golgi Morphology and Surfaceome Composition. *Int. J. Mol. Sci.* **2021**, *22*, 85.

* Authors contributed equally

Conference contributions

2017

Jochen Dobner, Indra M. Simons, Claudia Hoppen, Johannes G. Bode, Dieter Häussinger, Silke Hoffmann, Dieter Willbold

Efficient Method for the Generation of Multiple Knock Outs by CRISPR/Cas9 Based on a Multicolor FACS Approach

deLIVER 2017 - Technology in Hepatology, Düsseldorf 2017

2018

Jochen Dobner, Indra M. Simons, Julia L. Sanwald, Johannes G. Bode, Dieter Häussinger, Silke Hoffmann, Dieter Willbold

Elucidate unique functions of mATG8s by genome engineering

22nd STS Meeting 2018: Signal Transduction – Receptors, Mediators and Genes, Weimar 2018

2019

Jochen Dobner, Indra M. Simons, Julia L. Sanwald, Kerstin Rufinatscha, Johannes G. Bode, Dieter Häussinger, Silke Hoffmann, Dieter Willbold

Non-redundant roles of GABARAP subfamily members during surface protein trafficking

GBM / DGZ Fall Conference 2019, Age-Related Human Diseases Special Focus: Autophagy, Tübingen 2019

1. Kurzfassung/Summary

1.1 Kurzfassung

Während in Hefe ein einziges *autophagy-related* (*Atg*) *8* (*Atg8*) Gen exprimiert wird, haben sich daraus in Menschen zwei Unterfamilien entwickelt. Die *microtubule-associated protein 1 light chain 3* (MAP1LC3- oder kurz LC3-)Unterfamilie besteht aus LC3A, LC3B, LC3B2 und LC3C, während die *γ-aminobutyric acid type A receptor-associated protein* (GABARAP-)Unterfamilie aus GABARAP, GABARAP-*like* 1 (GABARAPL1) und GABARAP-*like* 2 (GABARAPL2) besteht. Mitglieder beider Unterfamilien weisen eine ubiquitinähnliche Tertiärstruktur auf und besitzen somit eine hohe interfamiliäre Strukturhomologie. Unter den vielfältigen Funktionen, die für humane ATG8-Proteine bereits beschrieben wurden, ist ihre Beteiligung an der Autophagie am besten charakterisiert. Autophagie bezeichnet einen evolutionär konservierten Abbauprozess, der durch Nährstoffmangel aktiviert wird und während dessen eine Zelle zytoplasmatische Bestandteile in einer Doppelmembran einschließt. Die resultierenden Vesikel werden als Autophagosomen bezeichnet. Diese maturieren durch Fusion mit Lysosomen zu Autophagolysosomen. Im sauren Milieu dieses Organells wird die eingeschlossene zytoplasmatische Fracht schließlich abgebaut. Die resultierenden recycelten Bausteine können anschließend genutzt werden, um das Zellüberleben sicherzustellen. Während jedes Schrittes der Autophagie, inklusive ihrer Initiierung, der Autophagosomen-Biogenese, deren Wachstum, Transport sowie ihrer Fusion mit Lysosomen ist eine Beteiligung von Proteinen der GABARAP-Unterfamilie beschrieben. Große Fortschritte wurden hinsichtlich der Entschlüsselung der autophagiebezogenen Funktionen, besonders in Bezug auf Proteine der GABARAP-Unterfamilie, erzielt.

Ursprünglich wurden GABARAP und seine Paraloge jedoch im Zusammenhang mit ihrer Beteiligung an vesikulären Transportprozessen und der Gruppierung von Zelloberflächenrezeptoren beschrieben. Aufgrund ihrer hohen strukturellen Ähnlichkeit ist die exakte Beteiligung der gesamten GABARAP-Unterfamilie und ihrer individuellen Mitglieder während dieser Prozesse noch nicht vollständig geklärt. Das Ziel dieser Arbeit war daher die Identifizierung einzigartiger Funktionen von Proteinen der GABARAP-Unterfamilie während autophagieunabhängiger Transportprozesse.

Um dies untersuchen zu können, wurde die CRISPR/Cas9-Methode zur Genomeditierung angewendet, um Knock-outs (KOs) individueller *GABARAP* Gene sowie Zweifach-Kombinationen derer bis hin zur Ausschaltung der gesamten Unterfamilie in zwei verschiedenen Zelltypen zu erzeugen. Auf diese Weise konnten Zelllinien generiert werden, die eine Defizienz für jedes Unterfamilienprotein einzeln, Kombinationen von zweien oder eine komplette Defizienz für die gesamte Unterfamilie aufweisen. Diese Zelllinien leisteten

einen Beitrag zu einer Publikation, die einen institutseigenen GABARAP-spezifischen Antikörper für Immunfluoreszenz (IF-)Messungen beschreibt. Hier konnte gezeigt werden, dass die Validierung von Antikörpern für jede Anwendung individuell durchgeführt werden sollte, da kommerziell erhältliche Antikörper, die zwar für die Anwendung bei Immunoblotting-Experimenten validiert wurden, nicht in der Lage waren GABARAP während IF-Experimenten spezifisch zu detektieren. Von größerer Wichtigkeit in Bezug auf die vorliegende Dissertation war jedoch, dass die generierten KO-Zelllinien den Grundstein für die nachfolgenden Untersuchungen der biologischen Funktionen der GABARAP-Unterfamilie während des vesikulären Transports von Zelloberflächenproteinen bildeten.

Da bereits beschrieben wurde, dass einzelne Proteine der GABARAP-Unterfamilie eine Rolle bei der Oberflächenlokalisierung bestimmter Oberflächenrezeptoren spielen, stellte sich die Frage nach einem generelleren Einfluss auf deren Transport. Um dies zu analysieren, wurden Plasmamembran (PM-)ständige oberflächenexponierte Proteine von *triple* KO (dreifach KO, TKO-)Zellen, denen die ganze GABARAP-Unterfamilie fehlt, und Wildtyp (WT-)Zellen mit Biotin markiert und extrahiert. Die resultierenden Oberflächen-Proteome von TKO- und WT-Zellen wurden in Zusammenarbeit mit dem *Molecular Proteomics Laboratory* der Heinrich-Heine-Universität Düsseldorf mittels Massenspektrometrie identifiziert und quantifiziert. Vergleichende Datenanalysen offenbarten eine Untergruppe an Proteinen mit veränderter Oberflächenabundanz zwischen TKO- und WT-Zellen. Diese beinhalteten bereits bekannte GABARAP-Interaktoren, wie etwa den Transferrin-Rezeptor, aber auch potentiell neuartige Zielproteine, wie etwa eine Untergruppe bestehend aus Transport- und Kanalproteinen.

In einem gemeinsamen Projekt konnte zusätzlich gezeigt werden, dass TKO-Zellen einen beeinträchtigten vesikulären Transport von fluoreszenzmarkierten Lipiden und ein fragmentiertes Golgi-Netzwerk aufweisen. Beide Beobachtungen tragen wahrscheinlich zu den beobachteten Unterschieden der Zusammensetzung der Oberflächen-Proteome zwischen TKO- und WT-Zellen bei. Zusammenfassend bildet diese Arbeit einen Rahmen zur Identifizierung und Charakterisierung neuer Zielproteine, deren vesikulärer Transport von noch näher zu definierenden GABARAP/L1/L2-Funktionen abhängt. Außerdem zeigt sie die Notwendigkeit auf, autophagieabhängige und -unabhängige Auswirkungen der GABARAP-Unterfamilie während der Analyse ihrer Funktionen zu berücksichtigen.

Weil der unvoreingenommene Ansatz des vergleichenden Oberflächen-Proteoms intrinsisch keine profunden mechanistischen Einblicke zulässt, musste schließlich ein Modellsystem gefunden werden, das die Analyse des Einflusses der GABARAP-Unterfamilienproteine auf den endosomalen Transport und die Degradierung von Rezeptorproteinen ermöglicht. Der epidermale Wachstumsfaktor (EGF-)Rezeptor (EGFR) wurde schlussendlich identifiziert, alle nötigen Kriterien eines solchen Modellsystems zu erfüllen, da er bereits gut untersucht und

die notwendigen Werkzeuge zur Untersuchung seines intrazellulären Transports dadurch unmittelbar vorhanden waren. Zudem waren in der Literatur bereits Verknüpfungen zu GABARAP-Proteinen bekannt.

Durch die Anwendung von KO-Zelllinien und der Kombination von molekularbiologischen und biochemischen Techniken wurde eine neue und einzigartige Rolle von GABARAP während des intrazellulären Transports des EGFR sowie dessen Degradierung und Recycling entdeckt. Die bloße Abwesenheit von GABARAP, nicht aber eines der beiden anderen Paraloge, führte zu einer beschleunigten EGF-induzierten EGFR-Degradierung in zwei unabhängigen Zelllinien. Zudem waren die Signaltransduktion, die EGF-Aufnahme über die Zeit und die Genexpression von Zielgenen verringert. Weiterhin konnte gezeigt werden, dass GABARAP und EGFR während Co-Immunopräzipitationsexperimenten miteinander assoziieren. Um die Relevanz von GABARAP für den EGFR-Transport in lebenden Zellen zu untersuchen, wurde die codierende Sequenz für ein grünes fluoreszierendes Protein (GFP) mittels der CRISPR/Cas9-Methode zur Genomeditierung vor den *GABARAP* Genlokus eingebracht. Die resultierende *knock-in* (KI-)Zelllinie (GFP-GABARAP KI) exprimiert die Sequenz für ein GFP-GABARAP-Fusionsprotein unter der Kontrolle der endogenen regulatorischen Elemente und somit auf physiologischem Niveau. Erstmals wurden solche GFP-GABARAP KI-Zellen benutzt, um in einem Kooperationsprojekt zu zeigen, dass fluoreszenzmarkiertes EGF und GFP-GABARAP in lebenden Zellen transient dynamisch komigrieren.

Schlussfolgernd lässt sich sagen, dass die vorliegende Promotionsarbeit neuartige Einblicke in die autophagieunabhängigen Funktionen der GABARAP-Unterfamilie bietet. Zudem wurde eine einzigartige Funktion für GABARAP während des intrazellulären Transports und der Degradierung des EGFR identifiziert.

1.2 Summary

While in yeast a single *autophagy-related 8* (*Atg8*) gene is expressed, two subfamilies have evolved from it in humans. The microtubule-associated 1 protein light chain 3 (MAP1LC3 or short LC3) subfamily consists of LC3A, LC3B, LC3B2 and LC3C, while the γ-aminobutyric acid type A receptor-associated protein (GABARAP) subfamily consists of GABARAP, GABARAP-like 1 (GABARAPL1) and GABARAP-like 2 (GABARAPL2). Members of both subfamilies exhibit an ubiquitin-like fold and thus high cross-family structural similarity. Among the diverse functions described for human ATG8 proteins, their involvement during autophagy is best characterized. Autophagy designates an evolutionarily conserved degradation process activated by nutrient deficiency, during which a cell encloses components of the cytoplasm within a double membrane. The resulting vesicles contain cytoplasmic cargo and are termed autophagosomes. Autophagosomes mature by fusion with lysosomes into autolysosomes. The cytoplasmic cargo is degraded within the acidic environment of this organelle, whereupon the resulting building blocks are used to ensure cell survival. GABARAP subfamily proteins have been described to be involved in every step of autophagy initiation as well as autophagosome biogenesis, transport and their fusion with lysosomes. Much progress has been made in deciphering these autophagy-related functions, particularly for GABARAP.

Originally, however, GABARAP and its paralogs were recognized for their involvement in vesicular transport processes and the clustering of cell surface receptors. Due to the high structural redundancy, the exact involvement of the whole GABARAP subfamily and its individual members is not yet entirely clear for any of these processes. The aim of this work was therefore to identify unique and non-redundant functions of GABARAP subfamily proteins during autophagy-independent processes.

To achieve this, CRISPR/Cas9-mediated genome editing was applied to generate gene knockouts (KOs) of individual GABARAP subfamily members and combinations thereof, up to deletion of the complete subfamily, in two different cell lines. The resulting cell lines contributed to a publication describing an institute's own novel antibody specific for GABARAP during immunofluorescence (IF) measurements. Here, it could be shown that validation of antibodies should be performed for every application individually, as commercially available antibodies, which were readily validated for immunoblotting, failed to specifically detect GABARAP during IF. More importantly for the scope of the presented PhD thesis, the panel of KO cell lines generated laid the groundwork for subsequent analyses investigating biological functions of GABARAP subfamily proteins during vesicular trafficking of cell surface proteins.

Because GABARAP subfamily proteins had been described to be of importance for the surface abundance of individual surface receptors, the question of whether they had a more general impact on cell surface protein trafficking arose. To address this, plasma membrane (PM) located surface-exposed proteins of triple KO (TKO) cells lacking the whole GABARAP subfamily and wildtype (WT) cells were labelled by biotinylation and extracted. The resulting surface proteomes (surfaceomes) of TKO and WT cells were identified and quantified by mass-spectrometry in cooperation with the Molecular Proteomics Laboratory of the Heinrich-Heine-Universität Düsseldorf. Comparative data analysis revealed a subset of cell surface proteins with altered PM abundance between TKO and WT cells. These included already known GABARAP interactors such as transferrin receptor and novel hits such as e.g. a subgroup of transport and channel proteins. In a joint project, TKO cells were further shown to display impaired anterograde vesicular trafficking of fluorescently labelled lipids and a dispersed Golgi apparatus network morphology. Both observations likely contribute to the changes in surfaceome composition observed for TKO cells compared to WT controls. Taken together, this work provides a framework to identify and characterize novel targets of GABARAP subfamily-dependent vesicular trafficking and highlights the necessity to consider autophagy-independent functions during analysis of any of the functions of the GABARAP subfamily.

Since the unbiased surfaceome approach inherently cannot provide profound mechanistic insights, a model system to study the impact of GABARAP subfamily proteins on endosomal trafficking and degradation of receptor proteins in more detail had to be identified. Finally, the epidermal growth factor (EGF) receptor (EGFR) was identified to meet the criteria of such an optimal model system, as it was already well studied and provided the necessary tools to investigate its intracellular trafficking, and some links to GABARAP proteins had already been established in the literature.

By employing KO cell lines and combining molecular biological and biochemical techniques, a novel and unique role for GABARAP during EGFR trafficking and degradation was revealed. The mere absence of GABARAP, but not of any of the other GABARAP subfamily proteins, was shown to result in accelerated EGF-induced receptor degradation in two independent cell lines. This was accompanied by reduced signal transduction, EGF uptake over time and target gene expression. Furthermore, it could be shown that GABARAP and EGFR associate together during co-immunoprecipitation experiments. To investigate the relevance of GABARAP during EGFR trafficking in living cells, the coding sequence for a green fluorescent protein (GFP) was knocked in upstream of the *GABARAP* gene locus via CRISPR/Cas9-mediated genome editing. The resulting knock-in (KI) cell line expresses the sequence for a GFP-GABARAP fusion protein under control of endogenous regulatory elements at physiological expression levels. For the first time such a GFP-GABARAP KI cell

line was employed in a joint project to show transient dynamic comigration of fluorescently labelled EGF and GFP-GABARAP in living cells.

In summary, this work provides novel insights into autophagy-independent functions of the GABARAP subfamily and identified a unique function for GABARAP in mediating intracellular trafficking and degradation of the EGFR.

2. Introduction

2.1 The GABARAP subfamily of human ATG8 proteins

While in yeast there is only a *single autophagy-related 8* (*Atg8*) gene expressed, two subfamilies of human Atg8 (ATG8) have evolved. The microtubule associated protein 1 light chain 3 (MAP1LC3 or short LC3) subfamily consists of LC3A, LC3B, LC3B2 and LC3C whereas the γ-aminobutyric acid type A receptor ($GABA_AR$)-associated protein (GABARAP) subfamily consists of GABARAP and its paralogs GABARAP-like 1 (GABARAPL1) and GABARAP-like 2 (GABARAPL2) [1]. GABARAP is 14 kDa of size and exhibits a C-terminal ubiquitin-like fold, placing it in the superfamily of ubiquitin-like modifiers [2]. It shares high sequence and structural similarity with its paralogs GABARAPL1 and GABARAPL2 but also with members of the LC3 subfamily [3-7]. While at low, i.e. < 100 µM, concentrations GABARAP was found to be monomeric, higher order linear homopolymers at higher concentrations have also been reported [2, 8].

Subfamily members of human ATG8 proteins (from here on collectively referred to as LC3/GABARAP) have numerous protein-protein interactions via conserved interaction motifs [9]. While the LC3-interacting region (LIR), or Atg8-family interacting motif (AIM), has been described to mediate interactions for all subfamily members, more recently a specific GABARAP interaction motif (GIM) has been described which mediates protein interactions preferably with the GABARAP subfamily [10, 11]. The LIR concept has further been extended by the discovery of a non-canonical LIR motif involving an additional binding pocket within GABARAP [12], as well as by an extended LIR (xLIR) motif referring to negatively charged amino acids in neighborhood to the core LIR motif which positively influence interactions [13]. In addition, a motif closely related to the ubiquitin-interacting motif (UIM) binding to a different site on the LC3/GABARAP proteins was described [14]. Given the fact that the consensus core LIR motif (W/F/Y)-X-X-(L/I/V) (where X may be any amino acid) is only four amino acids long, it is eminent that a huge number of potential protein interaction partners exist.

Atg8 was originally discovered in the yeast *Saccharomyces cerevisiae* as an essential protein in the degradative autophagy pathway [15]. Autophagy will thus be introduced in the following chapter and the impact of LC3/GABARAP proteins, especially the GABARAP subfamily, on this process will be highlighted.

2.1.1 GABARAP subfamily proteins in macroautophagy

The term autophagy is composed of the two Greek words αυτος (autos: he/himself) and φαγειν (phagein: eating). It describes a cellular degradation process during which cytosolic

components are engulfed by a double membrane and targeted for degradation within lysosomes. The expression was coined by Christian De Duve at the *Ciba Foundation Symposium on Lysosomes* in 1963 [16]. Macroautophagy is a rather unselective degradative process occurring under nutrient starvation [17]. Autophagosome formation can be roughly divided into three steps:

1) Initiation of autophagosome biogenesis
2) Elongation, growth and closure of autophagosomes
3) Fusion of mature autophagosomes with lysosomes, resulting in degradation of the former inner membrane and breakdown of autophagosomal cargo [18].

Although LC3/GABARAP proteins have originally been identified to act downstream of autophagy initiation [19], more recent data provides evidence that LC3/GABARAP subfamily proteins are influencing events during every step of autophagosome formation [20]. In the following chapters the involvement of particularly the GABARAP subfamily during these steps will be highlighted.

2.1.1.1 Initiation of autophagosome biogenesis

Three macromolecular complexes are involved in the initiation of autophagosome biogenesis and they act in a hierarchical manner. The most upstream complex involved is the mammalian target of rapamycin complex 1 (mTORC1) which is a sensor for extra- and intracellular nutrient levels and thus a master regulator of starvation-induced autophagy [21]. Under nutrient-rich conditions, mTORC1 associates with the UNC51-like kinase 1 (ULK1/ATG1) complex, consisting of ATG13, ATG101, ULK1 and focal adhesion kinase (FAK) family-interacting protein of 200 kDa (FIP200), causing its inactivation by phosphorylation of ULK1 and ATG13 [22, 23]. Upon nutrient starvation, mTORC1 dissociates from the ULK1 complex, resulting in reduced inactivating phosphorylation of ULK1 and ATG13, and subsequent activation of the complex which leads to induction of autophagy [22, 23]. Activated ULK1 complex locates to the autophagosome initiation site via vesicular trafficking [24, 25]. The current consensus is that autophagosome biogenesis is initiated near contact sites of the endoplasmic reticulum (ER) and mitochondria, which are termed omegasomes due to their characteristic appearance in fluorescence microscopy [26]. GABARAP was recently reported to be tethered to the Golgi-apparatus resident 130 kDa *cis*-Golgi matrix protein (GM130) and released by WW domain-containing adaptor with coiled-coil activity in response to starvation to subsequently localize to omegasomes to activate the ULK1 complex and promote autophagy [27]. Recent data further reported a direct interaction

between ULK1, ATG13 and LC3/GABARAP family proteins to either enhance (GABARAP) or downregulate (LC3B) autophagy by directly modulating ULK1 complex activity [28].

At the omegasome, the class III phosphatidylinositol 3 (PI3)-kinase (PI3KC3) complex (PI3KC3-C) is recruited. This complex is comprised of a core of PI3K catalytic subunit type 3 (PIK3C3/hVps34) and PI3K regulatory subunit 4 (PIK3R4) which, by association with Beclin-1 (BECN1), form the class 1 PI3KC3 (PI3KC3-C1) [29-32]. BECN1 is a central protein during autophagy initiation as it is phosphorylatable by a multitude of interaction partners to subsequently induce or suppress autophagy by various downstream interactions [33]. Autophagy-suppressing BECN1 interactors include e.g. apoptosis regulatory B-cell lymphoma 2 (BCL2) proteins [34], RUN domain BECN1-interacting and cysteine-rich domain-containing protein (RUBICON) [29] and activated epidermal growth factor (EGF) receptor (EGFR) [35]. In response to starvation, autophagy is promoted by interactions resulting in release of BECN1 from BCL2 [36, 37]. Free BECN1 subsequently associates with ATG14 and within this complex both proteins are phosphorylated by ULK1 to initiate autophagy by enhancing activation of the PI3KC3-C1 and recruiting it to omegasomes [38-44]. Phosphorylation of activating molecule in BECN1-regulated autophagy protein 1 (AMBRA1) by ULK1 further facilitates translocation of PI3KC3-C1 to omegasomes [45]. PIK3C3/hVps34 is the only class III PI3K known in humans and phosphorylates PI3 within membranes to produce PI3-phosphate (PI3P) [46, 47]. Local PI3P is essential for autophagosome biogenesis and mediates recruitment of downstream effector molecules to the initiation site [48]. Intriguingly, preferably GABARAP proteins also interact with PIK3C3/hVps34, BECN1 and ATG14 of the PI3KC3-C1 directly through LIR motifs, potentially acting as scaffolds to ensure efficient autophagosome biogenesis [49]. Figure 1 illustrates these early events of autophagy initiation and shows GABARAP interactions with their key players.

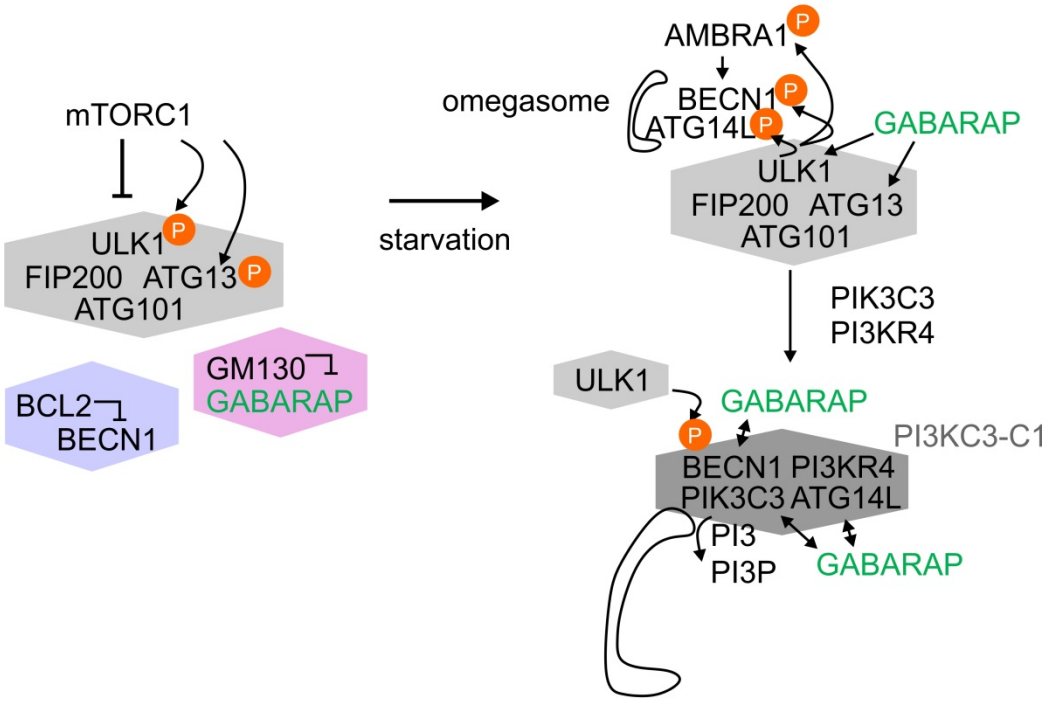

Figure 1: Regulation of starvation-induced autophagy by GABARAP interactions during early key events. Under nutrient-rich conditions, the mTORC1 inactivates the ULK1 complex by phosphorylation of ULK1 and ATG13. BCL2 binds and inhibits BECN1, while GM130 binds and inhibits GABARAP at the Golgi apparatus. In response to nutrient starvation or inhibition of mTORC1, the ULK1 complex localizes to the omegasome. Here GABARAP, potentially by acting as a scaffold protein, interacts with and activates ULK1 and ATG13 to enhance ULK1 autophagy-promoting activity. ULK1 further phosphorylates ATG14, BECN1 (both free and in complex with ATG14) and AMBRA1 to recruit PIK3C3/hVps34 and PI3KR4 to the omegasome where they interact with BECN1 and ATG14 to form the PI3KC3-C1. PIK3C3/hVps34 PI3-kinase activity results in local production of PI3P which is essential for initiation of autophagosome biogenesis. GABARAP furthermore interacts with components of the PI3K3C1, probably to stabilize the complex and facilitate initiation of autophagosome biogenesis. P = phosphorylated amino acid residue.

2.1.1.2 Elongation, growth and closure of autophagosomes

In order to engulf cytosolic cargo, the formation of fully closed autophagosomes is necessary for ultimate lysosomal cargo degradation. Growth of autophagosomes involves two ubiquitin-like conjugation systems. The first important step is the conjugation of ATG12 to ATG5 which is mediated by the E1- (E1L) and E2-like (E2L) enzymes ATG7 and ATG10 [50-52]. The resulting ATG12-ATG5 conjugate subsequently forms large tetrameric complexes with ATG16L which are associated with growing phagophores but absent from mature autophagosomes [53].

The second ubiquitin-like conjugation system during autophagosome biogenesis involves the conjugation of LC3/GABARAP subfamily proteins. They are cleaved at their C-terminus by ATG4 proteases to generate LC3/GABARAP-I, conjugated to the E2L protein ATG3 by E1L

activity of ATG7, followed by transfer to phosphatidylethanolamine (PE) to generate membrane associated LC3/GABARAP-II which is thus incorporated into growing autophagosomes during all stages of elongation and growth [54-56]. Especially accumulation of lipid-conjugated (lipidated) LC3B-II is therefore widely used as a marker for autophagosome formation and as a general readout for autophagy [57]. It has been shown that the ATG12-ATG5-ATG16L complex is recruited to omegasomes by the PI3P effector WD-40 repeat containing protein that interacts with PtdIns (WIPI) 2 (WIPI2), where it mediates attachment of LC3/GABARAP to PE via E3-like (E3L) activity [58, 59]. Subsequently, the ATG12-ATG5-ATG16L complex together with LC3/GABARAP forms a mesh-like layer with stabilizing properties on autophagic membranes [60]. Lipidation of LC3/GABARAP was also described to depend on the membrane curvature sensing properties of ATG3, thereby promoting membrane incorporation directly at the growing tips of autophagosomes [61]. Lipid-associated LC3/GABARAP proteins and their incorporation into membranes was further reported to alter properties and curvature of membranes directly [62].

Several membrane sources for growing autophagosomes were suggested in the past. They were believed to be either derived from an existing organelle (maturation model) or assembled from different lipid sources at their initiation site (assembly model) and evidence was reported to support both models [63]. Several studies reported autophagosomes to be positive for post-Golgi associated membrane sources such as lectins [64, 65]. Also mitochondria [66], ER exit sites [25, 67], ER-Golgi intermediates as well as the ER-Golgi fusion machinery [68, 69], recycling endosomes [70-72] and the PM [73] have been described to contribute membranes to autophagosome biogenesis. This illustrates that autophagy may utilize a multitude of membrane sources, probably depending on the cellular metabolic state. The transmembrane protein ATG9 seems to play a special role in this context, as cycling of ATG9-positive vesicles was described to not only be necessary for initiation, but also to transport membranes to omegasomes to promote autophagosome growth [74, 75].

How autophagosomes are finally closed, e.g. by membrane scission [76], is not fully understood yet [77], although PI3P phosphatases have been implicated to regulate autophagosome levels by negatively regulating local PI3P levels [78, 79]. Interestingly, the presence of LC3/GABARAPs is necessary to form fully sealed autophagosomes [80], potentially due to their ability to mediate membrane fusion processes during autophagosome biogenesis [81]. Importantly, a recently published study established a direct and essential role for GABARAP in autophagosome closure by interaction with ATG2A/B and WIPI4, whereas disruption of this interaction resulted in a block of autophagy [82]. Figure 2

highlights the involvement of GABARAP subfamily proteins during autophagosome growth as described within this chapter.

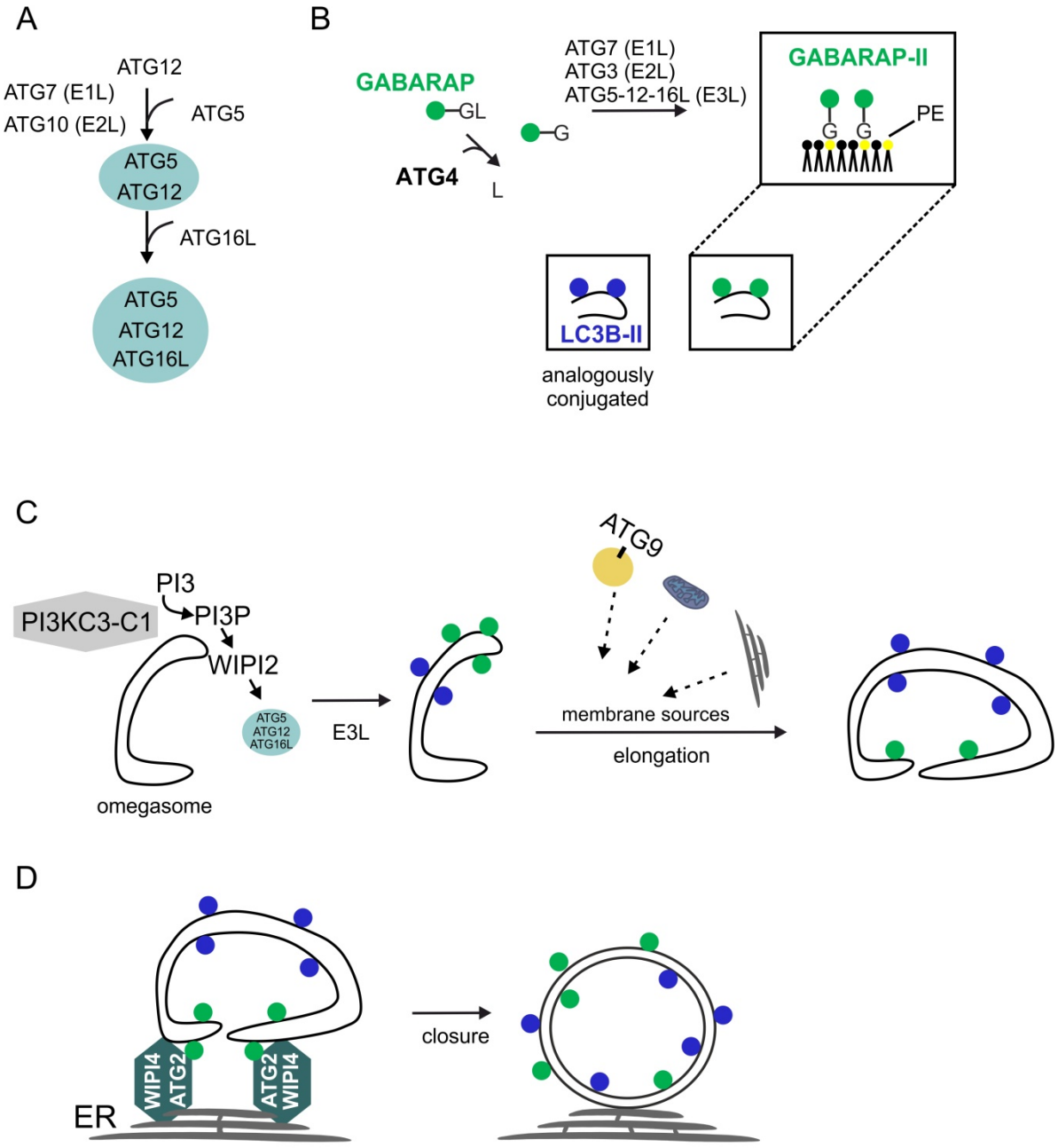

Figure 2: GABARAP is anchored into autophagic membranes by an ubiquitin-like conjugation system and is involved in autophagosome elongation, growth and closure. (A) ATG12 is conjugated to ATG5 by a ubiquitin-like conjugation process involving E1L activity of ATG7 and E2L activity of ATG10. The resulting ATG12-ATG5 conjugate subsequently forms a complex with ATG16L. (B) GABARAP family members are pre-processed by cleavage at C-terminal G by ATG4 protease activity and subsequently conjugated to phosphatidylethanolamine (PE) in a second ubiquitin like conjugation reaction involving E1L activity of ATG7 and E2L activity of ATG3 to generate membrane-associated GABARAP-II. LC3 family members represented by LC3B are conjugated to PE after C-terminal pre-procession analogously. (C) The E3L ATG12-5-16L complex is targeted to the omegasome by the PI3P-binding protein WIPI2 to mediate incorporation of GABARAP/LC3-II into

growing autophagosomes which are thereby tethering and recruiting lipids derived from various membrane sources including but not limited to ATG9-containing vesicles, mitochondria and ER. (D) Autophagosome closure is not yet fully understood but accomplished by an interaction involving GABARAP and ATG2 which is tethered to the ER by WIPI4 during autophagosome growth.

2.1.1.3 Transport of autophagosomes and their fusion with lysosomes

Fully closed autophagosomes are finally released from ER contact sites by regulation of local Ca^{2+} levels due to activity of vacuole membrane protein 1 (VMP1) [83]. Afterwards, free autophagosomes are transported along microtubules by dynein-mediated minus-end transport to encounter lysosomes which are concentrated in the perinuclear region [84, 85]. Proteins of the Ras-related in brain (RAB) family link both autophagosomes and lysosomes to microtubule transport by simultaneous binding to motor protein-linked adaptors [86]. In general, microtubule plus-end transport of vesicles is mediated by kinesin, while minus-end transport is mediated by dynein [87]. In this context, RAB7 both regulates minus- and plus-end transport of autophagosomes and lysosomes by interacting with e.g. FYVE and coiled-coil (CC) domain-containing protein 1 (FYCO1) [88], RAB7-interacting lysosomal protein (RILP) [89] and oxysterol-binding protein-related protein 1L (ORP1L) [90]. This bidirectional transport enables the control of autophagic flux by regulated encounter of autophagosomes and lysosomes. Since FYCO1 also interacts with LC3/GABARAP and kinesin to mediate plus-end transport, it was suggested to target pre-autophagosomal membranes to cytosolic target sites of cargo engulfment [91]. While FYCO1 was reported to preferentially associate with LC3 subfamily proteins [92, 93], it might in principle also bind to GABARAP subfamily members. Although LC3/GABARAP proteins have additionally been suggested to regulate autophagosome transport in a more direct manner, e.g. by microtubule-binding via their N-termini [94], experimental evidence to support such models is largely lacking.

After autophagosomes and lysosomes meet, their membranes fuse to form autophagolysosomes, resulting in degradation of intra-autophagosomal cargo and the inner membrane of the former autophagosome [95, 96]. This fusion step includes numerous anchor/tether molecules and protein complexes, among which the homeotypic fusion and protein sorting (HOPS) complex is best described. It shares a core with the class C core vacuole/endosome tethering (CORVET) complex and either of these complexes is then formed by addition of two unique subunits [97-99]. While the CORVET complex is responsible for tethering and facilitating endosome-endosome fusion, the HOPS complex tethers endosomes and other vesicles to lysosomes and mediates their fusion by recruiting effector proteins [97-99]. The HOPS complex interacts with RAB7 on late endosomes (LEs) and autophagosomes and is tethered via pleckstrin homology domain-containing protein

family member 1 (PLEKHM1) and simultaneous RAB7 and LC3/GABARAP binding to autophagosomes [100, 101].

Autophagosome-lysosome (AL) fusion is enabled by binding of the HOPS complex to the soluble N-ethyl-maleimide-sensitive factor (NSF) attachment protein (SNAP) receptor (SNARE) syntaxin17 (STX17) and its interaction with the lysosomal SNARE vesicle-associated membrane protein 8 (VAMP8) via SNAP29, enabling lipid mixing and fusion by bringing the two organelles in close proximity [102, 103]. Oligomeric ATG14 further stabilizes the STX17, VAMP8, SNAP29 interaction to facilitate AL fusion [104]. Importantly, the BIR repeat-containing ubiquitin-conjugating enzyme (BRUCE) has been shown to directly interact with GABARAP, STX17 and SNAP29 to facilitate AL fusion [105].

SNARE-mediated membrane fusion in general is based on the presence of distinct SNARE proteins associated to either of the vesicles about to fuse: one v-SNARE (vesicular SNARE) and two or three t-SNAREs (target SNAREs) bind to form a *trans*-SNARE complex bringing the two lipid bilayers in close enough proximity to overcome the energetic barrier and enable lipid mixing and finally fusion without organelle lysis [106]. Afterwards, the resulting *cis*-SNARE complex binds NSF and a specific SNAP to disassemble the SNARE complex under ATP consumption [107]. Additionally, PI3K3C3-C2, consisting of PIK3C3/hVps34, PI3KR4, BECN1 and UV radiation resistance-associated gene (UVRAG) protein, facilitates fusion by enhancing HOPS complex and RAB7 activity [32, 108]. GABARAP was recently reported to recruit phosphatidylinositol 4-kinase IIα (PI4KIIα) to mature autophagosomes and due to subsequent local phosphatidylinositol 4-phosphate (PI4P) production mediate AL fusion [109]. Within the resulting autophagolysosome, the inner membrane, including LC3/GABARAP, of the former autophagosome is degraded by acidic phospholipases [110, 111]. Subsequently, autophagosomal cargo is degraded by acidic proteases such as cathepsins [112]. The catabolites resulting from lysosomal breakdown of macromolecules are then exported via specific catabolite exporters to the cytoplasm where they can be reutilized to maintain cellular homeostasis [113].

Notably, the ATG8 conjugation machinery was described to be necessary not only for correct closure of autophagosomes, but also for the degradation of the former inner autophagosome membrane within lysosomes, although fusion itself was not affected [96]. Figure 3 illustrates the events described in this chapter and highlights involvement of GABARAP subfamily proteins during AL fusion.

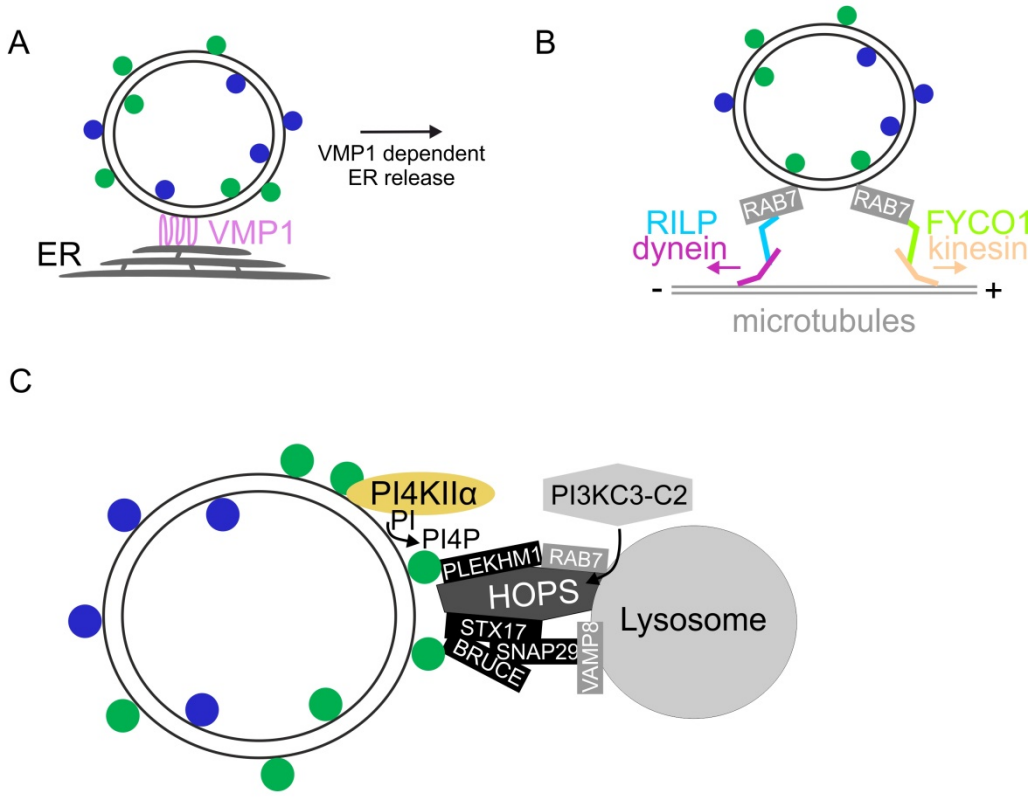

Figure 3: GABARAP is involved in autophagosome transport and fusion of autophagosomes with lysosomes. (A) Fully closed autophagosomes are released from ER contact sites by VMP1 activity. (B) Transport of autophagosomes along the microtubule network involves simultaneous binding of the effector protein RILP to RAB7 on autophagosomes as well as the motorprotein dynein, resulting in movement of autophagosomes along the microtubule minus-end. Microtubule plus-end transport is mediated analogously and involves interaction of RAB7, FYCO1 and kinesin. (C) GABARAP recruits PI4KIIα to autophagosomes, potentially to recruit effectors needed for fusion with lysosomes by local PI4P production. GABARAP subfamily proteins facilitate fusion of autophagosomes with lysosomes by interacting with the tethering factors PLEKHM1 and BRUCE to enable SNARE interaction.

2.1.2 GABARAP proteins in selective autophagy

In addition to canonical bulk degradation of cytoplasmic content via macroautophagy, several highly selective forms of autophagy exist. They result e.g. in degradation of (damaged) organelles, protein aggregates, lipid droplets but also exogenous material such as viruses, bacteria and parasites [114, 115]. Macroautophagy and selective autophagy mainly utilize the same set of proteins for autophagosome biogenesis and AL fusion, including LC3/GABARAP subfamily proteins, but substantially differ in their mode of cargo recognition which is highly specific in case of selective autophagy. Another important difference is the recruitment of the initiation machinery (2.1.1.1), including ULK1 complex,

which, in case of selective autophagy, is recruited only after cargo recognition and binding in an mTORC1 independent manner [116-118].

The current understanding of the cargo selection process is that oligomeric selective autophagy receptors (SARs) simultaneously bind to proteins marked by polyubiquitination and LC3/GABARAP proteins via LIR motifs, thereby targeting cargo into growing autophagosomes [114]. The first mechanistic observations of selective targeting of proteins into autophagosomes in mammalian cells described the targeting of polyubiquitinated protein aggregates to autophagosomes by oligomeric sequestosome-1 (SQSTM1/p62) through simultaneous binding to LC3/GABARAP proteins [119, 120]. Autophagic clearance of peroxisomes was also shown to be SQSTM1/p62-dependent [121].

Subsequently, the role of LC3/GABARAP proteins involved in the selective degradation of mitochondria, termed “mitophagy”, was established [80, 122]. In general, the mitochondrial serine/threonine-protein kinase PINK1 accumulates at the outer mitochondrial membrane (OMM) of damaged mitochondria and phosphorylates ubiquitin which causes recruitment of the SARs optineurin and nuclear dot 52 kDa protein, which in turn direct the ULK1-containing autophagosomal initiation machinery to compromised mitochondria [123, 124]. Subsequent depolarization of mitochondrial membranes leads to the relocalization of the inner mitochondrial membrane (IMM) resident proteins NipSnap homolog 1 and 2 which enhance selective mitophagy by binding to LC3/GABARAPs and SARs [125]. In addition, forms of mitophagy involving LC3/GABARAP proteins, independent of PINK1, by further SARs in response to different stressors have been described [126-128]. Particularly interesting is the involvement of AMBRA1 as a SAR in this regard [129] because AMBRA1 was found to preferably bind to GABARAP subfamily proteins [130]. As described in chapter 2.1.1.1, AMBRA1 is also involved in initiation of mTORC1-dependent autophagy which might provide another link of involvement of GABARAP during the process.

The turnover of the ER, termed “ER-phagy”, is another form of selective autophagy involving LC3/GABARAP proteins and several distinct forms have been described depending on the inducing factor and/or ER component to be degraded [131-133]. Further forms of selective autophagy involving LC3/GABARAP proteins exist, following the same general principle as described for aggrephagy, mitophagy and ER-phagy (they are reviewed e.g. in [114]).

2.1.3 GABARAP proteins in surface receptor trafficking

Although most of the recent studies focus on autophagy-related functions of the GABARAP subfamily, it was originally discovered in mammalians for its role in surface receptor trafficking. The eponymous $GABA_AR$ negatively regulates signals in GABAergic neurons and GABARAP was discovered as a binding protein simultaneously interacting with the

receptor's γ2 subunit and the cytoskeleton to promote receptor cluster formation and surface expression [134-136]. Simultaneous association with $GABA_AR$ and tubulin was also described for GABARAPL1 [137]. GABARAP was further shown to promote trafficking of $GABA_AR$-containing vesicles by binding to the motor protein kinesin-1 family member 5 A [138]. Because GABARAP itself was not found in high abundance at the synapse, it was later suggested to influence $GABA_AR$ clustering by mediating its trafficking via interaction with NSF [139]. Prior to this finding, GABARAPL2 was already reported to interact with NSF and enhance its ATPase activity, thereby promoting vesicular trafficking at the Golgi apparatus [140]. Later, GABARAPL1 was also reported to interact with NSF [141]. In contrast, NSF interaction has not been assigned to any of the LC3 family proteins to date. This feature thus discriminates the GABARAP from the LC3 subfamily and highlights the potentially unique role of GABARAP proteins during vesicular (receptor) trafficking. GABARAP and GABARAPL1 were also reported to interact with the splicing variant PX-RICS of Rho GTPase-activating protein (RICS) containing a phosphoinositide-binding (PX) domain, which is involved in ER to Golgi transport of a N-cadherin/β-catenin complex [142] and $GABA_AR$ trafficking [143]. Interaction of GABARAP with the transferrin receptor (TFRC) has been reported [5], but no mechanistic function for this interaction has been assigned to date. In contrast, GABARAP proteins have been reported to be associated with several cell surface receptors and to promote their surface expression. Interaction of GABARAP with transient receptor potential cation channel subfamily V member 1 (TRPV1) was found to directly influence its kinetics [144], illustrating the physiological relevance of the interaction. GABARAP further interacts with the angiotensin 1 receptor (AT_1R) to enhance its surface expression and positively modulate its signaling activity [145]. Consistently, deficiency for GABARAP was reported to result in increased levels of solute carrier family 34 member 1 (SLC34A1) at the renal brush border membrane, causing decreased urinary P_i levels in GABARAP KO mice [146, 147]. GABARAPL1 was reported to interact with κ-opioid receptor (KOR) and increase its surface expression [148]. Additionally, it was found to be required for increased surface expression of the EGFR, but only under hypoxic conditions [149]. Recently, GABARAPL2 has been described to interact with parkin-associated endothelin receptor-like receptor (PAELR) and to reduce its levels upon overexpression [150].

In summary, involvement of GABARAP subfamily proteins has been described for a variety of cell surface receptor proteins and while presence of a distinct GABARAP was often reported to be associated with increased surface expression of the analyzed receptor, also downregulation of receptors was reported. Notably, autophagic turnover of tumor necrosis factor receptor superfamily member 12 A (TNFRSF12A) is mediated by GABARAP subfamily proteins with GABARAP and GABARAPL2 fulfilling different roles in the process [151]. In general, degradation of proteins via autophagy contributes to their turnover and

thereby directly regulates cellular homeostasis [152]. Table 1 summarizes the known effects of GABARAP subfamily proteins on cell surface receptor trafficking. Despite these isolated observations, general models of how GABARAP and its paralogs influence cell surface protein trafficking are rather limited. Therefore, systematic analyses are necessary to shape a better understanding of the underlying processes.

Table 1: Reported interactions of GABARAP subfamily proteins with surface receptor proteins.

Surface receptor	GABARAP subfamily protein	Function
AT_1R	GABARAP	Direct interaction modulates surface expression and signaling activity
SLC34A1	GABARAP	Deficiency results in increased receptor levels at brush border membrane
TFRC	GABARAP	Direct interaction with unknown function
TRPV1	GABARAP	Direct interaction influences receptor kinetics and surface expression
$GABA_AR$	GABARAP/GABARAPL1	Direct interaction promotes receptor clustering
KOR	GABARAP/GABARAPL1	Direct interaction increases surface expression
TNFRSF12A	GABARAP/GABARAPL2	Selective regulation of turnover via autophagy
EGFR	GABARAPL1	Necessary for increased surface expression in response to hypoxia
PAELR	GABARAPL2	Overexpression reduces receptor levels

2.2 The endolysosomal system explained by epidermal growth factor receptor trafficking

The involvement of GABARAP subfamily proteins in both anterograde surface receptor trafficking as well as their autophagic turnover (2.1.3) illustrates how the functions of the GABARAP subfamily during (selective) autophagy are interconnected with functions directly related to (vesicular) receptor trafficking. Both autophagy and the endosomal system indeed share a subset of key proteins and therefore naturally overlap at a number of nodes. The endolysosomal system will thus be introduced in the following chapter with the example of EGF-induced EGFR intracellular trafficking. Selected proteins involved in both processes are highlighted.

2.2.1 The epidermal growth factor receptor

The EGFR belongs to the superfamily of ErbB receptors [153, 154]. It consists of an extracellular part with four domains, one single transmembrane domain, a small juxtamembrane segment, an intrinsically inactive kinase domain consisting of a C-lobe and a N-lobe as well as a flexible regulatory cytoplasmic tail containing several phosphorylatable Y residues (figure 4) [155-158]. It is thus a receptor tyrosine kinase (RTK) localized at the PM and as such responsible for receiving extracellular inputs and transducing them into intracellular signals to promote e.g. development, growth, cellular homeostasis, regeneration and proliferation [159, 160]. The inputs for such signals are provided by a variety of ligands, some of which bind to and activate several ErbB family members [161]. The eponymous EGF binds exclusively to the EGFR [162] and will thus be used in the following chapters to describe EGFR activation, signaling, subsequent internalization and trafficking within the endosomal system leading either to the receptor's recycling back to the PM or degradation within the lumen of lysosomes.

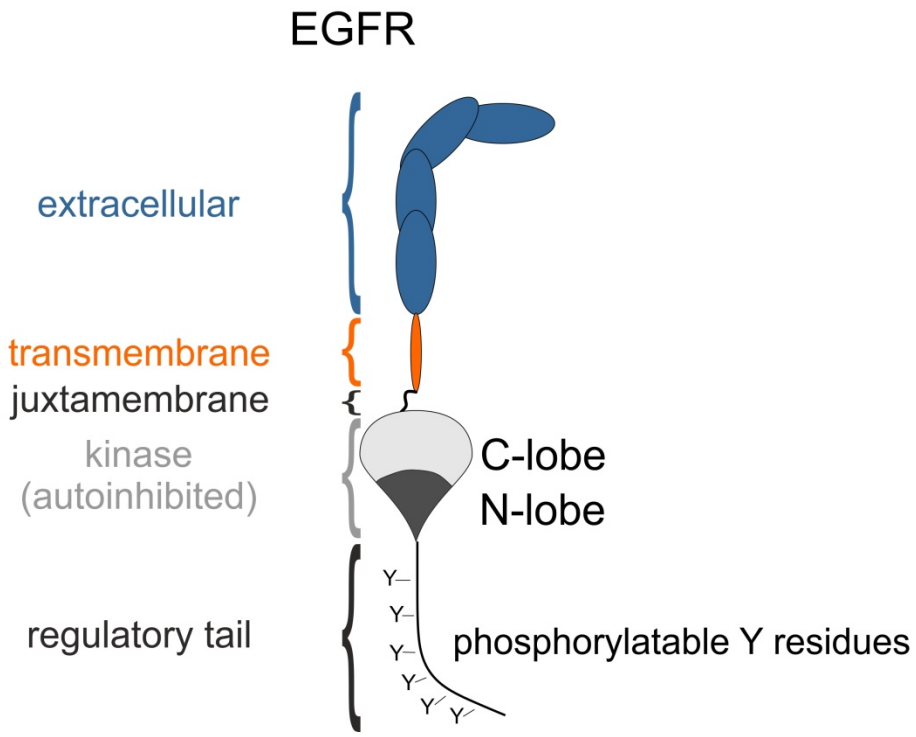

Figure 4: Structural composition of monomeric EGFR. The EGFR consists of an extracellular ligand-sensing domain, a single transmembrane segment which is connected by a small juxtamembrane segment to the kinase domain. The kinase domain is autoinhibited under conditions of ligand-unavailability and consists of two distinct lobes termed C and N lobe, respectively. Adjacent to the kinase domain, EGFR contains a cytoplasmic regulatory C-terminal tail which contains several phosphorylatable Y residues. Adapted and modified according to [157].

2.2.2 Epidermal growth factor receptor activation and signaling

Under steady-state conditions, ligand-unbound EGFR is present at the PM either as a monomer or as a preformed symmetric dimer [163-165]. The affinities of EGF for either a single monomer (220 pM) or a monomer within a symmetric dimer (190 pM) are basically equivalent, indicating that both are functionally relevant in living cells [166]. Upon EGF binding, the extracellular domains form a pocket like structure, the orientation of the C- and N-lobes change, which, in case of preformed dimers, results in an asymmetric dimer through rotation and the thus activated kinase domain of the EGF bound monomer auto-phosphorylates Y residues in the cytoplasmic regulatory tail of the unoccupied monomer [157, 167, 168]. Additionally, ligand-bound monomers associate with unoccupied monomers to form asymmetric dimers [169]. Notably, due to conformational changes, the affinity of EGF for the unoccupied monomer in an asymmetric dimer is approximately ten-fold (2.9 nM) lower compared to single monomers or monomers in preformed symmetric dimers (negative cooperativity) [166, 170]. The resulting double occupied dimers are rather unstable and tend

to separate, which results in two ligand-bound single monomers [166]. These ligand-bound EGFR monomers are then free to recruit unoccupied monomers, phosphorylating their C regulatory tails and thus laterally propagate the signal to subsequently recruit downstream effector proteins of diverse signaling pathways [166, 171]. At saturating concentrations of EGF (i.e. ≥ 10 ng/ml), however, relative levels of double ligand-bound symmetric dimers accumulate, resulting in phosphorylation of the remaining cytoplasmic regulatory tail of the initially EGF-bound EGFR monomer [166, 172]. Figure 5 summarizes binding kinetics of EGF to EGFR in such a model of negative cooperativity.

EGFR also forms higher state oligomers, thereby increasing local EGFR concentration and signaling activity through enhanced relative levels of cytoplasmic tail phosphorylation by oligomerization of activated kinase domains [172, 173]. Oligomerization of EGFR is ligand-dependent and thus explains how different ligands mediate different signaling outcomes through stabilization of distinct homo- or hetero-dimers and/or oligomers [174, 175].

Downstream of receptor oligomerization, several signaling pathways are activated and include PI3K/protein kinase B (PKB/AKT) and mitogen-activated protein kinase/extracellular-signal regulated kinase (MAPK/ERK) signaling which subsequently promote cell growth, motility, differentiation and proliferation via activation of downstream targets [176-180].

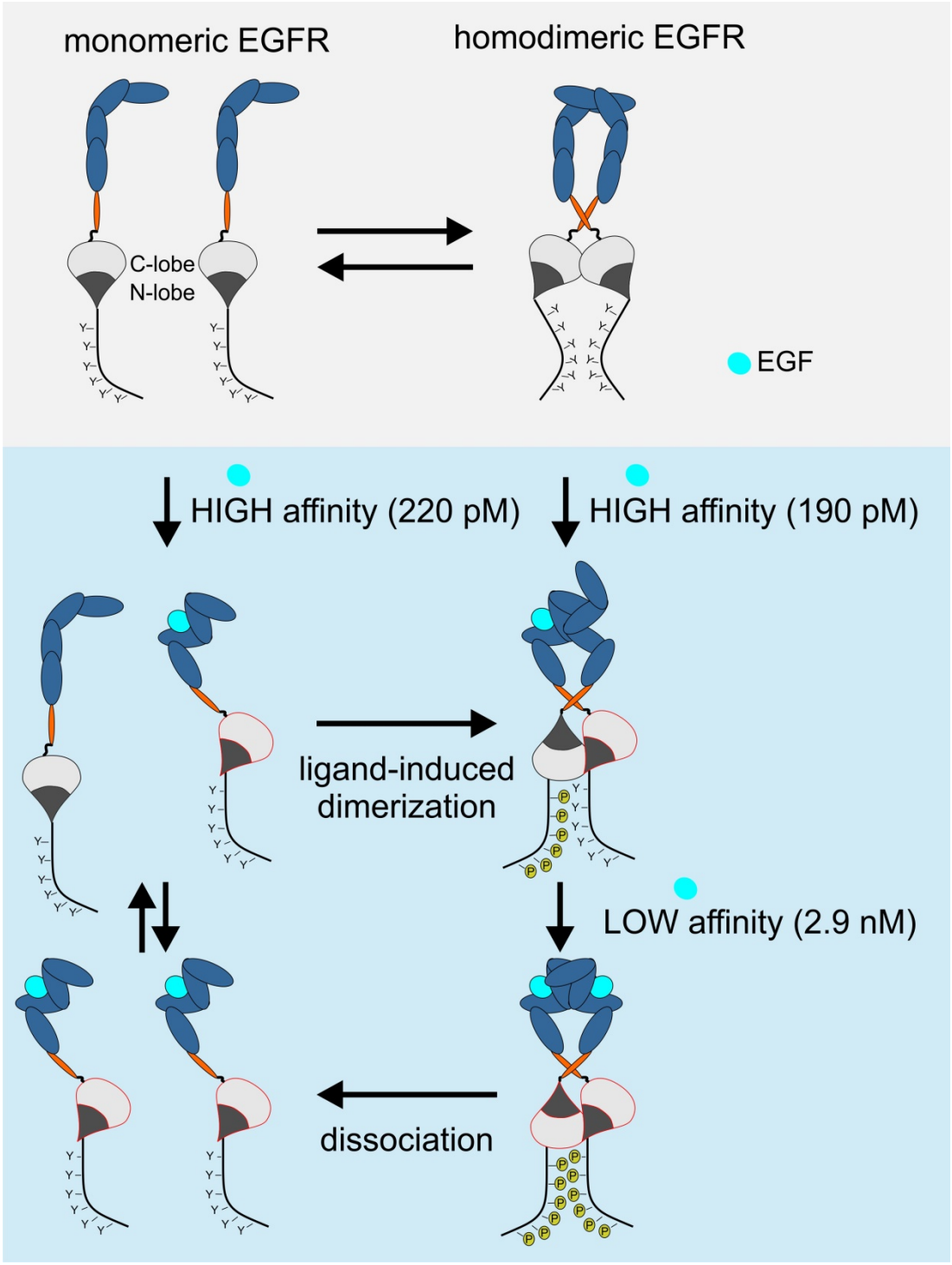

Figure 5: EGF:EGFR binding in a model of negative cooperativity. Under ligand-free conditions, EGFR is present at the PM either as a single monomer or as a symmetric homodimer. Upon EGF stimulation, both monomeric and homodimeric EGFR bind EGF with high affinity. Subsequently, asymmetric homodimers are either formed by ligand-induced dimerization in case of EGF bound monomeric EGFR or by rotation in case of preformed homodimeric EGFR. Within asymmetric EGFR dimers, the kinase domain of the EGF bound monomer is activated due to conformational changes and *trans*-phosphorylates Y residues in the regulatory tail of the unbound monomer within the dimer. The affinity of EGF to the unoccupied EGFR monomer within an asymmetric single-occupied dimer is approximately ten-fold lower compared to unoccupied symmetric dimers or unoccupied monomers which leads to rapid dissociation of double-bound asymmetric dimers, thereby laterally propagating

EGF-induced signaling by formation of additional asymmetric dimers with unoccupied monomeric EGFR. Active kinase domains are depicted by red margins. P = phosphorylated Y residues. Adapted and modified according to [166].

2.2.3 EGFR internalization, endosomal trafficking and degradation

To prevent sustained activation and uncontrolled signal transduction, the EGFR is internalized via endocytosis and sorted within the endolysosomal system, resulting either in recycling back to the PM or degradation within lysosomes [181].

Internalization in response to EGF binding and activation can be mainly divided into two different branches: at low EGF concentrations (i.e. < 10 ng/ml), the receptor is internalized via clathrin-coated pits by clathrin-mediated endocytosis (CME), whereas higher EGF levels promote clathrin-independent endocytosis (CIE) [182, 183]. The question of how receptors translate low and high EGF concentration into distinct cellular responses has evoked the concept of low and high affinity EGFR subsets [184]. However, the model of negative cooperativity for EGFR indicates that these subsets are based on the lowered binding affinity of EGF to the unoccupied monomer in an asymmetric dimer (2.2.2) [166]. “Lowly activated” receptors are thus likely represented by asymmetric dimers where only one EGFR cytoplasmic tail is phosphorylated in response to low concentrations of EGF which trigger lower levels of oligomeric EGFR species and thus lower net activation of receptors [173]. These receptors are internalized via CME and primarily sorted within RAB5-positive endosomes. As described, EGFR activation leads to recruitment of PI3K/AKT (2.2.2) which produces phosphatidylinositol-3,4,5-triphosphate (PIP3) which acts as an effector molecule to recruit RAB5 via binding of early endosomal antigen 1 (EEA1) [185]. RAB5 tethered to early endosomes by EEA1 subsequently recruits the CORVET complex to trigger fusion of RAB5-containing endosomes [186, 187]. RAB5 has further been described to interact with the effector fused toes (FTS)-hook-FTS and hook-interacting protein to mediate dynein-driven transport of early endosomes to the microtubule minus-end which directs endosomes towards the perinuclear region [188, 189]. Here, phosphatases of the protein tyrosine phosphatase (PTB) family reside at the ER [190, 191] and prototypic PTB1B dephosphorylates EGFR, thereby shutting down its signaling activity [191, 192]. The resulting vesicles containing inactivated EGFR mature into RAB11-positive recycling endosomes and are trafficked back to the PM, where recycled receptors again can react to extracellular stimuli [193-195]. Roughly two thirds of EGFRs internalized by CME are recycled back to the PM, the rest is degraded [196].

In contrast, highly activated, i.e. double phosphorylated oligomeric, receptors are internalized more rapidly via CIE and mainly undergo a different fate: here, approximately

85 % of the internalized receptors are targeted for degradation and only approximately 15 % are recycled [196, 197]. In this context, hyperubiquitination mediated by the E3 ubiquitin-protein ligase CBL in response to EGF stimulation serves as a sorting signal for endosomal trafficking towards degradation [198-200]. Vesicles containing hyperubiquitinated EGFR also acquire RAB5, fuse with other endosomes accordingly and travel towards the perinuclear region. However, in case of highly activated and ubiquitinated receptors, these vesicles mature into RAB7-positive LEs [201]. This is facilitated by dephosphorylation of RAB7 by phosphatase and tensin homolog (PTEN) on endosomes and subsequent recruitment of the vacuolar fusion protein MON1 homolog A-Vacuolar fusion protein/CCZ1 homolog complex which acts as an activator of RAB7 and mediates its incorporation into endosomal membranes [202]. Subsequently, LEs fuse and their membranes are invaginated to form multivesicular bodies (MVBs). In order to mature into intraluminal vesicles (ILV) of such MVBs, ubiquitinated receptors are dephosphorylated by PTBs and ILV formation is mediated by endosomal sorting complexes required for transport (ESCRT) activity. ESCRT protein complexes act hierarchically: ESCRT-0 recognizes and clusters ubiquitinated EGFR, ESCRT-I and ESCRT-II take over and bend LE membranes which are finally processed by ESCRT-III to generate ILVs devoid of ESCRT complexes but containing EGFR [203]. Successful maturation of EGFR-containing MVBs has also been reported to be dependent on proteasome-mediated deubiquitination [204].

To finally target EGFR for degradation, RAB7 recruits the effector proteins ORP1L and RILP to LEs/MVBs to drive microtubule minus-end transport to ensure their trafficking towards the perinuclear region [205]. In parallel, RAB7-RILP interaction on lysosomes facilitates their trafficking to the perinuclear region where both vesicular compartments meet [89]. Finally, LEs/MVBs fuse with lysosomes and form endolysosomes [206]. The mechanism mediating endosome-lysosome fusion involves recruitment of HOPS complex, PLEKHM1, RAB7 and is similar to AL fusion (2.1.1.3). Within the lysosomal lumen, acidic hydrolases finally degrade both EGF and EGFR and the resulting amino acids can be repurposed by the cell [207]. Figure 6 shows a simplified schematic representation of the events described in this chapter.

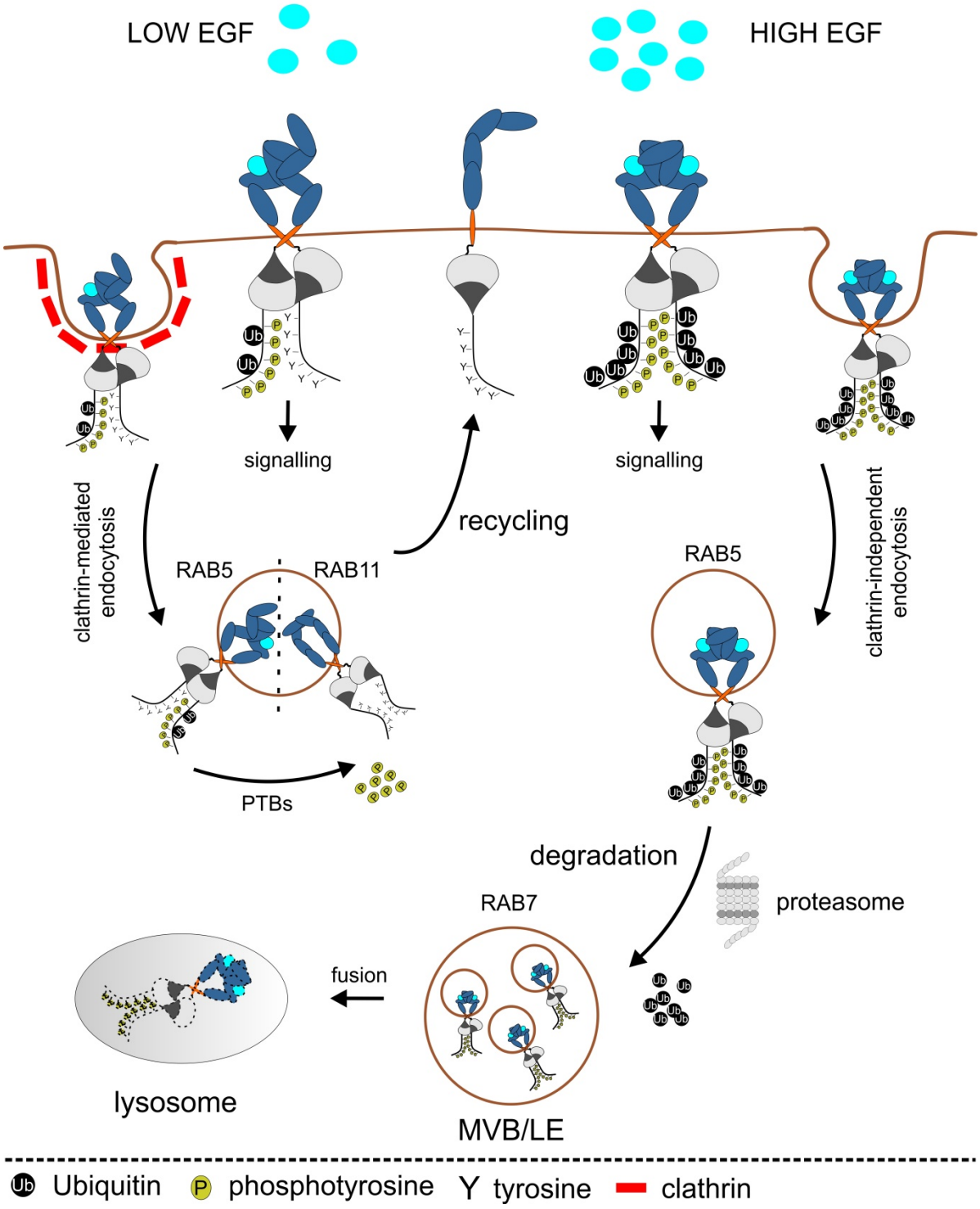

Figure 6: Scheme depicting trafficking of EGFR within the endolysosomal system. Upon extracellular ligand binding, EGFR is internalized via CME or CIE. Internalized EGFR is sorted via the endosomal system within RAB5-positive early endosomes and either targeted for recycling by RAB11-positive endosomes (preferred under low ligand availability) or degradation via RAB7-positive LEs/MVBs (enhanced under high ligand availability). Prior to lysosomal degradation, EGFR is deubiquitinated by proteasome-associated deubiquitinases which is a prerequisite for its engulfment into MVBs through ILVs. MVB = multivesicular body, LE = late endosome, PTBs = protein tyrosine phosphatases.

2.2.4 Interconnections between autophagy and the endolysosomal system

As described (2.1.1, 2.2.3), some general aspects, such as the trafficking of autophagosomes and endosomes along the microtubule network and their fusion with lysosomes obviously depend on similar mechanisms in both pathways. Furthermore, several proteins initially thought to be involved in only one of them, fulfill specific roles during both processes.

Apart from its role during endosomal trafficking, RAB5 has additionally been described to interact with PIK3C3/hVps34 and BECN1 during initiation of macroautophagy [208]. RAB5 was also found to be involved in closure of autophagosomes [209] via interaction with ESCRT proteins [210]. Furthermore, RAB11-positive compartments associated with endosomal recycling have been reported to additionally function as sites of autophagosome assembly [211]. As outlined in chapters 2.1.1.3 and 2.2.3, RAB7 facilitates fusion of both autophagosomes and LEs/MVBs with lysosomes. It also regulates their directed transport towards each other by acting as a link between motor proteins and autophagic, endosomal as well as lysosomal vesicles by interaction with e.g. FYCO1, RILP and ORP1L to mediate transport along the microtubule network. Finally, the HOPS complex is involved in tethering factors necessary for fusion between autophagosomes and lysosomes as well as endosomes and lysosomes. Intriguingly, endosomes and autophagosomes frequently fuse with each other to form amphisomes [212]. This clearly indicates that both processes represent closely related mechanisms to maintain cellular homeostasis and great caution needs to be exercised when interpreting experiments with focus on only one pathway.

Notably, two distinct pathways employing components of the core autophagic machinery during endo- and phagocytosis have been described. During LC3-associated phagocytosis (LAP), LC3 is recruited to single membrane phagosomes containing pathogens and targets them for killing by fusion with lysosomes [213, 214]. Quite recently, LC3-associated endocytosis (LANDO) has been described to facilitate clearance of β-amyloid aggregates, which are a hallmark of neurodegenerative diseases, by endocytosis of LC3-positive endosomes and subsequent lysosomal degradation [215]. These two examples show that LC3/GABARAP proteins are potentially able to be targeted to single membranes and subsequently facilitate fusion with lysosomal compartments to target e.g. pathogens for degradation. Intriguingly, GABARAP lipidation was found to be not necessary for its coexistence with PI4KIIα on cytoplasmic vesicles, providing direct experimental evidence for recruitment of GABARAP to single lipid bilayer membranes independent of lipidation [216]. However, in contrast to the hierarchical recruitment of proteins of the GABARAP subfamily, which is well studied in the case of autophagy-related processes, the mechanism(s) and importance of their association with single lipid bilayer membranes are incompletely understood.

2.3 Methodological obstacles during identification of non-redundant GABARAP subfamily protein functions

As described in chapter 2.1, GABARAP subfamily proteins exhibit high sequence and structural homology. They also bind to protein interaction partners through the same or similar interaction motifs (LIR/GIM) and were thus suggested to exhibit a high degree of functional redundancy. From the perspective of cellular homeostasis, a certain level of redundancy, especially during essential processes such as autophagy, is indeed favorable and thus very likely. However, studies which performed unbiased approaches and identified binding of only one or two subfamily members to a protein of interest (e.g. [145]), strongly suggest the existence of non-redundant functions of individual paralogs in parallel. However, at the start of this PhD project, there were several methodological constraints which had to be overcome in order to allow dissection of the non-redundant functions of GABARAP subfamily proteins at all.

These included the issue of antibody specificity which is a prerequisite for reliable discrimination between GABARAP, GABARAPL1 and GABARAPL2, e.g. during immunoblotting (IB) and immunofluorescence (IF) imaging experiments. It was described that use of polyclonal antibodies raised against either GABARAP or GABARAPL1 could not distinguish between the two, implying that any polyclonal antibody targeting one subfamily member likely cross-reacts with other paralogs [57, 137, 217-219].

One possible solution to deal with this situation is the use of transient or stable overexpression of fluorescent-protein (FP)-tagged individual GABARAP subfamily proteins [51]. Unfortunately, a variety of detrimental side effects exist which might strongly affect any results obtained. The use of different transfection reagents was reported to be associated with a change in cellular gene expression which was mainly caused by introduction of exogenous DNA, such as empty vector controls alone, thereby potentially masking the effect of the protein of interest [220-222]. To further complicate matters, alterations in protein abundance as a result of plasmid transfection are cell type specific [223]. Induction of autophagy by transfection procedures [224] represents another important confounding factor, because it likely interferes with analysis of any of the functions of GABARAP subfamily proteins. Other potential side effects of transient or stable gene overexpression include cytotoxicity [225, 226], activation of immune response and cytokine production [227, 228], modulation of growth rates depending on the used reporter or plasmid backbones [229], protein aggregation [230], mutagenicity [231], epigenetic instability [232], random integration of plasmid DNA in the genome [233, 234] and alteration of cellular signaling caused by non-physiological amounts of the protein of interest [235].

Another possibility is the use of RNA interference to knock down undesired members of the GABARAP subfamily and thus only analyze the remaining paralog(s) [217]. However, transiently introducing exogenous RNA sequences interferes with the endogenous cellular RNA machinery which was reported to result in its saturation and cause undesired side effects [236, 237]. Additionally, delivery by transfection was reported to alter lipid metabolism of primary and hepatocyte-derived liver cells [238, 239] which likely interferes with analysis of vesicular trafficking and/or autophagy.

In summary, the potentially high number of possible confounding factors complicates interpretation of such experiments and illustrates the need for techniques requiring as little manipulation as possible within a given experiment. As described (2.2.4), the involvement of GABARAP subfamily proteins in interdependent processes such as autophagy and (vesicular) protein trafficking further complicates analysis of non-redundant functions in specific processes.

2.3.1 CRISPR/Cas9-mediated genome editing

In order to address unique non-redundant functions, tools are needed to establish analyses without interference of other GABARAP subfamily members. One way to achieve this is the use of genome engineering to generate KO cells lacking a protein of interest or KI cells which, e.g., express the coding sequence of a fluorescent protein under control of endogenous regulatory elements of the gene of interest.

The clustered regularly interspaced short palindromic repeats/CRISPR-associated endonuclease Cas9 (CRISPR/Cas9) system, which was originally discovered as a type of adaptive immunity in bacteria, provides that [240-243]. Here, foreign DNA, e.g. from invading bacteriophages, is cleaved by bacterial endonucleases at distinct recognition sites and fragments of approximately 25 to 50 nucleotides (nt) length are inserted into the bacterial genome at distinct (proto)spacer sequences [244, 245]. Upon reinfection, these sequences are transcribed into small CRISPRRNAs (crRNAs) which are assembled with the endonuclease Cas9 via a *trans*-activating crRNA and directed to the DNA sequence of the invading bacteriophage where the target DNA is cleaved by Cas9 endonuclease activity [245-248].

This mechanism was adapted to mammalian cells and enables to direct a conjugate of Cas9 and a single guide RNA (sgRNA) consisting of a 20 nt target sequence to a specific genomic locus by binding of complementary nucleotides to perform genome editing [249-251]. Targeting additionally requires a protospacer adjacent motif (PAM) which precedes the targeting sequence on the target genome side and determines Cas9 cleavage activity [252].

Upon targeting of Cas9 to a specific genomic locus via the guide sequence, endonuclease activity of Cas9 results in cleavage of genomic DNA and subsequently in DNA double-strand breaks (DSBs). Because compromised DNA integrity represents a major threat to any cell [253-256], repair mechanisms have evolved. Among these, fast and efficient non-homologous end-joining (NHEJ) is mainly employed to ligate ends of DNA double-strands whereupon the DSB is closed [257-259]. Alternatively, sequences as present in single-stranded overhangs on breakage ends, serve as matrices for a ligase complex closing the gap with nucleotides [260]. Rather rarely in case of compatible overhangs and more often in case of incompatible overhangs, NHEJ results in imprecise repair and small insertions or deletions (indels) of nucleotides [261]. Such indel mutations can cause frameshifts and result in premature stop codons or aberrant amino acid sequences and thus loss of functional protein [250]. The endonuclease Cas9 is constitutively targeted to intact recognition sequences by its associated sgRNA. DNA cleavage is therefore also constitutive as long as the target sequence remains intact. Thus, imprecisely repaired genomic DNA accumulates and targeting of Cas9 consequently only stops when the target sequence is altered due to erroneous repair. Because of the high efficiency of Cas9 to introduce DSBs into the genome, care must be taken to prevent off-target effects resulting in undesired genomic mutations [262]. Besides usage of advanced systems, e.g. endonucleases from different sources requiring alternative PAMs [263] or double nickase systems [264], this can be achieved by sgRNA selection via advanced computational off-target prediction models [265].

The second main mechanism for repair of double-strand breaks is the homology-directed repair (HDR) pathway which is relatively slow and occurs less frequently compared to NHEJ [259, 266]. With regards to CRISPR/Cas9-mediated genome editing, the DSB can be repaired using a co-transfected engineered DNA template containing homology arms adjacent to the DSB site which can be used by the cellular repair machinery as a template for repair via homologous recombination [250, 267, 268]. Because HDR is rather error-free, it can be used to knock in specific sequences at desired genomic loci [269]. The KI of DNA sequences enables small introductions of a few nucleotides of length, or introduction of larger constructs, e.g. of fluorescent tags such as green fluorescent protein (GFP), which enable live-cell imaging of the protein of interest at physiological levels under control of the endogenous regulatory elements of the targeted gene [270-272]. Figure 7 shows a schematic representation of the application of CRISPR/Cas9-mediated genome editing.

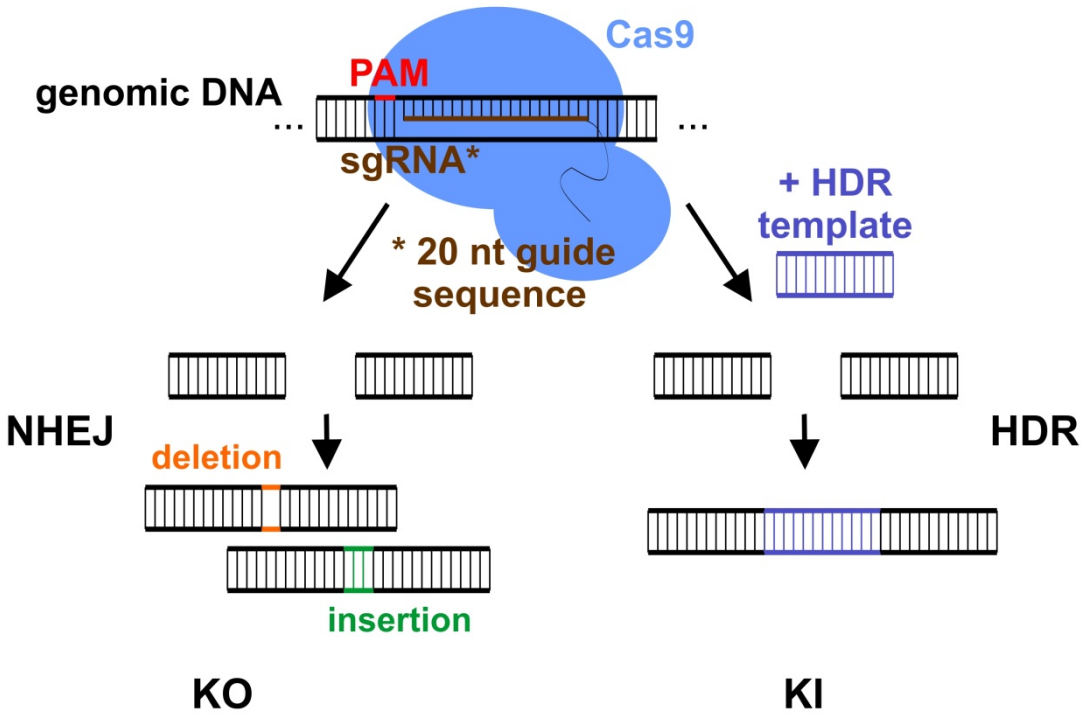

Figure 7: CRISPR/Cas9-mediated genome editing. A sgRNA sequence of 20 nt of length targets the associated endonuclease Cas9 to a specific genomic locus preceded by a distinct PAM. Here, Cas9 endonuclease activity results in DNA DSBs which are either repaired by NHEJ or HDR. In the former case, DSBs occur as long as the sequence is repaired correctly, resulting in stochastic accumulation of small indel mutations which, in some cases, result in premature stop codons in the coding region of the targeted gene and subsequent loss of functional protein. In case of HDR, simultaneous introduction of an artificial repair template containing homologous regions neighboring the cleavage site and a sequence, e.g. coding for a fluorescent protein, can result in repair by homologous recombination and insertion of the desired sequence.

3. Aims

Although research is mostly focused on the whole subfamily rather than individual proteins, the involvement of the GABARAP subfamily during autophagy is relatively well-investigated. In contrast, their impact on (surface) protein trafficking is largely neglected. Identification of non-redundant functions in either context is further complicated by the high degree of structural similarity between GABARAP subfamily members, their supposed high degree of functional redundancy and their involvement in the general process of autophagy. Given the role of individual GABARAP subfamily proteins during intracellular trafficking and anterograde transport of cell surface receptors described in the literature, the question arises whether the GABARAP subfamily fulfills a more general role during these processes. The aim of this work was therefore to investigate the role of the GABARAP subfamily in surface protein biology and dissection of unique functions of individual family members.

After establishing genome-edited cell lines lacking one, two or all three GABARAP subfamily proteins, this question should be addressed by employing a general unbiased approach. Quantitative surfaceome analysis represents such a method and should first be applied to cells deficient for the whole GABARAP subfamily. The surfaceome consists of all PM-located proteins at a given time point and thus under steady-state conditions represents the basal surface proteome. By comparative analysis of cells lacking the GABARAP subfamily and WT cells, proteins with altered surface abundance under basal conditions should be identified. Upon their identification, analysis should be conducted to identify potential subgroups within these proteins, based on e.g. functionality, membrane protein type, secretion pathway and involvement in disease.

While the surfaceome approach is suitable to identify proteins whose basal cell surface localization might be dependent on one, two or all three members of the GABARAP subfamily, it inherently cannot provide detailed information on the mechanistic role of GABARAP subfamily proteins on individual trafficking processes. Hence, a model system of surface receptor trafficking allowing for the investigation of single intracellular trafficking steps such as internalization, recycling and degradation should be identified and employed to investigate the role of individual GABARAP subfamily proteins within distinct phases of cell surface protein trafficking. Such model system should essentially be well-studied, meaning that reliable established tools such as antibodies and qPCR primers should be available. It should be possible to activate it in a specific and controllable manner, provide a clear readout and its subcellular localization should be traceable during live-cell microscopy. Further desirable characteristics of such a model system include a potential direct interaction of the respective protein candidate with GABARAP subfamily proteins, e. g. through an

interaction motif, ubiquitous expression levels in several cell types to ensure generalizability and ideally a basis of evidence already linking GABARAP subfamily proteins to its fate.

Once the ideal surface protein candidate had been identified, molecular biological and biochemical methods should be used to investigate the impact of individual GABARAP subfamily proteins on its intracellular trafficking under conditions not inducing autophagy. The greater aim of such analysis is to identify unique and non-redundant functions of GABARAP subfamily proteins and thus substantially enhance our knowledge of their autophagy-independent functions.

4. Results

4.1 The highly GABARAP specific rat monoclonal antibody 8H5 visualizes GABARAP in immunofluorescence imaging at endogenous levels

Title: The highly GABARAP specific rat monoclonal antibody 8H5 visualizes GABARAP in immunofluorescence imaging at endogenous levels.

Authors: Simons I.M., Mohrlüder J., Feederle R., Kremmer E., Zobel T., **Dobner J.**, Bleffert N., Hoffmann S., Willbold D.

Year of publication: 2019

Published in: Scientific Reports

5-year Impact Factor: 4.525 (2018)

Digital object identifier (DOI): 10.1038/s41598-018-36717-1

Contribution: Generation of the human embryonic kidney (HEK) 293 (HEK293) KO cell lines, validation of commercially available antibodies via immunoblotting in haploid 1 (HAP1) and HEK293 KO cell lines, editing of the manuscript

Reprint permission: This section contains a complete reprint of the publication published in Scientific Reports (www.nature.com/scientificreports/)

www.nature.com/scientificreports

SCIENTIFIC REPORTS
nature research

OPEN

Author Correction: The highly GABARAP specific rat monoclonal antibody 8H5 visualizes GABARAP in immunofluorescence imaging at endogenous levels

Published online: 11 December 2019

Indra M. Simons, Jeannine Mohrlüder, Regina Feederle, Elisabeth Kremmer, Thomas Zobel, Jochen Dobner, Nicole Bleffert, Silke Hoffmann & Dieter Willbold

Correction to: *Scientific Report* https://doi.org/10.1038/s41598-018-36717-1, published online 24 January 2019

This Article contains typographical errors in the Acknowledgements section.

"This study was funded by the Deutsche Forschungsgemeinschaft (DFG, German Research Foundation) – Projektnummer 190586431 – SFB 974, project B02 (D.W., I.M.S.), and project WE5343/1–1 (T.Z.), and by a grant from the Jürgen Manchot Foundation, Molecules of Infection Graduate School (MOI III) (D.W. and J.D.)."

should read:

"This study was funded by the Deutsche Forschungsgemeinschaft (DFG, German Research Foundation) – Projektnummer 267205415 – SFB 1208, project B02 (D.W., I.M.S.), and project WE5343/1–1 (T.Z.), and by a grant from the Jürgen Manchot Foundation, Molecules of Infection Graduate School (MOI III) (D.W. and J.D.)."

SCIENTIFIC REPORTS

Corrected: Author Correction

OPEN

The highly GABARAP specific rat monoclonal antibody 8H5 visualizes GABARAP in immunofluorescence imaging at endogenous levels

Received: 8 March 2018
Accepted: 25 November 2018
Published online: 24 January 2019

Indra M. Simons[1], Jeannine Mohrlüder[2], Regina Feederle[3], Elisabeth Kremmer[4], Thomas Zobel[5], Jochen Dobner[1], Nicole Bleffert[1], Silke Hoffmann[2] & Dieter Willbold[1,2]

The determination of unique functions of GABARAP (gamma-aminobutyric acid type A receptor-associated protein), a member of the highly conserved protein family of mammalian autophagy-related 8 protein (mATG8), within diverse cellular processes remains challenging. Because available anti-GABARAP antibodies perform inadequate, especially within various microscopy-based applications, we aimed to develop an antibody that targets GABARAP but not its close orthologs. Following the latest recommendations for antibody validation including fluorescence protein tagging, genetic and orthogonal strategies, we characterized the resulting anti-GABARAP (8H5) antibody during confocal immunofluorescence imaging in-depth. We compared the antibody staining pattern with that obtained for fluorescence protein tagged GABARAP, GABARAPL1 or GABARAPL2 each ectopically expressed in GABARAP knockout cells. Furthermore, we imaged cells expressing all mATG8 family members at endogenous levels and checked GABARAP knockout cells for unspecific staining under fed or macroautophagy-inducing conditions. Finally, we simultaneously stained cells for endogenous GABARAP and the common autophagosomal marker LC3B. Summarized, the presented antibody shows high specificity for GABARAP without cross-reactivity to other mATG8 family members in immunofluorescence imaging making it a valuable tool for the identification of unique GABARAP functions.

Autophagy-related 8 (ATG8) proteins form a highly conserved eukaryotic protein family, which generate small-sized products of approximately 15 kDa with high overall structural similarities[1]. Contrary to the situation in yeast which has one single *Atg8* gene, mammalian genomes code for several ATG8 paralogs. The respective proteins are divided in two subfamilies: the microtubule-associated protein 1 light chain 3 (MAP1LC3) subfamily (referred to as LC3s) including LC3A, LC3B, LC3B2, LC3C, and the GABARAP (γ-amino-butyric acid receptor-associated protein) subfamily (referred to as GABARAPs) with GABARAP, GABARAPL1/GEC1 (GABARAP-like 1/Glandular epithelial cell protein) and GABARAPL2/GATE-16 (GABARAP-like 2/Golgi-associated ATPase enhancer of 16 kDa) in humans. Mammalian (m)ATG8s show ubiquitous expression patterns, although for some family members increased expression levels are documented in certain tissues and their expression underlies regulation through various mechanisms[2].

The broad action spectrum of these adaptor-like proteins with partially overlapping features is far from being completely understood[3]. First described to participate in the trafficking of type-A receptors for the neurotransmitter gamma-aminobutyric acid (GABA) in neurons[4], GABARAP, the prototype of the GABARAP subfamily, is implicated in a variety of intracellular transport processes including the shipping and correct organization of further receptors[5–7] as well as in autophagy, an evolutionarily highly conserved process essential for cellular

[1]Institut für Physikalische Biologie, Heinrich-Heine-Universität, 40225, Düsseldorf, Germany. [2]Institute of Complex Systems, Structural Biochemistry (ICS-6), Forschungszentrum Jülich, 52425, Jülich, Germany. [3]Institute for Diabetes and Obesity, Monoclonal Antibody Core Facility, 85764, Neuherberg, Germany. [4]Institute for Molecular Immunology, Helmholtz Center Munich, German Research Center for Environmental Health, 85764, Neuherberg, Germany. [5]Department of Biology, Center for Advanced Imaging (CAi), Heinrich-Heine-Universität, 40225, Düsseldorf, Germany. Correspondence and requests for materials should be addressed to S.H. (email: si.hoffmann@fz-juelich.de) or D.W. (email: dieter.willbold@uni-duesseldorf.de)

homeostasis[8]. Like all ATG8s, GABARAP can undergo lipidation by an ubiquitin-like conjugation system[9,10] promoting its association to autophagosomal membranes[11,12] but likely also to (tubule)vesicular structures in GABARAP-mediated protein trafficking[13]. Meanwhile, functional divergences between the divers ATG8s became obvious, like their action at different stages of autophagosome biogenesis as well as during autophagosomal cargo recruitment, where specific interactions with divers scaffolding proteins or autophagic receptors are formed in selective autophagy[3,14]. Within the mATG8s, LC3B is considered as an established and widely accepted marker for autophagosomes[15]. In this context, recent studies point towards a crucial role of the GABARAP subfamily members especially in autophagosome and lysosome fusion[16]. Under nutrient rich conditions, GABARAP was shown to accumulate in the pericentriolar material from which it can be translocated to forming autophagosomes during starvation[17,18].

Despite this apparent progress, elucidation of unique roles for individual ATG8 members within a specific process remains to be a challenging task. Although fluorescent protein (FP)-tagged ATG8 reporters, which are widely used to study autophagy as well as ATG8s' functions, delivered multiple new insights, their application might be accompanied by artifacts resulting from overexpression or steric hindrance due to the bulky FP-tag. In parallel, available antibodies against diverse ATG8 family members often show cross-reactivity, and are frequently not sufficiently validated in a transparent manner for the user, especially regarding their performance within diverse applications. As long as such information is lacking, every ATG8-targeted antibody result has to be interpreted with caution unless specificity of the antibody in use has clearly been demonstrated for the application and the ATG8 member chosen[15].

In this study, we performed an in-depth characterization of an in-house generated rat monoclonal antibody (mAb) against human (h)GABARAP (anti-GABARAP (8H5) antibody) by taking the latest recommendations for antibody validation into account[19]. Thereby, we focused on immunofluorescence (IF) staining, and included genetic (knockout (KO) cell-based), orthogonal (autophagosome counting under growth factor depleted conditions), tagged-target protein expression and independent antibody-based (commercial anti-GABARAP and anti-LC3B) strategies as validation pillars. Our analysis revealed that the anti-GABARAP (8H5) antibody shows high specificity for GABARAP without cross-reactivity for GABARAPL1, -L2 or LC3 subfamily members in our set-up. With the help of this antibody we investigated the colocalization of GABARAP and LC3B under endogenous conditions. To our knowledge, anti-GABARAP (8H5) antibody outperforms so far available antibody resources during localization studies in fixed cells, and thus reasonably enlarges our current tool box that is needed to identify unique GABARAP activities with high quality and consistency in an unambiguous manner.

Results

Anti-GABARAP (8H5) antibody discriminates between purified recombinant GABARAP, -L1, and -L2. In order to generate a monoclonal GABARAP antibody that is able to discriminate GABARAP from its various related ATG8 family members, rats were immunized with full-length hGABARAP fused to GST (glutathione S-transferase) (GST-GABARAP). After fusion of their immune spleen cells with the myeloma cell line P3X63-Ag8.653, the resulting hybridoma supernatants were collected and confirmed to react with immobilized GST-GABARAP by ELISA (enzyme-linked immunosorbent assay) (data not shown). Next, selectivity of in total 38 reacting supernatants was assessed using the dot blot technique. To this end, recombinant purified GABARAP, -L1, -L2 as well as the LC3s A, B, and C were spotted as target. Approximately 80% of the tested GABARAP-reactive supernatants failed this quality check, because, besides GABARAP, they also bound to its closest relative, GABARAPL1, as exemplarily shown for the supernatant corresponding to clonal line 8E5 (Fig. 1A, top panel). A few, among them anti-GABARAP (8H5) and anti-GABARAP (15A11) mAb containing supernatants, showed selective binding to GABARAP demonstrating their high specificity in this application (Fig. 1A, mid and bottom panels). Finally, binding specificity of anti-GABARAP (8H5) and (15A11) antibodies was confirmed by ELISA (Fig. 1B) and western blot analysis (Fig. 1C), respectively. Again, immunoreactivity could exclusively be detected for GABARAP but not the other family members in both applications. Besides its good selectivity, particularly anti-GABARAP (8H5) antibody revealed a very good signal-to-noise ratio of the GABARAP-related ELISA signal, assuming a considerably high affinity of anti-GABARAP (8H5) antibody to its given antigen, a promising feature for immunostaining applications with fixed cells.

Anti-GABARAP (8H5) antibody recognizes the GABARAP amino-terminal region. To identify the binding epitope of anti-GABARAP (8H5) antibody which was raised against full-length GABARAP, an array-based oligo-peptide scanning was performed. In total 54 dodecapeptides (12mers) with a peptide-peptide overlap of 10 amino acids, which represent the complete sequence of hGABARAP, were spotted on a cellulose membrane. Anti-GABARAP (8H5) antibody showed a strong signal with the fourth 12mer and weak signals with the adjacent 12mers three and five, suggesting that the epitope recognized by anti-GABARAP (8H5) antibody is formed by the GABARAP residues ranging from position 7 to 18 (Fig. 2A). The alignment of GABARAP, -L1, and -L2 shows that the epitope forming region is highly similar between GABARAP and GABARAPL1, with 10 out of 12 positions being conserved (GABARAPL2: 7/12). In contrast, this region is much more variable when GABARAP is compared with the LC3s (Fig. 2B). Structurally, the identified epitope overlaps with the second half of helix α1 and first half of helix α2 (Fig. 2C), which N-terminally extend the ubiquitin-like fold that is highly conserved between all hATG8s. With K13 and S16 both non-conserved epitope residues between GABARAP and GABARAPL1 (and also -L2) expose their sidechains for antibody binding (Fig. 2D), suggesting that K13 and S16 define binding specificity of anti-GABARAP (8H5) antibody.

Anti-GABARAP (8H5) antibody specifically stains YFP-GABARAP but not YFP-GABARAPL1 and CFP-GABARAPL2 in HAP1 GABARAP-KO cells by IF staining. In order to study if anti-GABARAP (8H5) antibody successfully stains GABARAP in IF application in fixed cells, YFP (yellow fluorescent

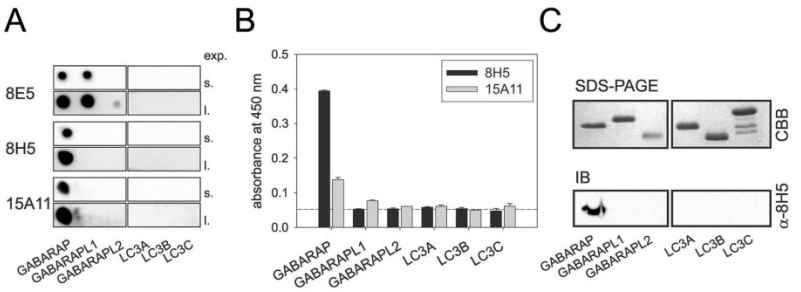

Figure 1. Anti-GABARAP (8H5) antibody does not react with LC3s and discriminates between GABARAP, GABARAPL1 and GABARAPL2. (**A**) Dot blots analysis using three different hybridoma supernatants to detect GABARAP binding and putative cross-reactivity to the other ATG8 family members. Purified recombinant proteins (10 µM each) were transferred to a cellulose nitrate membrane. Short (s.) and long (l.) exposure times of one representative blot each (n = 2) are given. (**B**) ELISA using anti-GABARAP (8H5) and anti-GABARAP (15A11) antibodies to confirm binding specificity and to assess the signal-to-noise ratio as a measure for mAb binding strength. Purified recombinant proteins (700 ng each) were coated on a 96-well plate and were incubated for 1 h at room temperature (RT) before antibody detection. Primary antibody containing hybridoma supernatants anti-GABARAP (8E5) and anti-GABARAP (15A11) and secondary goat anti-rat IgG-HRP antibody were incubated for 1 h at RT, respectively (n = 2). (**C**) Purified recombinant proteins (1 µg each) were subjected to SDS-PAGE in duplicate and were stained with Coomassie brilliant blue (CBB) to visualize the input or were used for immunoblotting with anti-GABARAP (8H5) mAb followed by HRP-coupled mouse anti-rat IgG2a antibody detection. Uncropped versions of (**A**) and (**C**) are given in Supplementary Fig. S3A,B.

protein)-GABARAP or YFP alone were transiently overexpressed in HAP1 GABARAP knockout (KO) cells. To do so, cells were incubated in growth factor-depleted medium in the presence of Bafilomycin A1 (BafA1). This macrolide antibiotic drug inhibits the vacuolar type H^+-ATPase (adenosine triphosphatase) and thereby blocks the autophagic flux by preventing the fusion between autophagosomes and lysosomes[20,21]. Under these conditions, the lipidated form of YFP-GABARAP is well known to be associated to the inner and outer lipid bilayer of mature autophagosomes, which under BafA1 treatment accumulates within the cytoplasm, and can be visualized easily as bright puncta in confocal imaging applications[2,12]. As expected, in the channel used for YFP detection, punctate YFP-GABARAP accumulations and a faint cytoplasmic stain were observed within the transfected HAP1 GABARAP KO cells (Fig. 3A, top, red). Likewise, immunostaining of these cells with anti-GABARAP (8H5) antibody and a secondary antibody conjugated with Cy5 produced many puncta (green) that showed a near to perfect colocalization with the YFP-GABARAP signals obtained (merge). In contrast, transfection with the YFP control vector produced fluorescence signals in the nuclear and cytoplasmic region solely in the channel for YFP detection (Fig. 3A, bottom, red), confirming that anti-GABARAP (8H5) antibody was reacting with the GABARAP part of the YFP-GABARAP fusion protein.

To further analyze the specificity of anti-GABARAP (8H5) antibody, plasmids encoding YFP-GABARAPL1 and CFP (cyan fluorescent protein)-GABARAPL2 were transfected in HAP1 GABARAP KO cells, respectively. Transfected cells showed fluorescence exclusively in the channels for YFP or CFP detection, but not after staining with anti-GABARAP (8H5) antibody (Fig. 3B), indicating that the antibody does not cross-react with its closest relatives, GABARAPL1 and GABARAPL2, even under overexpressing conditions.

Anti-GABARAP (8H5) antibody detects endogenous GABARAP, but not its close relatives -L1 and -L2 in IF. To further investigate if anti-GABARAP (8H5) antibody specifically stains endogenous GABARAP, HAP1 parental control cells expressing all ATG8s at endogenous levels, and HAP1 GABARAP KO cells, lacking GABARAP but expressing GABARAPL1 and -L2 were stained. Before fixation and immunostaining with anti-GABARAP (8H5) antibody, HAP1 cells were cultured in complete growth medium (IMDM + 10% FCS) without BafA1 or under growth factor deprivation (IMDM w/o FCS) with BafA1 to accumulate autophagosomes in the cells. As expected, we obtained a prominent cytoplasmic stain accompanied with some punctate structures when staining parental HAP1 cells with anti-GABARAP (8H5) antibody under basal autophagic conditions (Fig. 4A, top. left). After growth factor depletion and BafA1 treatment, anti-GABARAP (8H5) antibody staining revealed an accumulation of many bright GABARAP-positive puncta (Fig. 4A, top, right). Only a weak background stain was obtained with anti-GABARAP (8H5) antibody when cells lacking GABARAP but expressing all the other ATG8s at endogenous levels were used (immunoblot (IB) results of GABARAPL1, -L2 in HAP1 KO cells: please refer to Supplementary Fig. S1). A quantitative analysis of in total 513 parental cells and 460 GABARAP KO cells from 5 separate stains imaged under growth factor depletion and BafA1 treatment is given in Fig. 4B, confirming the selectivity of anti-GABARAP (8H5) antibody for GABARAP at high significance ($p < 0.0001$).

In parallel, we also tested three commercially available anti-GABARAP antibodies. Each of them selectively detects GABARAP in immunoblotting upon SDS-PAGE (see Supplementary Fig. S1B). Interestingly,

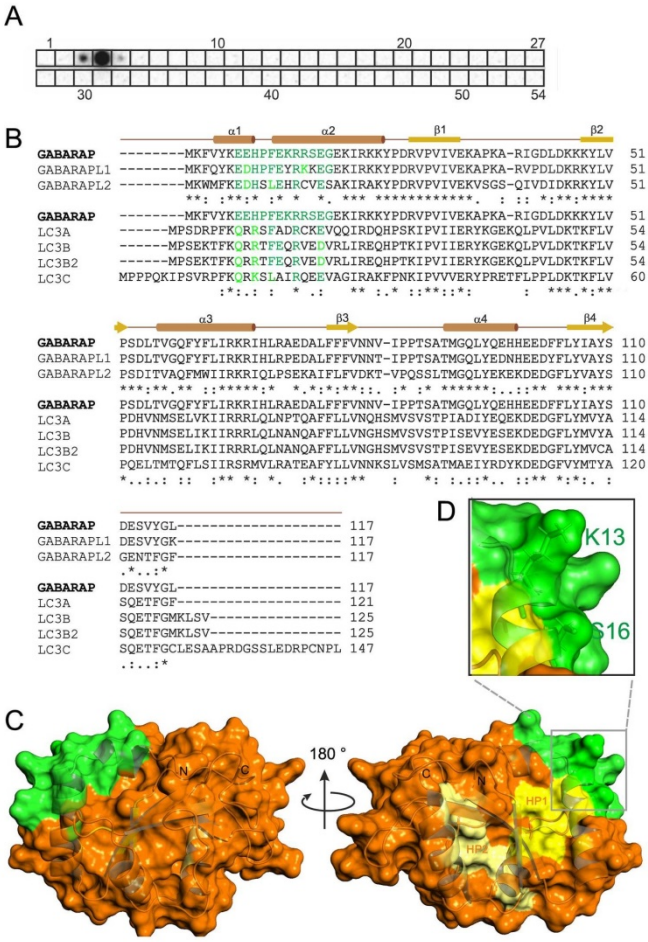

Figure 2. Anti-GABARAP (8H5) antibody binds an amino-terminally located epitope within GABARAP. (**A**) Peptide scanning was performed using a cellulose membrane loaded with 12mer peptides representing the complete sequence of human GABARAP and overlapping by 10 amino acids, respectively. Bound anti-GABARAP (8H5) antibody was detected using HRP-coupled mouse anti-rat IgG2a secondary antibody. Shown is one representative result. For reason of clarity peptide spot positions are boxed. Figure S3C includes source blots and membranes. (**B**) Sequence alignment of the GABARAPs (top) and of GABARAP with the LC3 family members (bottom) using Clustal Ω[42]. Regular secondary structure elements are depicted above the GABARAP sequence. The identified anti-GABARAP (8H5) antibody epitope is colored green within the GABARAP sequence. Identical residues in the sequences of the homologs listed are depicted in green, while highly similar residues are highlighted in light green. (**C**) Illustration of the anti-GABARAP (8H5) antibody epitope on the GABARAP structure (PDB ID: 1KOT) shown as combined ribbon and surface diagram using PyMOL (v1.860). Residues forming the epitope are shown in green, those forming the hydrophobic pockets HP1 and HP2 are colored dark and light yellow, respectively. In (**D**) the side chains of K13 and S16 are highlighted to illustrate their surface exposure and availability for anti-GABARAP (8H5) antibody binding.

the same antibodies showed pronounced unspecific staining in GABARAP KO cells during IF in our hands (see Supplementary Fig. S2), justifying the need for an in-depth application-based antibody characterization, and impressively illustrating that specificity features of antibodies should not be transferred between

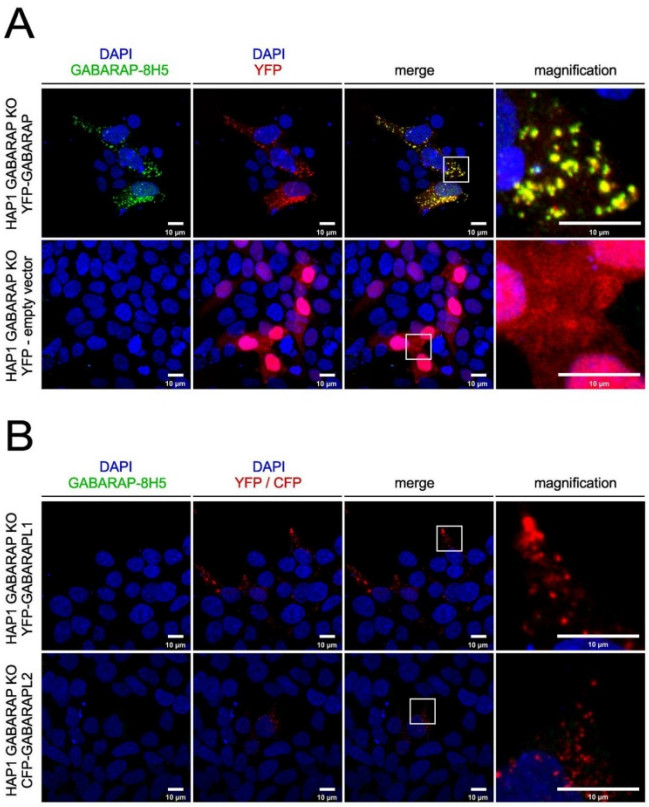

Figure 3. Anti-GABARAP (8H5) antibody detects YFP-GABARAP, but not YFP-GABARAPL1 and CFP-GABARAPL2 in immunofluorescence. HAP1 GABARAP KO cells were transfected with YFP-GABARAP and YFP-empty vector (**A**) or YFP-GABARAPL1 and CFP-GABARAPL2, respectively (**B**). After 48 h cells were incubated for 3 h with 100 nM Bafilomycin A1 (BafA1) in growth factor depleted medium (w/o FCS). Fixed cells (4% PFA) were immunolabeled with anti-GABARAP (8H5) antibody. Colocalization of GABARAP (green) and YFP (red) is indicated by yellow puncta. Nuclei were counterstained with DAPI.

different applications without separate experimental proof. In addition, we examined the performance of the anti-GABARAP (8H5) antibody in tissue sections in a preliminary manner. Therefore, two brain regions (motor-cortex, hippocampus) derived from mice with a GABARAP$^{+/+}$ background were applied to IF. In contrast to the negative control clear intracellular staining of different intensities could be obtained only in presence of anti-GABARAP (8H5) antibody (Supplementary Fig. S4). Thus, this anti-GABARAP antibody might also be applicable for IF-labelling of tissue sections.

Anti-GABARAP (8H5) antibody distinguishes LC3B^{+}/GABARAP^{+} from LC3B^{+}/GABARAP^{-} vesicular structures in two-color IF. Finally, we tested anti-GABARAP (8H5) antibody performance in two-color IF applications and chose LC3B as the second hATG8 to be targeted (to our knowledge, GABARAPL1 and -L2 trustworthy antibody-based analysis tools for IF are yet still lacking). We used anti-LC3B mAb clone 5F10 (anti-LC3B (5F10)), because this antibody reliably detects LC3B only and not the other LC3 family members[22]. LC3B is a common marker for autophagosomal structures[23], and consequently, anti-LC3B (5F10) antibody (Fig. 5A in red) stained a multitude of autophagosomes coated with endogenous LC3B under growth factor depletion and BafA1 treatment, regardless whether HAP1 parental or HAP1 GABARAP KO cells were imaged. Overall, anti-GABARAP (8H5) antibody (green) stained a smaller number of punctate structures compared to anti-LC3B (5F10) antibody in the parental cell line. Clearly, magnification and intensity plot (Fig. 5B) revealed that several of the imaged bright puncta are positive for LC3B but are negative for GABARAP under the conditions used. A comparable staining pattern, but with less GABARAP positive puncta after starvation, could also be observed in

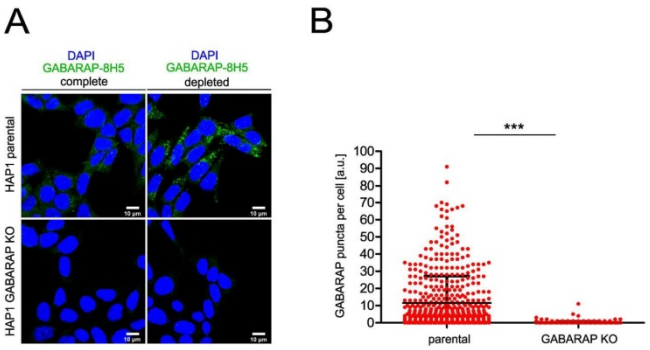

Figure 4. Anti-GABARAP (8H5) antibody specifically detects endogenous GABARAP in immunofluorescence. (**A**) HAP1 parental and GABARAP KO cells were incubated for 4 h in complete growth medium (IMDM + 10% FCS) and growth factor depleted medium (IMDM w/o FCS) with 100 nM Bafilomycin A1 (BafA1), respectively. Fixed cells were immunolabeled with anti-GABARAP (8H5) antibody. Nuclei were counterstained with DAPI. (**B**) Counted GABARAP puncta per cell in HAP1 cells. HAP1 cells grown under growth factor deprivation and BafA1 incubation (**A**) were analyzed. GABARAP puncta per cell from five individual experiments were measured in parental (n = 513) and GABARAP KO (n = 460) cells by Fiji analysis tool in combination with an in-house developed macro for puncta analysis. Error bars represent mean ± SD. Significance was determined using unpaired one-tailed t-test with Welch's correction (***$p < 0.0001$).

human embryonic kidney 293 (HEK293) cells (Supplementary Fig. S5). This is consistent with the common view that LC3s and GABARAPs have concerted but also can exhibit distinct, non-overlapping intracellular localizations, which is accompanied with at least partial functional divergences[2,16,22,24,25].

Discussion

Antibodies rank amongst the most widespread tools in basic life science research. Concurrently, an extensive discourse regarding antibody performance is ongoing with the task to guard against misleading conclusions drawn from experiments that included insufficiently validated antibodies[19,26]. A validated antibody must show specificity, selectivity, and reproducibility in the context of its application. But antibody validation beyond the datasheet knowledge can be tedious, is frequently underestimated, and thus is widely ignored in project scheduling. By comparing antibody-based IF stains with their respective fluorescence protein (FP)-tagged antigen location, a recent report impressively demonstrates the high error rates of inadequately validated polyclonal antibodies during IF applications under high throughput conditions[27].

Autophagy as well as the characterization of mATG8 function, one of the key players in this process, is subject of intensive studies. Because autophagy is proven to take part in several human e.g. neurodegenerative diseases[28,29], deciphering the common and the unique features of individual ATG8 family members would contribute to our understanding of their underlying molecular mechanisms. Antibodies specific for each single mATG8 would improve the toolbox needed to elucidate the unique ATG8s' functions. GABARAP, -L1, and -L2 are closely related, short-sized proteins with 117 aa (or 116 aa post processing through ATG4) in length. They, *per se*, display a limited number of epitopes, and cross-reactivity with antibodies that originally had been raised against one of their relatives, have frequently been observed in the past[15]. However, some of the available anti-GABARAP, -L1, and -L2 antibodies exhibit a specific performance with denatured proteins, e.g. in western blotting (Supplementary Fig. S1). To our knowledge, no single antibody with proven specificity during IF has been described in the literature yet. The reason for this may be that the number of exposed linear epitopes, and thus the chance of targeting a unique epitope (as basis for antibody specificity), is generally higher under denaturating than under native or semi-native conditions. Conversely, discontinuous epitopes are destroyed by denaturation, but are exposed under native or semi-native conditions, e.g. as prevailing during dot blot, ELISA or after mild cross-linking used in bio-imaging.

In this study, we positively-screened almost 40 cell clones, which generate monoclonal antibodies against hGABARAP. Out of them, we established and characterized clone 8H5 in particular with the aim to validate its performance especially during IF. In sum, hybridoma supernatants containing anti-GABARAP (8H5) antibody showed high specificity for GABARAP without cross-reactivity for the other (recombinant and purified) ATG8 homologues GABARAPL1, -L2 or LC3A, -B, and -C both in dot blot (Fig. 1A) and in western blotting (Fig. 1C). In addition to its good selectivity anti-GABARAP (8H5) antibody was our best performer during ELISA regarding binding strengths (Fig. 1B). Notably, anti-GABARAP (8H5) antibody failed to detect endogenous, SDS-PAGE-separated GABARAP from mammalian cell lysates during subsequent IB in our hands. Possible reasons are the low abundance of GABARAP in cell lysates compared to the applied amount of purified recombinant protein samples in Fig. 1C and/or the denaturation of the epitope recognized by 8H5 during western blotting[30,31]. Interestingly, epitope mapping of anti-GABARAP (8H5) antibody revealed that it interacts with the

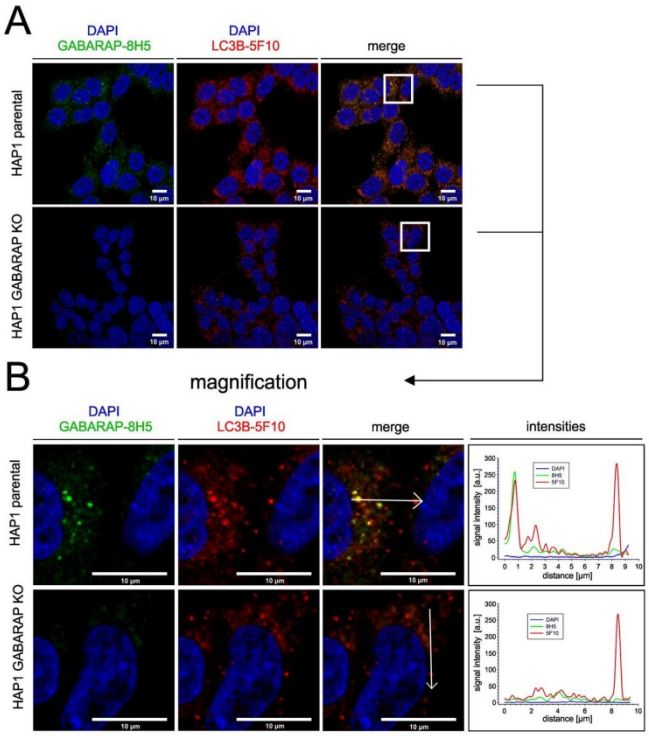

Figure 5. Anti-GABARAP (8H5) antibody detects endogenous GABARAP within some but not all LC3B$^+$ structures. (**A**) HAP1 parental and GABARAP KO cells were incubated for 3 h with 100 nM BafA1 in growth factor depleted medium. HAP1 cells were fixed with 4% PFA and immunolabeled with anti-GABARAP (8H5) and anti-LC3B (5F10) antibodies. Colocalization of LC3B (red) and GABARAP (green) is indicated by yellow puncta. Nuclei were counterstained with DAPI. (**B**) Intensity profiles of line segments (approx. 10 µm) drawn across the z-section shown for each channel. Overlap of anti-LC3B (5F10) (red) and anti-GABARAP (8H5) (green) antibodies' fluorescence intensity profiles (arbitrary units, a.u.) indicates colocalization of GABARAP with the autophagosomal marker LC3B.

α–helices 1 and 2 containing region (Fig. 2), suggesting that the existence of some α-helical secondary structure supports its efficient binding. According to the GABARAP structure a proper positioning of the non-conserved residues K13 and S16, which both are located within the binding epitope might be pivotal through acting as a GABARAP-unique platform for antibody binding. Because the complete GABARAP protein was applied as immunogen, it is likely, that under native conditions further parts of the GABARAP molecule contribute here by delivering the required scaffold for an optimal epitope presentation.

Following the latest recommendations for antibody validation[19], we next characterized the performance of anti-GABARAP (8H5) antibody during IF staining applications in-depth. We compared the anti-GABARAP (8H5) antibody-based staining with that of FP-tagged GABARAP, GABARAPL1, and GABARAPL2 ectopically expressed in HAP1 cells lacking endogenous GABARAP (Fig. 3A,B). Next, we compared the staining pattern of cells expressing all mATG8 family members at endogenous levels with that of cells lacking GABARAP, both under fed and growth-factor depleted/BafA1-treated conditions (Fig. 4). Furthermore, cells were simultaneously stained with anti-GABARAP (8H5) antibody and an antibody specifically recognizing LC3B, which is a common and independent marker for autophagosomes (Fig. 5).

Taken together, our results demonstrate that anti-GABARAP (8H5) antibody performs with high specificity in IF experiments. To our knowledge, we hereby provide the first staining results of endogenous GABARAP with an application- and target-specific in-depth validated antibody. In our opinion, this antibody can be very valuable for future studies that are aimed to resolve unique GABARAP functions in diverse cellular processes with already proven or assumed GABARAP-participation including autophagy, protein trafficking or unconventional secretion.

Recently, fluorescence protein-tagged, peptide-based sensors that can target mATG8s in a (semi)-specific manner have been published[32,33]. These sensors are based on peptides with LC3-interacting region (LIR) properties, showing selectivity, e.g. for GABARAP/GABARAPL1- or LC3B/LC3A-positive autophagosomes[32], or even for individual mATG8s[33]. Here, further engineering including the addition of domains for membrane recruitment or oligomerization, was necessary to achieve both selectivity and sufficient affinity of these sensors. While such sensors are very valuable for live-cell visualization of membrane-associated, lipidated mATG8 forms, and those ATG8 populations without tightly complexed intracellular LIR-containing binding partners, they likely fail to visualize both their soluble, unlipidated forms and their LIR-ligand complexed forms. We assume that anti-GABARAP (8H5) antibody can react with unlipidated GABARAP, and - because its epitope is largely separated from HP1 and HP2 - with such GABARAP molecules that are bound to an LIR-ligand. However, because its epitope includes with K13 one of the two ubiquitination sites (K13, K23) that recently have been identified for GABARAP[18], at least the K13-ubiquitinated GABARAP fraction will very likely not be stained by anti-GABARAP (8H5) antibody. Since its epitope overlaps with the microtubule-binding domain (amino acid residues 1–22) of GABARAP[34], further work is needed that has to clarify how anti-GABARAP (8H5) antibody performs with potentially microtubule-associated GABARAP molecules. Thus, anti-GABARAP (8H5) antibody not only discriminates GABARAP from its relatives but also opens avenues to distinguish between distinct cellular pools of GABARAP itself, a feature that can help to decipher distinct roles for the diverse variations of the same protein. Finally, because mammalian GABARAP sequences display 100% conservation, anti-GABARAP (8H5) antibody can be broadly used across mammalian species. Even within orthologous proteins from less related vertebrate, arthropode and nematode model organisms the anti-GABARAP (8H5) antibody epitope surrounding region is highly conserved (Supplementary Fig. S6). Thus, this antibody will likely be useful also in non-mammalian species. For improved results, the combination with anti-rat IgG2a subclass-specific secondary antibodies, especially for multiple labeling methods, is recommended.

Methods

Eukaryotic plasmids. Genes for GABARAP, GABARAPL1 and GABARAPL2 were subcloned from GST-fusion plasmids (Addgene IDs 73948, 73945 and 73518) by PCR amplification into the XhoI and BamHI sites of peYFP-C1 or peCFP-C1(Clontech), yielding peYFP-C1/GABARAP, peYFP-C1/GABARAPL1 and peCFP-C1/GABARAPL2.

Antibodies. The antibodies used throughout this study are listed in Supplementary Table S3.

Recombinant protein/antigen expression and purification. Cloning, expression and purification of human GABARAP (aa 1–117), GABARAPL1 (aa 1–117), GABARAPL2 (aa 1-117), MAP1-LC3A (aa 1–121), MAP1-LC3B (aa 1–125) and MAP1-LC3C (aa 1-147) was performed as previously described[35,36].

Antibody generation. Purified full length GABARAP protein N-terminally fused to glutathione-S-transferase (GST) was used as antigen for immunization. Approximately 50 µg of antigen dissolved in phosphate-buffered saline (PBS) was emulsified in an equal volume of incomplete Freund's adjuvant (Sigma-Aldrich, Germany) and 5 nmol CpG2006 (TIB MOLBIOL, Germany) and injected both intraperitoneally (ip) and subcutaneously (sc) into Lou/C rats. After 6 weeks, the animals received a booster injection (sc and ip) with 50 µg of antigen without Freund's adjuvant. Fusion of the myeloma cell line P3X63-Ag8.653[37] with immune spleen cells was performed according to the standard procedure described by Köhler and Milstein[38]. After fusion, the cells were cultured in 96-well cluster plates in standard medium supplemented with 20% fetal calf serum (FCS), 2% HCS (Capricorn Scientific, USA), and aminopterin (Life Technologies, Germany).

Hybridoma supernatants were tested in a solid-phase enzyme-linked immunoassay (ELISA). Plates were coated overnight with mouse-anti GST antibody (5 µg/ml) and after blocking with 2% FCS, GST-GABARAP fusion protein was added at 0.7 µg/ml for 60 min. Irrelevant GST-fusion protein served as negative control. Hybridoma supernatants (1:10 diluted) were added and GABARAP-bound antibodies were detected with a mixture of horseradish peroxidase (HRP)-coupled mouse monoclonal antibodies against rat IgG heavy chains. The secondary antibodies were visualized with 3,3′,5,5′-tetramethylbenzidine (TMB) substrate (Thermo Scientific, Germany) by measuring the absorbance at 650 nm with a microplate reader (Tecan, Switzerland). The IgG subclass was determined by ELISA with mouse anti-rat light chain antibodies as capture and HRP-coupled mouse anti-rat IgG subclass-specific antibodies for detection. The hybridoma cells of clone 8H5 (IgG2a/k) were stably subcloned twice by limiting dilution.

Dot blot analysis. Purified ATG8 family proteins (GABARAP, GABARAPL1, GABARAPL2, LC3A, LC3B and LC3C) were adjusted to a final concentration of 10 µM, respectively. 1 µl of each solution was transferred to a cellulose nitrate membrane considering an adequate spacing between all spots. After 5 min, membranes were blocked with tris-buffered saline-tween (TBS-T) (TBS, 0.1% Tween 20) including 5% nonfat-dried milk powder (AppliChem) for 30 min at room temperature (RT). The membrane was subsequently incubated with the primary antibody containing hybridoma supernatant (rat anti-GABARAP clone number 8H5) diluted in blocking buffer (1:1). Incubation was performed overnight at 4 °C. After three washing steps with TBS-T, HRP-coupled secondary antibody (mouse anti-rat-IgG2a-HRP; 1:1000) was applied for 1 h at RT. After three further washing steps with TBS-T, the membrane was incubated with the HRP substrate SuperSignal West Pico Chemiluminescent Substrate (Thermo Scientific, Germany) for 5 min at RT. Final quantification of immunosignal was performed using a chemiluminescence detection system (ChemiDoc, Bio-Rad, Hercules, CA, USA).

ELISA (for assessing binding specificity of selected hybridoma supernatants). 96 well Nunc-Immuno MicroWell Polysorp plates (Thermo Scientific, Germany) were coated with 700 ng of one GABARAP family protein per well and incubated for 1 h at RT. Wells were subsequently blocked for 30 min at RT

using TBS-T including 5% nonfat-dried milk powder (AppliChem, Germany). Hybridoma supernatant with primary antibody (rat anti-GABARAP clone 8H5) was diluted in blocking buffer (1:10) and was further transferred to 7 wells, respectively. Each of these wells contained a distinct protein of the GABARAP family. Incubation was performed for 1 h at RT. After three washing steps using TBS-T, a suitable HRP coupled secondary antibody (goat anti-rat IgG-HRP) was diluted (1:1000) and subsequently transferred to the wells. After 1 h of incubation at RT, each well was washed three times with TBS-T. The HRP substrate and TMB (Sigma-Aldrich, T5525, Germany) was finally applied to all wells according to manufacturer's instruction. Immunosignal was quantified at 450 nm (Fluostar Optima, BMG Labtechnologies GmbH, Germany).

Polyacrylamide gel electrophoresis and western blot analysis. Purified ATG8 family proteins (GABARAP, GABARAPL1, GABARAPL2, LC3A, LC3B and LC3C) were denatured at 95 °C for 5 min in SDS loading buffer (10% (v/v) glycerol, 2% (w/v) SDS, 2% (v/v) 2-mercaptoethanol, 50 mM Tris, pH 6.8, 0.75 g/l bromphenol blue). ATG8 family proteins (1 µg respectively) were then applied to a 12% SDS-PAGE and separated at 40 mA for 45 min. Gel staining was performed with coomassie staining solution (25% isopropanol, 10% acidic acid, 0.5 g/l coomassie brilliant blue R-250) and the destaining was done in hot water.

For western blot analysis, proteins were transferred to a PVDF membrane (pore size 0.2 µm) without preceding gel staining. Protein transfer was performed in a semi dry system at 25 V for 60 min. The membrane was subsequently washed in TBS-T and then blocked in TBS-T including 2.5% milk powder for 30 min. The blot was incubated with primary antibody containing hybridoma supernatant (rat anti-GABARAP (8H5) antibody) diluted in TBS-T (1:4) over night at 4 °C. After washing (3 times for 5 min, respectively) in TBS-T, the membrane was incubated with HRP-conjugated secondary antibody (goat anti-rat-HRP, Jackson 112–035–068, diluted 1:2000 in TBS-T) at RT for 1 h. The blot was washed (3 times for 5 min, respectively) in TBS-T and immunoreactivity was finally quantified as described for dot blot analysis.

Epitope mapping. Peptide scanning was performed using a cellulose membrane (Intavis AG, Germany) loaded with 12mer peptides representing the complete sequence of hGABARAP and overlapping by 10 amino acids, respectively. Every peptide was spotted on the membrane twice. Epitope mapping was done by washing the membrane with TBS-T, followed by a blocking step using TBS-T/5% nonfat-dried milk powder. After another washing step with TBS-T, primary antibody (rat anti-GABARAP (8H5) antibody hybridoma supernatant) was diluted with TBS-T (1:5) and applied over night at 4 °C. After 3 washing steps using TBS-T, HRP-coupled mouse anti-rat IgG2a antibody was diluted with TBS-T (1:2000) and applied for 2 h at RT. After another 3 washing steps with TBS-T, signal detection was performed by incubation with SuperSignal West Pico Chemiluminescent Substrate (Thermo Scientific, Germany) for 5 min at RT. Immunosignal was quantified using a chemiluminescence detection system (ChemiDoc, Bio-Rad, Hercules, CA, USA).

Cell culture and transfection. P3X63-Ag8.653 cells were cultured at 37 °C in a humidified 5% CO_2 incubator in standard medium RPMI 1640 (Sigma-Aldrich, Germany) supplemented with 1% glutamine, 1% non-essential amino acids, 1% sodium pyruvate, 1% penicillin/streptomycin (Sigma-Aldrich, Germany), and 2.5% FCS (Capricorn).

HAP1 cells are adherent human fibroblast-like cells with a near-haploid karyotype that have been derived from the male chronic myelogenous leukemia (CML) cell line KBM-7[39]. HAP1 parental (C631) and HAP1 GABARAP KO (HZGHC003054c004) cells were purchased from Horizon Discovery, UK. HAP1 cells were cultured at 37 °C in a humidified 5% CO_2 incubator in growth medium Iscove's Modified Dulbecco's Medium (IMDM – Gibco, Thermofisher Scientific, Germany) supplemented with 1% penicillin/streptomycin (Sigma-Aldrich, Germany), and 10% FCS (Sigma-Aldrich, Germany).

For transient transfection with peYFP-N1 empty vector (Clontech, USA), peYFP-GABARAP, peYFP-GABARAPL1, and peCFP-GABARAPL2 constructs, 1×10^5 HAP1 cells were seeded on a poly D-Lysine coated bottom dish (MatTek Corporation, MA, USA) and incubated in IMDM / 10% FCS, respectively. The next day transfection with 1.5 µg total DNA using Turbofectin 8.0 (OriGene, USA) was performed according to manufacturer's instructions.

Immunofluorescence. HAP1 cells (3×10^5) were seeded on a poly D-Lysine coated glass bottom dish (MatTek Corporation, MA, USA) and incubated in IMDM / 10% FCS. The next day, IMDM was removed and HAP1 cells were incubated for 3–4 h in IMDM medium with 10% FCS only or IMDM without 10% FCS including 100 nM Bafilomycin A1 (Sigma-Aldrich, Germany). Fixation with 4% (w/v) paraformaldehyde in PBS at RT for 10 min was followed by a washing step using PBS and addition of 0.2% TritonX-100 in PBS for 30 min at RT to permeabilize the cell membranes. After three washing steps with PBS, surfaces were blocked with 1% bovine serum albumin (BSA, Sigma-Aldrich, Germany) at RT for 60 min or overnight at 4–8 °C. Immunostaining was performed by addition of 1 mL undiluted hybridoma supernatant including anti-GABARAP (8H5) antibody and 1 µg/mL mouse monoclonal anti-LC3B (5F10) antibody and incubation for 60 min at RT under smooth shaking. Cells were washed three times for 5 min with PBS followed by incubation of an appropriate 1:250 diluted fluorescent labelled secondary antibody (goat anti-rat Alexa Fluor 488 for 8H5; goat anti-mouse Alexa Fluor 647 for mAb LC3B) for 60 min at RT in the dark, followed by two washing steps for 5 min with PBS. YFP, YFP-GABARAP, and YFP-GABARAPL1 transfected HAP1 cells were fixed 2 to 3 days after transfection. Fixing and staining procedure was done as described above, and a donkey anti-rat Cy5 secondary Ab (1:250) was used in combination with anti-GABARAP (8H5) antibody.

Image acquisition. Images were acquired using ZEN black 2009 on a LSM 710 confocal laser scanning system (Carl Zeiss MicroImaging Inc., Germany) with a Plan-Apochromat 63 × /1.40 Oil DIC M27 objective. The cell nuclei (DAPI) were measured in the 405 nm channel (MBS -405/760+). GABARAP puncta were detected

in the 488 nm channel (MBS 488/543/633) and LC3B puncta in the 633 nm channel (MBS 488/543/633), respectively. YFP was detected in channel 514 nm (MBS 458/514) and Cy5 in channel 633 nm (MBS 488/543/633).

Image evaluation. Image analysis was done using ImageJ / Fiji[40,41]. For quantitative and unbiased evaluation of anti-GABARAP (8H5) antibody a macro has been written and applied to images of parental and GABARAP KO cells. Within the macro a maximum intensity projection and a defined threshold (70/255) was used. After thresholding the images, a watershed algorithm was applied and puncta with a size >3 pixel were counted using the *Analyze Particles* tool of ImageJ. The puncta were analyzed in single cells using manually annotated regions of interest (ROIs) within the images. For better visibility in the print version, maximum intensity projections and an adjustment of brightness (20), contrast (40) and intensity (60) was applied equally for every figure using CorelDRAW 2017. For data analysis, GraphPad Prism Version 5.00 was used.

Data Availability Statement

No datasets were generated or analyzed during the current study.

References

1. Weiergräber, O. H., Schwarten, M., Strodel, B. & Willbold, D. Investigating Structure and Dynamics of Atg8 Family Proteins. *Methods in enzymology* **587**, 115–142, https://doi.org/10.1016/bs.mie.2016.09.056 (2017).
2. Le Grand, J. N. *et al.* GABARAPL1 (GEC1): original or copycat? *Autophagy* **7**, 1098–1107, https://doi.org/10.4161/auto.7.10.15904 (2011).
3. Schaaf, M. B., Keulers, T. G., Vooijs, M. A. & Rouschop, K. M. LC3/GABARAP family proteins: autophagy-(un)related functions. *FASEB journal: official publication of the Federation of American Societies for Experimental Biology* **30**, 3961–3978, https://doi.org/10.1096/fj.201600698R (2016).
4. Wang, H., Bedford, F. K., Brandon, N. J., Moss, S. J. & Olsen, R. W. GABA(A)-receptor-associated protein links GABA(A) receptors and the cytoskeleton. *Nature* **397**, 69–72, https://doi.org/10.1038/16264 (1999).
5. Green, F., O'Hare, T., Blackwell, A. & Enns, C. A. Association of human transferrin receptor with GABARAP. *FEBS Lett* **518**, 101–106 (2002).
6. Cook, J. L. *et al.* The trafficking protein GABARAP binds to and enhances plasma membrane expression and function of the angiotensin II type 1 receptor. *Circulation research* **102**, 1539–1547, https://doi.org/10.1161/CIRCRESAHA.108.176594 (2008).
7. Lainez, S. *et al.* GABAA receptor associated protein (GABARAP) modulates TRPV1 expression and channel function and desensitization. *FASEB journal: official publication of the Federation of American Societies for Experimental Biology* **24**, 1958–1970, https://doi.org/10.1096/fj.09-151472 (2010).
8. Ohsumi, Y. Historical landmarks of autophagy research. *Cell research* **24**, 9–23, https://doi.org/10.1038/cr.2013.169 (2014).
9. Ichimura, Y. *et al.* A ubiquitin-like system mediates protein lipidation. *Nature* **408**, 488–492, https://doi.org/10.1038/35044114 (2000).
10. Geng, J. & Klionsky, D. J. The Atg8 and Atg12 ubiquitin-like conjugation systems in macroautophagy. 'Protein modifications: beyond the usual suspects' review series. *EMBO reports* **9**, 859–864, https://doi.org/10.1038/embor.2008.163 (2008).
11. Tanida, I., Komatsu, M., Ueno, T. & Kominami, E. GATE-16 and GABARAP are authentic modifiers mediated by Apg7 and Apg3. *Biochem Biophys Res Commun* **300**, 637–644 (2003).
12. Kabeya, Y. *et al.* LC3, GABARAP and GATE16 localize to autophagosomal membrane depending on form-II formation. *Journal of cell science* **117**, 2805–2812, https://doi.org/10.1242/jcs.01131 (2004).
13. Chen, Z. W., Chang, C. S., Leil, T. A. & Olsen, R. W. C-terminal modification is required for GABARAP-mediated GABA(A) receptor trafficking. *J Neurosci* **27**, 6655–6663, https://doi.org/10.1523/JNEUROSCI.0919-07.2007 (2007).
14. Lee, Y. K. & Lee, J. A. Role of the mammalian ATG8/LC3 family in autophagy: differential and compensatory roles in the spatiotemporal regulation of autophagy. *BMB reports* **49**, 424–430 (2016).
15. Klionsky, D. J. *et al.* Guidelines for the use and interpretation of assays for monitoring autophagy (3rd edition). *Autophagy* **12**, 1–222, https://doi.org/10.1080/15548627.2015.1100356 (2016).
16. Nguyen, T. N. *et al.* Atg8 family LC3/GABARAP proteins are crucial for autophagosome-lysosome fusion but not autophagosome formation during PINK1/Parkin mitophagy and starvation. *The Journal of cell biology* **215**, 857–874, https://doi.org/10.1083/jcb.201607039 (2016).
17. Joachim, J. *et al.* Activation of ULK Kinase and Autophagy by GABARAP Trafficking from the Centrosome Is Regulated by WAC and GM130. *Mol Cell* **60**, 899–913, https://doi.org/10.1016/j.molcel.2015.11.018 (2015).
18. Joachim, J. *et al.* Centriolar Satellites Control GABARAP Ubiquitination and GABARAP-Mediated Autophagy. *Curr Biol* **27**, 2123–2136 e2127, https://doi.org/10.1016/j.cub.2017.06.021 (2017).
19. Uhlen, M. *et al.* A proposal for validation of antibodies. *Nature methods* **13**, 823–827, https://doi.org/10.1038/nmeth.3995 (2016).
20. Werner, G., Hagenmaier, H., Drautz, H., Baumgartner, A. & Zahner, H. Metabolic products of microorganisms. 224. Bafilomycins, a new group of macrolide antibiotics. Production, isolation, chemical structure and biological activity. *J Antibiot (Tokyo)* **37**, 110–117 (1984).
21. Drose, S. & Altendorf, K. Bafilomycins and concanamycins as inhibitors of V-ATPases and P-ATPases. *J Exp Biol* **200**, 1–8 (1997).
22. Koukourakis, M. I. *et al.* Autophagosome Proteins LC3A, LC3B and LC3C Have Distinct Subcellular Distribution Kinetics and Expression in Cancer Cell Lines. *PLoS One* **10**, e0137675, https://doi.org/10.1371/journal.pone.0137675 (2015).
23. Mizushima, N., Yoshimori, T. & Levine, B. Methods in mammalian autophagy research. *Cell* **140**, 313–326, https://doi.org/10.1016/j.cell.2010.01.028 (2010).
24. Joachim, J. & Tooze, S. A. Control of GABARAP-mediated autophagy by the Golgi complex, centrosome and centriolar satellites. *Biol Cell* **110**, 1–5, https://doi.org/10.1111/boc.201700046 (2018).
25. Hiyama, M. *et al.* Nutrient starvation affects expression of LC3 family at the feto-maternal interface during murine placentation. *J Vet Med Sci* **77**, 305–311, https://doi.org/10.1292/jvms.14-0490 (2015).
26. Meliopoulos, V. A. & Schultz-Cherry, S. Although it's painful: The importance of stringent antibody validation. *PLoS Pathog* **14**, e1006701, https://doi.org/10.1371/journal.ppat.1006701 (2018).
27. Skogs, M. *et al.* Antibody Validation in Bioimaging Applications Based on Endogenous Expression of Tagged Proteins. *Journal of proteome research* **16**, 147–155, https://doi.org/10.1021/acs.jproteome.6b00821 (2017).
28. Jiang, P. & Mizushima, N. Autophagy and human diseases. *Cell research* **24**, 69–79, https://doi.org/10.1038/cr.2013.161 (2014).
29. Kim, M., Ho, A. & Lee, J. H. Autophagy and Human Neurodegenerative Diseases-A Fly's Perspective. *Int J Mol Sci* **18**, https://doi.org/10.3390/ijms18071596 (2017).
30. Willingham, M. C. Conditional epitopes. is your antibody always specific? *J Histochem Cytochem* **47**, 1233–1236, https://doi.org/10.1177/002215549904701002 (1999).
31. Bordeaux, J. *et al.* Antibody validation. *Biotechniques* **48**, 197–209, https://doi.org/10.2144/000113382 (2010).

32. Lee, Y. K. *et al.* Development of LC3/GABARAP sensors containing a LIR and a hydrophobic domain to monitor autophagy. *The EMBO journal.* https://doi.org/10.15252/embj.201696315 (2017).
33. Stolz, A. *et al.* Fluorescence-based ATG8 sensors monitor localization and function of LC3/GABARAP proteins. *The EMBO journal* **36**, 549–564, https://doi.org/10.15252/embj.201695063 (2017).
34. Wang, H. & Olsen, R. W. Binding of the GABA(A) receptor-associated protein (GABARAP) to microtubules and microfilaments suggests involvement of the cytoskeleton in GABARAPGABA(A) receptor interaction. *Journal of neurochemistry* **75**, 644–655 (2000).
35. Ma, P. *et al.* Interaction of Bcl-2 with the autophagy-related GABAA receptor-associated protein (GABARAP): biophysical characterization and functional implications. *The Journal of biological chemistry* **288**, 37204–37215, https://doi.org/10.1074/jbc.M113.528067 (2013).
36. Krichel, C. *et al.* Sequence-specific 1H, 15N, and 13C resonance assignments of the autophagy-related protein LC3C. *Biomolecular NMR assignments* **10**, 41–43, https://doi.org/10.1007/s12104-015-9633-z (2016).
37. Kearney, J. F., Radbruch, A., Liesegang, B. & Rajewsky, K. A new mouse myeloma cell line that has lost immunoglobulin expression but permits the construction of antibody-secreting hybrid cell lines. *J Immunol* **123**, 1548–1550 (1979).
38. Kohler, G. & Milstein, C. Continuous cultures of fused cells secreting antibody of predefined specificity. *Nature* **256**, 495–497 (1975).
39. Carette, J. E. *et al.* Ebola virus entry requires the cholesterol transporter Niemann-Pick C1. *Nature* **477**, 340–343, https://doi.org/10.1038/nature10348 (2011).
40. Schindelin, J. *et al.* Fiji: an open-source platform for biological-image analysis. *Nature methods* **9**, 676–682, https://doi.org/10.1038/nmeth.2019 (2012).
41. Schneider, C. A., Rasband, W. S. & Eliceiri, K. W. NIH Image to ImageJ: 25 years of image analysis. *Nature methods* **9**, 671–675 (2012).
42. Sievers, F. *et al.* Fast, scalable generation of high-quality protein multiple sequence alignments using Clustal Omega. *Mol Syst Biol* **7**, 539, https://doi.org/10.1038/msb.2011.75 (2011).

Acknowledgements

We thank S. Weidtkamp-Peters for advice on image acquisition, M. Schwarten for help with PyMol, P. Ma for FP-fusion plasmid cloning, J. Post-Schulz for supporting IF staining of mouse brain slices and J. Fabig for valuable technical assistance. This study was funded by the Deutsche Forschungsgemeinschaft (DFG, German Research Foundation) – Projektnummer 190586431 – SFB 974, project B02 (D.W., I.M.S.), and project WE5343/1–1 (T.Z.), and by a grant from the Jürgen Manchot Foundation, Molecules of Infection Graduate School (MOI III) (D.W. and J.D.).

Author Contributions

D.W. and J.M. generated the original hypothesis. E.K., R.F. and J.M. generated and screened the antibody, J.M. purified the recombinantly expressed proteins, performed the dot blot assay and did the epitope mapping. I.M.S. conducted the cell culture experiments, IF-stainings, image acquisition and evaluation. T.Z. established the image analysis tool. I.M.S. and J.D. generated the HEK293 KO lines and performed the related IB experiments. D.W., J.M., S.H., provided intellectual contributions throughout and supervised the project. S.H., I.M.S. and J.M. took primary responsibility for writing the manuscript. All authors edited the manuscript.

Additional Information

Supplementary information accompanies this paper at https://doi.org/10.1038/s41598-018-36717-1.

Competing Interests: The authors declare no competing interests.

Publisher's note: Springer Nature remains neutral with regard to jurisdictional claims in published maps and institutional affiliations.

Supplementary Info

The highly GABARAP specific rat monoclonal antibody 8H5 visualizes GABARAP in immunofluorescence imaging at endogenous levels

Indra M. Simons[1], Jeannine Mohrlüder[2], Regina Feederle[3], Elisabeth Kremmer[4], Thomas Zobel[5], Jochen Dobner[1], Nicole Bleffert[1], Silke Hoffmann[2], Dieter Willbold[1,2]

[1]Institut für Physikalische Biologie, Heinrich-Heine-Universität, 40225 Düsseldorf, Germany

[2]Institute of Complex Systems, Structural Biochemistry (ICS-6), Forschungszentrum Jülich, 52425 Jülich, Germany

[3]Institute for Diabetes and Obesity, Monoclonal Antibody Core Facility [4]Institute for Molecular Immunology Helmholtz Center Munich, German Research Center for Environmental Health, 85764 Neuherberg, Germany

[5]Department of Biology, Center for Advanced Imaging (CAi), Heinrich-Heine-Universität, 40225 Düsseldorf, Germany

Supplementary Methods are related to Figure S1, S2, S4 and S5

Supplementary Figure 1 is related to all Figures dealing with HAP1 cells (Fig. 3, 4, 5)
Supplementary Figure 2 is related to Figure 4
Supplementary Figure 3 is related to Figures 1A, 1C, 2A, S1A and S1B
Supplementary Figure 4
Supplementary Figure 5 is related to Figure 5
Supplementary Figure 6
Supplementary Table 1 is related to Figure S1 B
Supplementary Table 2 is related to Figure Table S1 and Supplementary Figure S1 B
Supplementary Table 3 is related to all figures

Supplementary References are related to Figure S1

Supplementary Methods

Western blotting of mammalian cell lysates

For immunoblots depicted in figure S1, cells were washed once with warm PBS, dissociated with Trypsin-EDTA (Cytogen, Wetzlar, Germany) for 5 min, resuspended in medium and centrifuged for 3 min at 4 °C and 900 g. Afterwards, cell pellets were washed once with cold PBS and resuspended in lysis buffer (136 mM NaCl, 20 mM Tris-HCl, 10 % Glycerin, 2 mM EDTA, 50 mM β-Glycerophosphat, 20 mM Na-Pyrophosphat, 0.2 mM Pefablock, 5 µg/ml Aprotinin, 5 µg/ml Leupeptin, 4 mM Benzamidin, 1 mM Na_3VO_4 , 0.2 % SDS, pH 7.4) and frozen for 20 min at -20 °C. Subsequently, samples were thawed, sonicated thrice for 15 seconds at 100 % on ice and centrifuged for 15 min at 4 °C and 20 000 g to get rid of cell debris. Supernatants were transferred to fresh tubes and protein content measured with Bradford protein assay (Biorad, California, USA). 40 µg of whole cell protein lysates were then subjected to 12 % polyacrylamid SDS-PAGE. Proteins were then transferred onto a PVDF membrane via Semi-Dry Western Blot. Membranes were blocked with either 5 % milk in TBS-T or 5 % BSA in TBS-T for 1 h at room temperature (RT), followed by three times 20 min washing with TBS-T at RT incubation with primary antibody overnight at 4 °C and secondary HRP-coupled antibody for 1 h at RT. Blots were visualized by chemiluminescence (Western Lightning Plus-ECL, Perkin Elmer, Massachusetts, USA) and documented using the ChemiDoc system (Biorad, California, USA) or film (Amersham Hyperfilm ECL, GE, UK).

Generation of HEK293 knockout cell lines

HEK293 cells were nucleofected (Lonza, Basel, CH) with KO plasmids targeting *GABARAP* exon 1, -*L1* exon 2 and -*L2* exon 2 coexpressing either GFP, CFP or mCherry. KO plasmids are based on plasmid pSpCas9(BB)-2A-GFP (PX458), which was a gift from Feng Zhang (Addgene plasmid # 48138)[1]. Clonal lines were created by growth of single cell sorted FP positive cells via fluorescence activated cell sorting (FACS). Genomic mutations were validated via Sanger sequencing of PCR amplificates of the sgRNA target region +/- 200 bp (table S1) and analysed by TIDE and Crisp-ID[2,3], as listed in table S2.

Ethics statement

All animal experiments were performed in accordance with the German Law on the protection of animals (TierSchG §§ 7-9) and with permit from the local ethic committee (Landesamt für Natur, Umwelt und Verbraucherschutz Nordrhein-Westfalen (LANUV), North Rhine-Westphalia, Germany; AZ 84-02.04.2015.A106 and AZ 84-02.04.2014.A423).

Immunofluorescent analysis of mouse brain slices

Endogenous GABARAP in tissue sections was assessed by immunofluorescence analysis using 20 µm thick, sagittal sections of 20 weeks old mice divided by a cryostat (CM3050 S, Leica Biosystems Nussloch GmbH, Wetzlar, Germany). Formalin embedded brain sections were fixed for 10 min with 4 % PFA, three times washed for 5 min with (Tris-buffered saline) TBS and treated for 10 min with 70 % formic acid for antigen retrieval, followed by another three 5 min washing steps with TBS. After permeabilization with 1 % TBS-Triton-X (TBS-T) for 30 min, brain sections were blocked with 1 % BSA in TBS over night at 4 °C. Incubation with anti-GABARAP (8H5) antibody was performed with undiluted hybridoma supernatant for 2 h at RT. After three washing steps for 5 min with TBS, sections were incubated for 1 h with a goat anti-rat IgG+IgM (H&L) Alexa Fluor 488 secondary antibody (112-545-068, Dianova, 1:250 in 1 % BSA in TBS), followed by three 5 min washing steps with TBS. In addition, the secondary antibody was applied in the absence of primary antibody, to assess the specificity of the stain, and all residual staining was considered to be non-specific. Immunofluorescent sections were counterstained by DAPI (4,6-Diamidin-2-phenylindol) (Merck, Germany) and again washed as described. Brain sections were mounted with Aqua Poly/Mount (18606, Polysciences, Inc. Warrington, Pennsylvania, USA). Images were taken with a LSM 710 confocal laser scanning system (Carl Zeiss MicroImaging Inc., Germany) equipped with a EC Plan-Neofluar 20x/0.50 M27a or a Plan-Apochromat 63x/1.40 Oil DIC M27 objective.

Immunofluorescence

HEK293 cells (3 x 10^5) were seeded on a fibronectin (Sigma-Aldrich, Germany) coated glass bottom dish (ibidi, Germany) and incubated in DMEM supplemented with 10 % FCS for 24 hours. The next day, DMEM was removed and HEK293 cells were incubated for 3 h – 4 h in DMEM medium without 10 % FCS or Earle's Balanced Salts (EBSS, Sigma-Aldrich, Germany) including 100 nM Bafilomycin A1 (Sigma-Aldrich, Germany). Fixation with 4 % (w/v) paraformaldehyde (PFA) in PBS at RT for 10 min was followed by a washing step using PBS and addition of 0.2 % TritonX-100 in PBS for 30 min at RT to permeabilize the cell membranes. After three washing steps with PBS, surfaces were blocked with 1 % bovine serum albumin (BSA, Sigma-Aldrich, Germany) overnight at 4-8 °C. Immunostaining was performed by addition of 1 mL undiluted hybridoma supernatant including anti-GABARAP (8H5) and 1 µg/mL mouse monoclonal anti-LC3B (5F10) antibody and incubation for 60 min at RT under smooth shaking. Cells were washed three times for 5 min with PBS followed by incubation of an appropriate 1:250 diluted fluorescent labelled secondary antibody (goat anti-rat Alexa Fluor 488 for 8H5; goat anti-mouse Alexa Fluor 647 for mAb LC3B) for 60 min at RT in the dark, followed by two washing steps for 5 min with PBS.

HAP1 parental and GABARAP KO cells were cultured under growth factor deprivation with 100 nM BafA1 for 3 h. Cells were fixed with 4 % (w/v) PFA in PBS at RT or with 100 % methanol for 15 min at – 20 °C, both followed by washing twice for 5 min. Cells were immunolabeled with polyclonal

(pAb) GABARAP (Proteintech 1:200, abgent 1:25) or monoclonal GABARAP (Cell Signaling E1J4E, 1:200) antibodies followed by staining with Alexa Fluor 555 (pAb – 1 (Proteintech)) and with Alexa Fluor 488 (mAb (E1J4E) and pAb – 2 (abgent)).

106 **Supplementary Figure S1**

107

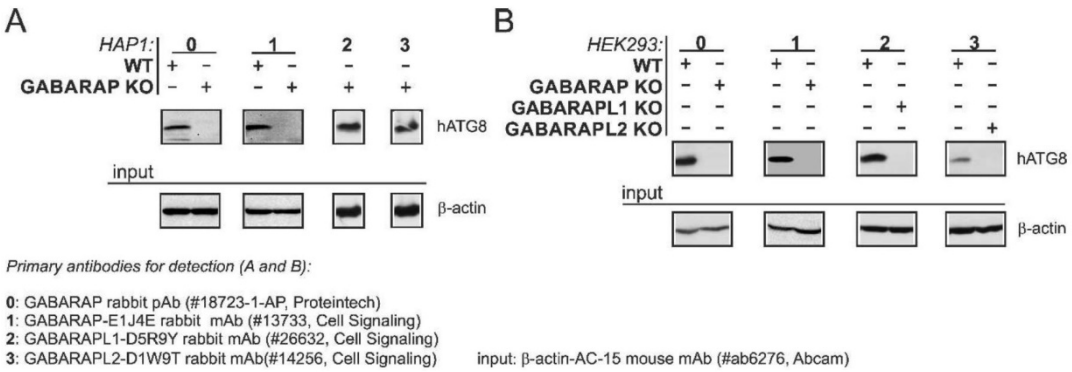

Primary antibodies for detection (A and B):

0: GABARAP rabbit pAb (#18723-1-AP, Proteintech)
1: GABARAP-E1J4E rabbit mAb (#13733, Cell Signaling)
2: GABARAPL1-D5R9Y rabbit mAb (#26632, Cell Signaling)
3: GABARAPL2-D1W9T rabbit mAb(#14256, Cell Signaling) input: β-actin-AC-15 mouse mAb (#ab6276, Abcam)

109 **Supplementary Figure S1. Expression analysis of GABARAP, GABARAPL1, and GABARAPL2 in HAP1 (A) and**
110 **HEK293 (B) cell lysates.** (B) KO-validation of the primary antibodies used in (A) demonstrating their target specificity
111 during immunoblotting applications. GABARAP TKO cells were created using the CRISPR/Cas9 system[1]. HEK293 KO cell
112 lines in (B) were used to validate specificity of the antibodies used against GABARAP, GABARAP-L1 and GABARAP-L2
113 during immunoblotting. "hATG8" stands for the corresponding GABARAP-subfamily member, detected by the respective
114 antibody. The corresponding full-length blots are given in Supplementary Fig. S3.

115

Supplementary Figure S2

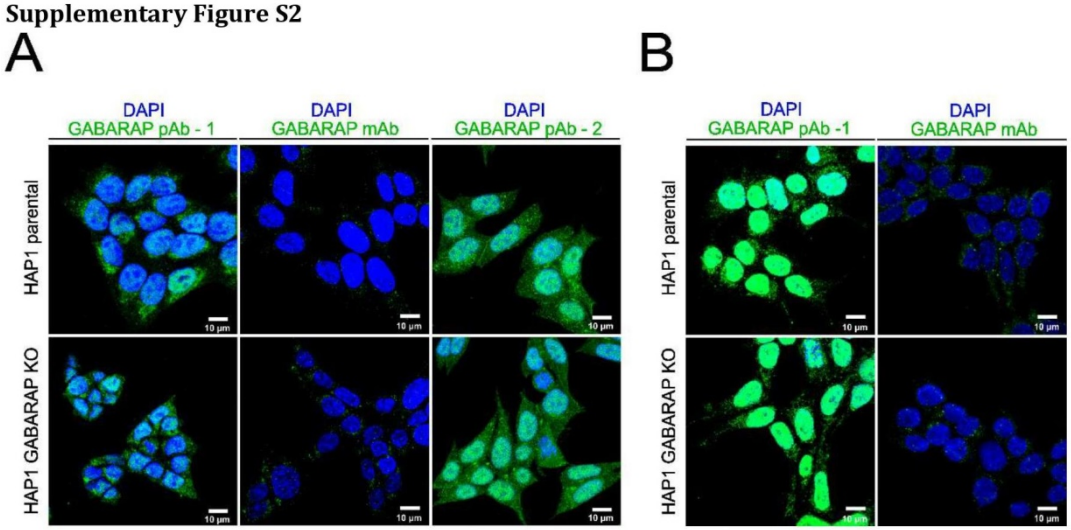

Supplementary Figure S2. Commercial antibodies fail to detect endogenous GABARAP in immunofluorescence in a specific manner. HAP1 parental and GABARAP KO cells were cultured under growth factor deprivation with 100 nM BafA1 for 3 h. Fixed cells were immunolabeled with polyclonal (pAb) GABARAP or monoclonal GABARAP antibodies. Under (A) a 4 % PFA fixation and a staining with Alexa555 (pAb – 1 (Proteintech)) and with Alexa488 (mAb (E1J4E) and pAb – 2 (abgent)) was applied. Under (B) a fixation with 4 % PFA and a staining with Alexa488 (pAb) and a methanol-based fixation protocol as recommended by the supplier for GABARAP mAb E1J4E with Alexa488 as secondary antibody was used, respectively. Nuclei were counterstained with DAPI.

Supplementary Figure S3

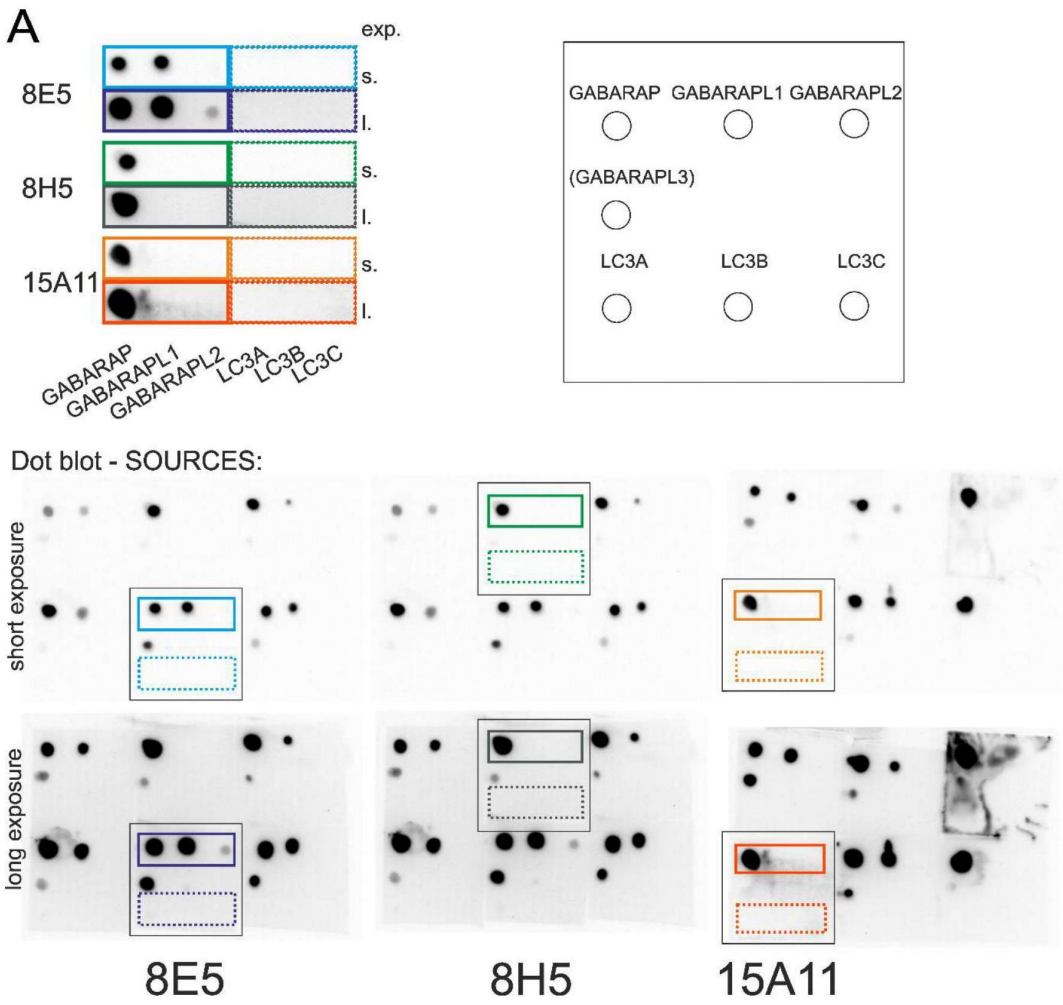

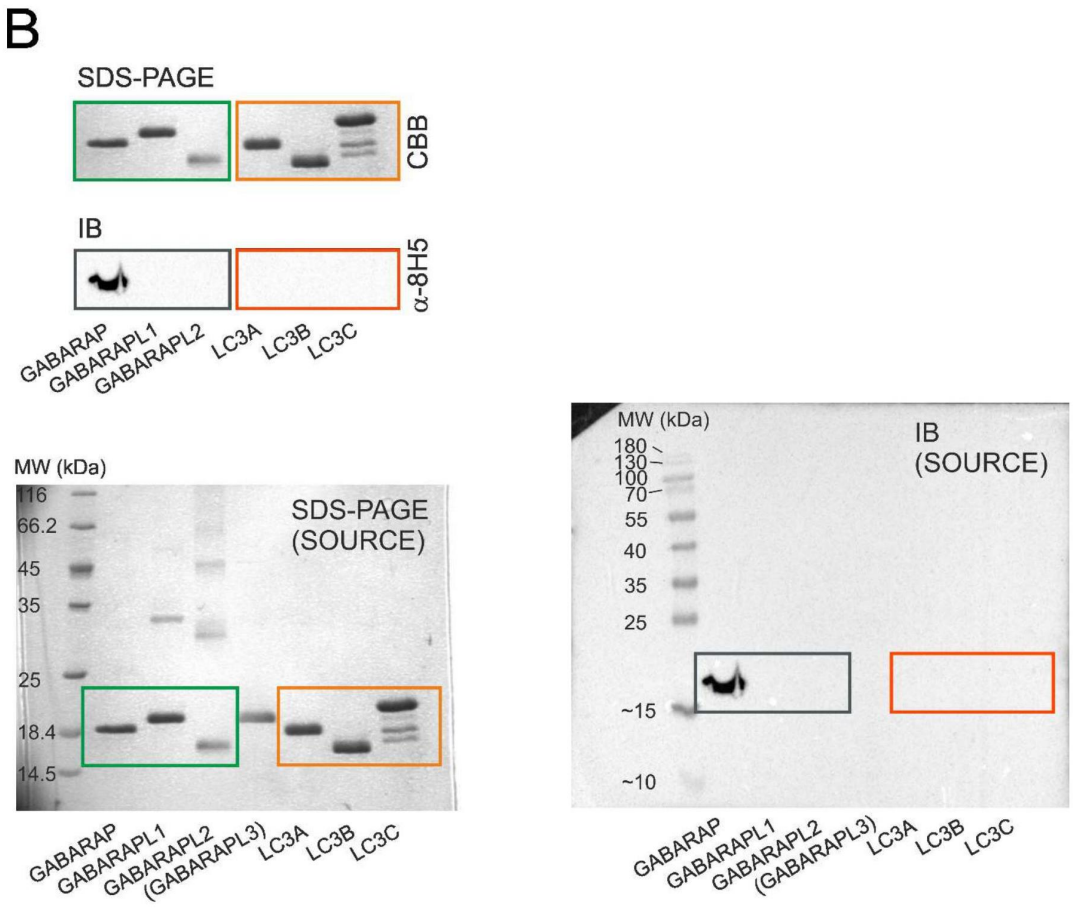

129

130

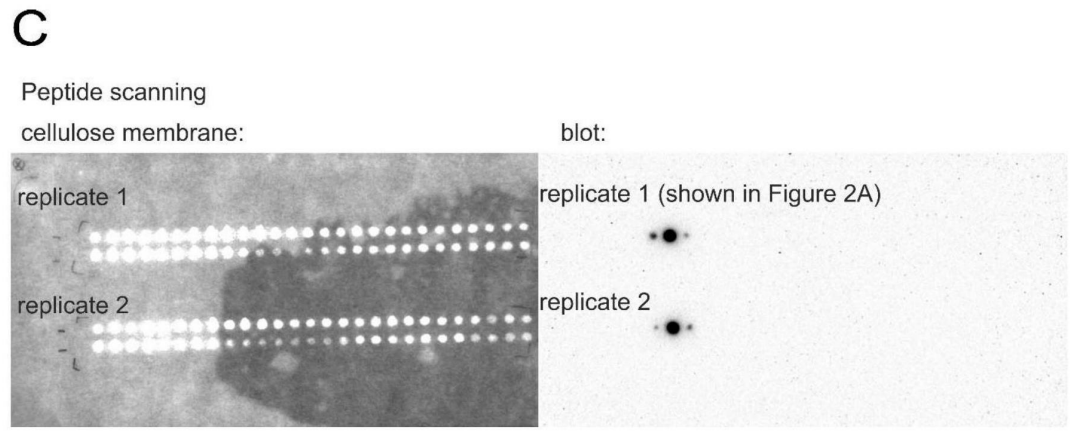

131

132

133

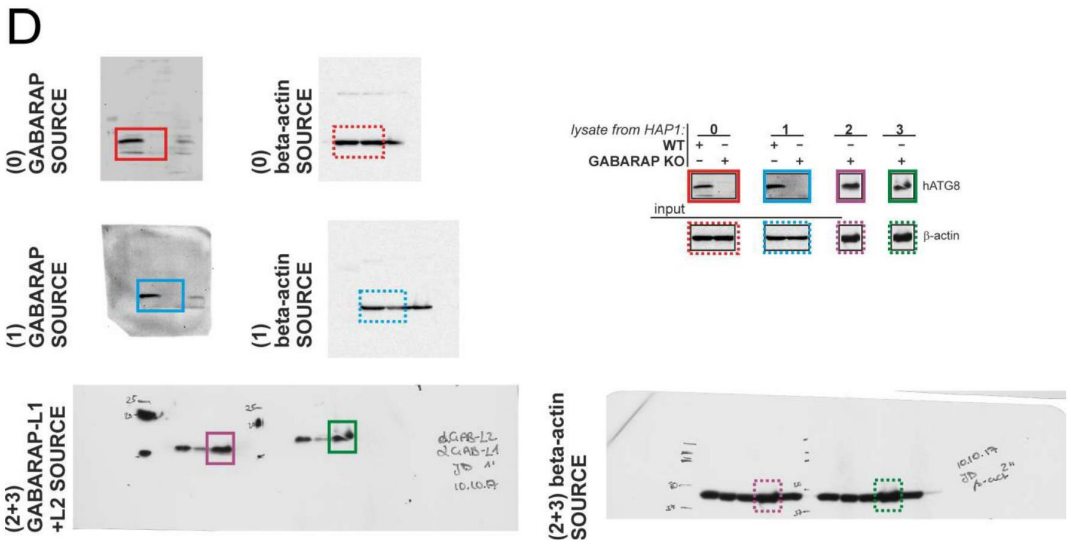

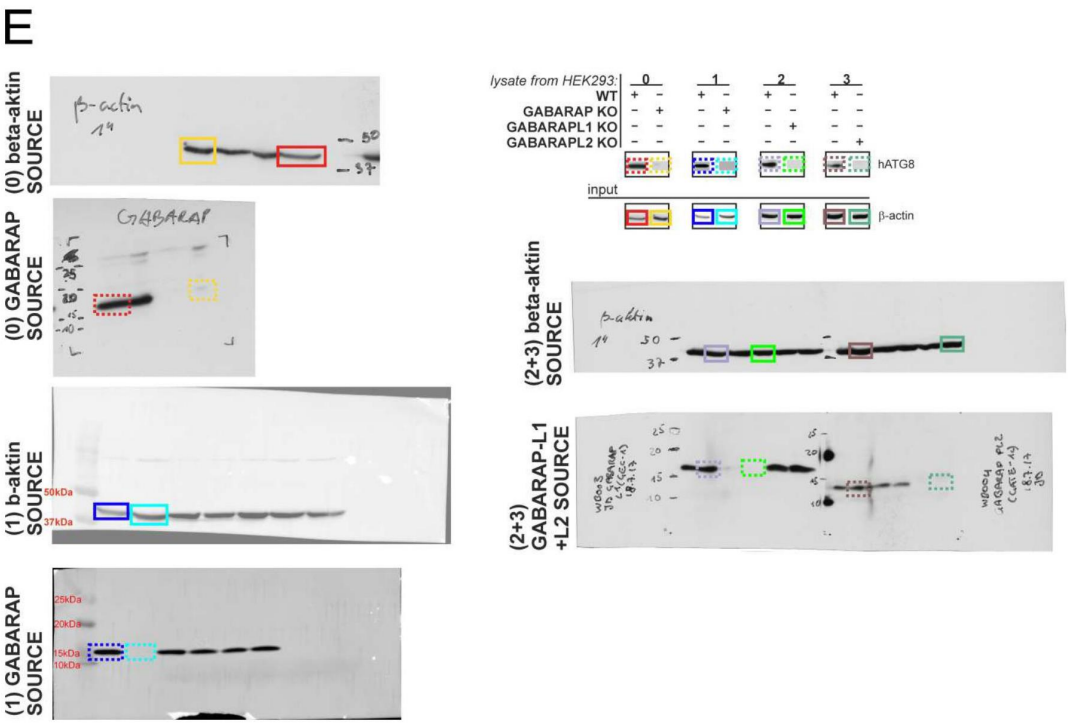

Supplementary Figure S3. Full-length-blots. (A) Uncropped dot blots related to Figure 1A. Note: Each individual exposure includes six blots incubated with one of six different hybridoma supernatants each. Only those incubated with GABARAP-8E5, -8H5 and -15A11 containing supernatants are highlighted. Beside purified GABARAP, -L1, -L2, LC3A, -B and –C the hybridoma supernatants were also tested for their reactivity with GABARAPL3. Because GABARAPL3 is assumed to be a "pseudogene", it was excluded during further analysis. (B) Uncropped SDS-PAGE and western blot membrane related to Figure 1C. (C) Uncropped cellulose membrane shown in Figure 2A used for epitope mapping of GABARAP-8H5. Transillumination and blot are given for both replicates. (D, E) Uncropped western blot membranes related to Supplementary Figure S1A, B.

Supplementary Figure S4

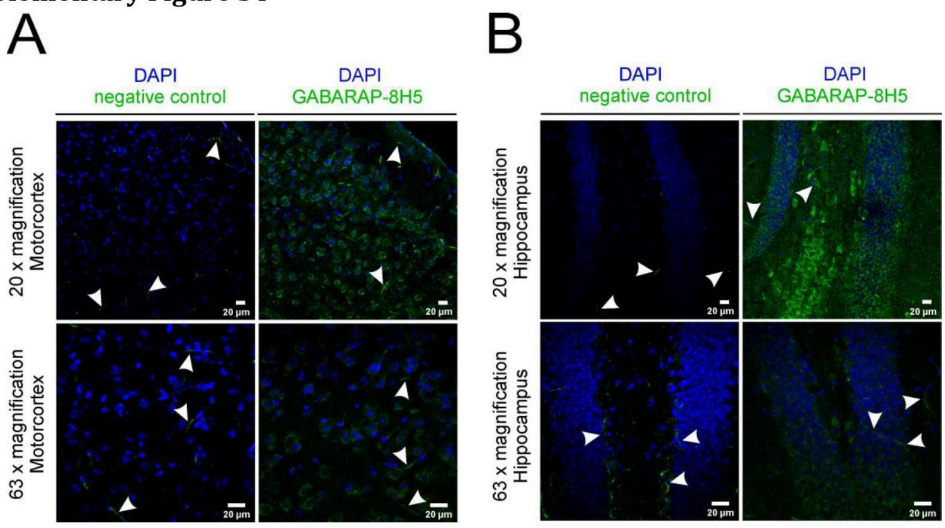

Supplementary Figure S4. Performance of anti-GABARAP (8H5) antibody during immunofluorescent analysis of mouse brain slices. Representative immunofluorescence images of motorcortex (A) or the hippocampal regions (B) of 20 weeks old mice stained with a goat anti-rat IgG+IgM (H&L) Alexa Fluor 488 secondary antibody in the absence (left panels) or presence of anti-GABARAP (8H5) primary antibody (right panels). All residual staining visible in the left panels is considered as non-specific, and likely represents blood vessels (white arrowheads). In the presence of anti-GABARAP (8H5) antibody a clear intra-cellular staining occurs (right panels). Interestingly, an antigen retrieval step as specified in the methods section was obligatory for positive staining results. Note that mouse and human GABARAP sequences display 100 % conservation. Counterstaining was performed with DAPI.

Supplementary Figure S5

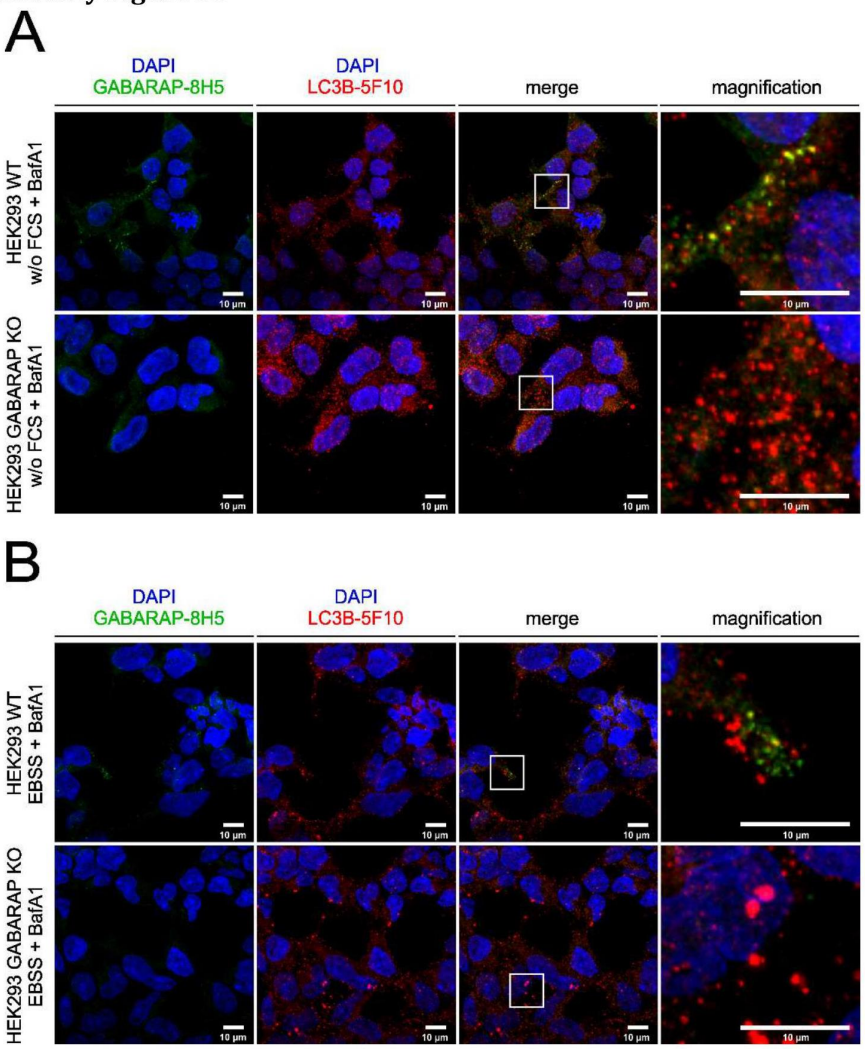

Supplementary Figure S5. Performance of anti-GABARAP (8H5) in HEK293 cells. HEK293 wildtype and GABARAP KO cells were incubated for 3 h in growth factor depleted medium (A) or in EBSS (B) both including 100 nM BafA1 each. Cells were fixed with 4 % PFA and immunolabeled with anti-GABARAP (8H5) and anti-LC3B (5F10) primary antibodies in combination with goat anti-rat IgG+IgM (H&L) Alexa Fluor 488 and anti-mouse IgG Alexa Fluor 647 secondary antibodies, respectively. Colocalization of LC3B (red) and GABARAP (green) is indicated by yellow puncta. Nuclei were counterstained with DAPI.

Supplementary Figure S6

Supplementary Figure S6. The epitope for anti-GABARAP (8H5) antibody shows high conservation between GABARAP proteins from organisms of diverse phylogenetic classes. Aligned are the GABARAP residues 1 to 20 of human GABARAP with those of selected vertebrate, arthropode and nemathode orthologs using Boxshade 3.2.3. UniProtKB accession numbers of the entries used are: O95166 (Homo sapiens); Q9DCD6 (Mus musculus); A0A1L1RN80 (Gallus gallus); Q6PSS4 (Danio rerio); Q6NUG7 (Xenopus laevis); Q9W2S2 (Drosophila melanogaster; protein name: Atg8a); Q09490 (Caenorhabditis elegans; protein name: lgg-1).

Supplementary Table S1. Genotyping primers for sequencing analysis the HEK293 knockout cell lines.

Gene	Exon	Primer direction	Primer sequence (5' to 3')	PCR product (bp)
GABARAP	1	forward	GGGTTGGTGAATAGGGAAGTGG	392
GABARAP-L1	2	forward	TGCAGCTATAACCTCATGAAGCC	400
GABARAP-L2	2	forward	CTTGCTGGGAGCTAGTAGGG	402
GABARAP	1	reverse	CACTCCTTTCATCCTGGGTCC	392
GABARAP-L1	2	reverse	ACTCCAGAGCATCCCACTCA	400
GABARAP-L2	2	reverse	TGAGGCACCCTGAACAGCA	402

Supplementary Table S2. CRISPR sequence details and genotyping results of the knockout cell lines used.

Gene symbol	Uniprot	Gene ID/ location	Targeting strategy	CRISPR gRNA (PAM)	Main clone	unique alleles	Mutation	Protein impact
GABARAP	O95166	11337/NC_000017.11	first exon	GGATCTTCTCGCCCTCAGAGCGG	C2	1	c.[152_153insT]	p.[fs*0]
GABARAP-L1	Q9H0R8	23710/NC_000012.12	second exon	AGAGAAGGCTCCAAAAGCCAGGG	C10	2	c.[352_357del];[353_356]	p.[K38Tfs*10];[K38Nfs*3]
GABARAP-L2	P60520	11345/NC_000016.1	second exon	TCCCACAGAACACAGATGCGTGG	#8	1	c.[179_180insT]	p.[C15Lfs*27]

Formatting of indels detected in the knockout cell lines (Mutation column) and their resulting proteins (Protein impact column) is according to Human Genome Variation Society (http://varnomen.hgvs.org/). Mutation positions are determined in respect to the canonical isoform annotated in Uniprot, if more than one form exists. The numbers after the asterisks represent the number of amino acids present from the first amino acid changed to the next sequential stop codon. del, deletion; ins, insertion; c., coding DNA; p., protein; fs, frame shift; *, stop codon.

185 **Supplementary Table S1. Antibodies used throughout this study.**

Antibody	Company	Species	Catalog number (antigen used for antibody production)
primary Abs:			
anti-GABARAP clone 8H5	in-house	rat	(GST-hGABARAP_aa1-117)
anti-LC3B clone 5F10	Nanotools	mouse	0231-100 (synthetic peptide from N-terminus of hLC3B)
anti-GABARAP pAb	Proteintech	rabbit	18723-1-AP (GABARAP full-length protein)
anti-GABARAP clone E1J4E	Cell Signaling	rabbit	13733 (synthetic peptide surrounding R40 of hGABARAP)
anti-GABARAP pAb clone RB11846	Abgent/antibodies-online	rabbit	AP1821a/ABIN388564 (synthetic peptide between 1-31 aa from the N-terminal region of GABARAP)
anti-GABARAPL1 clone D5R9Y	Cell Signaling	rabbit	26632 (synthetic peptide corresponding to residues near the N-terminus of hGABARAPL1)
anti-GABARAPL2 clone D1W9T	Cell Signaling	rabbit	14256 (synthetic peptide corresponding to residues near the C-terminus of hGABARAPL2)
secondary Abs:			
anti-rat IgG2a-HRP	in-house	mouse	(rat IgG 2a)
anti-rat-IgG-HRP	Sigma	goat	A9037
anti-rat-IgG Alexa Fluor 488	Jackson ImmunoResearch	goat	112-545-068
anti-rat-IgG Cy5	Jackson ImmunoResearch	donkey	712-175-153
anti-mouse IgG Alexa Fluor 647	Abcam	goat	ab150115
anti-rabbit IgG Alexa Fluor 555	Abcam	donkey	ab150074
anti-rabbit IgG Alexa Fluor 647	Abcam	donkey	ab150075

186

187

Additional References

1. Ran, F.A., et al. Genome engineering using the CRISPR-Cas9 system. *Nat Protoc* **8**, 2281-308, doi:10.1038/nprot.2013.143 (2013).
2. Dehairs, J., et al. CRISP-ID: decoding CRISPR mediated indels by Sanger sequencing. *Sci Rep* **6**, 28973, doi: 10.1038/srep28973 (2016).
3. Etard, C., et al. Tracking of Indels by DEcomposition is a Simple and Effective Method to Assess Efficiency of Guide RNAs in Zebrafish. *Zebrafish* **14**, 586-588, doi: 10.1089/zeb.2017.1454 (2017).

4.2 Lack of GABARAP-Type Proteins Is Accompanied by Altered Golgi Morphology and Surfaceome Composition

Title: Lack of GABARAP-Type Proteins Is Accompanied by Altered Golgi Morphology and Surfaceome Composition

Authors: Sanwald, J.L. *, **Dobner, J. ***, Simons, I.M., Poschmann, G., Stühler, K., Üffing, A. Hoffmann, S., Willbold D.

* Authors contributed equally

Year of publication: 2020

Published in: International Journal of Molecular Sciences

5-year Impact Factor: 4.653 (2019)

Digital object identifier (DOI): 10.3390/ijms22010085

Contribution: Surfaceome isolation, analysis of mass spectrometry data, gene ontology analysis, statistical analysis, generation of figures, main responsibility (together with Julia Sanwald) for writing and editing of the manuscript.

International Journal of
Molecular Sciences

MDPI

Communication

Lack of GABARAP-Type Proteins is Accompanied by Altered Golgi Morphology and Surfaceome Composition

Julia L. Sanwald [1,2,†], Jochen Dobner [1,†], Indra M. Simons [1,2], Gereon Poschmann [3], Kai Stühler [3,4], Alina Üffing [1,2], Silke Hoffmann [2,*] and Dieter Willbold [1,2,*]

[1] Institut für Physikalische Biologie, Heinrich-Heine-Universität Düsseldorf, Universitätsstraße 1, 40225 Düsseldorf, Germany; julia.sanwald@uni-duesseldorf.de (J.L.S.); j.dobner@fz-juelich.de (J.D.); indra.simons@uni-duesseldorf.de (I.M.S.); a.ueffing@fz-juelich.de (A.Ü.)
[2] Institute of Biological Information Processing (IBI-7: Structural Biochemistry), Forschungszentrum Jülich, Leo-Brandt-Straße, 52428 Jülich, Germany
[3] Institute of Molecular Medicine I, Proteome Research, Heinrich-Heine-Universität Düsseldorf, Universitätsstraße 1, 40225 Düsseldorf, Germany; gereon.poschmann@uni-duesseldorf.de (G.P.); kai.stuehler@uni-duesseldorf.de (K.S.)
[4] Molecular Proteomics Laboratory, Biologisch-Medizinisches Forschungszentrum (BMFZ), Heinrich-Heine-Universität Düsseldorf, Universitätsstraße 1, 40225 Düsseldorf, Germany
* Correspondence: si.hoffmann@fz-juelich.de (S.H.); d.willbold@fz-juelich.de (D.W.); Tel.: +49-2461-619389 (S.H.); +49-2461-612100 (D.W.)
† Authors contributed equally to this work.

Abstract: GABARAP (γ-aminobutyric acid type A receptor-associated protein) and its paralogues GABARAPL1 and GABARAPL2 comprise a subfamily of autophagy-related Atg8 proteins. They are studied extensively regarding their roles during autophagy. Originally, however, especially GABARAPL2 was discovered to be involved in intra-Golgi transport and homotypic fusion of post-mitotic Golgi fragments. Recently, a broader function of mammalian Atg8s on membrane trafficking through interaction with various soluble *N*-ethylmaleimide-sensitive factor-attachment protein receptors (SNAREs) was suggested. By immunostaining and microscopic analysis of the Golgi network, we demonstrate the importance of the presence of individual GABARAP-type proteins on Golgi morphology. Furthermore, triple knockout (TKO) cells lacking the whole GABARAP subfamily showed impaired Golgi-dependent vesicular trafficking as assessed by imaging of fluorescently labelled ceramide. With the Golgi apparatus being central within the secretory pathway, we sought to investigate the role of the GABARAP-type proteins for cell surface protein trafficking. By analysing the surfaceome composition of TKOs, we identified a subset of cell surface proteins with altered plasma membrane localisation. Taken together, we provide novel insights into an underrated aspect of autophagy-independent functions of the GABARAP subfamily and recommend considering the potential impact of GABARAP subfamily proteins on a plethora of processes during experimental analysis of GABARAP-deficient cells not only in the autophagic context.

Keywords: Atg8; GABARAP; Golgi apparatus; surfaceome

Citation: Sanwald, J.L.; Dobner, J.; Simons, I.M.; Poschmann, G.; Stühler, K.; Üffing, A.; Hoffmann, S.; Willbold, D. Lack of GABARAP-Type Proteins Is Accompanied by Altered Golgi Morphology and Surfaceome Composition. *Int. J. Mol. Sci.* **2021**, *22*, 85. https://dx.doi.org/10.3390/ijms22010085

Received: 6 November 2020
Accepted: 22 December 2020
Published: 23 December 2020

1. Introduction

The autophagy-related 8 (Atg8) proteins, consisting of members of the microtubule-associated proteins 1A/1B light chain 3 (MAP1LC3, hereafter LC3) subfamily and the γ-aminobutyric acid type A ($GABA_A$) receptor-associated protein (GABARAP) subfamily, are mainly recognised for their functions during autophagy.

In that context, the GABARAP-type proteins were shown to be involved in the later steps, involving autophagosome closure [1] and autophagosome-lysosome fusion [2], thereby enabling the autophagic degradation and recycling of cellular components. Interdependence of autophagy, endocytosis, and secretion pathways has been reported by a growing number of studies (reviewed in [3]). Notably, the three members of the

GABARAP family, GABARAP, GABARAP-like 1 (GABARAPL1), and GABARAP-like 2 (GABARAPL2), were initially discovered in the context of transport and trafficking processes. Early studies described an association of GABARAP with the eponymous $GABA_A$ receptor [4], and subsequently with other receptors including, e.g., the transferrin receptor (TFRC) [5]. Participation of GABARAP in vesicular transport along microtubules has also been reported [6,7]. Similarly, GABARAPL1 was also found to associate with tubulin [8] and to facilitate, e.g., κ opioid receptor trafficking [9]. The third member of the GABARAP family, GABARAPL2, was identified as an intra-Golgi transport modulator interacting both with the *N*-ethylmaleimide-sensitive factor (NSF) and the Golgi v-SNARE GOS-28 [10,11], and was reported to be required during post-mitotic Golgi reassembly [12]. In both processes, GABARAPL2 is deemed to act as a Golgi-SNARE protector [13]. Consistent with this idea, recent reports show direct interactions of all LC3 and GABARAP proteins with other types of SNARE proteins [14,15].

Furthermore, GABARAP was shown to interact with NSF [16] and 130 kDa *cis*-Golgi matrix protein (GM130), which tethers a certain pool of GABARAP proteins to the Golgi [17]. Other examples for Golgi-associated proteins interacting with GABARAP include PX-RICS, a splicing variant of Rho GTPase-activating protein (RICS) containing a phosphoinositide-binding (PX) domain that by interaction with GABARAP mediates ER-to-Golgi transport [18], and optineurin, that interacts with various human Atg8 paralogues and is involved in various cellular processes, including Golgi maintenance [19,20]

In non-mitotic mammalian cells, the Golgi apparatus consists of interconnected stacks of cisternae [21,22]. During conventional protein transport and secretion, the Golgi serves as a central trafficking organelle. After translation in the endoplasmic reticulum (ER), respective proteins are loaded into coatomer protein complex-II (COPII)-coated vesicles, transported to an ER-Golgi intermediate compartment (ERGIC), and translocated in an anterograde manner by passing the *cis*-, the *medial*-, and the *trans*-Golgi. Once a protein has reached the *trans*-Golgi network (TGN), it is sorted by coat proteins for its destination, for example the plasma membrane (PM) [23]. However, not only the transport of proteins, but also that of lipids is a central Golgi function. One of these lipids is ceramide, which is transported from the ER to the Golgi by ceramide transfer protein (CERT) [24]. Once it has reached the Golgi, ceramide is metabolised by sphingomyelin synthases. Ceramide metabolites are further transported to the PM or other membranes [25].

In this work, we employed various knockout (KO) cell lines to study the role and importance of the GABARAP subfamily in maintaining Golgi morphology and on lipid transport in a ceramide chase experiment. Finally, we comparatively analysed the surfaceomes of wild-type (WT) cells and of cells deficient for the GABARAP subfamily. Taken together, we demonstrate that the GABARAP subfamily, additionally to its well-described roles during autophagy, is involved in Golgi apparatus morphology maintenance, secretory vesicular trafficking of lipids and cell surface proteins. We thus suggest considering these autophagy-independent effects when analysing GABARAP-type protein function.

2. Results

2.1. GABARAP- and/or GABARAPL2-Deficient Cells Display Altered Golgi Morphology

To investigate the impact of individual GABARAP family members on Golgi morphology, we used a panel of human embryonic kidney 293 (HEK293) KO cell lines which exhibit a single KO (SKO), a double KO (DKO) combination, or a triple KO (TKO) of the respective GABARAP-type protein gene locus [26,27]. Golgi morphology was studied via visualisation of both the TGN by anti-TGN46 staining (Figure 1A) and the complete Golgi by BODIPY-FL C5-ceramide staining (Supplementary Figure S1). For both markers, consistent patterns for each of the analysed cell lines were observed, cross validating the observed results. Next, because of its more distinct staining profile, we categorised the signal obtained for TGN46 as compact (I), partly compact (II), and dispersed (III) Golgi pattern (Figure 1B), technically always considering all individual planes of each recorded z-stack during analysis. As summarised in Figure 1C, the vast majority of the stains

from WT cells, expressing all three GABARAP-type proteins, were classified as category I or II. Hence, WT cells had a compact or partly compact Golgi morphology in most of the cases (46% and 39%, respectively), while category III patterns indicating extensive Golgi fragmentation were rare. Cells with a GABARAPL1^{SKO} displayed only mild alterations with a slight tendency towards lower Golgi compactness, but overall showed the most WT-like phenotype of all genotypes analysed. In contrast, both GABARAPSKO and GABARAPL2^{SKO} cells showed category I patterns in less than 20% of the cases, and more than 60% the fraction of category II was considerably increased compared to WT. However, the percentage of category III was similar between all the three SKO lines and thus also resembled the WT situation. While SKO-like results were obtained for GABARAPL1/L2^{DKO} cells, GABARAP/L1^{DKO} cells showed a further reduction of category I (to 8%), accompanied with an increase of category II (to 71%). Strikingly, 36% of the GABARAP/L2^{DKO} cells exhibited even more category III Golgi structures than GABARAP/L1/L2^{TKO} cells (33%) and thus displayed the highest degree of disorganisation among all genotypes (Figure 1C). Overall, there was a significant association between the genotype analysed and Golgi compactness as calculated by Pearson's chi-squared test (χ^2 (14) = 414.62, $p < 0.001$). Based on the obtained standardised residuals (Figure 1D), which represent the standard deviation of the actual from the expected count, lack of GABARAP or GABARAPL2 alone or in combination with a lack of GABARAPL1 was associated with a shift from a compact to a more dispersed Golgi morphology. Strikingly, GABARAP/L1^{DKO} cells specifically showed an enrichment of partly compact Golgi morphology, whereas GABARAP/L2^{DKO} and GABARAP/L1/L2^{TKO} cells showed an enrichment of dispersed Golgi morphology. The representative 3D visualisations of the recorded confocal stacks after TGN46-staining can be found in Supplementary Figure S2. Consistently, also staining of the *cis*-Golgi marker protein GM130 (Figure S3A), followed by the categorization as applied for TGN46 staining (Figure 1), revealed a shift from compact to partly compact and completely dispersed Golgi morphology in GABARAP/L2^{DKO} and GABARAP/L1/L2^{TKO} cells compared to WT (Figure S3B,C). The same was true for another marker of *cis*-Golgi, Golgi reassembly-stacking protein of 65 kDa (GRASP65), which was analysed accordingly (Figure S3D–F). Taken together, these results indicate that besides GABARAPL2, at least also GABARAP seems to be involved in Golgi maintenance.

2.2. GABARAP-Type Protein Deficiency is Accompanied by Impaired Ceramide Trafficking

As the Golgi plays a fundamental role in conventional protein secretion and PM-directed transport [28], and because of the described transport-related functions of GABARAP and its two paralogues [4,9,10], we hypothesised that a lack of all GABARAP subfamily members at once should considerably impact membrane trafficking from the Golgi to the PM. It is well known that ceramide, after being transported by CERT from the ER to the Golgi apparatus, is converted to sphingomyelin, glucosylceramide, and more complex glycosphingolipids before it reaches the PM, and can therefore be used to study lipid metabolism and vesicle-mediated lipid transport from the Golgi to the PM [29]. Fluorescently labelled probes such as 6-((*N*-(7-Nitrobenz-2-Oxa-1,3-Diazol-4-yl)amino)hexanoyl)Sphingosine (NBD C_6-ceramide) or BODIPY-FL C_5-ceramide are selective stains for the Golgi in living and fixed cells [30] and therefore are applicable to study both Golgi morphology and Golgi-related lipid transport.

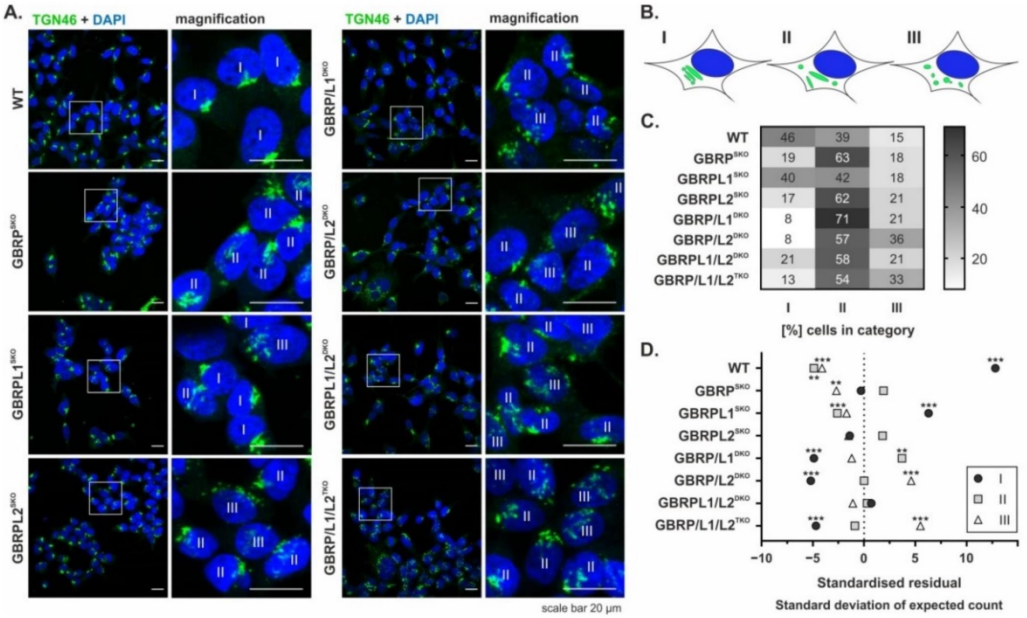

Figure 1. Influence of γ-aminobutyric acid type A ($GABA_A$) receptor-associated protein (GABARAP)-type protein deficiency on *trans*-Golgi morphology. (**A**) Wild type (WT) cells or cells deficient for one (SKO), two (DKO), or all three (TKO) GABARAP-type proteins (GBRPs) were fixed (4% PFA), immunolabelled with anti-human TGN46 antibody, and visualised by confocal fluorescence microscopy. Nuclei were counterstained with DAPI. Scale bar, 20 µm. (**B**) Scheme representing the categorisation of a compact (I), partly compact (II), and dispersed (III) Golgi structure. (**C**) Heatmap of percentage of cells per cell type assigned to Golgi category I, II, and III. Per cell type, in total ≥188 cells from ≥5 individual experiments were analysed. Cells were categorised by visual judgement. (**D**) Standardised residual values. Asterisks indicate significant differences from the mean based on the standardised residual distribution with: $|z| \geq 2.58$ ** ($p \leq 0.01$), $|z| \geq 3.29$ *** ($p \leq 0.001$).

Thus, as schematically depicted in Figure 2A, we followed the subcellular distribution of NBD C_6-ceramide over time in WT and GABARAP/L1/L2^{TKO} cells in the presence or absence of inhibitors of Golgi-related vesicular trafficking by live-cell fluorescence microscopy. The respective results are summarised in Figure 2B. While after 30 min a rather diffuse labelling of intracellular membranes was observed, after 90 min we noted an increase in staining intensity in the perinuclear region of WT cells, likely representing the Golgi apparatus. In GABARAP/L1/L2^{TKO} cells, on the other hand, the staining appeared in more punctate or vesicular structures compared to WT cells, a pattern which became even clearer after 24 h. Although WT cells also showed vesicular staining, they additionally exhibited staining at the PM which was only very faint in GABARAP/L1/L2^{TKO} cells. After 48 h, overall staining became less intense. At this timepoint, WT cells exhibited faint PM staining and diffuse intracellular labelling, while in GABARAP/L1/L2^{TKO} cells, still intensely labelled vesicular structures were found. When incubating the cells for 90 min with 10 µM Brefeldin A (BFA), ceramide additionally labelled perinuclear rims probably representing ER staining due to ER-to-Golgi fusion by BFA [31]. Interestingly, the overall staining pattern appeared similar between WT and GABARAP/L1/L2^{TKO} cells in the presence of BFA. Since BFA only inhibits vesicular transport without affecting ER-to-Golgi lipid transport by CERT [31], this indirectly suggests that GABARAP subfamily proteins do not have an impact on non-vesicular ER-to-Golgi transport of ceramide.

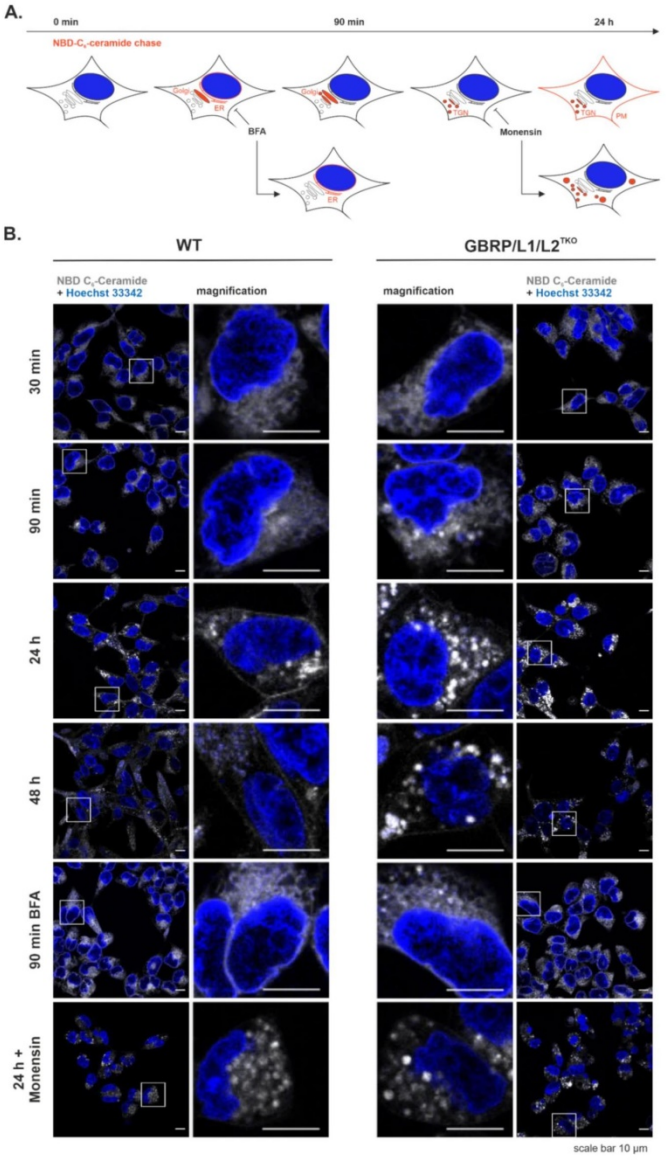

Figure 2. Intracellular ceramide distribution in WT and GABARAP/L1/L2^{TKO} cells. (**A**) Scheme representing the putative intracellular trafficking of NBD C_6-ceramide (shown here in red) in WT cells, including sites of action of BFA and Monensin. (**B**) Live cell confocal fluorescence microscopy of WT and GABARAP/L1/L2^{TKO} cells labelled with NBD C_6-ceramide (shown here in grey scale). After labelling for 1 h at 4 °C, the cells were further incubated at 37 °C for 30 min, 90 min, 24 h, or 48 h in full medium, or 90 min in full medium containing 10 µM Brefeldin A (BFA), or 24 h in full medium containing 10 µM Monensin. Nuclei were counterstained with Hoechst 33342. For each condition, one representative image from 5 individual experiments is shown. Scale bar, 10 µm.

Finally, incubation for 24 h with 10 µM Monensin, an ionophore known to cause disruption of the *trans*-Golgi apparatus [32], led to a similar phenotype in WT and GABARAP/L1/L2^{TKO} cells, resembling the ceramide distribution in GABARAP/L1/L2^{TKO} cells after 24 h without Monensin. Although, in principle, Monensin treatment can affect cell viability by causing oxidative stress [33], after 24 h of staining, cell nuclei were still intact, indicating that the cells were still viable. Taken together, these results hint towards a role of the GABARAP subfamily at least in *trans*-Golgi-to-PM trafficking of ceramide and its metabolites.

2.3. GABARAP-Type Protein Deficiency is Associated with Altered Surfaceome Composition

To investigate whether compromised Golgi integrity and impaired anterograde ceramide transport in the absence of the GABARAP subfamily is accompanied by altered cell surface protein expression, we finally analysed the surfaceome of GABARAP/L1/L2^{TKO} cells in comparison to WT cells.

To compare their cell surface proteomes, cultures of WT and GABARAP/L1/L2^{TKO} cells were exposed to surface biotinylation, lysed, subjected to streptavidin pull-down, and the protein pools obtained were processed by quantitative proteomics. Data were post-processed (for details refer to material and methods section) and normalised protein levels were analysed. As shown in Figure 3A (for raw data please refer to Supplementary Table S1), a total of 2710 different proteins were identified by this approach. By concentrating on already verified surface-located proteins, 216 of the initially identified hits were found to be surface annotated with high confidence (verified or putative) according to the cell surface protein atlas (CSPA, [34]). Notably, with 58 proteins, more than 25% of them displayed significantly different abundances and were therefore examined in more detail. Remarkably, 36 proteins displayed a significantly higher and 22 proteins displayed a significantly reduced surface abundance in GABARAP/L1/L2^{TKO} compared to WT cells. Figure 3B shows hierarchical clustering of these proteins, thereby demonstrating the high degree of conformity between individual replicates and the identity of the respective associated proteins (for more detailed information please refer to Supplementary Table S2).

Among all differentially abundant surface annotated proteins, a gene ontology (GO)/reactome pathway enrichment analysis revealed, among others, significant over-representation of proteins belonging to the category of sodium ion membrane transport ($-\log10\ p = 3.18$, 37.8-fold,) and cell adhesion ($-\log10\ p = 1.41$, 6.7-fold) as given in Figure 3C,D, respectively.

Most of the identified annotated surface proteins were single pass type I transmembrane proteins (32/58), but also single pass type II transmembrane proteins (4/58), multi pass transmembrane proteins (13/58), and GPI-anchored membrane proteins (2/58) were identified. Proteins with significantly higher abundance in GABARAP/L1/L2^{TKO} compared to WT cells included those with described or predicted transporter/channel activity or associated proteins thereof (CNNM4, CNNM2, SLC4A7, ASIC1, ABCC1, ANO6, SLC39A14, ATP1B3, ATP1A1, SLC3A2, ITPRIP) as well as receptor or receptor-associated proteins (ITGA7, ADAM15, INSR, PTPRF, TYRO3, M6PR, TFRC), cell adhesion associated proteins (PODXL2, KIRREL, NPTN, ALCAM/CD166, JAM3, CADM1), or proteins with described involvement in immunity (CD59, ALCAM/CD166, NCR3LG1, CD276, CADM1).

Proteins with known ER and/or Golgi association (GGCX, TMED7, SMPDL3B, SEL1L) were also identified within the group of higher surface abundance in GABARAP/L1/L2^{TKO} cells. Proteins with significantly lower abundance at the PM of GABARAP/L1/L2^{TKO} compared to WT cells were functionally more dispersed and included proteins associated with immunity (HLA-A, HLA-C, CD46), autophagy (CAPNS1), Ca^{2+} channel activity (CACHD1), receptor proteins (EPHA4), adhesion (MCAM/CD146, EPCAM, F11R, LGALS3BP), and proteins associated with ER and/or Golgi (RPN1, MIA3, EMC1, TMEM259, STT3A).

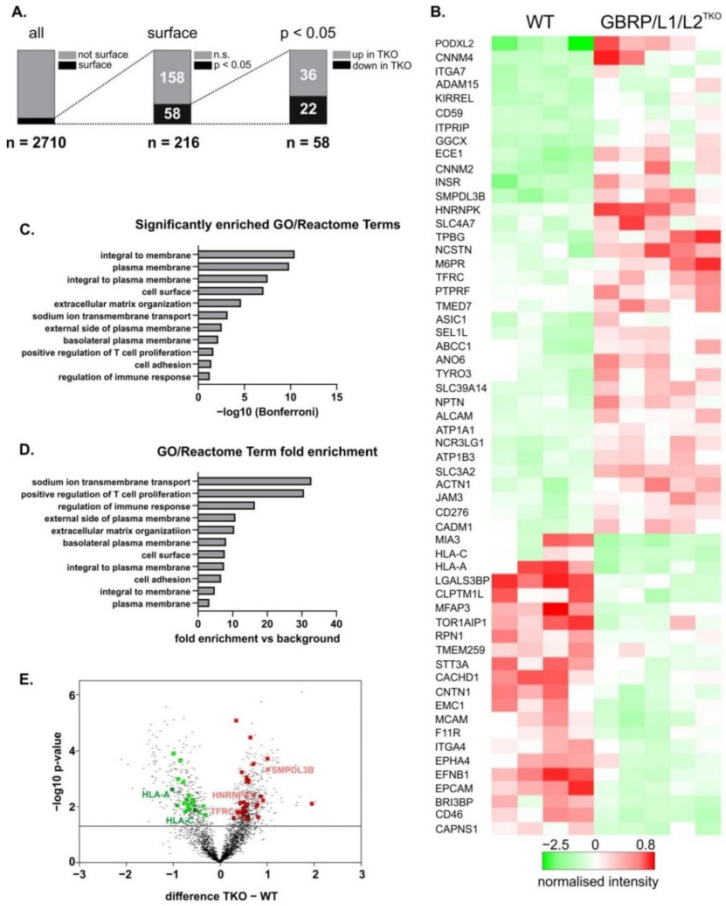

Figure 3. Comparative surfaceome composition analysis between WT and GABARAP/L1/L2^{TKO} cells. (**A**) Representation of filtering and statistical testing workflow. Mass spectrometry of isolated cell surface proteins revealed 2710 proteins of which 216 were surface annotated with high confidence (verified or putative) according to the cell surface protein atlas (CSPA) [34]. Of these 216, 58 showed significantly different abundances between WT and GABARAP/L1/L2^{TKO} cells. (**B**) Heatmap visualising the hierarchical clustering of normalised abundances for the 58 proteins described in (**A**) considering the individual replicates. (**C**,**D**) Relative enrichment of categories of identified proteins as determined by Gene Ontology (GO)/reactome pathway enrichment analysis. (**E**) Scatter plot of independent t-test results of the 2710 proteins. Proteins with significantly higher abundance in GABARAP/L1/L2^{TKO} cells compared to WT cells are marked in red and proteins with significantly lower abundance are marked in green. Proteins further addressed are highlighted. In general, proteins are denoted by their gene names.

Finally, Figure 3E displays a scatter plot of the 2710 protein hits detected in this study. Among those proteins with significantly increased abundance in cells lacking the GABARAP-type proteins (red dots), we identified with TFRC one of the earliest described GABARAP interactors [5]. Although the functional relevance of this association has not been clarified to date, it is tempting to speculate that its surface trafficking and/or correct glycosylation are dependent on any or all GABARAP-type proteins. Importantly, abundance of the major histocompatibility I (MHC-I) subtypes HLA-A and HLA-C was found to be reduced in GABARAP/L1/L2^{TKO} cells. This is intriguing, because macroautophagy

has been implicated in MHC-I antigen presentation to the cell surface [35]. As a proof of concept, we monitored TFRC and HLA-A surface levels by IB of biotinylated and pulled surface-enriched proteins and fluorescence-activated cell sorting (FACS), respectively. Surface levels of TFRC were significantly increased (Figure S4A), while surface HLA-A levels were significantly decreased (Figure S4B) in GABARAP/L1/L2^{TKO} compared to WT cells, which is in agreement with the MS data (Table S2 and related Figure 3B,E).

A further interesting hit is the acid sphingomyelinase-like phosphodiesterase 3b (SMPDL3B) which was described to regulate the levels of ceramide metabolites ceramide-1-phosphate (C1P) and sphingosine-1-phosphate (S1P) [36]. SMPDL3B is a lipid raft associated enzyme and thus involved in regulation of membrane fluidity [37]. Notably, another member of the family of sphingomyelinases, the neutral sphingomyelinase 2 (nSMase2), has been linked to LC3, which directly interacts with the nSMase2 regulator FAN (factor associated with nSMase2 activation) to specify cargo loading, e.g., of heterogeneous nuclear ribonucleoprotein K (HNRNPK), into extracellular vesicles (EVs) [38]. Very recently, we detected HNRNPK also in GABARAP-containing EVs [39]. Intriguingly, here we identified increased abundances of both SMPDL3B and HNRNPK in the absence of GABARAP-type proteins. Whether HNRNPK secretion is directly influenced by the GABARAP subfamily will thus be very interesting to determine in the future.

3. Discussion

In this work, we demonstrate that the lack of GABARAP, GABARAPL1, and GABARAPL2, both individually and combined (DKO, TKO), alter Golgi morphology, and that a lack of the whole GABARAP subfamily influences important vesicle-mediated intracellular trafficking events like ceramide distribution and surface protein expression. Our results thus extend the current knowledge regarding GABARAP-type protein functions in Golgi-related processes, which was limited to GABARAPL2 so far [13], to the two closely related paralogues GABARAP and GABARAPL1, which have not been investigated in this context yet.

First, we show that in addition to the expected effect of GABARAPL2 deficiency on Golgi morphology, also a lack of GABARAP significantly impacts the Golgi, shifting it from a compact to a more dispersed phenotype. Based on transcriptional data of HEK293 cells [40], it can be assumed that both proteins are expressed at comparable levels, thus suggesting that GABARAP and GABARAPL2 act in parallel to maintain the Golgi structure. This notion is further supported by the fact that double deficiency for GABARAP and GABARAPL2 drastically increased the Golgi disorganisation observed in this study, which would not be explainable if either protein was the only key player in this regard. The minor effect seen for GABARAPL1-deficient cells in this context might be based on the lower abundance of this paralogue in HEK293 cells, which can also be assumed from available gene expression data [40].

Golgi fragmentation and its functional impairment have been reported to be not necessarily causative, as in many Golgi fragmentation phenotypes cell surface transport processes function at normal kinetics [41–43]. Furthermore, it has been shown that Golgi fragmentation induced by gold nanoparticles, although not compromising the viability of individual cells, negatively affects cellular adhesion [44]. However, recently, DKO of GRASP55 and GRASP65 was reported to result in Golgi fragmentation accompanied by functional impairment [45]. Increased Golgi fragmentation has also been reported in the context of, e.g., cancer and neurodegenerative diseases such as Parkinson's disease or amyotrophic lateral sclerosis (ALS) as reviewed in [46]. Notably, also a KO of the GABARAP interactor GM130 led to a disruption of the Golgi, causing trafficking defects in mice [47]. Therefore, it is conceivable that alterations in Golgi morphology caused by a GABARAP-type protein deficiency as shown in this study might also have functional implications.

In line with this notion, by studying fluorescently labelled ceramide as a well-characterised example for Golgi-mediated vesicular trafficking, we discovered impaired PM-directed

transport of fluorescently labelled ceramide and its metabolites in cells deficient for all three GABARAP-type proteins.

BFA treatment, which is known to inhibit vesicular ER-to-Golgi trafficking by fusion of ER with Golgi, had no additional effect on TKO cells, indicating that non-vesicular transport of ceramide by CERT seems to be unaffected in the absence of the GABARAP subfamily.

Strikingly, treatment of WT cells with the ionophore Monensin, which is known to cause a disruption of the *trans*-Golgi apparatus [32], mimicked the effect of GABARAP/L1/L2^{TKO} on ceramide trafficking, indicating that GABARAP subfamily proteins play a role during vesicular transport of ceramide and its reaction products. Furthermore, in GABARAP/L1/L2^{TKO} cells we observed a dispersed fluorescence signal when staining not only the TGN marker TGN46, but also with the pan-Golgi marker BODIPY-FL C_5-ceramide. We thus speculate that further Golgi compartments rely on the presence of at least one GABARAP paralogue to maintain compactness. An obvious explanation for these results is provided by a Golgi-SNARE protector function already suggested for GABARAPL2 [13] which prevents uncontrolled (re-)fusion of Golgi-associated membranes, and which may be redundant for GABARAP and/or GABARAPL1.

Another explanation might be given by the reported interaction of GABARAP with the phosphatidylinositol 4-kinase IIα (PI4KIIα) [48]. PI4KIIα produces the messenger lipid phosphatidylinositol-4-phosphate (PI4P) which is, e.g., implicated in endosomal trafficking [49,50]. Locally increased PI4P levels furthermore lead to an accumulation of Golgi-derived endosomes [51]. GABARAP-type proteins might be involved in subcellular targeting of PI4P by PI4KIIα and thus influence local lipid homeostasis. Absence of GABARAP-type proteins might lead to PI4KIIα mislocalisation which could explain the accumulation of intensely NBD C_6-ceramide-labelled structures observed in this work.

Consistent with the hypothesis that Golgi fragmentation is linked with disturbed membrane transport, our comparative analysis of the surfaceomes of WT and GABARAP/L1/L2^{TKO} cells revealed a substantial number of proteins with significantly different surface abundance. This suggests that the trafficking of surface proteins is influenced by the GABARAP subfamily in a far more general manner than supposed to date. The fact that some of the surface-located proteins identified during our proteomics study were up-regulated, while others were downregulated, is particularly interesting and most likely reflects the plethora of cellular processes that GABARAP-type proteins participate in, mainly as providing interaction platforms for protein complexes [52–55]. It must thus be considered that GABARAP-type protein deficiency provokes a pleiotropy of potentially counteracting effects. For example, a reduction of overall degradation kinetics due to the function of the GABARAP-type proteins during lysosomal fusion events [2,56] might be counteracted by non-redundant roles of single paralogues, as, e.g., shown by the enhanced degradation of EGFR in the absence of GABARAP [26]. This adds further complexity to the picture and illustrates how several opposing effects might be evoked simultaneously. Accordingly, altered Golgi dynamics, probably in concert with inputs of further processes, likely determine the actual degree of the surface abundance of an individual protein. It is also conceivable that the diverse processes vary in their impact depending on the nature of each surface protein affected and the respective metabolic status of the cell system investigated. In parallel, deficiency of the GABARAP-type subfamily may additionally directly disturb the intracellular distribution of surface proteins, especially those containing functional interaction motifs [52]. Interestingly, recent results from a yet unpublished study show altered surfaceome composition of *Atg5*$^{-/-}$ mouse embryonic fibroblasts [57]. ATG5 is a key component of the LC3/GABARAP lipidation machinery which is essential for their integration into autophagy-related and unrelated membranes [53]. The effect of GABARAP subfamily protein lipidation on cell surface protein trafficking will be interesting to determine in future studies.

However, it has to be kept in mind that many surface proteins have been described to bypass the canonical Golgi secretion pathway [28]. Particularly, autophagy-dependent secretion [58] is likely influenced by a lack of GABARAP subfamily proteins. Deficiency of

GABARAP-type proteins might furthermore result in Golgi bypass of proteins which are usually secreted conventionally. This would lead to a subset of dysfunctional PM-associated proteins due to altered glycosylation patterns [59].

In summary, the presented work demonstrates a significant impact of GABARAP subfamily proteins on Golgi morphology, ceramide trafficking and surfaceome composition in cultured cells. The variety of proteins in terms of molecular function with altered surface abundance is broad and illustrates how many processes are potentially affected by the absence of all GABARAP-type proteins. We therefore conclude that the lack of the GABARAP subfamily is associated with impairment of a multitude of processes on a cellular and likely also organismal level. Hence, we suggest consideration of general cellular integrity which might be compromised on several levels. Attention should not be limited to autophagy, but also be given to phenotypical Golgi morphology and, if applicable, also to the extent of surface expression and functionality of selected proteins when working with GABARAP subfamily-deficient systems.

4. Materials and Methods

4.1. Antibodies

For immunofluorescence, primary TGN46 antibody (Cat. No. AHP500GT, Bio-Rad Laboratories, Hercules, CA, USA) was used at a concentration of 1:250. Goat anti-GRASP65 antibody (Cat. No. sc-19481, Santa Cruz Biotechnology, Dallas, TX, USA) and goat anti-GM130 antibody (Cat. No. sc-16268, Santa Cruz Biotechnology, Dallas, TX, USA) were used at a concentration of 1:50. Sheep-488 (Cat. No. A-11015, Thermo Fisher Scientific, Waltham, MA, USA) and Donkey Anti-Goat IgG H&L Alexa Fluor 647 (Cat. No. ab150131, abcam, Cambridge, UK) were used as a secondary antibody at a concentration of 1:200 and 1:250, respectively.

4.2. Eukaryotic Plasmids

KO plasmids are based on plasmid pSpCas9(BB)-2A-GFP (PX458) which was a gift from Feng Zhang (Addgene plasmid # 48138) [60].

4.3. Cell Culture

Human embryonic kidney 293 Flp-In T-REx (HEK293 Flp-In T-REx; Cat. No. R78007, Thermo Fisher Scientific, Waltham, MA, USA) cells were cultured at 37 °C and 5% CO_2 in Dulbecco's Modified Eagle's Medium (DMEM, Cat. No. D5796, Sigma-Aldrich, St. Louis, MO, USA) supplemented with 10% Foetal Calf Serum (FCS, Cat. No. F9665, Sigma-Aldrich, St. Louis, MO, USA). Cells were routinely checked for mycoplasma contamination.

4.4. CRISPR/Cas9 Mediated KO Generation

KO cell lines were generated and validated as described previously [26,27]. In brief, HEK293 Flp-In T-REx cells were transfected with KO plasmids based on pSpCas9(BB)-2A-GFP (PX458) [60] and single sorted for fluorescence protein (FP) positive signals via fluorescence-activated cell-sorting (FACS) in wells of 96 well plates. Clonal lines were recovered, and occurrence of genome editing was verified via amplification of a 400 bp product flanking the target site and sanger sequencing as well as on a protein level with specific antibodies.

4.5. Ceramide Chase

The ceramide chase experiment was conducted according to [29]. Briefly, HEK293 Flp-In T-REx cells (3×10^5) were seeded into fibronectin-coated 35 mm imaging dishes (Cat. No. 81158, ibidi, Gräfelfing, Germany) and cultured for 24 h in phenol red-free DMEM (Cat. No. 21063029, Thermo Fisher Scientific) supplemented with 10% FCS. Fluorescent NBD C_6-Ceramide, Cat. No. N1154, Thermo Fisher Scientific, Waltham, MA, USA) was dissolved in 95% ethanol to a stock concentration of 1 mM. Cells were labelled with 10 nmol/mL NBD C_6-Ceramide in Hanks' Balanced Salt Solution (Cat. No. 14025050, Thermo Fisher Scientific,

Waltham, MA, USA) containing 0.68 mg/mL bovine serum albumin (BSA) for 1 h at 4 °C in the dark. After labelling, the medium was aspirated, and the cells were rinsed two times with HBSS and further incubated at 37 °C and 5% CO_2 for 30 min, 90 min, 24 h, and 48 h. As inhibitors of Golgi function, Brefeldin A (Cat. No. 00-4506-51, Life Technologies, Carlsbad, CA, USA) and Monensin (Cat. No. 00-4505-51, Life Technologies, Carlsbad, CA, USA) were used at a concentration of 10 µM each. Cells were incubated with Hoechst 33342 (Cat. No. R37605, Invitrogen, Carlsbad, CA, USA) according to the manufacturer's instructions for nuclei staining.

4.6. Immunofluorescence (IF)

HEK293 Flp-In T-REx cells (3×10^5) were seeded in the presence of 1% penicillin/streptomycin (Cat. No. P0781, Sigma-Aldrich, St. Louis, MO, USA) into fibronectin-coated 35 mm imaging dishes (Cat. No. 81158, ibidi, Gräfelfing, Germany) and cultured for 24 h in DMEM supplemented with 10% FCS. For immunostaining with anti-TGN46 antibody, Flp-In T-REx 293 cells (Cat. No. R78007, Invitrogen, Carlsbad, CA, USA) (WT and as GABARAP(s) SKO, DKO, or TKO) were fixed at 37 °C for 10 min with 4% (*w*/*v*) paraformaldehyde (PFA; pH 6.5), washed two times with PBS, pH 7.4, and permeabilised by shaking in 0.2% Triton-X-100 for 30 min at RT. Cells were blocked by incubation in 1% BSA over night at 4 °C and incubated on the following day first with primary antibody for 1 h shaking at RT, washed three times with PBS, and then incubated with secondary antibody for 1 h shaking at RT under exclusion of light. Again, the cells were washed two times, stored in long storage buffer (0.05% sodium azide in PBS), and applied to image acquisition.

4.7. Image Acquisition–Laser Scanning Microscopy (LSM)

For image acquisition, an LSM 710 confocal microscope (Zeiss, Oberkochen Germany) equipped with ZEN black 2009 software (Zeiss, Oberkochen, Germany) and a Plan-Apochromat 63x/1.40 Oil DIC M27 objective was used. Nuclei (DAPI or Hoechst 33342) were visualised using the 405 nm channel (MBS -405), TGN46 using the 488 nm channel (MBS 488) and NBD C_6-Ceramide using the 458 nm channel (MBS 458). The number of focal planes (z-frames) with a z-distance of 0.4 µm was set between 11 and 18 or 11 and 34 for the recording of TGN46- or BODIPY-stained cells, respectively.

4.8. Image Evaluation

Image analysis was done using ImageJ/Fiji [61,62]. All individual planes of the z-stacks recorded were combined in ImageJ by applying the function „SUMSLICES". Morphology of *trans*-Golgi was qualitatively judged for each cell visually by categorizing the obtained TGN46-staining patterns according to Figure 1B. The 3D visualisations of the recorded confocal stacks from the TGN46-stains were obtained by using ZEN 2.3 SP1 FP1 (black edition). All images have been arranged using CorelDRAW 2017 (version 20, Corel Corporation, Ottawa, Canada). Data analysis and visualisation were done using GraphPad Prism (version 8, GraphPad Software, San Diego, CA, USA). Pearson's chi-square test statistic and standardised residuals representing z-scores were calculated using the statistical analysis software package (SPSS, version 22, SPSS Inc., Chicago, IL, USA).

4.9. Isolation, Identification, Quantification and Analysis of Surfaceomes

PM-based proteins were isolated as described before using the Pierce Cell Surface Protein Isolation Kit according to the manufacturer's instructions (89881, Thermo Fisher Scientific, Waltham, MA, USA) [26].

Briefly, for each individual experiment, four T75 flasks were prepared, pooled and further processed at >80% confluency. On the day of surface protein isolation, flasks were labelled with Sulfo-NHS-SS Biotin at 4 °C on a shaker. After quenching, cells were pelleted and lysed with periodical sonication and vortexing steps. Biotinylated surface proteins were bound to NeutrAvidin beads, eluted and prepared for mass spectrometric measure-

ments by in-gel digestion essentially as described [63]. Briefly, proteins were separated over a short distance (about 5 mm) in a polyacrylamide gel, stained, reduced with dithiothreitol, alkylated with iodoacetamide and digested with trypsin overnight. Peptides were extracted from the gel and reconstituted in 0.1% (*v*/*v*) trifluoroacetic acid in water. Liquid chromatography coupled with mass spectrometry were essentially carried out as described [63]. Then, 500 ng peptides per sample were separated using a 2 h gradient on C18 material using an Ultimate 3000 Rapid Separation Liquid Chromatography system (Thermo Fisher Scientific, Waltham, MA, USA) online coupled via a nano-source electrospray interface to a QExactive plus (Thermo Fisher Scientific, Waltham, MA, USA) mass spectrometer operated in positive data dependent mode. First, survey scans were recorded at a resolution of 70,000 and subsequently, up to 10 two- and three-fold charged precursors were selected by the quadrupole of the instrument (2 m/z isolation window), fragmented by higher-energy collisional dissociation and analysed at a resolution of 17,500.

Recorded mass spectra were further analysed by MaxQuant (version 1.6.2.10, Max Planck institute for biochemistry, Planegg, Germany) enabling peptide and protein identification and label-free quantification (LFQ). Searches were carried out with standard parameters if not indicated otherwise and were based on 73,112 protein entries from the homo sapiens reference proteome (UP000005640, downloaded on 18 August 2018 from the UniProt Knowledgebase). Label-free quantification was enabled as well as the 'match between runs' option. Peptides and proteins were identified at a false discovery rate of 1% and only proteins considered for further analysis showing at least 2 different peptides.

Positive hits were inferred when at least three valid values were detected in at least one group (WT or GABARAP/L1/L2^{TKO}). Log_2 transformed intensities were normalised by subtracting the median from every value. Afterwards, missing values were imputed by replacing them with random values from the normal distribution (downshift 1.8 SD, width 0.3 SD). One n (WT) was removed, because principle component analysis revealed lack of similarity to the other WT samples. Two-tailed two-sample Student's T-test was calculated (S0: 0, FDR: 5%) for a surface-annotated subset according to the CSPA [34]. Hierarchical clustering was calculated (Euclidean distance, pre-processed with κ-means, average linkage) for differentially expressed annotated surface proteins. High confidence surface proteins (CSPA annotated) with significantly different abundances between WT and GABARAP/L1/L2^{TKO} analysed for relative enrichment of gene ontology (GO)/reactome terms where all identified proteins during mass spectrometry were set as a background database.

Supplementary Materials: Supplementary Materials can be found at https://www.mdpi.com/1422-0067/22/1/85/s1.

Author Contributions: Conceptualisation, S.H. and D.W.; data curation, J.L.S., J.D., G.P., and S.H.; formal analysis, J.L.S., J.D., and S.H.; funding acquisition, K.S. and D.W.; investigation, J.L.S., J.D., I.M.S. and A.Ü.; methodology, J.L.S., J.D., and S.H.; project administration, D.W.; resources, K.S. and D.W.; supervision, S.H. and D.W.; validation, J.L.S., J.D., and S.H.; visualisation, J.L.S. and J.D.; writing—original draft preparation, J.L.S. and J.D.; writing—review and editing, J.L.S., J.D., I.M.S., G.P., K.S., A.Ü., S.H., and D.W. All authors have read and agreed to the published version of the manuscript.

Funding: This work was funded by the Deutsche Forschungsgemeinschaft (DFG, German Research Foundation)–Project-ID 267205415–SFB 1208, project B02 (D.W.) and Z01 (K.S.), and by a grant from the Jürgen Manchot Foundation, Molecules of Infection Graduate School (MOI III) (D.W. and J.D.).

Institutional Review Board Statement: Not applicable.

Informed Consent Statement: Not applicable.

Data Availability Statement: The data presented in this study are available in the article and supplementary material.

Conflicts of Interest: The authors declare no conflict of interest.

References

1. Weidberg, H.; Shvets, E.; Shpilka, T.; Shimron, F.; Shinder, V.; Elazar, Z. LC3 and GATE-16/GABARAP subfamilies are both essential yet act differently in autophagosome biogenesis. *EMBO J.* **2010**, *29*, 1792–1802. [CrossRef] [PubMed]
2. Nguyen, T.N.; Padman, B.S.; Usher, J.; Oorschot, V.; Ramm, G.; Lazarou, M. Atg8 family LC3/GABARAP proteins are crucial for autophagosome-lysosome fusion but not autophagosome formation during PINK1/Parkin mitophagy and starvation. *J. Cell Biol.* **2016**, *215*, 857–874. [CrossRef] [PubMed]
3. Birgisdottir, Å.B.; Johansen, T. Autophagy and endocytosis—Interconnections and interdependencies. *J. Cell Sci.* **2020**, *133*, jcs228114. [CrossRef] [PubMed]
4. Wang, H.; Bedford, F.K.; Brandon, N.J.; Moss, S.J.; Olsen, R.W. GABAA-receptor-associated protein links GABAA receptors and the cytoskeleton. *Nature* **1999**, *397*, 69–72. [CrossRef]
5. Green, F.; O'Hare, T.; Blackwell, A.; Enns, C.A. Association of human transferrin receptor with GABARAP. *FEBS Lett.* **2002**, *518*, 101–106. [CrossRef]
6. Asano, S.; Nemoto, T.; Kitayama, T.; Harada, K.; Zhang, J.; Harada, K.; Tanida, I.; Hirata, M.; Kanematsu, T. Phospholipase C-related catalytically inactive protein (PRIP) controls KIF5B-mediated insulin secretion. *Biol. Open* **2014**, *3*, 463–474. [CrossRef]
7. Nakajima, K.; Yin, X.; Takei, Y.; Seog, D.-H.; Homma, N.; Hirokawa, N. Molecular Motor KIF5A Is Essential for GABAA Receptor Transport, and KIF5A Deletion Causes Epilepsy. *Neuron* **2012**, *76*, 945–961. [CrossRef]
8. Mansuy, V.; Boireau, W.; Fraichard, A.; Schlick, J.-L.; Jouvenot, M.; Delage-Mourroux, R. GEC1, a protein related to GABARAP, interacts with tubulin and GABAA receptor. *Biochem. Biophys. Res. Commun.* **2004**, *325*, 639–648. [CrossRef]
9. Chen, C.; Li, J.G.; Chen, Y.; Huang, P.; Wang, Y.; Liu-Chen, L.Y. GEC1 interacts with the kappa opioid receptor and enhances expression of the receptor. *J. Biol. Chem.* **2006**, *281*, 7983–7993. [CrossRef]
10. Legesse-Miller, A.; Sagiv, Y.; Porat, A.; Elazar, Z. Isolation and characterization of a novel low molecular weight protein involved in intra-Golgi traffic. *J. Biol. Chem.* **1998**, *273*, 3105–3109. [CrossRef]
11. Sagiv, Y.; Legesse-Miller, A.; Porat, A.; Elazar, Z. GATE-16, a membrane transport modulator, interacts with NSF and the Golgi v-SNARE GOS-28. *EMBO J.* **2000**, *19*, 1494–1504. [CrossRef] [PubMed]
12. Müller, J.M.M.; Shorter, J.; Newman, R.; Deinhardt, K.; Sagiv, Y.; Elazar, Z.; Warren, G.; Shima, D.T. Sequential SNARE disassembly and GATE-16-GOS-28 complex assembly mediated by distinct NSF activities drives Golgi membrane fusion. *J. Cell Biol.* **2002**, *157*, 1161–1173. [CrossRef] [PubMed]
13. Elazar, Z.R.; Shouval, S.; Shorer, H. Involvement of LMA1 and GATE-16 family members in intracellular membrane dynamics. *Biochim. Biophys. Acta Mol. Cell Res.* **2003**, *1641*, 145–156. [CrossRef]
14. Kumar, S.; Jain, A.; Farzam, F.; Jia, J.; Gu, Y.; Choi, S.W.; Mudd, M.H.; Claude-Taupin, A.; Wester, M.J.; Lidke, K.A.; et al. Mechanism of Stx17 recruitment to autophagosomes via IRGM and mammalian Atg8 proteins. *J. Cell Biol.* **2018**, *217*, 997–1013. [CrossRef] [PubMed]
15. Gu, Y.; Princely Abudu, Y.; Kumar, S.; Bissa, B.; Choi, S.W.; Jia, J.; Lazarou, M.; Eskelinen, E.-L.; Johansen, T.; Deretic, V. Mammalian Atg8 proteins regulate lysosome and autolysosome biogenesis through SNAREs. *EMBO J.* **2019**, *38*, e101994. [CrossRef] [PubMed]
16. Kittler, J.T.; Rostaing, P.; Schiavo, G.; Fritschy, J.M.; Olsen, R.; Triller, A.; Moss, S.J. The subcellular distribution of GABARAP and its ability to interact with NSF suggest a role for this protein in the intracellular transport of GABA(A) receptors. *Mol. Cell. Neurosci.* **2001**, *18*, 13–25. [CrossRef]
17. Joachim, J.; Jefferies, H.B.J.; Razi, M.; Frith, D.; Snijders, A.P.; Chakravarty, P.; Judith, D.; Tooze, S.A. Activation of ULK Kinase and Autophagy by GABARAP Trafficking from the Centrosome Is Regulated by WAC and GM130. *Mol. Cell* **2015**, *60*, 899–913. [CrossRef]
18. Nakamura, T.; Hayashi, T.; Nasu-Nishimura, Y.; Sakaue, F.; Morishita, Y.; Okabe, T.; Ohwada, S.; Matsuura, K.; Akiyama, T. PX-RICS mediates ER-to-Golgi transport of the N-cadherin/beta-catenin complex. *Genes Dev.* **2008**, *22*, 1244–1256. [CrossRef]
19. Ryan, T.A.; Tumbarello, D.A. Optineurin: A Coordinator of Membrane-Associated Cargo Trafficking and Autophagy. *Front. Immunol.* **2018**, *9*, 1024. [CrossRef]
20. Toth, R.P.; Atkin, J.D. Dysfunction of Optineurin in Amyotrophic Lateral Sclerosis and Glaucoma. *Front. Immunol.* **2018**, *9*, 1017. [CrossRef]
21. Farquhar, M.G.; Palade, G.E. The Golgi apparatus (complex)-(1954-1981)-from artifact to center stage. *J. Cell Biol.* **1981**, *91 Pt 2*, 77s–103s. [CrossRef]
22. Ladinsky, M.S.; Mastronarde, D.N.; McIntosh, J.R.; Howell, K.E.; Staehelin, L.A. Golgi structure in three dimensions: Functional insights from the normal rat kidney cell. *J. Cell Biol.* **1999**, *144*, 1135–1149. [CrossRef] [PubMed]
23. Szul, T.; Sztul, E. COPII and COPI traffic at the ER-Golgi interface. *Physiology* **2011**, *26*, 348–364. [CrossRef] [PubMed]
24. Kumagai, K.; Hanada, K. Structure, functions and regulation of CERT, a lipid-transfer protein for the delivery of ceramide at the ER-Golgi membrane contact sites. *FEBS Lett.* **2019**, *593*, 2366–2377. [CrossRef] [PubMed]
25. Liu, Y.-Y.; Li, Y.-T. Ceramide glycosylation catalyzed by glucosylceramide synthase and cancer drug resistance. *Adv. Cancer Res.* **2013**, *117*, 59–89.
26. Dobner, J.; Simons, I.M.; Rufinatscha, K.; Hansch, S.; Schwarten, M.; Weiergraber, O.H.; Abdollahzadeh, I.; Gensch, T.; Bode, J.G.; Hoffmann, S.; et al. Deficiency of GABARAP but not its Paralogs Causes Enhanced EGF-induced EGFR Degradation. *Cells* **2020**, *9*, 1296. [CrossRef]

27. Simons, I.M.; Mohrlüder, J.; Feederle, R.; Kremmer, E.; Zobel, T.; Dobner, J.; Bleffert, N.; Hoffmann, S.; Willbold, D. The highly GABARAP specific rat monoclonal antibody 8H5 visualizes GABARAP in immunofluorescence imaging at endogenous levels. *Sci. Rep.* **2019**, *9*, 526. [CrossRef]
28. Grieve, A.G.; Rabouille, C. Golgi bypass: Skirting around the heart of classical secretion. *Cold Spring Harb Perspect Biol.* **2011**, *3*, a005298. [CrossRef]
29. Madison, K.C.; Howard, E.J. Ceramides are transported through the Golgi apparatus in human keratinocytes in vitro. *J. Invest. Dermatol.* **1996**, *106*, 1030–1035. [CrossRef]
30. Pagano, R.E.; Martin, O.C.; Kang, H.C.; Haugland, R.P. A novel fluorescent ceramide analogue for studying membrane traffic in animal cells: Accumulation at the Golgi apparatus results in altered spectral properties of the sphingolipid precursor. *J. Cell Biol.* **1991**, *113*, 1267–1279. [CrossRef]
31. Hanada, K. Intracellular trafficking of ceramide by ceramide transfer protein. Proceedings of the Japan Academy. *Ser. B Phys. Biol. Sci.* **2010**, *86*, 426–437.
32. Mollenhauer, H.H.; Morré, D.J.; Rowe, L.D. Alteration of intracellular traffic by monensin; mechanism, specificity and relationship to toxicity. *Biochim. Biophys. Acta* **1990**, *1031*, 225–246. [CrossRef]
33. Ketola, K.; Vainio, P.; Fey, V.; Kallioniemi, O.; Iljin, K. Monensin is a potent inducer of oxidative stress and inhibitor of androgen signaling leading to apoptosis in prostate cancer cells. *Mol. Cancer Ther.* **2010**, *9*, 3175–3185. [CrossRef] [PubMed]
34. Bausch-Fluck, D.; Hofmann, A.; Bock, T.; Frei, A.P.; Cerciello, F.; Jacobs, A.; Moest, H.; Omasits, U.; Gundry, R.L.; Yoon, C.; et al. A Mass Spectrometric-Derived Cell Surface Protein Atlas. *PLoS ONE* **2015**, *10*, e0121314. [CrossRef]
35. Crotzer, V.L.; Blum, J.S. Autophagy and its role in MHC-mediated antigen presentation. *J. Immunol.* **2009**, *182*, 3335–3341. [CrossRef]
36. Mitrofanova, A.; Mallela, S.K.; Ducasa, G.M.; Yoo, T.H.; Rosenfeld-Gur, E.; Zelnik, I.D.; Molina, J.; Varona Santos, J.; Ge, M.; Sloan, A.; et al. SMPDL3b modulates insulin receptor signaling in diabetic kidney disease. *Nat. Commun.* **2019**, *10*, 2692. [CrossRef]
37. Heinz, L.X.; Baumann, C.L.; Koberlin, M.S.; Snijder, B.; Gawish, R.; Shui, G.; Sharif, O.; Aspalter, I.M.; Muller, A.C.; Kandasamy, R.K.; et al. The Lipid-Modifying Enzyme SMPDL3B Negatively Regulates Innate Immunity. *Cell Rep.* **2015**, *11*, 1919–1928. [CrossRef]
38. Leidal, A.M.; Huang, H.H.; Marsh, T.; Solvik, T.; Zhang, D.; Ye, J.; Kai, F.; Goldsmith, J.; Liu, J.Y.; Huang, Y.-H.; et al. The LC3-conjugation machinery specifies the loading of RNA-binding proteins into extracellular vesicles. *Nat. Cell Biol.* **2020**, *22*, 187–199. [CrossRef]
39. Sanwald, J.L.; Poschmann, G.; Stuhler, K.; Behrends, C.; Hoffmann, S.; Willbold, D. The GABARAP Co-Secretome Identified by APEX2-GABARAP Proximity Labelling of Extracellular Vesicles. *Cells* **2020**, *9*, 1468. [CrossRef]
40. Thul, P.J.; Åkesson, L.; Wiking, M.; Mahdessian, D.; Geladaki, A.; Ait Blal, H.; Alm, T.; Asplund, A.; Björk, L.; Breckels, L.M.; et al. A subcellular map of the human proteome. *Science* **2017**, *356*, eaal3321. [CrossRef]
41. Cole, N.B.; Sciaky, N.; Marotta, A.; Song, J.; Lippincott-Schwartz, J. Golgi dispersal during microtubule disruption: Regeneration of Golgi stacks at peripheral endoplasmic reticulum exit sites. *Mol. Biol. Cell* **1996**, *7*, 631–650. [CrossRef] [PubMed]
42. Bexiga, M.G.; Simpson, J.C. Human diseases associated with form and function of the Golgi complex. *Int. J. Mol. Sci.* **2013**, *14*, 18670–18681. [CrossRef] [PubMed]
43. Gosavi, P.; Gleeson, P.A. The Function of the Golgi Ribbon Structure—An Enduring Mystery Unfolds! *BioEssays* **2017**, *39*, 1700063. [CrossRef] [PubMed]
44. Ma, X.; Sun, J.; Zhong, L.; Wang, Y.; Huang, Q.; Liu, X.; Jin, S.; Zhang, J.; Liang, X.-J. Evaluation of Turning-Sized Gold Nanoparticles on Cellular Adhesion by Golgi Disruption in Vitro and in Vivo. *Nano Lett.* **2019**, *19*, 8476–8487. [CrossRef] [PubMed]
45. Bekier, M.E.; Wang, L.; Li, J.; Huang, H.; Tang, D.; Zhang, X.; Wang, Y. Knockout of the Golgi stacking proteins GRASP55 and GRASP65 impairs Golgi structure and function. *Mol. Biol. Cell* **2017**, *28*, 2833–2842. [CrossRef]
46. Makhoul, C.; Gosavi, P.; Gleeson, P.A. Golgi Dynamics: The Morphology of the Mammalian Golgi Apparatus in Health and Disease. *Front. Cell Dev. Biol.* **2019**, *7*, 112. [CrossRef]
47. Liu, C.; Mei, M.; Li, Q.; Roboti, P.; Pang, Q.; Ying, Z.; Gao, F.; Lowe, M.; Bao, S. Loss of the golgin GM130 causes Golgi disruption, Purkinje neuron loss, and ataxia in mice. *Proc. Natl. Acad. Sci. USA* **2017**, *114*, 346–351. [CrossRef]
48. Wang, H.; Sun, H.-Q.; Zhu, X.; Zhang, L.; Albanesi, J.; Levine, B.; Yin, H. GABARAPs regulate PI4P-dependent autophagosome:lysosome fusion. *Proc. Natl. Acad. Sci. USA* **2015**, *112*, 7015–7020. [CrossRef]
49. Minogue, S.; Waugh, M.G.; De Matteis, M.A.; Stephens, D.J.; Berditchevski, F.; Hsuan, J.J. Phosphatidylinositol 4-kinase is required for endosomal trafficking and degradation of the EGF receptor. *J. Cell Sci.* **2006**, *119*, 571–581. [CrossRef]
50. Henmi, Y.; Morikawa, Y.; Oe, N.; Ikeda, N.; Fujita, A.; Takei, K.; Minogue, S.; Tanabe, K. PtdIns4KIIα generates endosomal PtdIns(4)P and is required for receptor sorting at early endosomes. *Mol. Biol. Cell* **2016**, *27*, 990–1001. [CrossRef]
51. Mao, D.; Lin, G.; Tepe, B.; Zuo, Z.; Tan, K.L.; Senturk, M.; Zhang, S.; Arenkiel, B.R.; Sardiello, M.; Bellen, H.J. VAMP associated proteins are required for autophagic and lysosomal degradation by promoting a PtdIns4P-mediated endosomal pathway. *Autophagy* **2019**, *15*, 1214–1233. [CrossRef] [PubMed]
52. Johansen, T.; Lamark, T. Selective Autophagy: ATG8 Family Proteins, LIR Motifs and Cargo Receptors. *J. Mol. Biol.* **2020**, *432*, 80–103. [CrossRef]

53. Martens, S.; Fracchiolla, D. Activation and targeting of ATG8 protein lipidation. *Cell Discov.* **2020**, *6*, 23. [CrossRef] [PubMed]
54. Schaaf, M.B.; Keulers, T.G.; Vooijs, M.A.; Rouschop, K.M. LC3/GABARAP family proteins: Autophagy-(un)related functions. *FASEB J.* **2016**, *30*, 3961–3978. [CrossRef] [PubMed]
55. Wesch, N.; Kirkin, V.; Rogov, V.V. Atg8-Family Proteins-Structural Features and Molecular Interactions in Autophagy and Beyond. *Cells* **2020**, *9*, 2008. [CrossRef]
56. Vaites, L.P.; Paulo, J.A.; Huttlin, E.L.; Harper, J.W. Systematic Analysis of Human Cells Lacking ATG8 Proteins Uncovers Roles for GABARAPs and the CCZ1/MON1 Regulator C18orf8/RMC1 in Macroautophagic and Selective Autophagic Flux. *Mol. Cell Biol.* **2018**, *38*, e00392-17. [CrossRef] [PubMed]
57. Baines, K.; Lane, J.D. The ATG5 Interactome Links Clathrin Vesicular Trafficking With The ATG8 Lipidation Machinery For Autophagosome Assembly. *bioRxiv* **2019**, 769059. [CrossRef]
58. Keulers, T.; Schaaf, M.; Rouschop, K. Autophagy-Dependent Secretion: Contribution to Tumor Progression. *Front. Oncol.* **2016**, *6*, 251. [CrossRef]
59. Chang, I.J.; He, M.; Lam, C.T. Congenital disorders of glycosylation. *Ann. Transl. Med.* **2018**, *6*, 477. [CrossRef]
60. Ran, F.A.; Hsu, P.D.; Wright, J.; Agarwala, V.; Scott, D.A.; Zhang, F. Genome engineering using the CRISPR-Cas9 system. *Nat. Protoc.* **2013**, *8*, 2281–2308. [CrossRef]
61. Schindelin, J.; Arganda-Carreras, I.; Frise, E.; Kaynig, V.; Longair, M.; Pietzsch, T.; Preibisch, S.; Rueden, C.; Saalfeld, S.; Schmid, B. Fiji: An open-source platform for biological-image analysis. *Nat. Methods* **2012**, *9*, 676–682. [CrossRef] [PubMed]
62. Schneider, C.A.; Rasband, W.S.; Eliceiri, K.W. NIH Image to ImageJ: 25 years of image analysis. *Nat. Methods* **2012**, *9*, 671–675. [CrossRef] [PubMed]
63. Grube, L.; Dellen, R.; Kruse, F.; Schwender, H.; Stuhler, K.; Poschmann, G. Mining the Secretome of C2C12 Muscle Cells: Data Dependent Experimental Approach to Analyze Protein Secretion Using Label-Free Quantification and Peptide Based Analysis. *J. Proteome Res.* **2018**, *17*, 879–890. [CrossRef] [PubMed]

Lack of GABARAP-type proteins is accompanied by altered Golgi morphology and surfaceome composition

Julia L. Sanwald [1,2 †], Jochen Dobner [1 †], Indra M. Simons [1,2], Gereon Poschmann [3], Kai Stühler [3,4], Alina Üffing [1,2], Silke Hoffmann [2], Dieter Willbold [1,2]

[1] Institut für Physikalische Biologie, Heinrich-Heine-Universität Düsseldorf, Universitätsstraße 1, 40225 Düsseldorf, Germany
[2] Institute of Biological Information Processing (IBI-7: Structural Biochemistry), Forschungszentrum Jülich, Leo-Brandt-Straße, 52428 Jülich, Germany
[3] Institute of Molecular Medicine I, Proteome Research, Heinrich-Heine-Universität Düsseldorf, Universitätsstraße 1, 40225 Düsseldorf, Germany; gereon.poschmann@uni-duesseldorf.de (G.P.); kai.stuehler@uni-duesseldorf.de (K.S.)
[4] Molecular Proteomics Laboratory, Biologisch-Medizinisches Forschungszentrum (BMFZ), Heinrich-Heine-Universität Düsseldorf, Universitätsstraße 1, 40225 Düsseldorf, Germany
[†] Authors contributed equally to this work

Supplementary Methods are related to Figures S1, S4

Supplementary Figure S1 is related to Figure 1

Supplementary Figure S2 is related to Figure 1

Supplementary Figure S3 is related to Figure 1

Supplementary Figure S4 is related to Figure 3

Supplementary Figure S5 is related to Figure S4

Supplementary Table S1 is related to Figure 3B

Supplementary Methods

Live-cell imaging with fluorescently labelled ceramide

HEK293 Flp-In T-REx cells (3×10^5) were seeded into fibronectin coated 35 mm imaging dishes (Cat. No. 81158, ibidi) and cultured for 24 h in DMEM supplemented with 10 % FCS. Staining of the cells (WT and as GABARAP(s) SKO, DKO, or TKO) with BODIPY-FL C5-ceramide (Cat. No. B-22650, Life Technologies) was conducted according to the manufacturer's instructions. Briefly, cells were rinsed in HBSS and incubated for 30 min at 4 °C with 5 µM BODIPY-FL C5-ceramide. Then, the cells were rinsed three times in ice-cold HBSS and incubated 30 min in phenol red-free DMEM supplemented with 10 % FCS. Finally, the cells were rinsed once in HBSS and stored in phenol red-free DMEM supplemented with 10 % FCS. Cells were incubated with Hoechst 33342 (Cat. No. R37605, Invitrogen, Carlsbad, CA, USA) according to the manufacturer's instructions for nuclei staining. BODIPY-FL C5-ceramide was visualised by LSM using the 488 nm channel (MBS 488).

Fluorescence-activated cell sorting

Surface levels of HLA-A were analysed under steady-state conditions in HEK293 WT and GABARAP/L1/L2^{TKO} cells. In brief, 1 * 10^6 cells of 90 % confluent cells were washed twice with ice-cold PBS and resuspended in 100 µl ice-cold FACS buffer (2 mM EGTA, 1 %FBS, 25 mM HEPES in PBS) containing 1:20 diluted HLA-A3 antibody conjugated to PE (ThermoFisher Scientific, 12-5754-42) or APC (ThermoFisher Scientific, 17-5754-42). Isotype controls (ThermoFisher Scientific, PE: Mouse IgG2a K, 12-4724-81, APC: Mouse IgG2a K, 17-4724-81) After 30 min incubation on ice in the dark, cells were washed thrice with ice-cold FACS buffer, resuspended in 0.5 ml FACS buffer and analysed by flow cytometry (Aria III, BD Bioscience, Franklin Lakes, USA). Cells were gated according to their size (SSC-A x FSC-A) and being single cells (FSC-A x FSC-H). Median fluorescence intensity of GABARAP/L1/L2^{TKO} cells was calculated relative to HEK293 WT intensity. Statistical significance was inferred as calculated by Welch's t-test using GraphPad Prism (version 8).

Immunoblotting

For proof-of-method immunoblotting, 10 µg of surface-enriched proteins were diluted with 4 x Lämmli's buffer (250 mM Tris-HCl pH 6.8, 40 % glycerol, 5 % SDS, 0.005 % bromophenol blue) containing 8 % fresh 2-mercaptoethanol. After samples were boiled for 5 min at 95 °C, surface fraction lysates were applied on 8 % SDS-PAA gel. After gel electrophoresis, semi-dry blotting of proteins onto 0.4 µm µm polyvinyliden fluoride membrane was performed for 1 h 30 min at 77 mA constant current. Unspecific binding sites were blocked for 1 h at RT with 5 % BSA in TBS-T (TBS, 0.1 % Tween-20) and membrane incubated with primary antibody for TFRC (#13208, Cell Signaling Technologies, Danvers, USA) at 1:1000 dilution overnight at 4 °C. After washing (three times with TBS-T) and incubation with 1:5000 diluted fluorescently labelled secondary antibody (ab150083, abcam) for 1 h at RT, target protein was

visualised using BioRad Imager. Statistical significance was inferred as calculated by Student's t-test using GraphPad Prism (version 8).

3

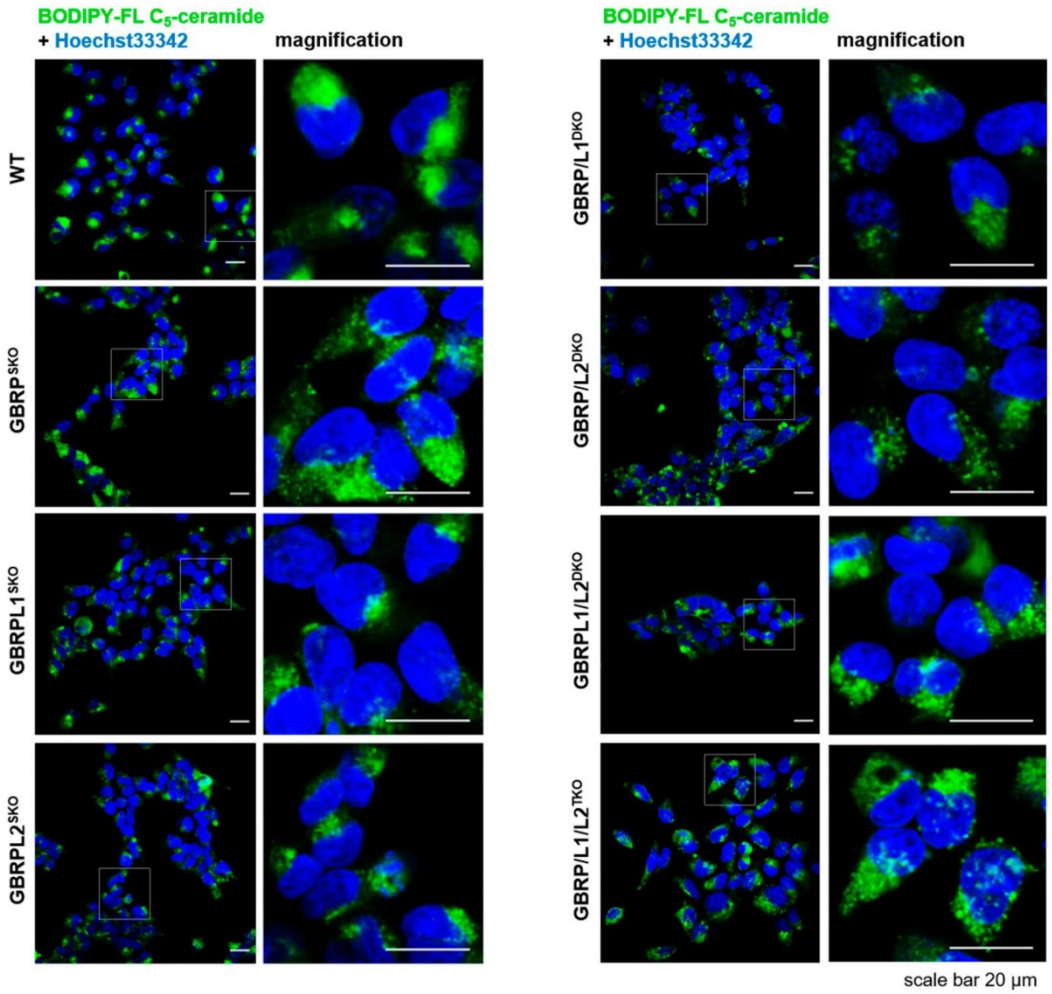

Supplementary Figure S1. Loss of GABARAP leads to a redistribution of Golgi-localised ceramide. HEK^{WT} (WT) or HEK cells with deficiency for one (SKO), two (DKO), or all three (TKO) of the GABARAPs (GBRPs) were cultured for 24 h at 37 °C and 5 % CO_2 in fibronectin coated 35 mm imaging dishes, stained with BODIPY-FL C_5-ceramide according to the manufacturer's instructions (Cat. No. B-22650, Life Technologies), and visualised by confocal fluorescence microscopy. Nuclei were counterstained with Hoechst 33342. Cells were recorded as z-stacks and the slices of each stack were combined in ImageJ by applying the function „SUMSLICES". For each condition, a representative image of five frames is shown. Scale bar, 20 µm.

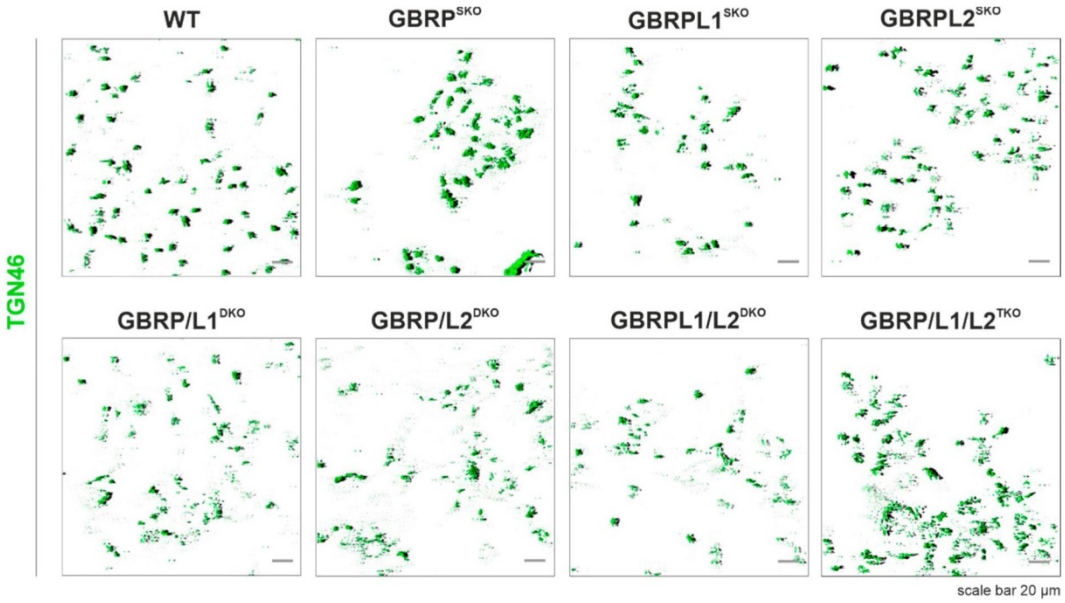

Supplementary Figure S2. 3D visualisation of the *trans*-Golgi morphology in HEK293 WT cells and under various GABARAP-type protein deficiencies. Individual planes of each stack were displayed as 3D image in ZEN 2.3 SP1 FP1 (black edition). The reconstructions relate to the respective images in Figure 1A. Scale bar, 20 µm.

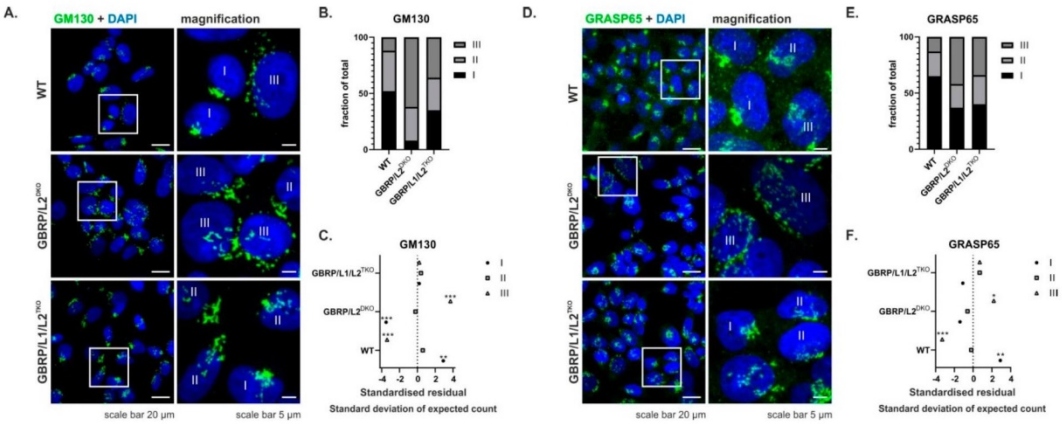

Supplementary Figure S3. Influence of GABARAP-type protein deficiency on *cis*-Golgi morphology. (A) WT, GABARAP/L2^{DKO} or GABARAP/L1/L2^{TKO} cells were fixed (4 % PFA), immunolabelled with anti-human GM130 antibody, and visualised by confocal fluorescence microscopy. Nuclei were counterstained with DAPI. Scale bar total = 20 µm, scale bar zoom-in = 5 µm. (B) Distribution of percentage of cells per cell type assigned to Golgi structure category I (compact), II (partly compact), and III (dispersed) according to GM130 staining. (C) Standardised residual distribution of analysed genotypes. Per cell type, in total ≥ 63 cells from three individual experiments were analysed and categorised by visual judgement. Asterisks indicate significant differences from the mean based on the standardised residual distribution with: $|z| \geq 2.58$ ** ($p \leq 0.01$), $|z| \geq 3.29$ *** ($p \leq 0.001$). (D) WT, GABARAP/L2^{DKO} or GABARAP/L1/L2^{TKO} cells were fixed (4 % PFA), immunolabelled with anti-human GRASP65 antibody, and visualised by confocal fluorescence microscopy. Nuclei were counterstained with DAPI. Scale bar total = 20 µm, scale bar zoom-in = 5 µm. (B) Distribution of percentage of cells per cell type assigned to Golgi structure category I (compact), II (partly compact), and III (dispersed) according to GRASP65 staining. (C) Standardised residual distribution of analysed genotypes. Per cell type, in total ≥ 103 cells were analysed and categorised by visual judgement. Asterisks indicate

significant differences from the mean based on the standardised residual distribution with: $|z| \geq 1.96$ * ($p \leq 0.05$), $|z| \geq 2.58$ ** ($p \leq 0.01$), $|z| \geq 3.29$ *** ($p \leq 0.001$).

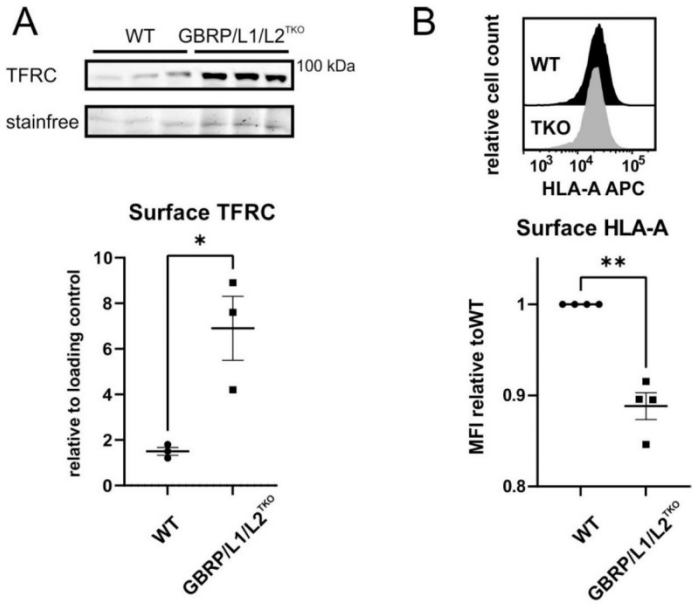

Supplementary Figure S4. Validation of surface proteome mass-spectrometry analysis by two independent methods. (A) Cell surface protein-enriched fractions were analysed by immunoblot. Surface levels of TFRC are shown for three independent experiments. Asterisk marks significant differences between GABARAP/L1/L2^{TKO} and WT cells as calculated using independent t-test. $p \leq 0.05$ = *. (B) Surface levels of MHC-I subtype HLA-A were analysed by fluorescence-activated cell sorting. Representative histograms of four independent experiments of single cells stained with HLA-A antibody are shown. Significant differences of median fluorescence intensities (MFI) between WT and GABARAP/L1/L2^{TKO} cells are marked by asterisk as calculated by Welch's t-test. $p \leq 0.01$ = **. GBRP = GABARAP. APC = Allophycocyanin.

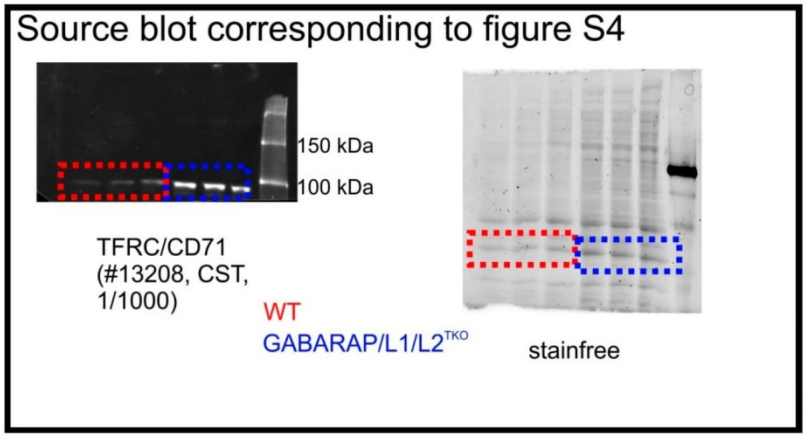

Supplementary Figure S5. Source blot corresponding to Figure S4. Regions used for display and analysis are indicated.

Supplementary Table S1. Raw data of mass-spectrometry analysis of surface-enriched proteomes of HEK293 WT and GABARAP/L1/L2^{TKO} cells can be found in the attached excel file Table S1 Mass-spectrometry data set.

Supplementary Table S2. Significantly different expressed surface-annotated proteins. For consistency, proteins are sorted as depicted in Figure 3B. Respective raw data are given in Supplementary Table S1.

GENE SYMBOL	GENE NAME	GENE ID	UNIPROT	CSPA CONFIDENCE LEVEL	DIFFERENCE TKO-WT
PODXL2	podocalyxin like 2	50512	Q9NZ53	1	1.95089
CNNM4	cyclin and CBS domain divalent metal cation transport mediator 4	26504	Q6P4Q7	1	0.801802
ITGA7	integrin subunit alpha 7	3679	Q13683	1	0.516933
ADAM15	ADAM metallopeptidase domain 15	8751	Q13444	1	0.575086
KIRREL	Kin of IRRE-like protein 1	55243	Q96J84	1	0.514684
CD59	CD59 molecule (CD59 blood group)	966	P13987	1	0.559599
ITPRIP	inositol 1,4,5-trisphosphate receptor interacting protein	85450	Q8IWB1	1	0.417335
GGCX	gamma-glutamyl carboxylase	2677	P38435	2	0.703851
ECE1	endothelin converting enzyme 1	1889	P42892	1	1.0075
CNNM2	cyclin and CBS domain divalent metal cation transport mediator 2	54805	Q9H8M5	1	0.859415
INSR	Insulin receptor	3643	P06213	1	0.912155
SMPDL3B	sphingomyelin phosphodiesterase acid like 3B	27293	Q92485	1	1.01647
HNRNPK	heterogeneous nuclear ribonucleoprotein K	3190	P61978	1	0.694312
SLC4A7	solute carrier family 4 member 7	9497	Q9Y6M7	1	0.592821
TPBG	trophoblast glycoprotein	7162	Q13641	1	0.787366
NCSTN	nicastrin	23385	Q92542	1	0.772031
M6PR	mannose-6-phosphate receptor, cation dependent	4074	P20645	1	0.557621
TFRC	transferrin receptor	7037	P02786	1	0.422732
PTPRF	protein tyrosine phosphatase receptor type F	5792	P10586	1	0.287566
TMED7	transmembrane p24 trafficking protein 7	51014	Q9Y3B3	1	0.367156
ASIC1	acid sensing ion channel subunit 1	41	P78348	1	0.541489
SEL1L	SEL1L adaptor subunit of ERAD E3 ubiquitin ligase	6400	Q9UBV2	1	0.604953
ABCC1	ATP binding cassette subfamily C member 1	4363	P33527	1	0.578134
ANO6	anoctamin 6	196527	Q4KMQ2	1	0.478563
TYRO3	TYRO3 protein tyrosine kinase	7301	Q06418	1	0.544295
SLC39A14	solute carrier family 39 member 14	23516	Q15043	1	0.594535
NPTN	neuroplastin	27020	Q9Y639	1	0.499769

ALCAM	activated leukocyte cell adhesion molecule	214	Q13740	1	0.458814
ATP1A1	ATPase Na+/K+ transporting subunit alpha 1	476	P05023	1	0.340416
NCR3LG1	natural killer cell cytotoxicity receptor 3 ligand 1	374383	Q68D85	1	0.578246
ATP1B3	ATPase Na+/K+ transporting subunit beta3	483	P54709	1	0.570178
SLC3A2	solute carrier family 3 member 2	6520	P08195	1	0.643518
ACTN1	actinin alpha 1	87	P12814	1	0.712156
JAM3	junctional adhesion molecule 3	83700	Q9BX67	1	0.468754
CD276	CD276 molecule	80381	Q5ZPR3	1	0.428201
CADM1	cell adhesion molecule 1	23705	Q9BY67	1	0.497293
MIA3	MIA SH3 domain ER export factor 3	375056	5JRA6	1	-0.909785
HLA-C	major histocompatibility complex, class I, C	3107	P10321	1	-0.539395
HLA-A	major histocompatibility complex, class I, A	3105	P04439	1	-1.0196
LGALS3BP	galectin 3 binding protein	3959	Q08380	1	-0.991107
CLPTM1L	cleft palate transmembrane protein 1-like	81037	Q96KA5	2	-0.741051
MFAP3	microfibril associated protein 3	4238	P55082	1	-0.768297
TOR1AIP1	torsin 1A interacting protein 1	26092	Q5JTV8	2	-0.685934
RPN1	ribophorin 1	6184	P04843	1	-0.358063
TMEM259	transmembrane protein 259	91304	Q4ZIN3	2	-0.314032
STT3A	STT3 oligosaccharyltransferase complex catalytic subunit A	3703	P46977	2	-0.59739
CACHD1	cache domain containing 1	57685	Q5VU97	1	-0.580828
CNTN1	contactin 1	1272	Q12860	1	-0.711767
EMC1	ER membrane protein complex subunit 1	23065	Q8N766	1	-0.646965
MCAM	melanoma cell adhesion molecule	4162	P43121	1	-0.682648
F11R	F11 receptor	50848	Q9Y624	1	-0.478582
ITGA4	integrin subunit alpha 4	3676	P13612	1	-0.446824
EPHA4	EPH receptor A4	2043	P54764	1	-0.57585
EFNB1	ephrin B1	1947	P98172	1	-0.896389
EPCAM	epithelial cell adhesion molecule	4072	P16422	1	-0.78135
BRI3BP	BRI3 binding protein	140707	Q8WY22	2	-0.665538
CD46	CD46 molecule	4179	P15529	1	-0.848529
CAPNS1	calpain small subunit 1	826	P04632	1	-0.562122

10

4.3 Deficiency of GABARAP but Not Its Paralogs Causes Enhanced EGF-Induced EGFR Degradation

Title: Deficiency of GABARAP but Not Its Paralogs Causes Enhanced EGF-induced EGFR Degradation

Authors: **Dobner, J.;** Simons, I.M.; Rufinatscha, K.; Hänsch, S.; Schwarten, M.; Weiergräber, O.H.; Abdollahzadeh, I.; Gensch, T.; Bode, J.G.; Hoffmann, S.; Willbold, D.

Year of publication: 2020

Published in: Cells

5-year Impact Factor: 5.276 (2018)

Digital object identifier (DOI): 10.3390/cells9051296

Contribution: Project development (theory and methodology), main responsibility for writing and editing of the manuscript (original and revised versions), generation and validation of the human hepatoma (Huh) 7.5 (Huh7.5) and HEK293 CRISPR/Cas9 KO and KI cell lines, IB experiments (EGFR degradation, inhibitor experiments), gene expression experiments, surface protein isolation experiments, FACS-based EGF uptake experiment, co-immunoprecipitation experiments, transient transfection experiments, statistical analysis, generation of figures and tables.

Reprint permission: This section contains a complete reprint of the publication published in Cells (www.mdpi.com/journal/cells).

.

cells

MDPI

Article

Deficiency of GABARAP but Not Its Paralogs Causes Enhanced EGF-Induced EGFR Degradation

Jochen Dobner [1], Indra M. Simons [1,2], Kerstin Rufinatscha [3], Sebastian Hänsch [4], Melanie Schwarten [2], Oliver H. Weiergräber [2], Iman Abdollahzadeh [2,5], Thomas Gensch [5], Johannes G. Bode [3], Silke Hoffmann [2] and Dieter Willbold [1,2,*]

1 Institut für Physikalische Biologie, Heinrich-Heine-Universität Düsseldorf, 40225 Düsseldorf, Germany; j.dobner@fz-juelich.de (J.D.); i.simons@fz-juelich.de (I.M.S.)
2 Institute of Biological Information Processing: Structural Biochemistry (IBI-7), Forschungszentrum Jülich, 52425 Jülich, Germany; m.schwarten@fz-juelich.de (M.S.); o.h.weiergraeber@fz-juelich.de (O.H.W.); i.abdollahzadeh@fz-juelich.de (I.A.); si.hoffmann@fz-juelich.de (S.H.)
3 Department of Gastroenterology, Hepatology and Infectiology, University Hospital, Heinrich-Heine-Universität Düsseldorf, 40225 Düsseldorf, Germany; rufinats@hhu.de (K.R.); Johannes.Bode@med.uni-duesseldorf.de (J.G.B.)
4 Department of Biology, Center for Advanced Imaging (CAi), Heinrich-Heine-Universität Düsseldorf, 40225 Düsseldorf, Germany; Sebastian.Haensch@uni-duesseldorf.de
5 Institute of Biological Information Processing: Molecular and Cell Physiology (IBI-1), Forschungszentrum Jülich, 52425 Jülich, Germany; t.gensch@fz-juelich.de
* Correspondence: d.willbold@fz-juelich.de; Tel.: +49-2461-61-2100

Received: 27 February 2020; Accepted: 20 May 2020; Published: 22 May 2020

Abstract: The γ-aminobutyric acid type A receptor-associated protein (GABARAP) and its close paralogs GABARAPL1 and GABARAPL2 constitute a subfamily of the autophagy-related 8 (Atg8) protein family. Being associated with a variety of dynamic membranous structures of autophagic and non-autophagic origin, Atg8 proteins functionalize membranes by either serving as docking sites for other proteins or by acting as membrane tethers or adhesion factors. In this study, we describe that deficiency for GABARAP alone, but not for its close paralogs, is sufficient for accelerated EGF receptor (EGFR) degradation in response to EGF, which is accompanied by the downregulation of EGFR-mediated MAPK signaling, altered target gene expression, EGF uptake, and EGF vesicle composition over time. We further show that GABARAP and EGFR converge in the same distinct compartments at endogenous GABARAP expression levels in response to EGF stimulation. Furthermore, GABARAP associates with EGFR in living cells and binds to synthetic peptides that are derived from the EGFR cytoplasmic tail in vitro. Thus, our data strongly indicate a unique and novel role for GABARAP during EGFR trafficking.

Keywords: EGFR; GABARAP; receptor trafficking; degradation; Atg8; genome editing

1. Introduction

The epidermal growth factor receptor (EGFR/ErbB1) is a plasma membrane bound receptor tyrosine kinase (RTK) that is expressed in many different cell types and plays an important role in numerous processes, such as development, tissue homeostasis, and regeneration [1,2], by binding a variety of ligands, including transforming growth factor-α (TGF α) [3], amphiregulin [4], and the eponymous epidermal growth factor [5]. The binding of these ligands causes either homo- or heterodimerization with the other members of the erythroblastosis oncogene B (ErbB) superfamily ErbB2, ErbB3, and ErbB4 [6], leading to intrinsic kinase activation and autophosphorylation of distinct tyrosine residues in the C-terminal cytoplasmic region of the receptor [7,8]. The subsequent

recruitment and activation of various downstream signaling pathways causes a plethora of cellular effects, depending on which pathway is activated, including cell growth, proliferation, differentiation, and motility [9–11]. Dephosphorylation and/or degradation of the activated receptor are necessary to strictly control and regulate these signaling events, thus preventing the sustained activation and uncontrolled cell growth that are found in many types of cancer [12,13].

Ligand-associated EGFR undergoes rapid internalization [14,15], which can either be clathrin-dependent [16] or independent [17]. Whereas the former mainly occurs under low ligand concentrations, leading to sustained EGFR signaling and enhanced recycling back to the plasma membrane through a non-degradative sorting pathway, with the latter being accompanied by monoubiquitination at several sites and packaging of activated receptors in intraluminal vesicles (ILV) of multivesicular bodies (MVB), followed by maturation to late endosomes and ultimately fusion with the lysosome where the receptor is degraded by pH-dependent hydrolases [18].

Autophagy is an intracellular degradation pathway [19]. Upon stress conditions, such as nutrient starvation, but also in response to oxidative stress and pathogen infection [20], membrane cisternae in the cytosol of cells arise and engulf cargo either non-selectively or selectively. Their closure finally yields double-membrane vesicles, termed autophagosomes. Ultimately, their fusion with the lysosome leads to the degradation of autophagosomal content [21]. This enables cells to survive by repurposing amino acids and other resources, to get rid of damaged organelles [22], but also to eliminate pathogens [23]. The autophagic degradation of RET (receptor tyrosine kinase Proto-oncogene tyrosine-protein kinase receptor) and associated proto-oncogene tyrosine-protein kinase SRC via autophagy has also been reported [24,25]. Apart from degradation, components of the autophagic machinery are also implicated in the secretion processes by facilitating a form of unconventional protein secretion [26,27]. Proteins of the autophagy-related (Atg) protein family have first been identified in yeast and they are involved in every step of the autophagic process [28,29]. While, in yeast only a single *Atg8* gene exists [30], in mammalian cells the family has expanded into a number of paralogs [31]. The microtubule-associated proteins 1A/1B light chain 3 (LC3) proteins A, B, and C are grouped in the LC3 subfamily, whereas γ-aminobutyric acid type A receptor-associated protein (GABARAP) and its two paralogs GABARAPL1 and GABARAPL2 form the GABARAP subfamily, according to their degree of relation. Besides (canonical) autophagy, GABARAP subfamily members have been described to play pivotal roles in many cellular processes, such as immunity, receptor trafficking, unconventional secretion of leaderless proteins [32–34], and interaction with viral proteins [35–37]. However, because they share high sequence and structural similarity [38] within and between subfamilies, the elucidation of their exact and especially non-redundant functions requires the development of highly specific and sensitive readout systems. Progress towards this goal has been made in the field of autophagy, especially regarding their roles during autophagosome biogenesis (e.g., [39–41]) as well as selective cargo loading via cargo receptor interaction ([42–44]). Respective overviews can be found in several recent reviews (e.g., [32,34,45–48]). The direct binding of interaction partners to Atg8 proteins is mediated by a canonical interaction motif, generally known as LC3-interacting region (LIR) or GABARAP interaction motif (GIM) in the case of GABARAP subfamily ligands [49], which can reach various levels of specificity [50]. Very recently, an additional motif, related to the ubiquitin interacting motif (UIM), was described utilizing a binding region localized opposite to the LIR/GIM-docking site on the Atg8 protein surface [51].

Additionally, it has long been known that the proteins of the GABARAP subfamily are involved in the regulation of cell surface receptor trafficking. GABARAP was first described to be associated to the name-giving GABAA receptor [52] and implicated in its trafficking [53]. It was also described to be associated with the Transferrin receptor [54] and be important in the clustering of Transient receptor potential cation channel subfamily V member 1 (TRPV1) at the cell surface [55]. Furthermore, angiotensin II type 1 (AT1) receptor plasma membrane expression was described to be mediated by GABARAP [56], while sodium-dependent phosphate transport protein 2A (SLC34A1) levels were found to be increased in its absence [57]. Recently, GABARAPL2 was reported to be directly involved in

regulating the protein levels of Parkin associated endothelin like receptor (PAELR) [58]. GABARAPL1, in turn, has also been described to be implicated in trafficking of the GABAA receptor [59] and the κ-opioid receptor [60]. Importantly, GABARAPL1 has already been connected with increased EGFR surface expression under hypoxic conditions without altering the total EGFR levels [61]. However, in almost all above-mentioned autophagy-unrelated functions, systematic analysis revealing unique and non-redundant roles of the three human GABARAP subfamily members are largely lacking.

Therefore, the aim of this work was to analyze the role of the different members of the GABARAP subfamily of human Atg8 family proteins in trafficking, signaling, and degradation of the cell surface receptor EGFR as a model RTK.

2. Materials and Methods

2.1. Materials

A list of antibodies (Table A1) and RT-PCR primers (Table A2) used in this study can be found in Appendix A. Unless stated otherwise, antibodies were used at dilutions according to the manufacturer's instructions.

2.2. Cell Culture

Human hepatoma Huh7.5 cells [62] were maintained in Dulbecco's Modified Eagle Medium (DMEM) high glucose (F0445, Biochrom, Berlin, Germany) that was supplemented with 10% (*v*/*v*) heat-inactivated fetal bovine serum (FBS, 10270-106, ThermoFisher Scientific, Waltham, MA, USA), 2 mM L-glutamine (25040081, ThermoFisher Scientific), 1% penicillin/streptomycin (15140-122, ThermoFisher Scientific), 10 µL/mL non-essential amino acids (NEAA, 11140-035, ThermoFisher Scientific) at 37 °C and 5% CO_2. The use of the Huh7.5 cell line is covered by a material transfer agreement with Apath, L.L.C. (New York City, NY, USA). Human embryonic kidney 293 (HEK293) Flp-In T-Rex cells [63,64] were maintained in DMEM high glucose that was supplemented with 10% (*v*/*v*) heat-inactivated FBS at 37 °C and 5% CO_2. The cells were split regularly at 80% confluency and used for a maximum of 30 passages after thawing. Cells were routinely checked for mycoplasma contamination.

For treatment with EGF and inhibitors 0.14×10^6 cells were seeded two days prior treatment in wells of six-well plates. The cells were pretreated with either 10 µM lactacystin (L6785, Sigma–Aldrich, St. Louis, MO, USA) for 1 h, 100 µM chloroquine (14774, Cell Signaling Technologies, Danvers, MA, USA) for 2 h or left untreated, followed by treatment with 40 ng/mL EGF (11376454001, Roche, Basel, Switzerland) for up to 180 min.

2.3. CRISPR/Cas9 Mediated Knockout Generation

Knockout (KO) cell lines were generated, as described [65]. In brief, the cells were transfected with KO plasmids based on pSpCas9(BB)-2A-GFP (PX458) [66], single sorted for fluorescent protein (FP) positive signals via fluorescence-activated cell-sorting (FACS) in wells of 96-well plates, clonal lines recovered and occurrence of genome editing verified via the amplification of a 400 bp product flanking the target site and Sanger sequencing as well as on protein level with specific antibodies. Knock-in (KI) of an enhanced green fluorescent protein (EGFP) at the endogenous locus of GABARAP was achieved by transfecting a homology-directed repair (HDR-) plasmid containing homology arms 1 kbp up- and downstream of the CRISPR target site flanking the sequence for EGFP. The cells were serum starved 24 h prior transfection to enhance HDR, sorted by FACS as single cells in wells of 96-well plates, and recovered and analyzed as the KO cells. The resulting cell line was termed GFP-GABARAP. Sequences for primers used for Sanger sequencing can be found in Table S1.

2.4. Transient Transfection

Nucleofection was performed according to the manufacturer's instructions (Lonza, Basel, Switzerland) with 4D Nucleofector. In brief, HEK293 Flp-In T-REx cells were split 2–3 days prior to

nucleofection. On the day of nucleofection, 1×10^6 cells were nucleofected with 2 µg plasmid DNA and cell membranes recovered by adding warm RPMI (21875034, ThermoFisher Scientific) medium containing 10% FBS for 10 min. at 37 °C to each reaction. Afterwards, the cells were seeded into wells of 12-well plates and treated with 40 ng/mL EGF for up to 180 min. two days post nucleofection.

Lipofection with Lipofectamin2000 reagent was performed according to the manufacturer's instructions (11668019, Qiagen, Hilden, Germany). Briefly, one day prior transfection, 3×10^5 Huh7.5 cells were seeded in wells of 6-well plates in growth medium without antibiotics. On the day of transfection, 3 µg of each plasmid DNA and 10.5 µL Lipofectamin2000 reagent were diluted in 150 µL Opti MEM (1×) + GlutaMAX reduced serum medium (51985042, ThermoFisher Scientific), mixed and incubated for 5 min. at RT to form plasmid-lipid complexes. Afterwards, 250 µL of this solution were added dropwise to wells of the 6-well plates in order to reach a final plasmid amount of 2.5 µg per well and then incubated for two days at 37 °C until further experiments. EGFR-GFP was a gift from Alexander Sorkin (Addgene plasmid #32751).

2.5. Immunoblot

The cells were washed once with ice cold PBS and then harvested by scraping into cell lysis buffer (1% Triton, 20 mM Tris/HCl, pH 7.4, 13.6 mM NaCl, 2 mM EDTA, 50 mM β-glycerophosphate, 20 mM sodium pyrophosphate, 1 mM $Na3VO_4$, 4 mM benzamidine, 0.2 mM Pefabloc, 5 µg/mL aprotinin, 5 µg/mL leupeptin, 10% glycerol, and 0.2% SDS) on ice. Cell lysis was carried out by incubating samples on ice for 10 min. The supernatants were cleared by centrifugation at 20,000 g for 15 min. at 4 °C, transferred to fresh tubes, and protein concentration was determined by BCA assay. In general, 20–30 µg of whole cell protein lysate were supplemented with 4 × Lämmli buffer (250 mM Tris-HCl pH 6.8, 40% glycerol, 5% SDS, 0.005% bromophenol blue) supplemented with fresh 8% 2-mercaptoethanol, boiled for 7 min. at 95 °C and loaded on 10 or 12 %-PAA gels for SDS-PAGE. After SDS-PAGE, gels were imaged with BioRad Imager using the stain-free method in order to determine protein loading [67] and then transferred to 0.4 µm PVDF membrane via semidry blotting at 0.77 mA/cm^2 gel constant current for 1 h. The membranes were afterwards cut, washed for 5 min. with TBS containing 0.1% Tween20 (TBS-T) at RT, blocked with 5% BSA in TBS-T for 1 h at RT, and incubated with specific antibodies overnight at 4 °C. On the next day, blots were washed thrice with TBS-T at RT for 20 min. and incubated with fluorescently labeled secondary antibodies for 1 h at RT wrapped in aluminium foil. Afterward, membranes were washed thrice with TBS-T for 20 min. at RT. The protein levels were visualized either directly using BioRad Imager with detection settings specific for Alexa488 or Alexa647 in the case of fluorescent protein conjugated antibodies or after 2 min. incubation with Western Bright ECL spray (K-12049-D50, Advansta, San Jose, CA, USA) by chemiluminescence in case of HRP conjugated antibodies. The protein expression levels were normalized to total protein loading, as determined by stain-free analysis.

2.6. RT-PCR

The cells were washed once with PBS and harvested by scraping into cell lysis buffer RLT containing 0.01% 2-mercaptoethanol, followed by cell homogenization using Qiashredder spin columns (79656, Qiagen). The total RNA was extracted using RNeasy miniprep kit (74106, Qiagen). Concentration was determined by NanoDrop1000 and 1 µg total RNA was reverse transcribed into cDNA with Quantitect Reverse Transcription kit (205314, Qiagen) while using oligomeric (dT) primers and including a DNAse digestion step. The resulting cDNA was used in a 20 µL reaction mix containing 1 × SYBR green (A6002, Promega, Madison, WI, USA), 400 nM of each forward and reverse exon spanning specific primers, 1/250 diluted cDNA and RNAse free water. The mRNA levels were determined on Viia7 RT-PCR (ThermoFisher Scientific), normalized to *succinat dehydrogenase subunit a* (*SDHA*) as a reference gene, and expressed as fold-change compared to controls using the ΔΔCT method.

2.7. EGF Uptake Assay

For FACS-based EGF uptake assay, 0.07×10^6 cells were seeded in wells of 12-well plates two days prior experiment. On the day of experiment, the cells were stimulated for up to 180 min. with Alexa647 labelled EGF (E35351, ThermoFisher Scientific). Afterwards, the cells were harvested by trypsin-EDTA treatment for 4 min. at 37 °C, resuspended in ice cold FACS buffer (PBS containing 2 mM EGTA, 1% FBS), washed twice with fresh FACS buffer, and analyzed with FACS Aria III (BD Bioscience, Franklin Lakes, NJ, USA).

For pulse-based EGF uptake assay analyzed by immunofluorescence, Huh7.5 cells (2×10^5) were seeded on fibronectin (F1141, Sigma–Aldrich, St. Louis, MO, USA) coated glass bottom µ-dishes (81158, ibidi, Martinsried, Germany) one day before analysis. The next day, Huh7.5 cells were precooled on ice for 10 min. Afterwards, cells were incubated in cold medium supplemented with 40 ng/mL EGF-Alexa647 conjugate (E35351, ThermoFisher Scientific) for 1 h at 4 °C to enable prebinding to surface EGFR. The medium was then replaced by full medium without EGF-Alexa647 and cells were incubated in at 37 °C for 5, 10, 30, 60, 120, or 180 min. or directly washed once with high salt and low pH buffer (0.2 M sodium acetate and 0.5 M NaCl, pH 4.5) to remove unspecific binding, fixed for 10 min. with 4% PFA in PBS, and washed twice with PBS. After each incubation time point, corresponding cells were treated the same way.

For simultaneous immunofluorescence staining, fixed cells were permeabilized with 0.2% TritonX-100 in PBS for 30 min. at RT and then blocked with 1% bovine serum albumin (BSA, Sigma–Aldrich) at RT for 60 min. or overnight at 4–8 °C. Immunostaining was performed by incubation with primary antibodies for 60 min. at RT under gentle shaking. The cells were washed thrice for 5 min. with PBS followed by incubation with appropriate fluorescently labeled secondary antibody for 60 min. at RT in the dark, followed by two washing steps for 5 min. with PBS.

2.8. Confocal Laser Scanning Microscopy

Images were acquired using ZEN black 2009 software operating a LSM 710 confocal laser scanning system (Carl Zeiss MicroImaging Inc., Dunedin, FL, USA) with a Plan-Apochromat 63x/1.40 Oil DIC M27 objective. The cell nuclei were stained with DAPI and measured in the 405 nm channel (MBS -405/760+). GFP-GABARAP was detected in the 488 nm channel (MBS 488), Transferrin (Tf)-Alexa 555 conjugate (T35352, Thermo Fisher Scientific) in the 543 nm channel (MBS 458/543) and EGF-Alexa 647 conjugate in the 633 nm channel (MBS 488/543/633), respectively. HEK293 GFP-GABARAP KI cells (2×10^5) were seeded on fibronectin (F1141, Sigma–Aldrich) coated glass bottom µ-dishes (81158, ibidi), incubated overnight at 37 °C and 5% CO_2 in growth medium. Directly before measuring, medium was replaced by cold medium containing 40 ng/mL EGF-Alexa 647. Data were post-processed using ImageJ [68] (version: 2.0.0-rc-43/1.50e).

2.9. EGFR Surface Expression Analysis

Plasma membrane proteins exhibiting extracellular primary amines were isolated with Pierce Cell Surface Protein Isolation Kit (89881, Thermo Fisher Scientific) according to the manufacturer's instructions in order to analyze surface EGFR protein expression. In brief, two days prior labelling and isolation of plasma membrane proteins, 2×10^6 cells per flask for a total of four T75 flasks per cell line were seeded for each biological replicate. On the day of isolation, each flask was quickly washed twice with ice cold PBS on ice and then labeled with Sulfo-NHS-Biotin shaking for 30 min. at 4 °C. The labelling reaction was then quenched, cells were scraped into solution, centrifuged, and lysed with lysis buffer for 30 min. with additional vortexing (every 5 min.) and sonication (every 8 min.) steps. Lysates were cleared and biotinylated proteins bound to NeutrAvidin beads for 1 h at RT with end-over-end mixing. The proteins were eluted with elution buffer containing 50 mM DTT for 1 h at RT with end-over-end mixing. Protein concentrations of eluates were determined by BCA and equal amounts were processed and loaded on 10% PAA gels for immunoblot analysis.

2.10. Spinning Disc Confocal Fluorescence Microscopy

During measurement, the cells were maintained in a StageTop Incubator system (Okolab S.R.L., Pozzuoli, Italy) on the microscope stage at 37 °C, 85% humidity, and 5% CO_2. The spinning disk confocal fluorescence microscope (Acal BFI, Gröbenzell, Germany) is based on an inverted microscope (Eclipse Ti, Nikon Instruments Europe BV, Amsterdam, Netherlands) equipped with a multi-beam confocal scanner unit (CSU-W1, Yokogawa Deutschland GmbH, Ratingen, Germany) working according to the spinning disk confocal principle and two cw lasers for excitation at 488 nm (GFP-GABARAP) and 640 nm (EGF-Alexa647). The setup allows for fast (<50 ms) acquisition of confocal fluorescence images in three dimensions. Bright field images, as well as confocal fluorescence images with excitation at 488 and 640 nm, were recorded while using a 100 magnification oil immersion objective lens (CFI PLAN APOCHROMAT VC, NA = 1.40, Nikon) and appropriate multi-dichroic beamsplitter, an EMCCD camera (Ixon Ultra 897, Andor Technologies Ltd., Belfast, UK) as detector and an image splitting device (Optosplit II, Cairn Research, Faversham, UK) for the simultaneous observation of two spectral regions of the emitted light (EGFP: 540/75 nm (Omega Optics Filters, Brattleboro, VT, USA) and EGF-Alexa647: 675/67 nm Brightline HC (Semrock Optical Filters (IDEX Health & Science, Bristol, CT, USA), West Henrietta, NY, US), respectively). The software Andor IQ2 was used for image acquisition. The exposure time for single images was set between 300–500 ms, while the frame rate was set to the minimum. The laser power and number of focal planes (z-frames) were set for every measured cell individually between 1 and 3. Data were post-processed using ImageJ [68] (version: 2.0.0-rc-43/1.50e).

2.11. Image Analysis

The image analysis software "Imaris" (Bitplane, Zurich, Switzerland) was used for quantitative comparison of EGF-Alexa647 uptake over time. Z-Stacks of cells were acquired, as described before, applying the same microscopy hardware settings to ensure reproducibility between datasets and individual cells were extracted to single stacks manually. The EGF volumes were identified and rendered utilizing the "Imaris surface" feature. A surface smoothing factor of 0.05 µm was used as well as a volume thresholding based on absolute EGF signal intensity of 14. Touching objects were separated on a seed diameter of 1 µm. A set of minimum requirement feature filters were applied and repeatedly checked for quality by comparing it to non-rendered data to minimize background volumes. Final filter sets were set as following: Quality threshold of 1.89, Minimum number of Voxel of 1, Shortest axis of minimum 520 nm and minimum mean intensity of 21. The surface generation was applied in batch mode to all individual cells and mean intensity, surface volume, and surface number per cell were extracted for downstream analysis.

2.12. Bio-Layer Interferometry (BLI)

BLI was used to determine the binding affinity of GABARAP and EGFR derived peptides. Experiments were performed on an Octet Red 96 (FORTÉBIO, San Jose, CA, USA) while using solid-black 96-well plates at 25 °C and a shake speed of 1000 rpm. The BLI buffer contained 25 mM Tris-HCl, pH 7.5, 150 mM NaCl, 0.5 mM Tris(2-carboxyethyl)phosphin (TCEP), 0.1% Tween-20, 1 mg/mL bovine serum albumin (BSA). The EGFR peptides were synthesized and N-terminally biotinylated via an aminohexanoic acid linker as well as C-terminally amidated (CASLO, Lyngby, Denmark). GABARAP was expressed and purified, as described [69]. Peptides (50 µg/mL) or biotin (10 µg/mL) as reference were immobilized on High Precision Streptavidin (SAX) biosensors (FORTÉBIO, San Jose, CA, USA). The peptide immobilization levels were around 0.8 nm. GABARAP was used as analyte in increasing concentrations in 200 µL solution. Association of GABARAP was recorded for 300 s on ligand and reference biosensors, followed by a dissociation phase of 300 s. Steady-state evaluation was performed by plotting the respective response levels against the applied peptide concentrations.

The curves were fitted according to the following Langmuir's 1:1 binding model using OriginPro 2019 (OriginLab, Northampton, MA, USA):

$$\mathbf{y} = \frac{\mathbf{R_{max}x}}{\mathbf{K_D + x}}, \quad (1)$$

with y corresponding to the binding signal (response), R_{max} the saturation binding signal, x the applied GABARAP concentration, and K_D the equilibrium dissociation constant.

2.13. Co-immunoprecipitation

For co-immunoprecipitation (Co-IP) analysis, the GFP-Trap technology employing high affinity VHH domain containing nanobodies for GFP binding (gtak-20, Chromotek, Islandia, NY, USA) was used according to the manufacturer's instructions. In brief, Huh7.5 GABARAP SKO cells were transfected via lipofection, as described and stimulated with 40 ng/mL EGF for 10 min. or left untreated. Afterwards, the cells were placed on ice, washed once with ice-cold PBS, and two 6-wells per condition scraped into 200 µL NP-40 lysis buffer (10 mM Tris/HCl pH 7.5, 150 mM NaCl, 0.5 mM EDTA, 0.5% Nonidet™ P40 Substitute, 0.09% sodium azide) containing protease and phosphatase inhibitors (78430, ThermoFisher Scientific). Cell lysis was carried out on ice for 30 min., with 10 s vortexing after every 10 min. Lysates were then cleared by centrifugation for 10 min. at 17 000 g at 4 °C and the supernatants containing proteins transferred to pre-cooled reaction tubes. The lysates were diluted with 300 µL ice-cold washing buffer (10 mM Tris/HCl pH 7.5, 150 mM NaCl, 0.5 mM EDTA.

0.018% sodium azide) containing protease and phosphatase inhibitors and 10% saved for input analysis. 25 µL of anti-GFP nanobody coupled agarose bead slurry was equilibrated with washing buffer, separated via a magnetic rack, and for Co-IP lysates were bound overnight at 4 °C with end-over-end mixing. Afterwards, 50 µL were saved for flow through analysis, beads were washed four times with ice-cold washing buffer, and finally eluted with 80 µL 2× Lämmli's SDS sample buffer (120 mM Tris/HCl pH 6.8, 20% glycerol, 4% SDS, 0.04% bromophenol blue, 8% 2-mercaptoethanol) by heating to 95 °C for 5 min. The samples were then analyzed by immunoblotting, as described.

2.14. Statistical Analysis

All of the statistical analyses were performed with the statistical analysis software package (SPSS, version 22; SPSS Inc., Chicago, IL, USA), unless stated otherwise. Descriptive data are expressed as means ± standard error of means (SEM). Normal distribution was assessed using the Shapiro–Wilk test, and data was transformed or bias-corrected accelerated bootstrapping performed prior to analysis where necessary. Statistical testing was performed, as described individually. In general, statistical significance was inferred at a two-tailed p-value of ≤ 0.05. To test the influence of each GABARAP family protein on total EGFR protein levels, dichotomous dummy-coded variables were used to express each genotype as either wildtype for a specific paralog (1) or as a knockout (0). Afterwards, bivariate correlation analysis (Spearman) was performed and two-tailed statistical significance was calculated.

3. Results

3.1. Deficiency for GABARAP, but Not GABARAPL1 or GABARAPL2 Is Associated with Increased Degradation of EGFR in Huh7.5 and HEK293 Cells

We generated HEK293 knockout (KO) cells deficient for each GABARAP subfamily member alone (SKO) or in double (DKO) and triple (TKO) combination using the CRISPR/Cas9 system to systematically investigate the role of GABARAP-subfamily proteins during EGFR degradation (Figure S1A, Table S1).

The cells were then stimulated with 40 ng/mL EGF, which is known to promote receptor degradation [70], for up to 180 min., and whole cell lysates were analyzed for total EGFR protein levels by immunoblot (Figure 1A). Figure 1B shows densitometric analyses of the genome-edited HEK293 cell lysates compared to their matching controls. Evidently, GABARAP SKO cells displayed significantly lower EGFR levels in whole cell lysates after 10 (1.24-fold, $p \leq 0.05$), 120 (1.84-fold, $p \leq 0.05$), and by

trend 180 min. (1.42-fold, $p = 0.07$) of EGF treatment as compared to the control levels. In contrast, neither single lack of GABARAPL1 nor GABARAPL2 led to significant differences in the total EGFR levels when compared to their respective controls, although GABARAPL1 deficiency resulted in a slight increase in EGFR at most time points, and a trend towards reduced EGFR levels could be observed for GABARAPL2 SKO cells after 180 min. of EGF treatment (1.19-fold, $p = 0.1$). Consistently, GABARAP/L1 DKO cells showed no differences in the EGFR levels as compared to the wildtype controls, neither unstimulated nor in response to EGF treatment, indicating that GABARAP and GABARAPL1 have opposite functions regarding EGFR degradation dynamics in this cell type. GABARAP/L2 DKO cells had significantly less EGFR after 10 (1.52-fold, $p \leq 0.05$) and by trend after 60 (1.69-fold, $p = 0.06$), 120 (1.73-fold, $p = 0.08$), and 180 min. (1.9-fold, $p = 0.1$) of EGF treatment, respectively, and thus performed like lacking solely GABARAP. A lack of both GABARAPL1 and GABARAPL2 resulted in EGFR levels as in the control samples, suggesting that GABARAP is the decisive factor for a correct EGFR degradation phenotype in HEK293 cells. Notably, TKO cells, lacking the whole GABARAP subfamily, showed slightly elevated unstimulated EGFR without reaching statistical significance. This phenotype might reflect the participation of the whole GABARAP subfamily in general cellular processes such as autophagy or lysosome biogenesis [71], which, due to functional redundancy emerges, most if none of the family members are present. We used dichotomous dummy-coded variables to indicate the genotypic status for each GABARAP-subfamily member in all applied HEK293 cell lines to analyze the correlation between the presence of each of the GABARAP subfamily proteins and EGFR levels after EGF stimulation (Figure 1C) (for details see Materials and Methods).

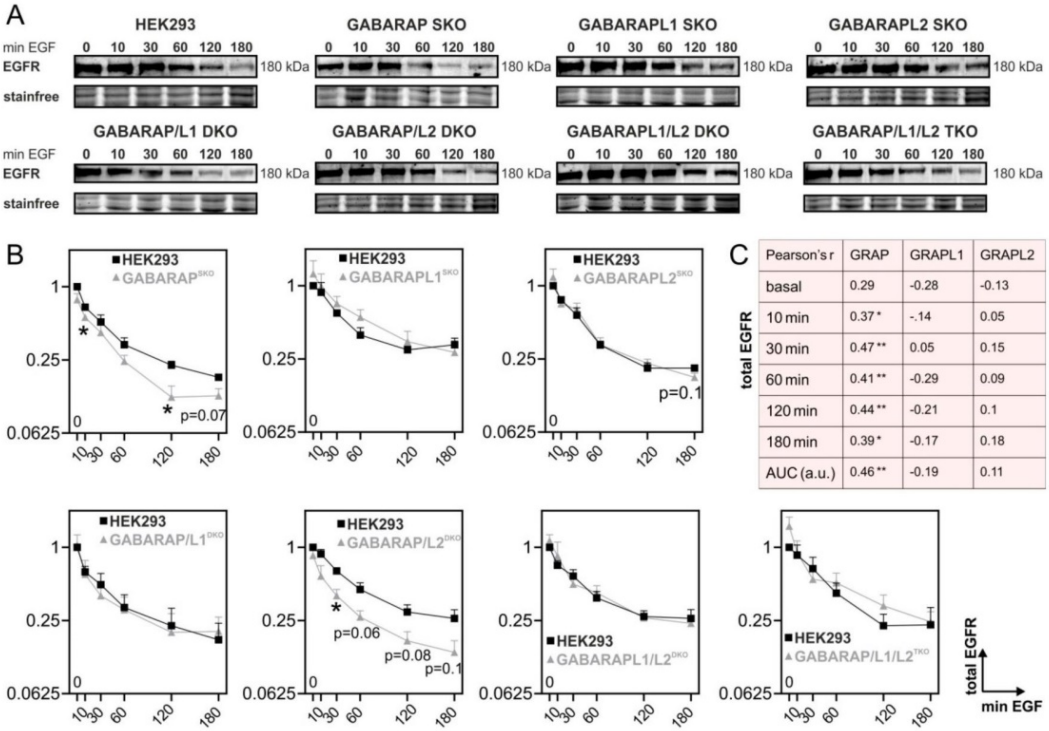

Figure 1. Epidermal growth factor (EGF)-induced EGF receptor (EGFR) degradation in HEK293 knockout (KO) cells. (**A**) Cells were treated with 40 ng/mL EGF for the indicated times. Afterwards, total EGFR protein levels in whole cell lysates were analyzed by immunoblot. Representative blots are shown for at least n = 3 independent experiments. (**B**) Densitometric analysis of at least n = 3 independent experiments. Controls are plotted for each experiment. Quantification of total EGFR protein levels was performed by normalization to stain-free loading control; levels are given relative to HEK293 control cells at unstimulated conditions (t = 0). Error bars represent standard error of means.

Asterisks mark significant differences versus the corresponding time point of control cells as calculated using independent t-test. $p \leq 0.05$ = *, $p \leq 0.01$ = **, $p \leq 0.001$ = ***. (**C**) Correlation of presence of each GABARAP with total EGFR levels in response to EGF treatment. Correlations were calculated taking every analyzed KO combination except GABARAP/L1/L2 TKO in HEK293 cells into account. Pearson correlation was used for calculation and two-tailed significances are denoted with asterisks: $p \leq 0.05$ = *, $p \leq 0.01$ = ** GRAP = GABARAP, GRAPL1 = GABARAPL1, GRAPL2 = GABARAPL2. Respective wildtype controls were run on the same PAGE for each KO cell line and can be found in Figure S6A which also shows the uncropped source blots.

As expected, the GABARAP availability was significantly and positively correlated with EGFR protein levels at each time point after EGF treatment (10 min., r = 0.37, $p \leq 0.05$; 30 min., r = 0.47, $p \leq 0.01$; 60 min., $r = 0.41$, $p \leq 0.01$; 120 min., $r = 0.44$, $p \leq 0.05$; 180 min., r = 0.39, $p \leq 0.05$) as well as with the corresponding integrated area under the curve (AUC, a.u.) of EGFR levels over time (r = 0.46, $p \leq 0.01$).

In addition to the above described experiments, we also applied the transient overexpression of GFP-fused EGFR to the same panel of genome-edited HEK293 cell lines and analyzed their respective EGFR-(GFP) levels upon EGF stimulation by immunoblot (Figure S2A). Densitometric analysis (Figure S2B) largely confirmed our results that were obtained for endogenous EGFR levels. Again, GABARAP deficiency alone or in combination with GABARAPL2 deficiency resulted in a significant reduction of EGFR levels. Interestingly, GABARAPL1/L2 DKO and GABARAP/L1/L2 TKO cells both showed significantly elevated EGFR levels under EGFR overexpression conditions, suggesting that some effects observed for overexpression are either dependent on receptor density or produced by the overexpression *per se*. In general, when comparing endogenous with overexpressed EGFR degradation dynamics, it is evident that EGFR overexpression strongly slows down degradation (Figure S2B, see EGFR-GFP vs. EGFR).

Overall, GABARAP deficiency appeared to accelerate EGFR degradation or, *vice versa*, GABARAP appeared to slow down EGFR degradation upon EGF stimulation in HEK293 cells.

We next used Huh7.5 cells for degradation analysis of endogenous EGFR to clarify whether the validity of the observed GABARAP-mediated effects on EGFR degradation can be extended to other cell lines and to rule out clonal effects of our genome-edited HEK293 cell lines. To that end, we first established Huh7.5 KO cells deficient for GABARAP, GABARAPL1, or GABARAPL2 alone or combinations of GABARAP/L2 and GABARAPL1/GABARAPL2 (Figure S1B, Table S1). Cells and lysates were treated, as described above, total EGFR was detected by immunoblotting (Figure 2A), and the respective densitometric analyses are summarized in Figure 2B. While the basal EGFR levels were unaltered in GABARAP SKO cells, the total EGFR levels were significantly reduced after 10 (1.3-fold, $p \leq 0.05$), 30 (2.14-fold, $p \leq 0.01$), 60 (2.7-fold, $p \leq 0.05$), 120 (3.56-fold, $p \leq 0.01$), and 180 min. (4.74-fold, $p \leq 0.001$) of treatment with EGF when compared to Huh7.5 control cells. GABARAPL1 and GABARAPL2 SKO cells were analyzed likewise with regards to EGFR protein levels in response to EGF treatment to analyze the role of the two other GABARAP subfamily members. Neither GABARAPL1 SKO nor GABARAPL2 SKO cells showed significantly reduced levels of EGFR in response to EGF stimulation when compared to Huh7.5 control cells. In fact, GABARAPL1 SKO cells displayed a slight trend towards higher EGFR total protein levels over time, while a slight but significant (1.32-fold, $p \leq 0.05$) increase in the basal total EGFR levels was observed for GABARAPL2 SKO cells. Strikingly, the only other analyzed Huh7.5 cell line showing the accelerated degradation of EGFR in response to EGF stimulation was the GABARAP/L2 DKO line after 10 (1.9-fold, $p \leq 0.05$), 30 (2.16-fold, $p \leq 0.05$), 60 (2-fold, $p \leq 0.05$), 120 (1.44-fold, $p \leq 0.01$), and 180 min. (3.29-fold, $p \leq 0.05$) of treatment with EGF, but not at basal levels as compared to Huh7.5 control cells. GABARAPL1/GABARAPL2 DKO cells displayed unaltered total EGFR levels when compared to Huh7.5 control cells, indicating that the lack of GABARAP alone was sufficient for driving accelerated EGFR degradation in these cells.

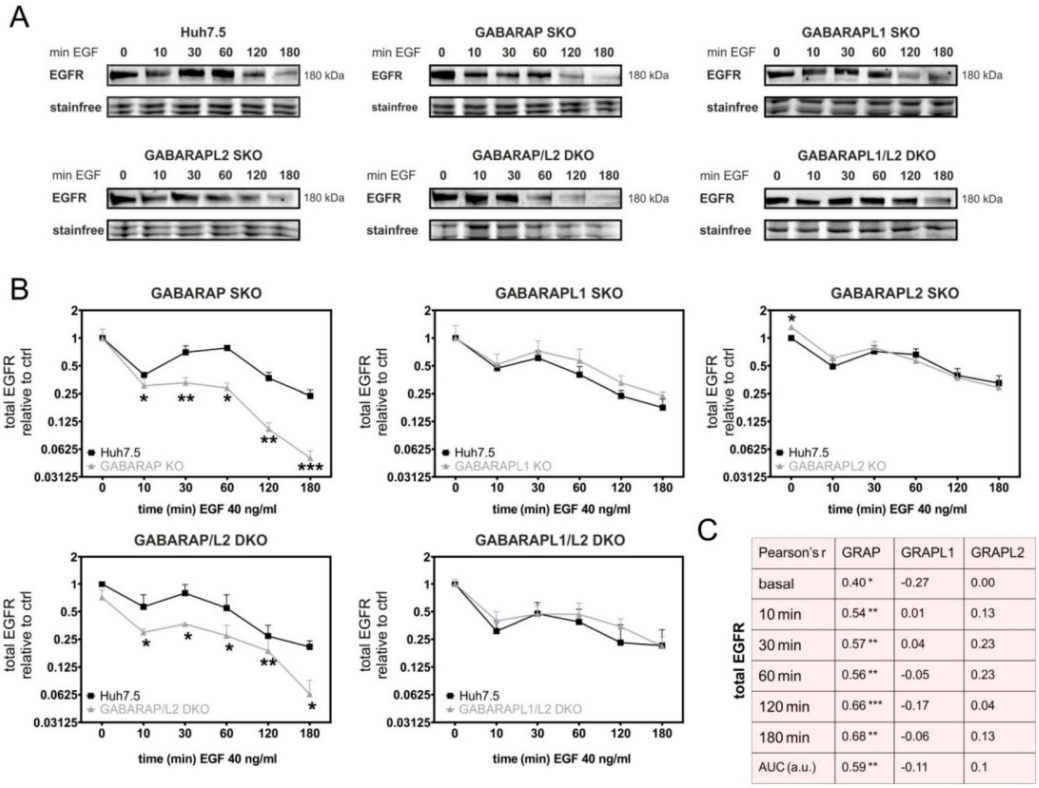

Pearson's r	GRAP	GRAPL1	GRAPL2
basal	0.40 *	-0.27	0.00
10 min	0.54 **	0.01	0.13
30 min	0.57 **	0.04	0.23
60 min	0.56 **	-0.05	0.23
120 min	0.66 ***	-0.17	0.04
180 min	0.68 **	-0.06	0.13
AUC (a.u.)	0.59 **	-0.11	0.1

Figure 2. EGF-induced EGFR degradation in Huh7.5 KO cells. (**A**) Cells were treated with 40 ng/mL EGF for the indicated times. Afterwards, total EGFR protein levels in whole cell lysates were analyzed by immunoblot. Representative blots are shown for n = 3 independent experiments. (**B**) Densitometric analysis of n = 3 independent experiments. Controls are directly plotted for each experiment. Quantification of EGFR protein levels was performed by normalization on stain-free loading control and calculated as percentage of Huh7.5 control cells at unstimulated conditions (t = 0). Representative blots are shown for a summary of n = 3 independent experiments. Error bars represent standard error of means. Asterisks mark significant differences versus the corresponding time point of control cells as calculated using independent t-test. $p < 0.05$ = *, $p < 0.01$ = **, $p < 0.001$ = ***. (**C**) Correlation of presence of each GABARAP with total EGFR levels in response to EGF treatment. Correlations were calculated taking every analyzed KO combination in Huh7.5 cells into account. Pearson correlation was used for calculation and two-tailed significances are denoted with asterisks: $p \leq 0.05$ = *, $p \leq 0.01$ = **. GRAP = GABARAP, GRAPL1 = GABARAPL1, GRAPL2 = GABARAPL2. Respective wildtype controls were run on the same PAGE for each KO cell line and can be found in Figure S6B which also shows the uncropped source blots.

The correlation analysis of EGFR degradation results from Huh7.5 cell derived lysates (Figure 2C) showed broad consistency with that based on the independent HEK293 cell lysates (Figure 1C): a strong and significant positive correlation of genotypes expressing GABARAP with total EGFR levels under basal conditions ($r = 0.4$, $p \leq 0.05$), as well as after 10 ($r = 0.54$, $p \leq 0.01$), 30 ($r = 0.57$, $p \leq 0.01$), 60 ($r = 0.56$, $p \leq 0.01$), 120 ($r = 0.66$, $p \leq 0.001$), and 180 ($r = 0.68$, $p \leq 0.01$) min. of EGF treatment, as well as with the integrated AUC of EGFR total protein levels ($r = 0.59$, $p \leq 0.01$) was revealed. No significant correlation for GABARAPL1 or GABARAPL2 with EGFR protein levels was found for any of the time points analyzed, although GABARAPL1 showed a trend towards negative correlation with EGFR levels at basal conditions ($r = -0.27$) and after 120 min. ($r = -0.17$) of EGF treatment. Clonal off-target effects as an explanation for the observed phenotype could be excluded with high confidence based on the close agreement of observations with two different cell lines.

In summary, the lack of GABARAP, either alone or in combination with GABARAPL2, was consistently and significantly associated with decreased total EGFR protein levels in response to EGF treatment in both Huh7.5 and HEK293 cells, whereas the presence of GABARAP in general was associated with higher EGFR total levels. Subsequently, we concentrated further efforts on the Huh7.5 GABARAP SKO cell line to analyze EGFR degradation dynamics and its implications in more detail.

3.2. GABARAP Deficiency Alters EGFR Signaling on Protein and Gene Expression Levels and Increases GABARAPL1 but Not GABARAPL2 Protein Expression

Next, we asked whether GABARAP deficiency is additionally accompanied by altered EGFR downstream signaling. Therefore, we analyzed the activation of EGFR itself as well as of EGFR-associated signaling, namely the phosphoinositide-3-kinase/proteinkinase B (PI3K/AKT) and mitogen-activated protein kinase/extracellular-signal regulated kinase (MAPK/ERK) signaling pathway, by immunoblot (Figure 3A). The phosphorylation of EGFR at Y1068 in GABARAP SKO cells was higher by trend after 10 min. of EGF treatment (1.36-fold, $p = 0.06$) as compared to Huh7.5 control cells, whereas it was not altered at later time points (Figure 3B). The activation of the PI3K/AKT pathway was analyzed by phosphorylation of AKT at S473 and it was not significantly influenced under the given circumstances (Figure 3C). Activating phosphorylation of ERK1/2 was reduced in GABARAP SKO cells at every time point analyzed with a significant reduction after 30 min. of EGF treatment (2.49-fold, $p \leq 0.05$, Figure 3D).

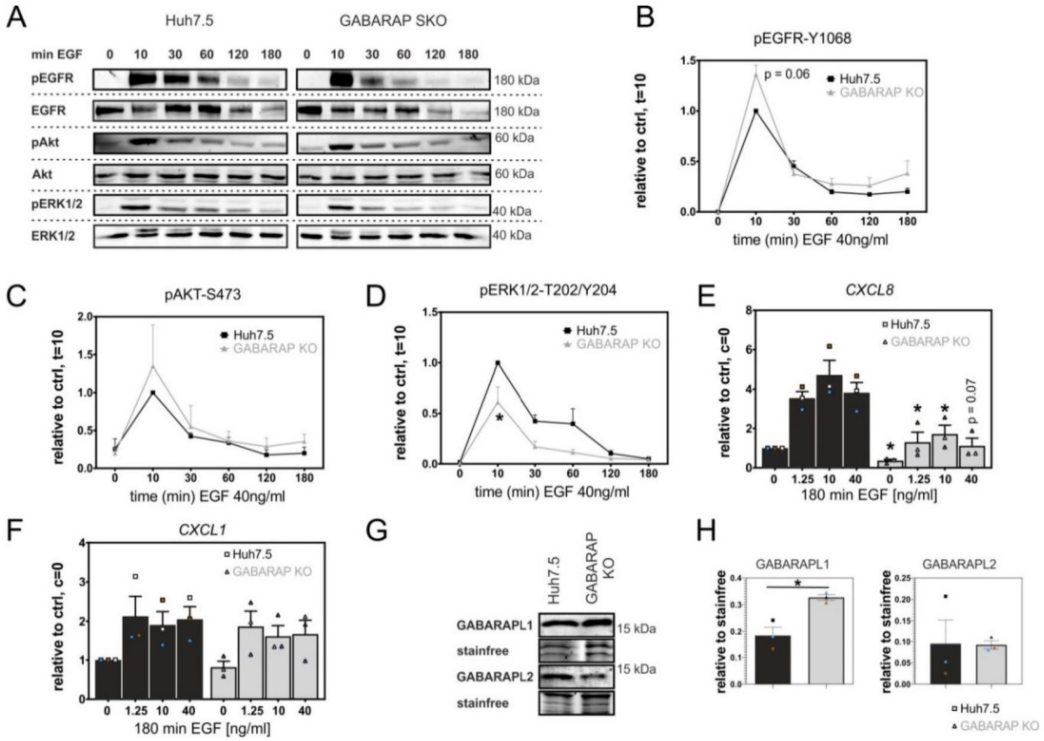

Figure 3. Analysis of EGF-induced EGFR phosphorylation, activation of downstream signaling and gene expression in GABARAP SKO and Huh7.5 control cells. (**A**) Huh7.5 and GABARAP SKO cells were treated with 40 ng/mL EGF for the indicated times. Afterwards, activating phosphorylations of the EGFR (**B**) and downstream PI3K/AKT (**C**) and MAPK/ERK (**D**) signaling pathways were analyzed by immunoblot. Quantification of phosphorylated proteins was performed by normalization to the corresponding total protein levels and calculated as percentage of Huh7.5 control cells after 10 min. of EGF treatment (t = 10). (**E** + **F**) Huh7.5 and GABARAP SKO cells were treated with the indicated concentrations of EGF for 180 min., followed by cell lysis, RNA extraction, reverse transcription and

quantitative real-time PCR (RT-PCR). Expression of target genes *CXCL8* (**E**) and *CXCL1* (**F**) was normalized to *succinate dehydrogenase* (*SDHA*) as reference gene and is expressed relative to unstimulated control cells. (**G**) Protein expression of GABARAP paralogs GABARAPL1 and GABARAPL2 was analyzed in Huh7.5 and GABARAP SKO cells and densitometric analysis performed to determine GABARAPL1 and GABARAPL2 protein levels in GABARAP SKO cells compared to Huh7.5 controls (**H**). Representative blots are shown for a summary of n = 3 independent experiments. Error bars represent standard errors of means. Asterisks mark significant differences versus the corresponding time point or concentration of control cells as calculated using independent t-test. $p \leq 0.05$ = *. (**E**,**F**,**H**) individual experiments are color-coded. Figure S6C shows uncropped source blots.

Next, the impact of GABARAP deficiency on EGFR target gene expression was analyzed. The mRNA levels of the C-X-C chemokine receptor 2 (CXCR2) ligand *CXCL8* alongside mRNA levels of another CXCR2 ligand, *CXCL1*, were analyzed after treatment with various concentrations of EGF because the gene expression of *CXCL8*was reported to be regulated by the EGFR/ERK signaling axis after HCV infection [72]. Strikingly, *CXCL8* transcripts were significantly reduced in GABARAP SKO cells at basal levels (2.75-fold, $p \leq 0.05$) and upon stimulation with 1.25 ng/mL (2.72-fold, $p \leq 0.05$), 10 ng/mL (2.75-fold, $p \leq 0.05$) and by trend 40 ng/mL EGF (3.42-fold, $p = 0.068$) for 180 min. compared to Huh7.5 control cells (Figure 3E). This was not the case for *CXCL1* (Figure 3F), suggesting different transcriptional regulation for these two chemokines through independent axes of EGFR transduced signaling.

In order to investigate the influence of GABARAP deficiency on protein levels of its paralogs GABARAPL1 and GABARAPL2, we analyzed their basal levels in Huh7.5 control and GABARAP SKO cells (Figure 3G). Interestingly, GABARAPL1 protein expression was significantly increased in GABARAP SKO cells (1.77-fold, $p \leq 0.05$), whereas the GABARAPL2 protein levels were not consistently influenced (Figure 3H) as compared to Huh7.5 control cells.

3.3. Basal EGFR Surface Expression Is Unaltered in GABARAP Deficient Cells, While EGF Uptake Capacity Is Impaired over Time

We isolated the surface proteins of Huh7.5 and GABARAP SKO cells via biotinylation (Figure 4A) and determined surface EGFR levels by immunoblot (Figure 4B) in order to check whether accelerated degradation of EGFR is simply caused by altered EGFR surface expression. Densitometric analysis revealed no alterations between GABARAP SKO and Huh7.5 control cells (Figure 4C), indicating that the trafficking of EGFR to the plasma membrane is not impaired in GABARAP SKO cells under basal levels of EGF. Consistent with unaltered EGFR total protein levels, the *EGFR* mRNA expression levels were not influenced by GABARAP deficiency (Figure 4D). We next asked whether the observed acceleration of EGFR degradation and alterations in downstream signaling events are caused by defects in EGF uptake or receptor endocytosis *per se*. Therefore, we carried out a FACS based assay. The cells were continuously treated with 40 ng/mL EGF that was conjugated to the fluorophore Alexa647 and the median fluorescence intensity (a.u.), reflecting the amount of intracellular EGF, was analyzed via FACS (Figure 4E). As EGFR is the only receptor for EGF, this directly reflects its internalization by endocytosis at early time points and accumulated intracellular EGF over time. However, Alexa647 is a pH-stable fluorophore and it is therefore not fully degraded by lysosomes similar to EGF quantum dots [73]. Hence, intracellular fluorescence at later time points might reflect free dye, at least to some extent. Nonetheless, this approach represented several cycles of EGFR internalization, which provides a measure of EGF uptake over time. Consistent with surface expression being unaltered, GABARAP SKO cells displayed unaltered median fluorescent intensity values after 10 min. of EGF-Alexa647 treatment, indicating that early internalization events are not impaired in GABARAP deficient cells. Over time, intracellular EGF-Alexa647 levels were lower in GABARAP SKO cells after 30, 60, and 120 min. by trend and significantly reduced after 180 min. (1.59-fold, $p \leq 0.01$) when compared to Huh7.5 control cells (Figure 4F). The obtained results with this continuous treatment conditions, which allow for several rounds of ligand binding and receptor cycling, indicate a shift from receptor recycling to

degradation in GABARAP SKO cells at later time points as compared to Huh7.5 control cells. This is in line with the immunoblot experiments and suggests that the reduction of EGF-Alexa647 levels is caused by a general reduction of EGFR protein levels over time in response to EGF treatment in GABARAP deficient cells.

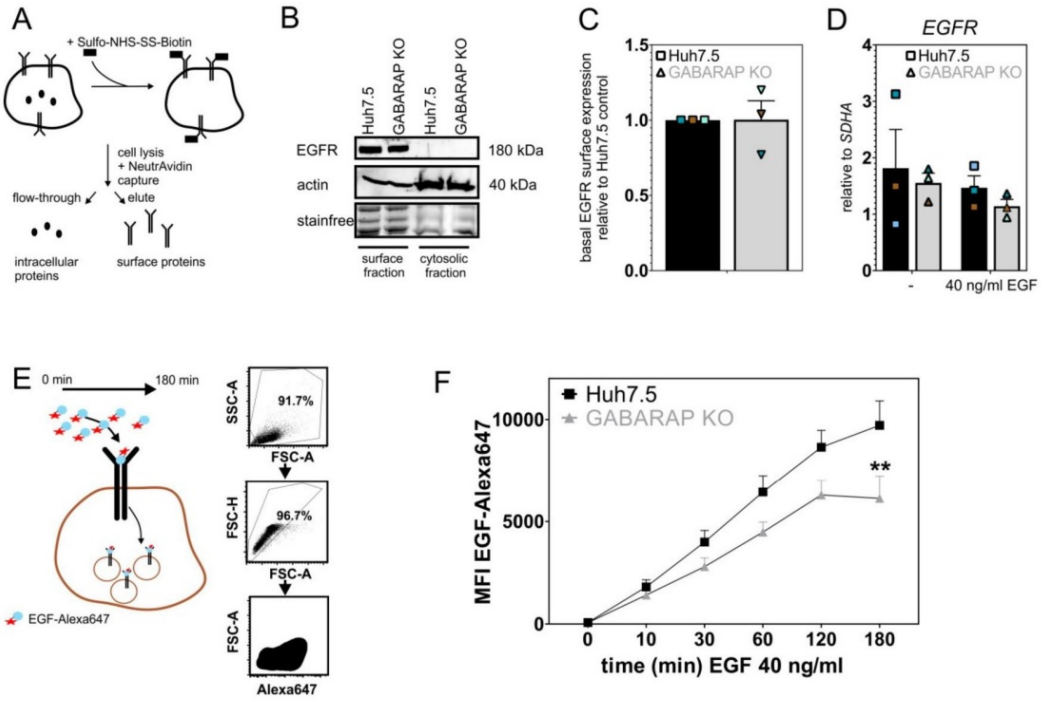

Figure 4. Analysis of EGFR surface expression by isolation of surface proteins and EGF-uptake in GABARAP SKO and Huh7.5 control cells by flow cytometry. (**A**) Primary amines of extracellular portions of plasma membrane proteins were conjugated to Sulfo-NHS-SS-Biotin. Afterwards, cells were lysed and biotinylated proteins captured via NeutrAvidin to separate surface from cytosolic proteins. (**B**) EGFR surface expression of Huh7.5 control and GABARAP SKO cells was determined by immunoblotting of the surface fraction lysate and (**C**) densitometric analysis performed to determine relative EGFR protein surface expression levels between Huh7.5 and GABARAP SKO cells (n = 3 independent experiments). (**D**) EGFR mRNA expression levels were analyzed at steady-state and after 180 min. of 40 ng/mL EGF treatment. Expression levels were normalized to *SDHA* expression and compared between Huh7.5 and GABARAP SKO cells. (**E**) Huh7.5 and GABARAP SKO cells were continuously treated with 40 ng/mL of Alexa647 labelled EGF over 180 min. Gates were set to get rid of debris and select for single cells. Intracellular EGF was determined by analyzing median fluorescence intensity (MFI) of EGF-Alexa647 positive cells (**F**). Line plot is a summary of n = 4 independent experiments. Error bars represent standard errors of mean. Asterisks mark significant differences to the corresponding time point of control cells as calculated using two-way analysis of variance with Bonferroni post-hoc testing with GraphPad Prism version 8.00 for Windows (GraphPad Software, La Jolla California US, www.graphpad.com). $p \leq 0.01$ = **. (**C** + **D**) Individual experiments are color-coded. Figure S6D shows uncropped source blots.

3.4. Tracking of Fluorescently-Labeled EGF Reveals Altered EGF Trafficking and Vesicular Composition in GABARAP Deficient Cells without Abrogation of General Endosomal Targeting

We used a pulse-based setup for confocal laser scanning microscopy imaging to address the question of whether GABARAP deficiency causes impaired intracellular trafficking of EGFR. The cells were pre-incubated with 40 ng/mL EGF-Alexa647 at 4 °C to saturate all EGFR binding sites at the plasma membrane, followed by acidic wash to remove unbound EGF and subsequent incubation at

37 °C to allow for internalization and trafficking of EGF pre-bound to EGFR (Figure 5A). As exemplarily shown for 5, 30 60, and 120 min. (Figure 5B), the cells were fixed at various time points after the EGF pulse and EGF accumulation was recorded as distinct dots, likely reflecting that EGFR accumulated in vesicles subsequent to ligand stimulation. EGF-Alexa647 containing vesicles were analyzed regarding the average number (Figure 5C), volume (Figure 5D) and intensity (Figure 5E) of individual vesicles per cell. Overall vesicular number per analyzed cell was significantly reduced after 60 (1.21-fold, $p \leq 0.05$) and 120 min. (1.29-fold, $p \leq 0.05$) of EGF-Alexa647 incubation. While the overall vesicular volume at 5 min. after the EGF-Alexa647 pulse was significantly increased in GABARAP SKO cells when compared to Huh7.5 control cells (1.15-fold, $p \leq 0.05$), it was found to be significantly lower after 30 min. (1.26-fold, $p \leq 0.001$) as compared to Huh7.5 control cells. Accordingly, the mean fluorescent intensity of analyzed vesicles after 5 min. of EGF-Alexa647 stimulation was significantly higher in GABARAP SKO cells when compared to Huh7.5 control cells (1.04-fold, $p \leq 0.05$), while it was found to be significantly decreased after 30 min. (1.07-fold, $p \leq 0.001$).

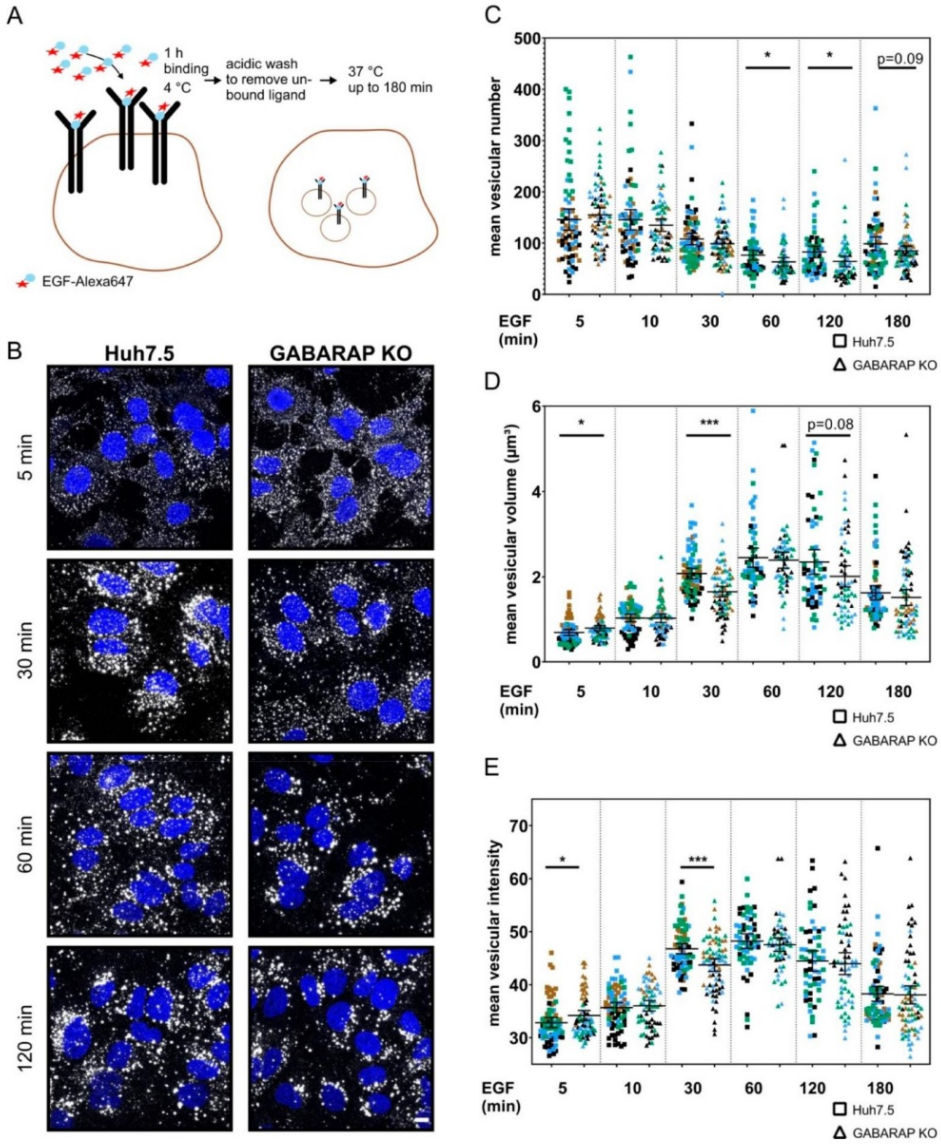

Figure 5. Analysis of EGF uptake in GABARAP SKO and Huh7.5 control cells via EGF-Alexa647 pulse by immunofluorescence imaging. (**A**) Huh7.5 and GABARAP SKO cells were treated with 40 ng/mL

Alexa647 labelled EGF at 4 °C to allow binding to EGFR. After rigorous washing, cells were placed at 37 °C and analyzed at distinct time points to assess EGF internalization. (**B**) Cells were fixed at basal levels and after 5, 10, 30, 60, 120, and 180 min. of EGF treatment. Nuclei were counterstained with DAPI and images of EGF positive puncta taken. Mean vesicular number (**C**), volume (**D**) and intensity (**E**) of imaged EGF-Alexa647 puncta were analyzed by Imaris. Single cells were cropped out of images, processed with ImageJ and Imaris (Bitplane, Zurich, Switzerland). Only vesicles with volumes > 0.1 μm^3) were taken into account. Fluorescent images are representative of at least n = 3 independent experiments. Individual experiments are color-coded; >50 cells per genotype and time point were analyzed. Error bars represent 95% confidence intervalls (CI) (**C**–**E**). Asterisks mark significant differences to the corresponding time point of control cells and were calculated using independent t-test. $p \leq 0.05$ = *, $p \leq 0.01$ = **, $p \leq 0.001$ = ***.

Next, we classified the obtained vesicle volumes and intensities into subgroups to visualize the more subtle differences that are not resolved by the global approach described above. The corresponding plots are shown in Supplementary Figure S3A,B. In summary, for vesicles of the smallest category (0.5–1 μm^3) similar numbers were found in GABARAP SKO and Huh7.5 control cells at all time points. Interestingly, for all other size categories and particularly at later stages starting at 30 min. post EGF-Alexa647 treatment, the numbers of observed vesicles were decreased in GABARAP deficient cells. Solely for the early 5 min. time point, increased numbers of vesicles of several categories were found for GABARAP SKO cells when compared to Huh7.5 control cells. Accordingly, vesicles of the lowest intensity (20–40) were not altered between GABARAP SKO and Huh7.5 cells, while vesicles of the remaining three intensity categories were significantly decreased, again especially starting at 30 min. post EGF-Alexa647 treatment. EGF-Alexa647 pulse-treated GABARAP SKO and Huh7.5 control cells were fixed and stained for early (RAB5), recycling (RAB11) or late (RAB7) endosomal marker proteins, to further analyze endosomal trafficking. Colocalization events of RAB5, RAB11, and RAB7 with EGF-Alexa647 (white arrows) were observed for GABARAP SKO and Huh7.5 control cells at every analyzed time point, indicating that the general ability of EGFR to reach the analyzed endosomal compartments is not abolished by GABARAP deficiency, as exemplarily shown for 10, 30, and 60 min. in Figure S3C. However, fixed cells and the analyzed set of time points might not be suitable to capture subtle and transient GABARAP-mediated interactions.

3.5. Accelerated EGFR Degradation in GABARAP Deficient Huh7.5 Cells Can Be Counteracted by Lysosomal and Proteasomal Inhibition

We then asked whether the acceleration in EGF-induced EGFR degradation in GABARAP deficient cells depends on the activity of the proteasomal or lysosomal machinery or whether degradation would occur through a different non-canonical mechanism. To this end, the inhibition of lysosomal or proteasomal activity was obtained by chloroquine or lactacystin treatment, respectively (Figure 6A), which are known to inhibit either lysosomal acidification (chloroquine) or proteasomal subunits (lactacystin) and cause delay in EGF-induced EGFR degradation [74–76]. The cells were treated with chloroquine and total EGFR levels as well as the activation of MAPK/ERK signaling in response to subsequent EGF stimulation was analyzed by immunoblot (Figure 6B). This led to a delay in EGF-induced EGFR degradation in Huh7.5 cells and could, at least partly, restore the declined EGFR levels observed in GABARAP SKO cells in response to EGF stimulation shown in Figure 2A, as the total EGFR levels were only significantly reduced after 60 min. (1.69-fold, $p \leq 0.05$), but not at any of the other time points compared to Huh7.5 control cells (Figure 6C). Interestingly, MAPK signaling assessed by activating phosphorylation of ERK1/2 was still found to be significantly reduced in GABARAP SKO cells after 30 (1.77-fold, $p \leq 0.01$), 120 (1.8-fold, $p \leq 0.05$), and 180 min. (1.82-fold, $p \leq 0.01$) of EGF treatment when compared to controls (Figure 6D). Next, lactacystin treatment was applied prior to EGF stimulation and immunoblot analysis (Figure 6E).

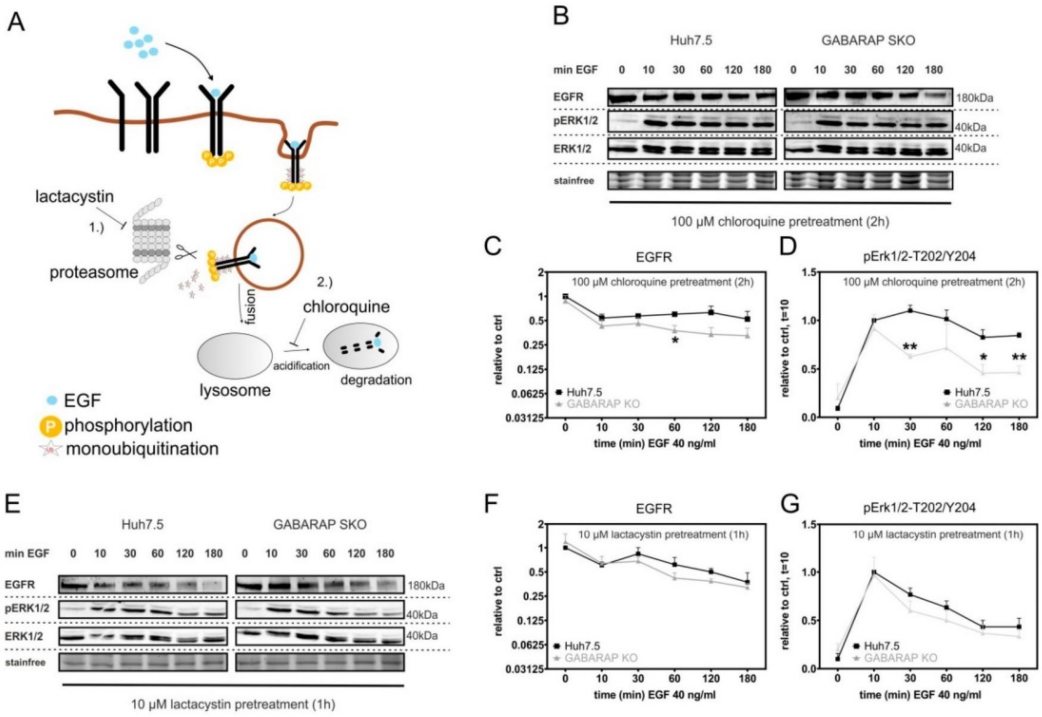

Figure 6. EGF-induced EGFR degradation after inhibition of lysosomal acidifcation and proteasomal inhibition in GABARAP SKO and Huh7.5 control cells. (**A**) Modes of action of the inhibitors used. Cells were pretreated with inhibitors of lysosomal acidifcation or proteasomal subunits and afterwards treated with 40 ng/mL EGF for the indicated times. (**B**–**D**) Cells were treated with lysosomal acidification inhibitor chloroquine. Total EGFR levels as well as activating phosphorylation of ERK1/2 at T202/Y204 were analyzed by immunoblotting and densitometry. (**D**–**G**) Cells were treated with proteasomal subunit inhibitor lactacystin. Total EGFR levels as well as activating phosphorylation of ERK1/2 at T202/Y204 were analyzed by immunoblotting and densitometry. Quantification of protein levels was performed by normalization to stain-free protein loading or the respective total levels of downstream signaling proteins and calculated as percentage of Huh7.5 control cells at unstimulated conditions (t = 0) for EGFR and peak activation levels (t = 10 min.) for ERK. Representative blots are shown for a summary of n ≥ 3 independent experiments. Error bars represent standard errors of means. Asterisk marks significant difference versus the corresponding time point of control cells as calculated using independent t-test. $p \leq 0.05$ = *. Figure S6E shows uncropped source blots.

Interestingly, this led to a delay in EGF-induced EGFR degradation in Huh7.5 control cells and abrogated the differences in EGFR protein between GABARAP SKO and Huh7.5 control cells after stimulation, as shown in Figure 2A, at any of the analyzed time points (Figure 6E). MAPK/ERK signaling was also found to be restored after lactacystin treatment in GABARAP SKO cells when compared to Huh7.5 control cells (Figure 6F). Taken together, these results indicated that GABARAP deficiency does not change the mechanism of EGFR degradation in general, but rather affects upstream events related to receptor trafficking. Impaired ERK signaling of GABARAP SKO cells under chloroquine treatment points to endosomal trafficking events when the cytoplasmic tail of the receptor is still able to contact the cytoplasm to activate downstream signaling molecules.

3.6. GABARAP and EGF Converge in Distinct Dynamic Vesicular Structures at Endogenous Expression Levels in HEK293 Cells

We asked whether both molecules localize to the same endosomal compartment after ligand stimulation to obtain an insight into the trafficking events underlying GABARAP-mediated regulation

of EGFR degradation. We generated a knock-in (KI) cell line expressing GFP-tagged GABARAP under control of the endogenous *GABARAP* promoter by CRISPR/Cas9 mediated genome editing to eliminate the impact of overexpression artifacts (Figure S1C, Table S1). The resulting GFP-GABARAP expression levels were sufficient for live cell microscopy, as demonstrated in Figure 7.

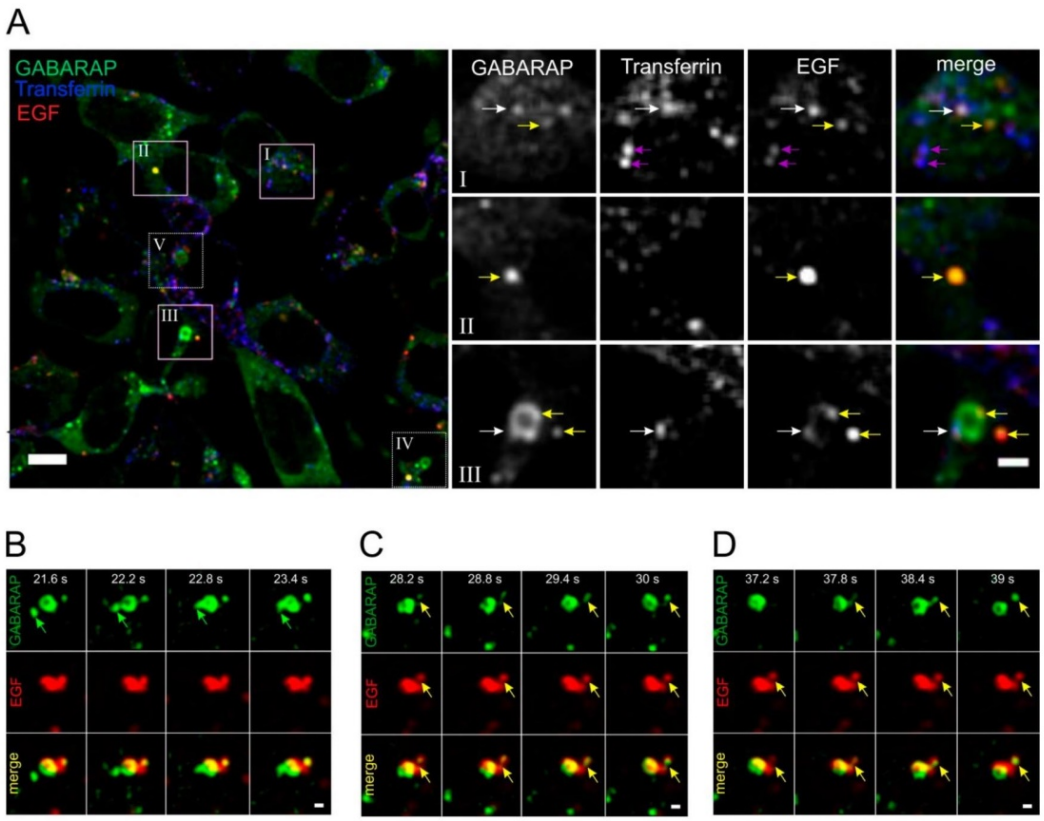

Figure 7. Live cell imaging of HEK293 knock-in cells expressing GFP-GABARAP under the endogenous *GABARAP* promoter after stimulation with EGF-Alexa647 and Tf-Alexa555. (**A**) HEK293 GFP-GABARAP knock-in (KI) cells were simultaneously treated with 40 ng/mL EGF-Alexa647 and 20 ng/mL Tf-Alexa555 for 60 min. and imaged under live-cell conditions by laser scanning confocal microscopy. White arrows highlight GABARAP/EGF/Tf triple-positive structures. Yellow arrows highlight GABARAP/EGF double-positive structures. Magenta arrowheads highlight EGF/Tf double-positive structures. In the merged images GABARAP fluorescence is depicted in green, EGF in red and Tf in blue. Snapshots are shown for selected time points of a 117 s time-lapse series consisting of 10 images with 13 s time intervals between images. In Figure S4, the complete time-lapse series of regions of interest I to V are shown, with a link to the corresponding movies. Scale bar in the overview = 10 µm, scale bar in close ups = 3 µm. (**B**–**D**) Spinning disk confocal fluorescence microscopy images of highly dynamic vesicles. GABARAP-only positive vesicles and large rings are highlighted by green arrows and GABARAP/EGF double-positive vesicles are highlighted by yellow arrows. In Figure S5 the complete time-lapse series is shown with a link to the corresponding movie. Scale bar = 3 µm.

GABARAP was found to be present in distinct structures in the cell's cytoplasm. These structures displayed different characteristics regarding their shape, size, and cargo, as determined by the simultaneous use of EGF-Alexa647 and Transferrin (Tf)-Alexa555 (Figure 7A, Figure S4 and Video S1). The latter was applied as a marker for endosomal compartments associated with recycling [77]. GABARAP and EGF frequently converged in punctate structures (yellow arrows), indicating that both

of the molecules are located within the same vesicle or at least adjacent vesicular structures. Some of these vesicles were additionally observed to be Tf-Alexa555 positive (white arrows), while others were found to be EGF and Tf double-positive (magenta arrows) without GABARAP localization. In contrast, we rarely observed GABARAP vesicles, which were additionally only Tf-positive. GABARAP and EGF also converged in Tf-negative ball-shaped structures (yellow arrows), indicating the accumulation of EGF and GABARAP within the same endosomal compartment, potentially associated with the degradative branch.

Strikingly, we frequently found large ring-like structures that were labeled with GABARAP (videos S1 III–V) of up to 3 µm in diameter. They were found at most once per cell and vesicles either double-positive for EGF and Tf or single-positive for EGF fused with the perimeters of these rings or budded off them. EGF accumulation was found in clusters resembling microdomains on these rings. Some, but not all, of these EGF clusters also contained Tf, suggesting that the respective parts of such rings might be associated with recycling. Altogether, these observations suggested that the large GABARAP-positive ring-like structures represent some sort of endosomal compartment, potentially a sorting endosome at the center of endosomal targeting either towards recycling or degradation.

We then subjected the GFP-GABARAP KI line to spinning disk confocal fluorescence microscopy to increase the temporal resolution (Figure 7B–D, Figure S5 and Video S2). After EGF-Alexa647 treatment, we could observe highly dynamic vesicular structures that were constantly fusing with and budding off the aforementioned GABARAP-positive rings. Figure 7B illustrates the fusion of a GABARAP single-positive vesicle with such a ring within a time frame as short as 1.2 s (green arrows). We also observed GABARAP vesicles that were EGF-Alexa647 positive (yellow arrows) and budded off the rings in a coordinated manner (Figure 7C). Frequently, these budding events were preceded by tubular protrusions (Figure 7D), which might represent molecules destined for recycling. Indeed, such cargo has been described to be sorted by tubular endosomal structures [78].

3.7. GABARAP Associates with EGFR during Co-Immunoprecipitation and Binds to Synthetic Peptides Derived from the EGFR Cytoplasmic Tail

We performed co-immunoprecipitation experiments, followed by *in vitro* interaction studies using purified GABARAP and synthetic peptides derived from the EGFR cytoplasmic tail, to investigate the nature of the transient co-migration observed during live cell imaging. As shown in Figure 8A, EGFR was co-immunoprecipitated by GFP-GABARAP but not by GFP from lysates of transiently transfected GABARAP SKO cells. This experiment confirmed an association between GABARAP and EGFR within cells. Interestingly, association was observed both under unstimulated conditions and after 10 min. of EGF treatment, supporting the idea of a GABARAP effect early in EGFR trafficking after ligand stimulation. The observed spatial overlap between GABARAP and EGFR during our live cell imaging studies, together with their observed co-immunoprecipitation, finally encouraged us to scan the EGFR sequence for canonical LIR/GIM motifs as putative direct GABARAP-binding sites. To address this, we used the iLIR tool [79]. Interestingly, EGFR indeed includes a putative extended LIR motif (xLIR) encompassing positions 1060 to 1065 (DTFLPV) within its cytoplasmic, regulatory tail (Figure 8B). Overall, this LIR motif contains four negatively charged and three phosphorylatable residues are located between P-8 and P-1, a further negatively charged residue at P + 5 and two phosphorylatable residues at P + 6 and P + 10. These features are in line with the established LIR-motifs of well-known GABARAP interactors, as demonstrated by alignment with the respective regions of ULK1, autophagy-related protein 13 (ATG13), Sequestosome-1 (SQSTM), pericentreolar material 1 (PCM1), and FIP200 [80].

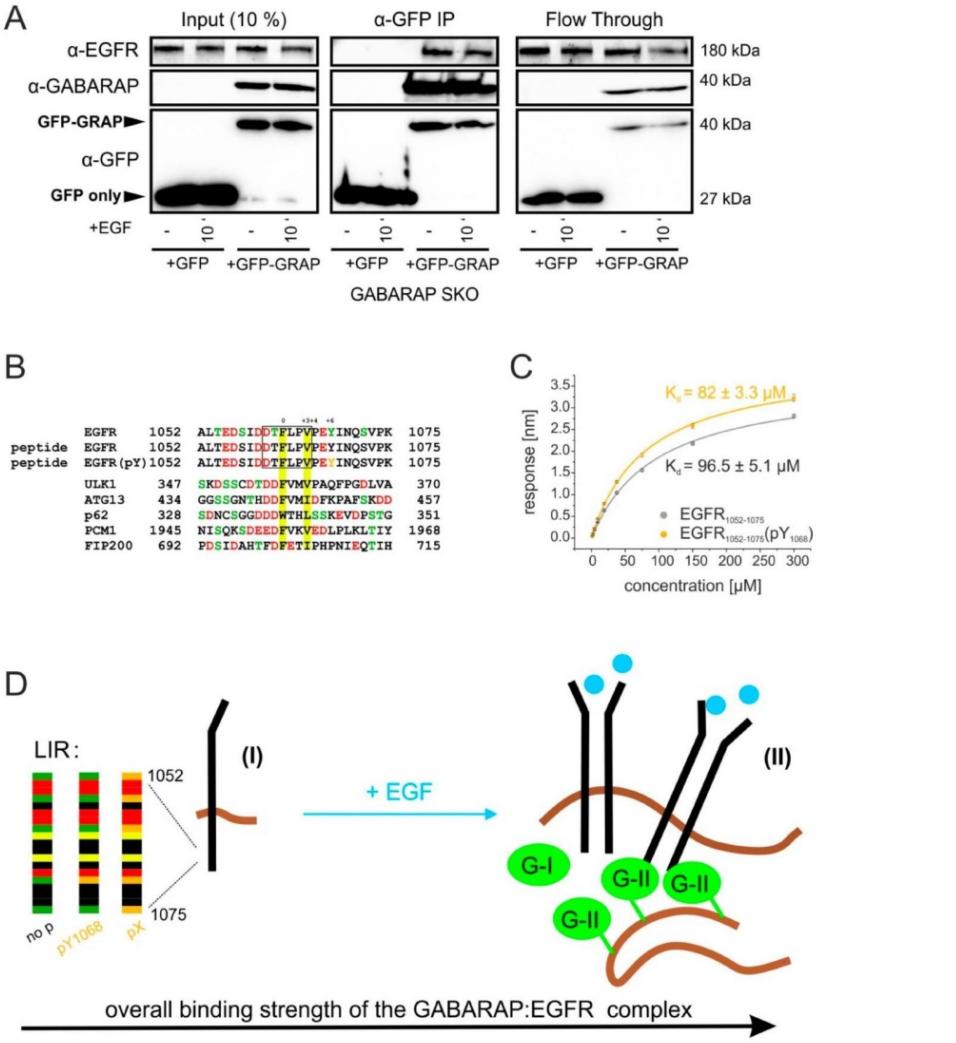

Figure 8. GABARAP associates with EGFR and binds to EGFR-derived peptides covering a putative LC3-interacting region (LIR) motif. (**A**) Co-Immunoprecipitation analysis between endogenous EGFR and transiently overexpressed GFP-GABARAP and GFP-only control in Huh7.5 GABARAP SKO cells. Figure S6F shows uncropped source blots. GRAP = GABARAP. (**B**) Sequence alignment of residues 1052 to 1075 of the cytoplasmic domain of EGFR with LIR-peptides from known GABARAP interaction partners. The core LIR motif is boxed and aromatic and hydrophobic residues in position 0 and +3 are depicted in yellow. Residues with negative charges are shown in red. Phosphorylatable residues are depicted in green. Both peptide sequences used for the BLI measurement shown in B are also depicted. Phosphorylated residue used in modified peptide is depicted in orange. Sequences were manually aligned according to the general core consensus (W/F/Y)-X-X-(L/I/V) where × may be any amino acid. (**C**) Ascending concentrations of recombinantly expressed and purified GABARAP were titrated to immobilized peptides and response measured by BLI. Measurements were performed in triplicates. Dissociation constants (Kd) of GABARAP were 96.5 ± 5.1 μM with the unmodified EGFR LIR peptide and 82 ± 3.3 μM with the phosphorylated peptide. (**D**) Model depicting modulation of binding affinity of GABARAP and EGFR. I: Phosphorylation of aa residues in the C-terminal tail of the receptor increases binding affinity through addition of negative charges. II: Increase of local concentration of EGFR due to ligand-induced dimerization and microclustering at the plasma membrane, as well as increase of local concentration of GABARAP due to lipidation, membrane association and possibly oligomerization increase avidity and, thus, overall binding strength of the GABARAP:EGFR complex. GABARAP is represented in green. G-I = unlipidated form of GABARAP, G-II = lipidated form of GABARAP.

Two aminoterminally biotinylated peptides covering the xLIR "DTFLPV" and additional eight positions up- and ten positions downstream, one of them phosphorylated at the regulatory Y1068, were subjected to biolayer interferometry (BLI) to analyze the binding affinity of GABARAP to this EGFR region. Figure 8C shows results of BLI measurements. The obtained dissociation constants were 96.5 µM (±5.1 µM) and 82 µM (±3.3 µM) for the unmodified and the modified peptide, respectively. These affinities appear relatively weak when compared to those of other known GABARAP protein interactors being in the low micromolar range [49]. Nonetheless, this interaction still might be of relevance e.g., in microdomains of locally clustered EGFR and GABARAP molecules (Figure 8D) by increasing overall avidity. Whether or not the xLIR motif is decisive for GABARAP binding to EGFR will be the subject of further investigation.

4. Discussion

In this study we identified a unique and novel role for GABARAP in EGF-induced trafficking and degradation of the EGFR, with implications for EGFR downstream signaling. Based on two independently generated HEK293 and Huh7.5 KO cell line panels, we could show that only cells lacking GABARAP, but not GABARAPL1 or GABARAPL2, displayed reduced total EGFR protein levels after EGF stimulation. We further showed that MAPK signaling downstream of EGFR was impaired in GABARAP deficient Huh7.5 cells, which translated into the reduction of EGFR target gene *CXCL8* expression. Consequently, we then explored the potential mechanistic role of GABARAP in the context of EGFR trafficking and degradation.

EGFR cycling can roughly be divided into five stages (Figure 9A): EGFR gene transcription and protein expression (1) are followed by post-translational modifications in the ER, trafficking through the Golgi-apparatus and surface targeting (2). Plasma membrane localized EGFR can then encounter extracellular stimuli, such as EGF. Ligand-bound EGFR is activated and internalized to strictly control signaling strength and duration (3). Subsequently, EGFR gets sorted within the endosomal system and is either recycled back to the plasma membrane (4) or targeted for degradation in the lysosome (5).

A

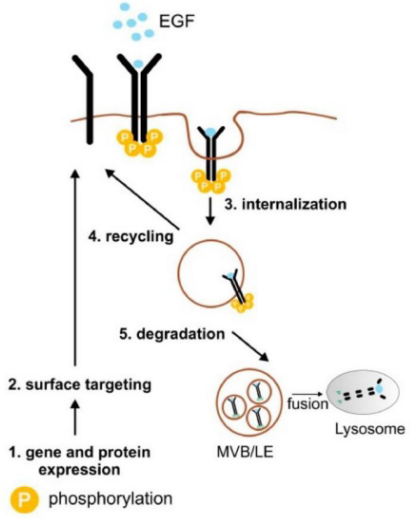

B

GABARAP protein interactions potentially influencing EGFR trafficking and degradation

level of interaction	affected process	interaction partner
direct	1 - 5	EGFR (figure 8)
indirect	3 [16, 70]	Clathrin [83]
	3 [84]	RTN3 [85]
	4 - 5 [88, 89]	NEDD4 [86]
	4 - 5 [88, 90]	CBL [25]
	5 [91]	CUL3 [92]
	4 [94]	TBC1D5/16 [95]
	5 [96]	RMC1 [41]
	3 + 4 [97]	OstIII [97]
	5 [101]	PLEKHM1 [49]

Figure 9. Scheme depicting EGFR internalization, trafficking and degradation including potential ways for GABARAP to take action. (**A**) 1. *EGFR* gene is expressed as mRNA and translated into protein followed by posttranslational modifications. 2. Trafficking through the Golgi apparatus regulates correct EGFR surface expression. 3. Upon extracellular ligand binding EGFR is internalized, sorted via the endosomal system and either targeted for recycling (4) or degradation (5). (**B**) List of processes that can be targeted by GABARAP either based on a direct interaction of GABARAP with EGFR as suggested in this study (grey) or indirectly by known or putative GABARAP interaction partners (light orange) with described activities in respective processes. MVB = multivesicular body, LE = late endosome.

An impact of GABARAP on basal protein levels of both total and cell surface localized EGFR seems unlikely, given our observations under unstimulated conditions. Additionally, steady state and EGF stimulated gene expression of the receptor was not influenced by GABARAP deficiency.

While we also did not observe an impact of GABARAP on the initial uptake of EGF-Alexa647, several hints strongly suggest that early internalization events might be slowed down by GABARAP. We found GABARAP deficiency associated with initially increased phosphorylation of EGFR Y1068, which is known to be associated with EGFR activation, growth factor receptor-bound protein 2 (GRB2), and E3 ubiquitin-protein ligase CBL binding, followed by internalization and subsequent degradation of the receptor [81]. We also observed higher volumes and intensities of EGF-containing vesicles as early as after 5 min. of EGF treatment in GABARAP deficient cells, indicating that GABARAP negatively influences the speed of early uptake events. Taken together, these observations suggest that GABARAP acts at an early stage of endosomal EGFR trafficking immediately downstream of ligand-induced receptor activation. In that way, increased EGFR degradation in GABARAP SKO cells would be a cumulative effect based on influencing early receptor dynamics.

Whether GABARAP influences EGFR activation through regulating the strength of dimer formation, as reported for different EGFR ligands [82], needs to be determined in further studies. As exemplarily shown in Figure 9B, a plethora of GABARAP interaction partners have already been reported to participate in endosomal sorting of the EGFR. The internalization of EGFR via clathrin-mediated endocytosis (CME) [16] might be modulated through direct interaction of GABARAP with the clathrin-heavy chain, which has already been described [83]. Interestingly, *CXCL8* expression was already reduced at low (i.e., 1.25 ng/mL) concentrations of EGF in the absence of GABARAP, indicating that CME, which is the major internalization route at low ligand concentrations [17], might be positively influenced by GABARAP. The high ligand concentrations that we mainly used in our study are known to activate clathrin-independent endocytosis (CIE), balancing the ratio of CME:CIE to about 1:1 [70]. CIE was reported to be mediated by ER/plasma membrane contact sites facilitated by reticulon 3 (RTN3) [84]. Intriguingly, RTN3 was recently described to interact with human Atg8 proteins through functional LIR motifs in the context of selective ER-phagy [85]. Thus, GABARAP could also sequester RTN3, hindering it from promoting CIE of EGFR. Thereby, GABARAP might shift the equilibrium towards enhanced CME and recycling.

Additionally, the E3 ubiquitin ligases NEDD4 and CBL have already been described to exhibit functional LIR motifs [25,86]. They take part in monoubiquitination of activated receptors, which is a signal for sorting into degradative compartments [87,88]. In particular, NEDD4 facilitates EGF-induced EGFR degradation by the ubiquitination of activated Cdc42-associated tyrosine kinase (ACK), leading to the degradation of both proteins [89]. Members of the E3 ubiquitin-protein ligase CBL family also target receptor tyrosine kinases for degradation by ubiquitination [90]. GABARAP might sequester these E3 ligases and, thus, prevent them from targeting receptors to degradation by monoubiquitination. With Cullin-3 (CUL3) another E3 ligase was reported to be positively involved in the maturation of late endosomes [91] and interact with GABARAP via KBTBD6/7 (Kelch repeat and BTB domain-containing protein 6/7) binding [92]. In this context, GABARAP might indirectly sequester CUL3 via KBTBD6/7, thereby inhibiting its positive effect on late endosome maturation and thus attenuate EGFR degradation.

Experimental evidence for GABARAP participating at the level of endosomal sorting comes from our EGF uptake results using confocal laser scanning microscopy, demonstrating that GABARAP SKO cells show altered vesicular size and EGF-Alexa647 loading, especially regarding larger vesicles with high fluorescence intensity at later time points upon stimulation.

The RAS-related in brain (RAB) protein family of small GTPases plays a major role in endocytic trafficking [93]. Several possibilities exist for GABARAP to influence RAB related processes. TBC1 domain family member 16 (TBC1D16) was described to be a negative regulator of RAB4A, thereby inhibiting the recycling of activated EGFR [94]. TBC1D16 was also reported to interact with Atg8 proteins in pulldown experiments, similar to other TBC domain containing proteins [95]. Whether

GABARAP directly interacts with TBC1D16 to counteract its negative effect on EGFR recycling or whether other TBC domain containing proteins are involved needs to be elucidated in future studies.

The association of the RAB proteins 5, 11, and 7 with EGF-Alexa647 was not found to be altered in GABARAP deficient cells during our experiments, implicating that GABARAP activity is not necessary for general endosomal targeting of EGFR. However, we cannot exclude that subtle or transient differences remained undetected under the experimental conditions used. Time-lapse live cell imaging while using KI cell lines expressing fluorescent protein tagged RABs can help to clarify this issue in more depth in the future.

KI cells expressing GFP-GABARAP under the endogenous *GABARAP* promoter enabled us to detect transient co-migration of GABARAP and EGF in the cytoplasm of cells under live conditions while using confocal laser scanning microscopy. Diverse punctate vesicular structures were frequently found along with GABARAP positive rings forming microdomain-like spots, which were either positive for EGF- or for the recycling compartment marker Transferrin, emphasizing the importance of GABARAP-related activity for EGFR trafficking. Using spinning disk confocal fluorescence microscopy we improved the temporal resolution up to 20-fold, enabling us to assess the dynamics of GABARAP- and EGF-containing vesicles. We observed highly dynamic GABARAP-, EGF- or GABARAP/EGF-containing vesicles fusing with or budding off such rings. These intracellular interactions strongly suggest that also later stages of endosomal trafficking that are not associated with Tf are affected by GABARAP, potentially correlating with a role in endosomal sorting and/or maturation.

A potential role of GABARAP in inhibiting endosome maturation is supported by the finding that the protein levels of the CCZ1/MON1 positive regulator RMC1 are elevated in cells deficient for the whole GABARAP subfamily [41]. CCZ1/MON1 acts as an activator of RAB7 [96]. The inhibition of late endosome maturation might be mediated by GABARAP preventing RMC1 from activating RAB7 through CCZ1/MON1. Another RAB regulator interacting with GABARAP is the RAC1 GEF Ost-III, which negatively regulates CME of receptors and it was found to be inhibited by ectopic GABARAP expression [97]. Two main degradative pathways play a role in EGF-induced EGFR degradation. First, proteasome-mediated deubiquitination of activated receptors is necessary for EGFR containing endosomes to mature into intraluminal vesicles (ILV) of multivesicular bodies (MVB) [98]. Second, processed receptors are targeted for degradation within the lysosomal compartment [99]. Proteasomal inhibition by lactacystin restored both EGFR protein levels and ERK1/2 phosphorylation to wildtype, indicating that GABARAP acts downstream or on the level of MVB maturation. In contrast, the inhibition of lysosomal acidification by chloroquine partly restored EGFR degradation towards wildtype levels. Notably, ERK1/2 phosphorylation was still impaired in GABARAP SKO cells. Chloroquine is known to inhibit EGFR degradation by preventing fusion of multivesicular bodies/late endosomes with the lysosome [100], indicating that GABARAP affects ERK1/2 activation earlier in the process. Thus, we hypothesize that GABARAP might act on the level of endosomal maturation and/or compartmentalization, e.g., by controlling maturation of EGFR containing vesicles into ILVs of MVBs upstream of lysosomal degradation.

Finally, Pleckstrin homology domain-containing family M member 1 (PLEKHM1) binding simultaneously to Atg8 family proteins and the homotypic fusion and protein sorting (HOPS) complex was reported to regulate ligand-induced EGFR degradation due to impaired lysosomal fusion [101]. Importantly, PLEKHM1 was found to contain a LIR displaying a much higher affinity to GABARAP subfamily proteins than LC3 subfamily proteins [49]. However, the binding of all GABARAP subfamily proteins was described to be in the low micromolar range, strongly suggesting that GABARAP function in this context might be redundant to GABARAPL1 and/or GABARAPL2.

GABARAP might also directly bind to EGFR under certain circumstances due to the existence of an xLIR motif, which we identified in the cytoplasmic domain of EGFR. The binding of EGFR LIR peptides to immobilized GABARAP was quite modest during our measurements as compared with most GABARAP interactions reported previously. Nevertheless, EGF stimulation is known to promote EGFR nanocluster formation [102,103] by receptor oligomerization and membrane bending [104] prior

to internalization [105]. GABARAP has also been described to form self-associated species [106]. Such clusters may increase the local EGFR and/or GABARAP concentration facilitating LIR-mediated binding. Indeed, we were able to show the co-immunoprecipitation of GFP-GABARAP and EGFR both with and without EGF treatment. These results and the observed comigration of GFP-GABARAP and EGF-Alexa647 strongly suggest an at least transient interaction between GABARAP and EGFR.

Such an interaction could either result in direct targeting of EGFR into autophagosomes or involve endosomal sorting. Direct autophagic targeting of proteins by GABARAP has recently been described for the nuclear receptor co-repressor 1 (NCOR1) [107]. On the other hand, EGFR activation actively suppresses autophagy by beclin 1 phosphorylation [108], and we did not use autophagy inducing conditions in our set up.

GABARAP might bind to EGFR-containing vesicles, presenting the xLIR motif on their outer face and thereby connect them to the microtubule network, which is known to associate with GABARAP [52]. In this case, EGFR vesicle transport would be mediated in a very direct manner.

Finally, several RTKs are associated with autophagy related processes. For example, protein turnover of TNFRSF12A (TNF receptor superfamily member 12 A) is regulated by mammalian Atg8 family proteins, with GABARAP and GABARAPL2 fulfilling different roles in this process [109]. Autophagy degraded the RTK ret proto-oncogene (RET) [24]. The former case supports the idea of non-redundant roles of GABARAP subfamily proteins, similar to what we observe for EGFR in Huh7.5 cells regarding GABARAP action.

5. Conclusions

Altogether, the presented data supports a unique and non-redundant role for GABARAP in the context of EGF-induced EGFR degradation. GABARAP may be able to influence EGFR trafficking on numerous levels, including, but very likely not limited to, a direct interaction with EGFR, as depicted in Figure 9. Therefore, further detailed studies will be necessary to determine the underlying molecular mechanism(s) of GABARAP interfering with EGFR trafficking and endosomal trafficking in general. It will also be of paramount importance to clarify the roles of the other two GABARAP subfamily proteins in that context. Lastly, we shall not forget the involvement of GABARAP subfamily proteins in important cellular processes, such as autophagy and lysosomal fusion, which cannot be ruled out to have an effect on most phenotypes in general. We have just started to uncover the mode of action of human Atg8 proteins and their contribution to cell surface receptor fate in general.

Supplementary Materials: The following are available online at http://www.mdpi.com/2073-4409/9/5/1296/s1, Figure S1: Verification of CRISPR/Cas9 knockout and knock-in cell lines on protein level, Table S1: CRISPR sequence details and genotyping results of the knockout cell lines used, Figure S2: Total EGFR levels in response to EGF treatment in HEK293 KO cells transiently overexpressing EGFR-GFP, Figure S3: Analysis of EGF-Alexa647 containing vesicles of GABARAP SKO and Huh7.5 cells by Imaris and analysis of endosomal markers RAB 5, RAB11 and RAB7 in response to EGF treatment in GABARAP SKO and Huh7.5 control cells, Figure S4: Montage of live cell imaging of HEK293 knock-in cells expressing GFP-GABARAP under the endogenous GABARAP promoter and stimulated with EGF-Alexa647 and Tf-Alexa555 by confocal laser scanning microscopy, Figure S5: Live cell imaging of HEK293 KI cells expressing GFP-GABARAP under the endogenous *GABARAP* promoter and stimulated with EGF-Alexa647 by spinning disk confocal fluorescence microscopy, Figure S6: Uncropped source blots of immunoblotting experiments, Movie S1: Live cell imaging of HEK293 knock-in cells expressing GFP-GABARAP under the endogenous GABARAP promoter and stimulated with EGF-Alexa647 and Tf-Alexa555 by confocal laser scanning microscopy and Movie S2: Live cell imaging of HEK293 KI cells expressing GFP-GABARAP under the endogenous GABARAP promoter and stimulated with EGF-Alexa647 by spinning disk confocal fluorescence microscopy.

Author Contributions: Conceptualization, J.D., O.H.W., J.G.B., S.H. and D.W.; Formal analysis, J.D., I.M.S., S.H. and M.S.; Funding acquisition, S.H. and D.W.; Investigation, J.D., I.M.S., K.R., M.S., I.A. and T.G.; Project administration, D.W.; Resources, S.H., T.G., J.G.B. and D.W.; Supervision, S.H. and D.W.; Validation, J.D. and I.M.S.; Visualization, J.D. and I.M.S.; Writing—original draft, J.D. and S.H.; Writing—review & editing, J.D., I.M.S., K.R., M.S., O.H.W., T.G., J.G.B., S.H. and D.W. All authors have read and agreed to the published version of the manuscript.

Funding: This work was supported by a grant from the Jürgen Manchot Foundation, Molecules of Infection Graduate School (MOI III) (J.D. and K.R.), funded by the Deutsche Forschungsgemeinschaft (DFG, German Research Foundation)–Project-ID 267205415–SFB 1208 (D.W.), funding for the Center for Advanced Imaging (WE5343/1-1) and by funding of the Vorstandsdoktorandenprogramm of the Forschungszentrum Jülich (I.A.). The authors declare that they have no conflicts of interest with the contents of this article.

Acknowledgments: We are grateful to Marianne Wammers for guidance with the FACS. We thank Claudia Hoppen for cloning of the original KO plasmids.

Conflicts of Interest: The authors declare no conflict of interest.

Appendix A

Table A1. Antibodies used in this study.

Antibody	Company	Species	Catalog Number/Dilution-Application (Antigen Used for Antibody Production)
primary Abs:			
anti-EGFR	Cell Signaling	rabbit	2232/1:1000-IB (synthetic peptide corresponding to residues surrounding Tyr1068 of human EGFR)
anti-EGFR	Cell Signaling	rabbit	4267/1:1000-IB (fusion protein containing the cytoplasmic domain of human EGFR)
anti-phospho-EGFR (Tyr1068)	Cell Signaling	rabbit	2234/1:1000–IB (synthetic peptide corresponding to residues surrounding Tyr1068 of human EGFR)
anti-Akt (pan)	Cell Signaling	mouse	2920/1:1000-IB (synthetic peptide at the carboxyterminal sequence of human Akt)
anti-phospho-Akt (Ser473)	Cell Signaling	rabbit	4060/1:1000-IB (synthetic phosphopeptide corresponding to residues around Ser473 of human Akt)
anti-p44/42 MAPK (Erk1/2)	Cell Signaling	rabbit	4695/1:1000-IB (synthetic peptide corresponding to residues near the C-terminus of rat p44 MAP kinase)
anti-phospho-p44/42 MAPK (Erk1/2) (Thr202/Tyr204)	Cell Signaling	mouse	9106/1:1000-IB (synthetic phospho-peptide (KLH-coupled) corresponding to residues surrounding Thr202/Tyr204 of human p44 MAP kinase)
anti-beta actin	Abcam	mouse	ab6276/1:15 000-IB (DDDIAALVIDNGSGK)
anti-GABARAP	Cell Signaling	rabbit	13733/1:1000-IB (synthetic peptide corresponding to residues surrounding Arg40 of human GABARAP)
anti-GABARAP	In-house	rat	In-house/undiluted-IF Institute for Diabetes and Obesity, Monoclonal Antibody Core Facility, GST-hGABARAP_aa1-117 [65]
anti-GABARAPL1	Cell Signaling	rabbit	26632/1:1000-IB (synthetic peptide corresponding to residues near the amino terminus of human GABARAPL1)
anti-GABARAPL2	Cell Signaling	rabbit	14256/1:1000-IB (synthetic peptide corresponding to residues near the carboxy terminus of human GABARAPL2)
anti-GFP (HRP-coupled)	Miltenyi Biotech	mouse	130-091-833/1:2000-IB (proprietary)
anti-RAB5	Cell Signaling	rabbit	3547S/1:100-IF (synthetic peptide corresponding to residues surrounding Gly190 of human Rab5A protein)
anti-RAB7	Cell Signaling	rabbit	9367S/1:100-IF (synthetic peptide corresponding to residues surrounding Glu188 of human Rab7 protein)

Table A1. *Cont.*

Antibody	Company	Species	Catalog Number/Dilution-Application (Antigen Used for Antibody Production)
anti-RAB11	Cell Signaling	rabbit	5589S/1:100-IF (synthetic peptide corresponding to residues near the amino terminus of human Rab11 protein.
secondary Abs:			
anti-Mouse IgG H&L (Alexa Fluor® 488)	Abcam	goat	150117/1:250–IF or 1:5000-IB (mouse IgG)
anti-Rabbit IgG H&L (Alexa Fluor® 647)	Abcam	goat	150083/1:250–IF or 1:5000-IB (rabbit IgG)
anti-rat IgG+IgM H&L (Alexa Fluor® 488)	Jackson ImmunoResearch	goat	112-545-068/1:250–IF (rat IgG + IgM)
anti-rabbit IgG H&L (Alexa Fluor® 555 preadsorbed)	Abcam	goat	150086/1:250–IF (rabbit IgG)

Table A2. Primers used in this study.

	Sequence (5′ → 3′)
qPCR	
CXCL8 forward	AGAAGTTTTTGAAGAGGGCTGAGA
CXCL8 reverse	CAGACCCACACAATACATGAAGTG
CXCL1 forward	CTGGCGGATCCAAGCAAAT
CXCL1 reverse	CATTCCCCTGCCTTCACAAT
SDHA forward	AGATGTGGTGTCTCGGTCGAT
SDHA reverse	CGTGATCTTTCTCAGGGCCA
EGFR forward	CATCCAGTGGCGGGACATAG
EGFR reverse	GGGACAGCTTGGATCACACT
Genotyping	
GABARAP forward	GGGTTGGTGAATAGGGAAGTGG
GABARAP reverse	CACTCCTTTCATCCTGGGTCC
GABARAPL1 forward	TGGGAACCTGATCCAAGACTC
GABARAPL1 reverse	GCCAGGAAGCTAGTCCAAAAC
GABARAPL2 forward	CTTGCTGGGAGCTAGTAGGG
GABARAPL2 reverse	TGAGGCACCCTGAACAGCA

References

1. Cohen, S.; Carpenter, G.; King, L. Epidermal growth factor-receptor-protein kinase interactions. Co-purification of receptor and epidermal growth factor-enhanced phosphorylation activity. *J. Biol. Chem.* **1980**, *255*, 4834–4842. [PubMed]
2. Chen, J.; Zeng, F.; Forrester, S.J.; Eguchi, S.; Zhang, M.-Z.; Harris, R.C. Expression and Function of the Epidermal Growth Factor Receptor in Physiology and Disease. *Physiol. Rev.* **2016**, *96*, 1025–1069. [CrossRef]
3. Roberts, A.B.; Lamb, L.C.; Newton, D.L.; Sporn, M.B.; De Larco, J.E.; Todaro, G.J. Transforming growth factors: Isolation of polypeptides from virally and chemically transformed cells by acid/ethanol extraction. *Proc. Natl. Acad. Sci. USA* **1980**, *77*, 3494–3498. [CrossRef] [PubMed]
4. Shoyab, M.; McDonald, V.L.; Bradley, J.G.; Todaro, G.J. Amphiregulin: A bifunctional growth-modulating glycoprotein produced by the phorbol 12-myristate 13-acetate-treated human breast adenocarcinoma cell line MCF-7. *Proc. Natl. Acad. Sci. USA* **2006**, *85*, 6528–6532. [CrossRef]
5. Cohen, S. Isolation of a mouse submaxillary gland protein accelerating incisor eruption and eyelid opening in the new-born animal. *J. Biol. Chem.* **1962**, *237*, 1555–1562.
6. Yarden, Y.; Sliwkowski, M.X. Untangling the ErbB signalling network. *Nat. Rev. Mol. Cell Biol.* **2001**, *2*, 127–137. [CrossRef]

7. Honegger, A.M.; Kris, R.M.; Ullrich, A.; Schlessinger, J. Evidence that autophosphorylation of solubilized receptors for epidermal growth factor is mediated by intermolecular cross-phosphorylation. *Proc. Natl. Acad. Sci. USA* **1989**, *86*, 925–929. [CrossRef]
8. Honegger, A.M.; Schmidt, A.; Ullrich, A.; Schlessinger, J. Evidence for epidermal growth factor (EGF)-induced intermolecular autophosphorylation of the EGF receptors in living cells. *Mol. Cell. Biol.* **1990**, *10*, 4035–4044. [CrossRef]
9. Xie, H.; Pallero, M.A.; Gupta, K.; Chang, P.; Ware, M.F.; Witke, W.; Kwiatkowski, D.J.; Lauffenburger, D.A.; Murphy-Ullrich, J.E.; Wells, A. EGF receptor regulation of cell motility: EGF induces disassembly of focal adhesions independently of the motility-associated PLCgamma signaling pathway. *J. Cell Sci.* **1998**, *111 Pt 5*, 615–624.
10. Wee, P.; Wang, Z. Epidermal growth factor receptor cell proliferation signaling pathways. *Cancers* **2017**, *9*, 52.
11. Uemura, T.; Kametaka, S.; Waguri, S. GGA2 interacts with EGFR cytoplasmic domain to stabilize the receptor expression and promote cell growth. *Sci. Rep.* **2018**, *8*, 1–14. [CrossRef] [PubMed]
12. Yarden, Y.; Pines, G. The ERBB network: At last, cancer therapy meets systems biology. *Nat. Rev. Cancer* **2012**, *12*, 553–563. [CrossRef] [PubMed]
13. Sigismund, S.; Avanzato, D.; Lanzetti, L. Emerging functions of the EGFR in cancer. *Mol. Oncol.* **2018**, *12*, 3–20. [CrossRef] [PubMed]
14. Carpenter, G.; Cohen, S. 125I-Labeled human epidermal growth factor: Binding, Internalization, and Degradation in Human Fibroblasts Antiserum to hEGF 1251-hEGF Binding Assay Iodination o f hEGF and Antiserum Autoradiography. *J. Cell Biol.* **1976**, *71*, 159–171. [CrossRef]
15. Haigler, H.T.; McKanna, J.A.; Cohen, S. Direct visualization of the binding and internalization of a ferritin conjugate of epidermal growth factor in human carcinoma cells A-431. *J. Cell Biol.* **1979**, *81*, 382–395. [CrossRef]
16. Hanover, J.A.; Willingham, M.C.; Pastan, I. Kinetics of transit of transferrin and epidermal growth factor through clathrin-coated membranes. *Cell* **1984**, *39*, 283–293. [CrossRef]
17. Sigismund, S.; Woelk, T.; Puri, C.; Maspero, E.; Tacchetti, C.; Transidico, P.; Di Fiore, P.P.; Polo, S. Clathrin-independent endocytosis of ubiquitinated cargos. *Proc. Natl. Acad. Sci. USA* **2005**, *102*, 2760–2765. [CrossRef]
18. Bakker, J.; Spits, M.; Neefjes, J.; Berlin, I. The EGFR odyssey—From activation to destruction in space and time. *J. Cell Sci.* **2017**, *130*, 4087–4096. [CrossRef]
19. Yu, L.; Chen, Y.; Tooze, S.A. Autophagy pathway: Cellular and molecular mechanisms. *Autophagy* **2018**, *14*, 207–215. [CrossRef]
20. Antonioli, M.; Di Rienzo, M.; Piacentini, M.; Fimia, G.M. Emerging Mechanisms in Initiating and Terminating Autophagy. *Trends Biochem. Sci.* **2017**, *42*, 28–41. [CrossRef]
21. Shibutani, S.T.; Yoshimori, T. A current perspective of autophagosome biogenesis. *Cell Res.* **2014**, *24*, 58–68. [CrossRef] [PubMed]
22. Anding, A.L.; Baehrecke, E.H. Cleaning House: Selective Autophagy of Organelles. *Dev. Cell* **2017**, *41*, 10–22. [CrossRef] [PubMed]
23. Mao, K.; Klionsky, D.J. Xenophagy: A battlefield between host and microbe, and a possible avenue for cancer treatment. *Autophagy* **2017**, *13*, 223–224. [CrossRef]
24. Sandilands, E.; Serrels, B.; Wilkinson, S.; Frame, M.C. Src-dependent autophagic degradation of Ret in FAK-signalling-defective cancer cells. *EMBO Rep.* **2012**, *13*, 733–740. [CrossRef] [PubMed]
25. Sandilands, E.; Serrels, B.; McEwan, D.G.; Morton, J.P.; MacAgno, J.P.; McLeod, K.; Stevens, C.; Brunton, V.G.; Langdon, W.Y.; Vidal, M.; et al. Autophagic targeting of Src promotes cancer cell survival following reduced FAK signalling. *Nat. Cell Biol.* **2012**, *14*, 51–60. [CrossRef]
26. Ponpuak, M.; Mandell, M.A.; Kimura, T.; Chauhan, S.; Cleyrat, C.; Deretic, V. Secretory autophagy. *Curr. Opin. Cell Biol.* **2015**, *35*, 106–116. [CrossRef]
27. Claude-Taupin, A.; Jia, J.; Mudd, M.; Deretic, V. Autophagy's secret life: Secretion instead of degradation. *Essays Biochem.* **2017**, *61*, 637–647.
28. Matsuura, A.; Tsukada, M.; Wada, Y.; Ohsumi, Y. Apg1p, a novel protein kinase required for the autophagic process in Saccharomyces cerevisiae. *Gene* **1997**, *192*, 245–250. [CrossRef]

29. Mizushima, N.; Yoshimori, T.; Ohsumi, Y. The Role of Atg Proteins in Autophagosome Formation. *Annu. Rev. Cell Dev. Biol.* **2011**, *27*, 107–132. [CrossRef]
30. Tsukada, M.; Ohsumi, Y. Isolation and characterization of autophagy-defective mutants of Saccharomyces cerevisiae. *FEBS Lett.* **1993**, *333*, 169–174. [CrossRef]
31. Shpilka, T.; Weidberg, H.; Pietrokovski, S.; Elazar, Z. Atg8: An autophagy-related ubiquitin-like protein family. *Genome Biol.* **2011**, *12*, 226. [CrossRef] [PubMed]
32. Weiergräber, O.; Mohrlüder, J.; Willbold, D. *Atg8 Family Proteins—Autophagy and Beyond. In Autophagy—A Double-Edged Sword—Cell Survival or Death?* InTech: Rijeka, Croatia, 2013; pp. 267–322.
33. Zhang, Z.; Xu, X.; Ma, J.; Wu, J.; Wang, Y.; Zhou, R.; Han, J. Gene Deletion of Gabarap Enhances Nlrp3 Inflammasome-Dependent Inflammatory Responses. *J. Immunol.* **2013**, *190*, 3517–3524. [CrossRef] [PubMed]
34. Keulers, T.G.; Schaaf, M.B.E.; Rouschop, K.M.A. Autophagy-dependent secretion: Contribution to tumor progression. *Front. Oncol.* **2016**, *6*, 251. [CrossRef] [PubMed]
35. Peng, G.; Yan, Y.; Zhu, C.; Wang, S.; Yan, X.; Lu, L.; Li, W.; Hu, J.; Wei, W.; Mu, Y.; et al. Borna Disease Virus P Protein Affects Neural Transmission through Interactions with Gamma-Aminobutyric Acid Receptor-Associated Protein. *J. Virol.* **2008**, *82*, 12487–12497. [CrossRef]
36. Chen, R.Y.; Shen, K.L.; Chen, Z.; Fan, W.W.; Xie, X.L.; Meng, C.; Chang, X.J.; Zheng, L.B.; Jeswin, J.; Li, C.H.; et al. White spot syndrome virus entry is dependent on multiple endocytic routes and strongly facilitated by Cq-GABARAP in a CME-dependent manner. *Sci. Rep.* **2016**, *6*. [CrossRef]
37. Boeske, A.; Schwarten, M.; Ma, P.; Tusche, M.; Mötter, J.; Möller, C.; Neudecker, P.; Hoffmann, S.; Willbold, D. Direct binding to GABARAP family members is essential for HIV-1 Nef plasma membrane localization. *Sci. Rep.* **2017**, *7*, 5797. [CrossRef]
38. Mohrlüder, J.; Schwarten, M.; Willbold, D. Structure and potential function of γ-aminobutyrate type A receptor-associated protein. *FEBS J.* **2009**, *276*, 4989–5005. [CrossRef]
39. Weidberg, H.; Shvets, E.; Shpilka, T.; Shimron, F.; Shinder, V.; Elazar, Z. LC3 and GATE-16/GABARAP subfamilies are both essential yet act differently in autophagosome biogenesis. *EMBO J.* **2010**, *29*, 1792–1802. [CrossRef]
40. Nguyen, T.N.; Padman, B.S.; Usher, J.; Oorschot, V.; Ramm, G.; Lazarou, M. Atg8 family LC3/GAB ARAP proteins are crucial for autophagosome-lysosome fusion but not autophagosome formation during PINK1/Parkin mitophagy and starvation. *J. Cell Biol.* **2016**, *215*, 857–874. [CrossRef]
41. Vaites, L.P.; Paulo, J.A.; Huttlin, E.L.; Harper, J.W. Systematic Analysis of Human Cells Lacking ATG8 Proteins Uncovers Roles for GABARAPs and the CCZ1/MON1 Regulator C18orf8/RMC1 in Macroautophagic and Selective Autophagic Flux. *Mol. Cell. Biol.* **2017**, *38*, e00392-17. [CrossRef]
42. Novak, I.; Kirkin, V.; McEwan, D.G.; Zhang, J.; Wild, P.; Rozenknop, A.; Rogov, V.; Löhr, F.; Popovic, D.; Occhipinti, A.; et al. Nix is a selective autophagy receptor for mitochondrial clearance. *EMBO Rep.* **2010**, *11*, 45–51. [CrossRef] [PubMed]
43. Rozenknop, A.; Rogov, V.V.; Rogova, N.Y.; Löhr, F.; Güntert, P.; Dikic, I.; Dötsch, V. Characterization of the interaction of GABARAPL-1 with the LIR motif of NBR1. *J. Mol. Biol.* **2011**, *410*, 477–487. [CrossRef] [PubMed]
44. Rogov, V.V.; Suzuki, H.; Fiskin, E.; Wild, P.; Kniss, A.; Rozenknop, A.; Kato, R.; Kawasaki, M.; McEwan, D.G.; Löhr, F.; et al. Structural basis for phosphorylation-triggered autophagic clearance of Salmonella. *Biochem. J.* **2013**, *454*, 459–466. [CrossRef] [PubMed]
45. Lee, Y.K.; Lee, J.A. Role of the mammalian ATG8/LC3 family in autophagy: Differential and compensatory roles in the spatiotemporal regulation of autophagy. *BMB Rep.* **2016**, *49*, 424–430. [CrossRef]
46. Zaffagnini, G.; Martens, S. Mechanisms of Selective Autophagy. *J. Mol. Biol.* **2016**, *428*, 1714–1724. [CrossRef]
47. Abdollahzadeh, I.; Schwarten, M.; Gensch, T.; Willbold, D.; Weiergräber, O.H. The Atg8 family of proteins-modulating shape and functionality of autophagic membranes. *Front. Genet.* **2017**, *8*, 109. [CrossRef]
48. Lystad. Simonsen Mechanisms and Pathophysiological Roles of the ATG8 Conjugation Machinery. *Cells* **2019**, *8*, 973. [CrossRef]
49. Rogov, V.V.; Stolz, A.; Ravichandran, A.C.; Rios-Szwed, D.O.; Suzuki, H.; Kniss, A.; Löhr, F.; Wakatsuki, S.; Dötsch, V.; Dikic, I.; et al. Structural and functional analysis of the GABARAP interaction motif (GIM). *EMBO Rep.* **2018**, *19*, e47268. [CrossRef]

50. Wirth, M.; Zhang, W.; Razi, M.; Nyoni, L.; Joshi, D.; O'Reilly, N.; Johansen, T.; Tooze, S.A.; Mouilleron, S. Molecular determinants regulating selective binding of autophagy adapters and receptors to ATG8 proteins. *Nat. Commun.* **2019**, *10*, 2055. [CrossRef]
51. Marshall, R.S.; Hua, Z.; Mali, S.; McLoughlin, F.; Vierstra, R.D. ATG8-Binding UIM Proteins Define a New Class of Autophagy Adaptors and Receptors. *Cell* **2019**, *177*, 766–781. [CrossRef]
52. Wang, H.; Bedford, F.K.; Brandon, N.J.; Moss, S.J.; Olsen, R.W. GABA(A)-receptor-associated protein links GABA(A) receptors and the cytoskeleton. *Nature* **1999**, *397*, 69–72. [CrossRef] [PubMed]
53. Chen, L.; Wang, H.; Vicini, S.; Olsen, R.W. The gamma -aminobutyric acid type A (GABAA) receptor-associated protein (GABARAP) promotes GABAA receptor clustering and modulates the channel kinetics. *Proc. Natl. Acad. Sci. USA* **2000**, *97*, 11557–11562. [CrossRef] [PubMed]
54. Green, F.; O'Hare, T.; Blackwell, A.; Enns, C.A. Association of human transferrin receptor with GABARAP. *FEBS Lett.* **2002**, *518*, 101–106. [CrossRef]
55. Laínez, S.; Valente, P.; Ontoria-Oviedo, I.; Estévez-Herrera, J.; Camprubí-Robles, M.; Ferrer-Montiel, A.; Planells-Cases, R. GABAA receptor associated protein (GABARAP) modulates TRPV1 expression and channel function and desensitization. *FASEB J.* **2010**, *24*, 1958–1970. [CrossRef] [PubMed]
56. Cook, J.L.; Re, R.N.; DeHaro, D.L.; Abadie, J.M.; Peters, M.; Alam, J. The trafficking protein GABARAP binds to and enhances plasma membrane expression and function of the angiotensin II type 1 receptor. *Circ. Res.* **2008**, *102*, 1539–1547. [CrossRef] [PubMed]
57. Reining, S.C.; Liesegang, A.; Betz, H.; Biber, J.; Murer, H.; Hernando, N. Expression of renal and intestinal Na/Pi cotransporters in the absence of GABARAP. *Pflug. Arch. Eur. J. Physiol.* **2010**, *460*, 207–217. [CrossRef]
58. Dutta, P.; Dargahi, L.; O'Connell, K.E.; Bolia, A.; Ozkan, B.; Sailer, A.W.; Dev, K.K. A novel modelling mechanism of PAEL receptor and GABARAPL2 interaction involved in Parkinson's disease. *Neurosci. Lett.* **2018**, *673*, 12–18. [CrossRef]
59. Mansuy, V.; Boireau, W.; Fraichard, A.; Schlick, J.L.; Jouvenot, M.; Delage-Mourroux, R. GEC1, a protein related to GABARAP, interacts with tubulin and GABA A receptor. *Biochem. Biophys. Res. Commun.* **2004**, *325*, 639–648. [CrossRef]
60. Chen, C.; Li, J.G.; Chen, Y.; Huang, P.; Wang, Y.; Liu-Chen, L.Y. GEC1 interacts with the κ opioid receptor and enhances expression of the receptor. *J. Biol. Chem.* **2006**, *281*, 7983–7993. [CrossRef]
61. Keulers, T.G.; Schaaf, M.B.E.; Peeters, H.J.M.; Savelkouls, K.G.M.; Vooijs, M.A.; Bussink, J.; Jutten, B.; Rouschop, K.M.A. GABARAPL1 is required for increased EGFR membrane expression during hypoxia. *Radiother. Oncol.* **2015**, *116*, 417–422. [CrossRef]
62. Blight, K.J.; McKeating, J.A.; Rice, C.M. Highly Permissive Cell Lines for Subgenomic and Genomic Hepatitis C Virus RNA Replication. *J. Virol.* **2002**, *76*, 13001–13014. [CrossRef] [PubMed]
63. O'Gorman, S.; Fox, D.T.; Wahl, G.M. Recombinase-mediated gene activation and site-specific integration in mammalian cells. *Science* **1991**, *251*, 1351–1355. [CrossRef] [PubMed]
64. Russell, W.C.; Graham, F.L.; Smiley, J.; Nairn, R. Characteristics of a Human Cell Line Transformed by DNA from Human Adenovirus Type 5. *J. Gen. Virol.* **1977**, *36*, 59–72.
65. Simons, I.M.; Mohrlüder, J.; Feederle, R.; Kremmer, E.; Zobel, T.; Dobner, J.; Bleffert, N.; Hoffmann, S.; Willbold, D. The highly GABARAP specific rat monoclonal antibody 8H5 visualizes GABARAP in immunofluorescence imaging at endogenous levels. *Sci. Rep.* **2019**, *9*, 526. [CrossRef]
66. Ran, F.A.; Hsu, P.D.; Wright, J.; Agarwala, V.; Scott, D.A.; Zhang, F. Genome engineering using the CRISPR-Cas9 system. *Nat. Protoc.* **2013**, *8*, 2281–2308. [CrossRef] [PubMed]
67. Rivero-Gutiérrez, B.; Anzola, A.; Martínez-Augustin, O.; De Medina, F.S. Stain-free detection as loading control alternative to Ponceau and housekeeping protein immunodetection in Western blotting. *Anal. Biochem.* **2014**, *467*, 1–3. [CrossRef]
68. Schindelin, J.; Arganda-Carreras, I.; Frise, E.; Kaynig, V.; Longair, M.; Pietzsch, T.; Preibisch, S.; Rueden, C.; Saalfeld, S.; Schmid, B.; et al. Fiji: An open-source platform for biological-image analysis. *Nat. Methods* **2012**, *9*, 676–682. [CrossRef]
69. Möckel, C.; Kubiak, J.; Schillinger, O.; Kühnemuth, R.; Della Corte, D.; Schröder, G.F.; Willbold, D.; Strodel, B.; Seidel, C.A.M.; Neudecker, P. Integrated NMR, Fluorescence, and Molecular Dynamics Benchmark Study of Protein Mechanics and Hydrodynamics. *J. Phys. Chem. B* **2019**, *123*, 1453–1480. [CrossRef]

70. Sigismund, S.; Argenzio, E.; Tosoni, D.; Cavallaro, E.; Polo, S.; Di Fiore, P.P. Clathrin-Mediated Internalization Is Essential for Sustained EGFR Signaling but Dispensable for Degradation. *Dev. Cell* **2008**, *15*, 209–219. [CrossRef]
71. Gu, Y.; Princely Abudu, Y.; Kumar, S.; Bissa, B.; Choi, S.W.; Jia, J.; Lazarou, M.; Eskelinen, E.; Johansen, T.; Deretic, V. Mammalian Atg8 Proteins Regulate Lysosome and Autolysosome Biogenesis Through SNAREs. *EMBO J.* **2019**, *38*, e101994. [CrossRef]
72. Groepper, C.; Rufinatscha, K.; Schröder, N.; Stindt, S.; Ehlting, C.; Albrecht, U.; Bock, H.H.; Bartenschlager, R.; Häussinger, D.; Bode, J.G. HCV modifies EGF signalling and upregulates production of CXCR2 ligands: Role in inflammation and antiviral immune response. *J. Hepatol.* **2018**, *69*, 594–602. [CrossRef] [PubMed]
73. Salova, A.V.; Belyaeva, T.N.; Leontieva, E.A.; Kornilova, E.S. EGF receptor lysosomal degradation is delayed in the cells stimulated with EGF-Quantum dot bioconjugate but earlier key events of endocytic degradative pathway are similar to that of native EGF. *Oncotarget* **2017**, *8*, 44335–44350. [CrossRef] [PubMed]
74. Sorkin, A.; Carter, R. Endocytosis of Functional Epidermal Growth Factor Receptor-Green Fluorescent Protein Chimera. *J. Biol. Chem.* **1998**, *273*, 35000–35007.
75. Ettenberg, S.A.; Magnifico, A.; Cuello, M.; Nau, M.M.; Rubinstein, Y.R.; Yarden, Y.; Weissman, A.M.; Lipkowitz, S. Cbl-b-dependent Coordinated Degradation of the Epidermal Growth Factor Receptor Signaling Complex. *J. Biol. Chem.* **2001**, *276*, 27677–27684. [CrossRef] [PubMed]
76. Alwan, H.A.J.; Van Zoelen, E.J.J.; Van Leeuwen, J.E.M. Ligand-induced lysosomal epidermal growth factor receptor (EGFR) degradation is preceded by proteasome-dependent EGFR de-ubiquitination. *J. Biol. Chem.* **2003**, *278*, 35781–35790. [CrossRef]
77. Mayle, K.M.; Le, A.M.; Kamei, D.T. The intracellular trafficking pathway of transferrin. *Biochim. Biophys. Acta (BBA)-Gen. Subj.* **2012**, *1820*, 264–281. [CrossRef] [PubMed]
78. Mesaki, K.; Tanabe, K.; Obayashi, M.; Oe, N.; Takei, K. Fission of tubular endosomes triggers endosomal acidification and movement. *PLoS ONE* **2011**, *6*, e19764. [CrossRef]
79. Jacomin, A.C.; Samavedam, S.; Promponas, V.; Nezis, I.P. iLIR database: A web resource for LIR motif-containing proteins in eukaryotes. *Autophagy* **2016**, *12*, 1945–1953. [CrossRef]
80. Kirkin, V.; Rogov, V.V. A Diversity of Selective Autophagy Receptors Determines the Specificity of the Autophagy Pathway. *Mol. Cell* **2019**, *76*, 268–285. [CrossRef]
81. Capuani, F.; Conte, A.; Argenzio, E.; Marchetti, L.; Priami, C.; Polo, S.; Di Fiore, P.P.; Sigismund, S.; Ciliberto, A. Quantitative analysis reveals how EGFR activation and downregulation are coupled in normal but not in cancer cells. *Nat. Commun.* **2015**, *6*, 7999. [CrossRef]
82. Freed, D.M.; Bessman, N.J.; Kiyatkin, A.; Salazar-Cavazos, E.; Byrne, P.O.; Moore, J.O.; Valley, C.C.; Ferguson, K.M.; Leahy, D.J.; Lidke, D.S.; et al. EGFR Ligands Differentially Stabilize Receptor Dimers to Specify Signaling Kinetics. *Cell* **2017**, *171*, 683–695. [CrossRef] [PubMed]
83. Mohrlüder, J.; Hoffmann, Y.; Stangler, T.; Hänel, K.; Willbold, D. Identification of clathrin heavy chain as a direct interaction partner for the γ-aminobutyric acid type A receptor associated protein. *Biochemistry* **2007**, *46*, 14537–14543. [CrossRef] [PubMed]
84. Caldieri, G.; Barbieri, E.; Nappo, G.; Raimondi, A.; Bonora, M.; Conte, A.; Verhoef, L.G.G.C.; Confalonieri, S.; Malabarba, M.G.; Bianchi, F.; et al. Reticulon 3-Dependent ER-PM contact sites control EGFR nonclathrin endocytosis. *Science* **2017**, *356*, 617–624. [CrossRef] [PubMed]
85. Grumati, P.; Morozzi, G.; Hölper, S.; Mari, M.; Harwardt, M.L.I.E.; Yan, R.; Müller, S.; Reggiori, F.; Heilemann, M.; Dikic, I. Full length RTN3 regulates turnover of tubular endoplasmic reticulum via selective autophagy. *Elife* **2017**, *6*, e25555. [CrossRef]
86. Sun, A.; Wei, J.; Childress, C.; Shaw, J.H.; Peng, K.; Shao, G.; Yang, W.; Lin, Q. The E3 ubiquitin ligase NEDD4 is an LC3-interactive protein and regulates autophagy. *Autophagy* **2017**, *13*, 522–537. [CrossRef]
87. Haglund, K.; Sigismund, S.; Polo, S.; Szymkiewicz, I.; Di Fiore, P.P.; Dikic, I. Multiple monoubiquitination of RTKs is sufficient for their endocytosis and degradation. *Nat. Cell Biol.* **2003**, *5*, 461–466. [CrossRef]
88. Critchley, W.; Pellet-Many, C.; Ringham-Terry, B.; Harrison, M.; Zachary, I.; Ponnambalam, S. Receptor Tyrosine Kinase Ubiquitination and De-Ubiquitination in Signal Transduction and Receptor Trafficking. *Cells* **2018**, *7*, 22. [CrossRef]
89. Lin, Q.; Wang, J.; Childress, C.; Sudol, M.; Carey, D.J.; Yang, W. HECT E3 Ubiquitin Ligase Nedd4-1 Ubiquitinates ACK and Regulates Epidermal Growth Factor (EGF)-Induced Degradation of EGF Receptor and ACK. *Mol. Cell. Biol.* **2010**, *30*, 1541–1554. [CrossRef]

90. Mohapatra, B.; Ahmad, G.; Nadeau, S.; Zutshi, N.; An, W.; Scheffe, S.; Dong, L.; Feng, D.; Goetz, B.; Arya, P.; et al. Protein tyrosine kinase regulation by ubiquitination: Critical roles of Cbl-family ubiquitin ligases. *Biochim. Biophys. Acta (BBA)-Mol. Cell Res.* **2013**, *1833*, 122–139. [CrossRef]
91. Huotari, J.; Meyer-Schaller, N.; Hubner, M.; Stauffer, S.; Katheder, N.; Horvath, P.; Mancini, R.; Helenius, A.; Peter, M. Cullin-3 regulates late endosome maturation. *Proc. Natl. Acad. Sci. USA* **2012**, *109*, 823–828. [CrossRef]
92. Genau, H.M.; Huber, J.; Baschieri, F.; Akutsu, M.; Dötsch, V.; Farhan, H.; Rogov, V.; Behrends, C. CUL3-KBTBD6/KBTBD7Ubiquitin Ligase Cooperates with GABARAP Proteins to Spatially Restrict TIAM1-RAC1 Signaling. *Mol. Cell* **2015**, *57*, 995–1010. [CrossRef] [PubMed]
93. Wandinger-Ness, A.; Zerial, M. Rab proteins and the compartmentalization of the endosomal system. *Cold Spring Harb. Perspect. Biol.* **2014**, *6*, a022616. [CrossRef] [PubMed]
94. Goueli, B.S.; Powell, M.; Finger, E.C.; Pfeffer, S.R. TBC1D16 is a Rab4A GTPase activating protein that regulates receptor recycling and EGF receptor signaling. *Proc. Natl. Acad. Sci. USA* **2012**, *109*, 15787–15792. [CrossRef] [PubMed]
95. Popovic, D.; Akutsu, M.; Novak, I.; Harper, J.W.; Behrends, C.; Dikic, I. Rab GTPase-Activating Proteins in Autophagy: Regulation of Endocytic and Autophagy Pathways by Direct Binding to Human ATG8 Modifiers. *Mol. Cell. Biol.* **2012**, *32*, 1733–1744. [CrossRef]
96. Nordmann, M.; Cabrera, M.; Perz, A.; Bröcker, C.; Ostrowicz, C.; Engelbrecht-Vandré, S.; Ungermann, C. The Mon1-Ccz1 complex is the GEF of the late endosomal Rab7 homolog Ypt7. *Curr. Biol.* **2010**, *20*, 1654–1659. [CrossRef]
97. Ieguchi, K.; Ueda, S.; Kataoka, T.; Satoh, T. Role of the guanine nucleotide exchange factor Ost in negative regulation of receptor endocytosis by the small GTPase Rac. *J. Biol. Chem.* **2007**, *282*, 23296–23305. [CrossRef]
98. Longva, K.E.; Blystad, F.D.; Stang, E.; Larsen, A.M.; Johannessen, L.E.; Madshus, I.H. Ubiquitination and proteasomal activity is required for transport of the EGF receptor to inner membranes of multivesicular bodies. *J. Cell Biol.* **2002**, *156*, 843–854. [CrossRef]
99. Luzio, J.P.; Pryor, P.R.; Bright, N.A. Lysosomes: Fusion and function. *Nat. Rev. Mol. Cell Biol.* **2007**, *8*, 622–632. [CrossRef]
100. Oksvold, M.P.; Skarpen, E.; Wierød, L.; Paulsen, R.E.; Huitfeldt, H.S. Re-localization of activated EGF receptor and its signal transducers to multivesicular compartments downstream of early endosomes in response to EGF. *Eur. J. Cell Biol.* **2001**, *80*, 285–294. [CrossRef]
101. McEwan, D.G.; Popovic, D.; Gubas, A.; Terawaki, S.; Suzuki, H.; Stadel, D.; Coxon, F.P.; MirandadeStegmann, D.; Bhogaraju, S.; Maddi, K.; et al. PLEKHM1 regulates autophagosome-lysosome fusion through HOPS complex and LC3/GABARAP proteins. *Mol. Cell* **2015**, *57*, 39–54. [CrossRef]
102. Ariotti, N.; Liang, H.; Xu, Y.; Zhang, Y.; Yonekubo, Y.; Inder, K.; Du, G.; Parton, R.G.; Hancock, J.F.; Plowman, S.J. Epidermal Growth Factor Receptor Activation Remodels the Plasma Membrane Lipid Environment To Induce Nanocluster Formation. *Mol. Cell. Biol.* **2010**, *30*, 3795–3804. [CrossRef] [PubMed]
103. Liang, S.I.; van Lengerich, B.; Eichel, K.; Cha, M.; Patterson, D.M.; Yoon, T.Y.; von Zastrow, M.; Jura, N.; Gartner, Z.J. Phosphorylated EGFR Dimers Are Not Sufficient to Activate Ras. *Cell Rep.* **2018**, *22*, 2593–2600. [CrossRef] [PubMed]
104. Needham, S.R.; Roberts, S.K.; Arkhipov, A.; Mysore, V.P.; Tynan, C.J.; Zanetti-Domingues, L.C.; Kim, E.T.; Losasso, V.; Korovesis, D.; Hirsch, M.; et al. EGFR oligomerization organizes kinase-active dimers into competent signalling platforms. *Nat. Commun.* **2016**, *7*, 13307. [CrossRef] [PubMed]
105. Heukers, R.; Vermeulen, J.F.; Fereidouni, F.; Bader, A.N.; Voortman, J.; Roovers, R.C.; Gerritsen, H.C.; Van Bergen En Henegouwen, P.M.P. Endocytosis of EGFR requires its kinase activity and N-terminal transmembrane dimerization motif. *J. Cell Sci.* **2013**, *126*, 4900–4912. [CrossRef] [PubMed]
106. Pacheco, V.; Ma, P.; Thielmann, Y.; Hartmann, R.; Weiergräber, O.H.; Mohrlüder, J.; Willbold, D. Assessment of GABARAP self-association by its diffusion properties. *J. Biomol. NMR* **2010**, *48*, 49–58. [CrossRef] [PubMed]
107. Saito, T.; Kuma, A.; Sugiura, Y.; Ichimura, Y.; Obata, M.; Kitamura, H.; Okuda, S.; Lee, H.C.; Ikeda, K.; Kanegae, Y.; et al. Autophagy regulates lipid metabolism through selective turnover of NCoR1. *Nat. Commun.* **2019**, *10*, 1567. [CrossRef]

108. Wei, Y.; Zou, Z.; Becker, N.; Anderson, M.; Sumpter, R.; Xiao, G.; Kinch, L.; Koduru, P.; Christudass, C.S.; Veltri, R.W.; et al. EGFR-Mediated Beclin 1 Phosphorylation in Autophagy Suppression, Tumor Progression, and Tumor Chemoresistance. *Cell* **2013**, *154*, 1269–1284. [CrossRef]
109. Winer, H.; Fraiberg, M.; Abada, A.; Dadosh, T.; Tamim-Yecheskel, B.C.; Elazar, Z. Autophagy differentially regulates TNF receptor Fn14 by distinct mammalian Atg8 proteins. *Nat. Commun.* **2018**, *9*, 3744. [CrossRef]

Supplementary Figures

Deficiency of GABARAP but not its paralogs causes enhanced EGF-induced EGFR degradation

Jochen Dobner[1], Indra M. Simons[1, 2], Kerstin Rufinatscha[3], Sebastian Hänsch [4], Melanie Schwarten[2], Oliver H. Weiergräber[2], Iman Abdollahzadeh[2, 5], Thomas Gensch[5], Johannes G. Bode[3], Silke Hoffmann[2], Dieter Willbold[1, 2] *

[1] Institut für Physikalische Biologie, Heinrich-Heine-Universität Düsseldorf, Universitätsstraße 1, 40225 Düsseldorf, Germany
[2] Institute of Biological Information Processing: Structural Biochemistry (IBI-7), Forschungszentrum Jülich, 52425 Jülich, Germany
[3] Department of Gastroenterology, Hepatology and Infectiology, University Hospital, Heinrich-Heine-Universität Düsseldorf, Moorenstraße 5, 40225 Düsseldorf, Germany
[4] Department of Biology, Center for Advanced Imaging (CAi), Heinrich-Heine-Universität Düsseldorf, Universitätsstraße 1, 40225 Düsseldorf, Germany
[5] Institute of Biological Information Processing – Molecular and Cell Physiology (IBI-1), Forschungszentrum Jülich, 52425 Jülich, Germany

Supplementary Figure S1 is related to Figures 1-8
Supplementary Figure S2 is related to Figure 1
Supplementary Figure S3 is related to Figure 5
Supplementary Figure S4 is related to Figure 7 and Movie S1
Supplementary Figure S5 is related to Figure 7 and Movie S2
Supplementary Figure S6 is related to Figures 1-4, 6, 8 and Figure S2
Supplementary Table S1 is related to Figures 1-8
Movie S1 is related to Figures 7 and S4
Movie S2 is related to Figures 7 and S5

Supplemental Figures S1 - 6, Table S1, Movies S1 - 2

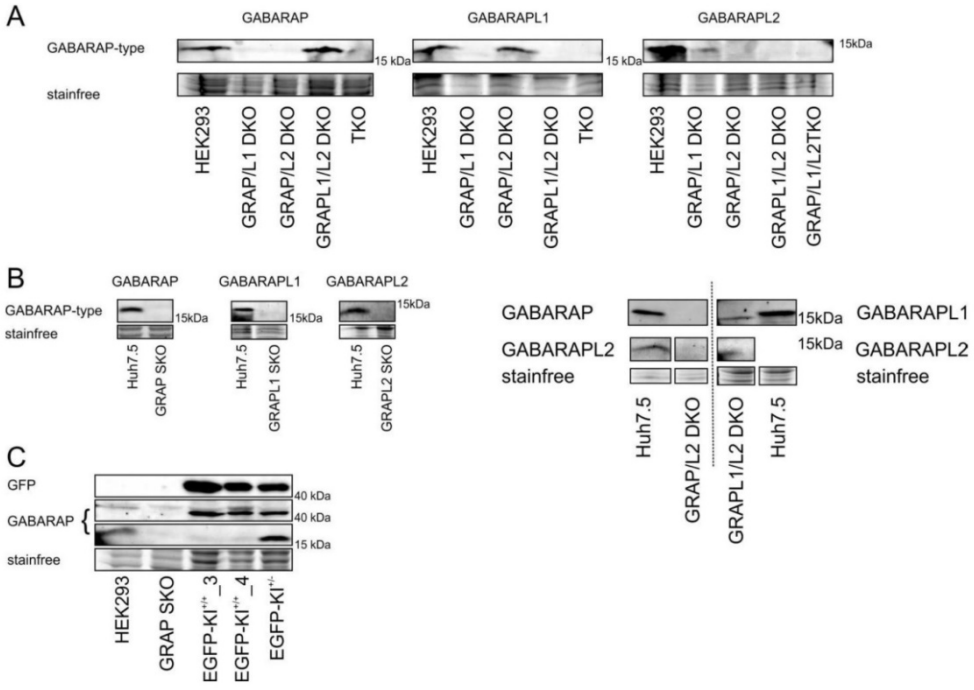

Figure S1: Verification of CRISPR/Cas9 knockout and knock-in cell lines on protein level. Whole cell protein lysates were isolated and analyzed for presence of the indicated GABARAP subfamily member. (A) HEK293 based clonal KO cell lines. (B) Huh7.5 based clonal KO cell lines. (C) HEK293 based KI clonal lines. GRAP = GABARAP, GRAPL1 = GABARAPL1, GRAPL2 = GABARAPL2, TKO = GABARAP/L1/L2 TKO. SKO = single knockout, DKO = double knockout, TKO = triple knockout. Figure S7 G shows uncropped source blots

Table S1: CRISPR sequence details and genotyping results of the knockout cell lines used.

HEK293 GABARAP, GABARAPL1 and GABARAPL2 SKOs have already been published (Simons *et al.*, 2019).

Gene Symbol	Uniprot	GeneID/ Location	Targeting strategy	CRISPR gRNA (PAM)	Main clone	Unique Alleles	Mutation	Protein Impact
Huh7.5								
GABARAP	O95166	11337/NC_000017.11	first exon	GGATCTTCTCGCCCTCAGAG CGG	3	1	c.[152_153insT]	p.[fs*0]
GABARAPL1	Q9H0R8	23710/NC_000012.12	second exon	AGAGAAGGCTCCAAAAGCC AGGG	G5	3	c.[352_358_del];[353_356del];[154_355del]	p.[K38Gfs*9];[K38Gfs*11];[K38Sfs*3]
GABARAPL2	P60520	11345/NC_000016.1	second exon	TCCCACAGAACACAGATGCG TGG	F6	1	c.[179_180insT]	p.[C15Lfs*27]
GABARAP/L2 DKO	O95166	11337/NC_000017.11	first exon	GGATCTTCTCGCCCTCAGAG CGG	G8	2	c.[152_153insTT];[152_154insGG]	p.[E17Lfs*36];[E17Gfs*14]
	P60520	11345/NC_000016.1	second exon	TCCCACAGAACACAGATGCG TGG		2	c.[179_180insT];[179_180insTG]	p.[C15Lfs*27];[V16Afs*15]
GABARAPL1/L2 DKO	Q9H0R8	23710/NC_000012.12	second exon	AGAGAAGGCTCCAAAAGCC AGGG	F5	2	c.[354_355del];[355del]	p.[K38Nfs*3];[A39Pfs*10]
	P60520	11345/NC_000016.1	second exon	TCCCACAGAACACAGATGCG TGG		1	c.[179_180insT]	p.[C15Lfs*27]
HEK293								
GABARAP	O95166	11337/NC_000017.11	first exon	GGATCTTCTCGCCCTCAGAG CGG	C2	1	c.[152_153insT]	p.[fs*0]
GABARAPL1	Q9H0R8	23710/NC_000012.12	second exon	AGAGAAGGCTCCAAAAGCC AGGG	C10	2	c.[352_357del];[353_356]	p.[K38Tfs*10];[K38Nfs*3]
GABARAPL2	P60520	11345/NC_000016.	second	TCCCACAGAACACAGATGCG	#8	1	c.[179_180insT]	p.[C15Lfs*27]

		1	exon	TGG				
GABARAP/L1 DKO	O95166	11337/NC_000017.11	first exon	GGATCTTCTCGCCCTCAGAG CGG	A11 (based on C10)	2	c.[152_153insT];[148_151del]	p.[fs*0];[K23Nfs*6]
GABARAP/L2 DKO	P60520	11345/NC_000016.1	second exon	TCCCACAGAACACAGATGCG TGG	#8 (based on C2)	1	c.[179_180insT]	p.[C15Lfs*27]
GABARAPL1/L2 DKO	P60520	11345/NC_000016.1	second exon	TCCCACAGAACACAGATGCG TGG	B3 (based on C10)	1	c.[179_180insT]	p.[C15Lfs*27]
GABARAP/L1/L2 TKO	O95166 P60520	11337/NC_000017.11 11345/NC_000016.1	first exon second exon	GGATCTTCTCGCCCTCAGAG CGG TCCCACAGAACACAGATGCG TGG	#3 (based on C10)	1 1	c.[152_153insT] c.[179_180insT]	p.[fs*0] p.[C15Lfs*27]
GABARAP	O95166	11337/NC_000017.11	first exon +linearized HDR plasmid	TACACGAACTTCATCCTCCC GGG	3	1	c.[ins717+21bpEGFP+linker]	p.[ins239+7aaEGFP+linker]

Formatting of indels detected in the knockout cell lines (Mutation column) and their resulting proteins (Protein impact column) is according to Human Genome Variation Society (http://varnomen.hgvs.org/). Mutation positions are determined in respect to the canonical isoform annotated in Uniprot, if more than one form exists. The numbers after the asterisks represent the number of amino acids present from the first amino acid changed to the next sequential stop codon. del, deletion; ins, insertion; c., coding DNA; p., protein; fs, frame shift; *, stop codon.

5 of 20

50

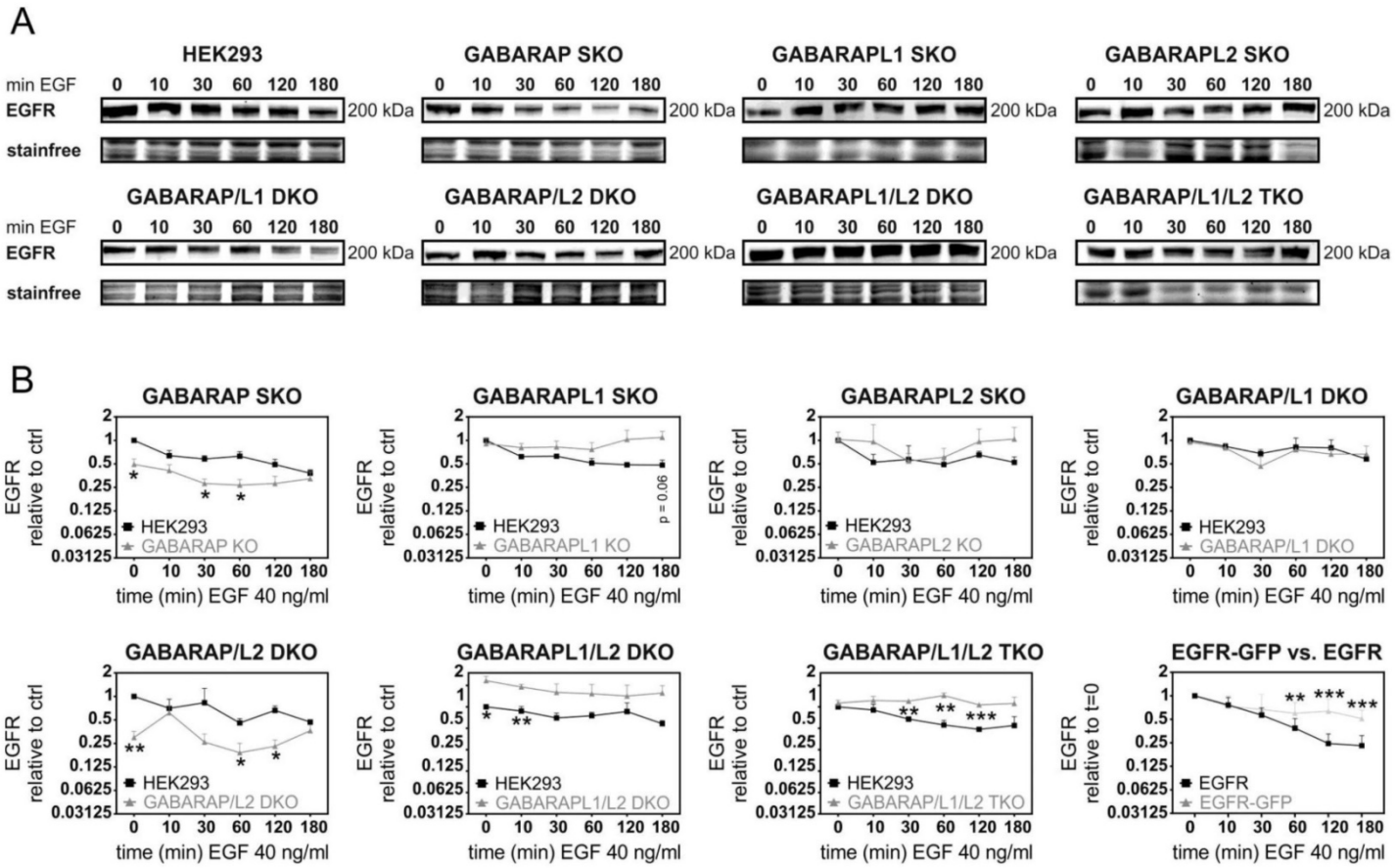
A
HEK293
GABARAP SKO
GABARAPL1 SKO
GABARAPL2 SKO
min EGF 0 10 30 60 120 180
EGFR
200 kDa
stainfree
GABARAP/L1 DKO
GABARAP/L2 DKO
GABARAPL1/L2 DKO
GABARAP/L1/L2 TKO
B
GABARAP SKO
GABARAPL1 SKO
GABARAPL2 SKO
GABARAP/L1 DKO
GABARAP/L2 DKO
GABARAPL1/L2 DKO
GABARAP/L1/L2 TKO
EGFR-GFP vs. EGFR
EGFR relative to ctrl
EGFR relative to t=0
2 1 0.5 0.25 0.125 0.0625 0.03125
HEK293
GABARAP KO
GABARAPL1 KO
GABARAPL2 KO
GABARAP/L1 DKO
GABARAP/L2 DKO
GABARAPL1/L2 DKO
GABARAP/L1/L2 TKO
EGFR
EGFR-GFP
p = 0.06
time (min) EGF 40 ng/ml

51

Figure S2: Total EGFR levels in response to EGF treatment in HEK293 KO cells transiently overexpressing EGFR-GFP.

(A) Cells were transfected with 2 μg EGFR-GFP expression plasmid and two days post transfection treated with 40 ng/ml EGF for the indicated time points. Afterwards, total EGFR protein levels in whole cell lysates were analyzed by immunoblot. Representative blots are shown for at least n = 3 independent experiments. (B) Densitometric analysis of at least n = 3 independent experiments. Controls are directly associated to each experiment. Kinetics of EGF-induced EGFR-GFP degradation in EGFR-GFP transfected HEK293 compared to endogenous EGFR degradation is shown (EGFR-GFP n = ≥ 23, EGFR n = 20). Quantification of EGFR(-GFP) protein levels was performed by normalization on stain-free loading control and calculated as percentage of HEK293 control cells at unstimulated conditions (t = 0). For comparison between EGFR-GFP overexpression and endogenous EGFR, kinetics of each level of EGFR expression (overexpression or endogenous) is displayed (t = 0 for each condition individually). Error bars represent standard error of means. Asterisks mark significant differences versus the corresponding time point of control cells and were calculated using independent t-test. $p \leq 0.05$ = *, $p \leq 0.01$ = **, $p \leq 0.001$ = ***. Respective wildtype controls were run on the same PAGE for each KO cell line and can be found in figure S7 H which also shows the uncropped source blots.

A mean vesicular volume distribution

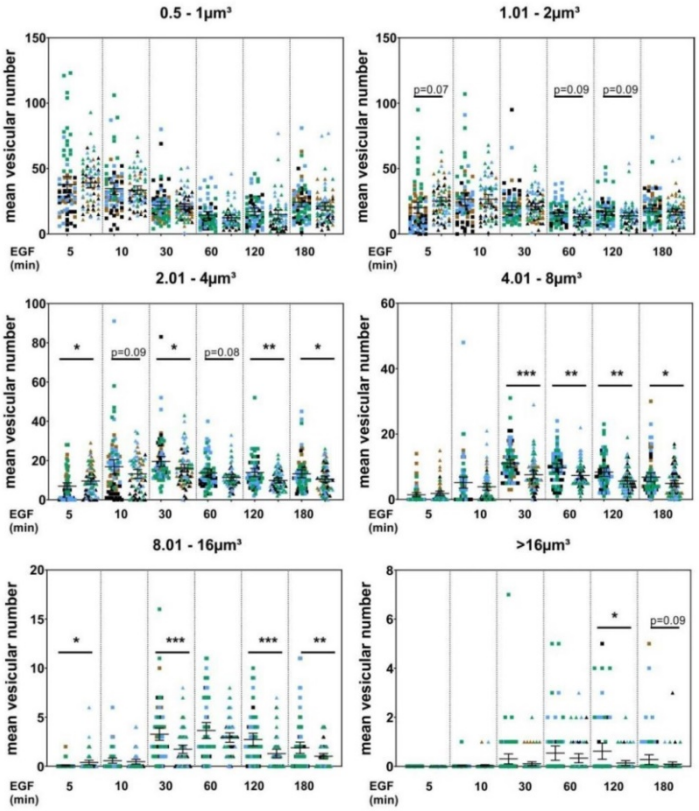

B mean vesicular intensity distribution

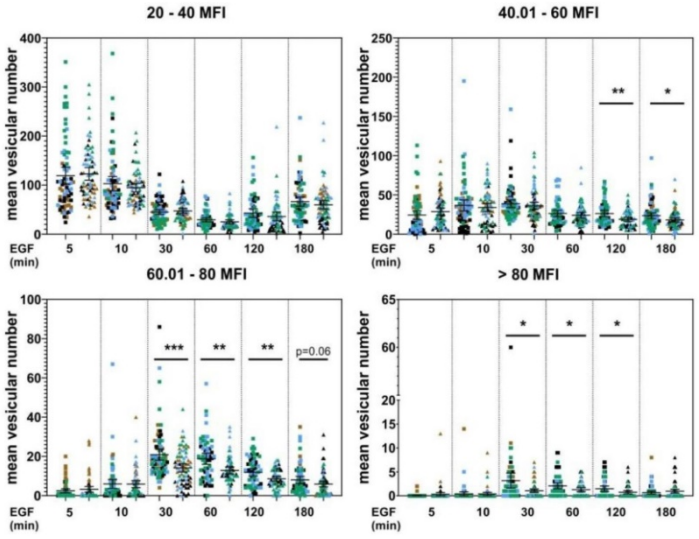

62

C

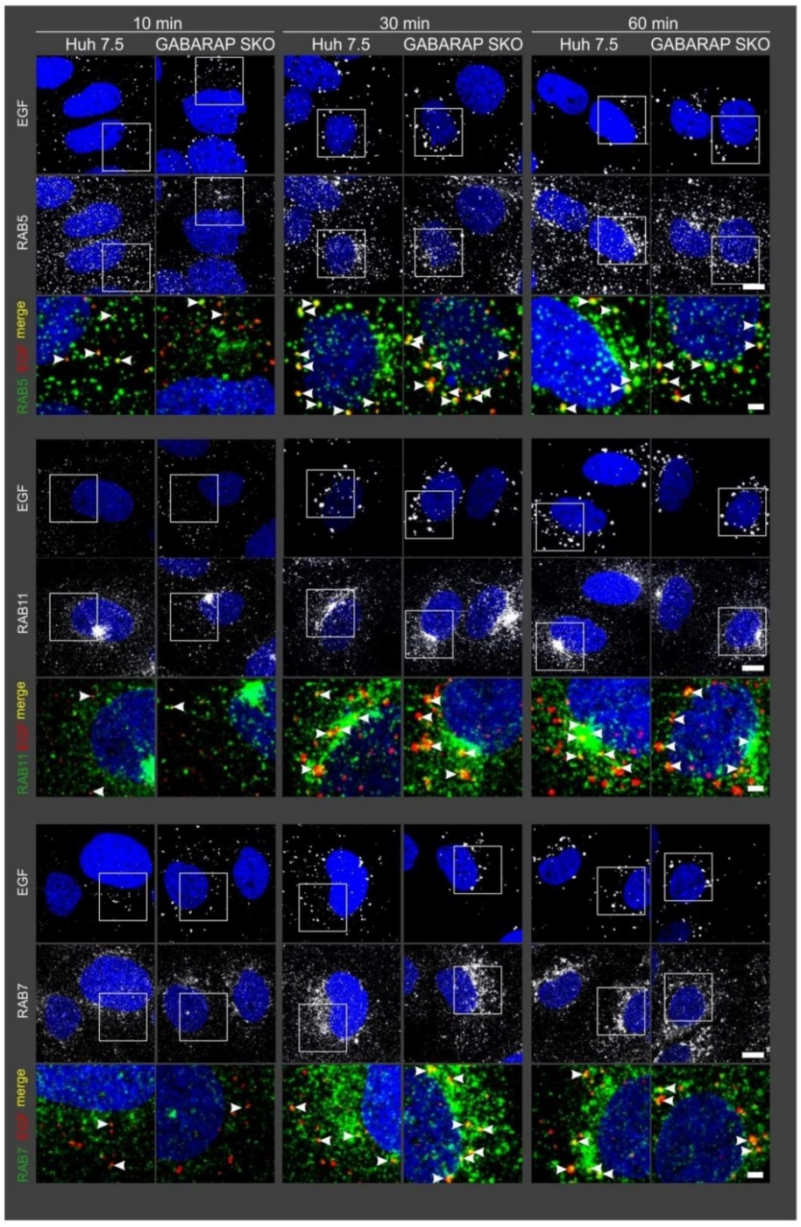

63

64 **Figure S3: Analysis of EGF-Alexa647 containing vesicles of GABARAP SKO and Huh7.5 cells by**
65 **Imaris and analysis of endosomal markers RAB 5, RAB11 and RAB7 in response to EGF treatment**
66 **in GABARAP SKO and Huh7.5 control cells.**

Vesicles of GABARAP SKO and Huh7.5 control cells which were treated with 40 ng/ml EGF-Alexa647 were modelled with Imaris imaging analysis software (described in detail in figure 5 and materials and methods section). (A) Mean vesicular volumes were largely unaffected by GABARAP-deficiency in GABARAP SKO cells although tendency for less vesicles with a diameter of 16 – 32 μm^3 was observable for GABARAP SKO cells after 30 min of treatment. Asterisks mark significant differences at indicated time points versus control cells as calculated using independent t-test. $p \leq 0.01$ = **. (B) Mean fluorescence intensities of EGF-Alexa647 positive vesicles classified into four arbitrary groups for GABARAP SKO and Huh7.5 control cells revealed significantly less vesicles with highest mean fluorescence intensities > 80 for GABARAP SKO cells compared to Huh7.5 control cells after 30 min of treatment. (B+C) Individual experiments are color-coded; > 50 cells per genotype and time point were analyzed. Error bars represent 95 % CI (C-E). Asterisks mark significant differences to the corresponding time point of control cells and were calculated using independent t-test. $p \leq 0.05$ = *, $p \leq 0.01$ = **, $p \leq 0.001$ = ***. (C) Huh7.5 and GABARAP SKO cells were pulse-treated with 40 ng/ml EGF-Alexa647 at 4 °C to allow binding to EGFR. After rigorous washing, cells were placed at 37 °C, fixed at distinct time points and stained for early (RAB5), recycling (RAB11) or late (RAB7) endosomes. All analyzed RAB proteins strongly accumulated within the first 30 min after EGF-Alexa647 pulse. Colocalization analysis of RAB proteins with EGF-Alexa647 (white arrowheads) revealed no alterations between GABARAP SKO and Huh7.5 control cells. MFI = mean fluorescence intensity Scale bar = 10 μm, scale bar zoom = 3 μm.

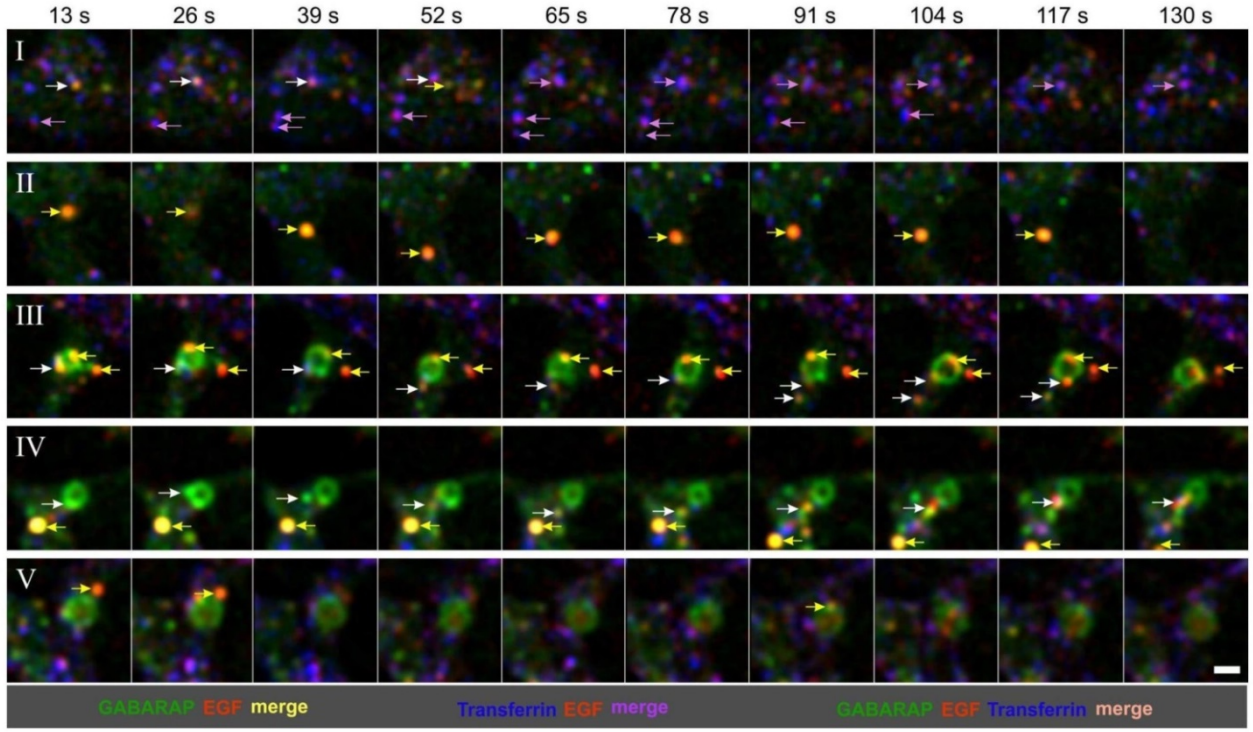

Figure S4: Montage of live cell imaging of HEK293 knock-in cells expressing GFP-GABARAP under the endogenous *GABARAP* promoter and stimulated with EGF-Alexa647 and Tf-Alexa555 by confocal laser scanning microscopy.

HEK293 GFP-GABARAP KI cells were simultaneously treated with 40 ng/ml EGF-Alexa647 and 20 ng/ml Tf-Alexa555 for 60 min and imaged under live-cell conditions by laser scanning microscopy. The montage shows snapshots of regions of interest I to V indicated in figure 7 A, covering a 117 s time frame. Images were taken at intervals of 13 s. Selected GABARAP/EGF positive signals are marked with yellow arrows,

GABARAP/EGF/Tf positive structures with white arrows and EGF/Tf positive vesicles with magenta arrows. Video can be found under movie S1. Scale bar = 3 μm.

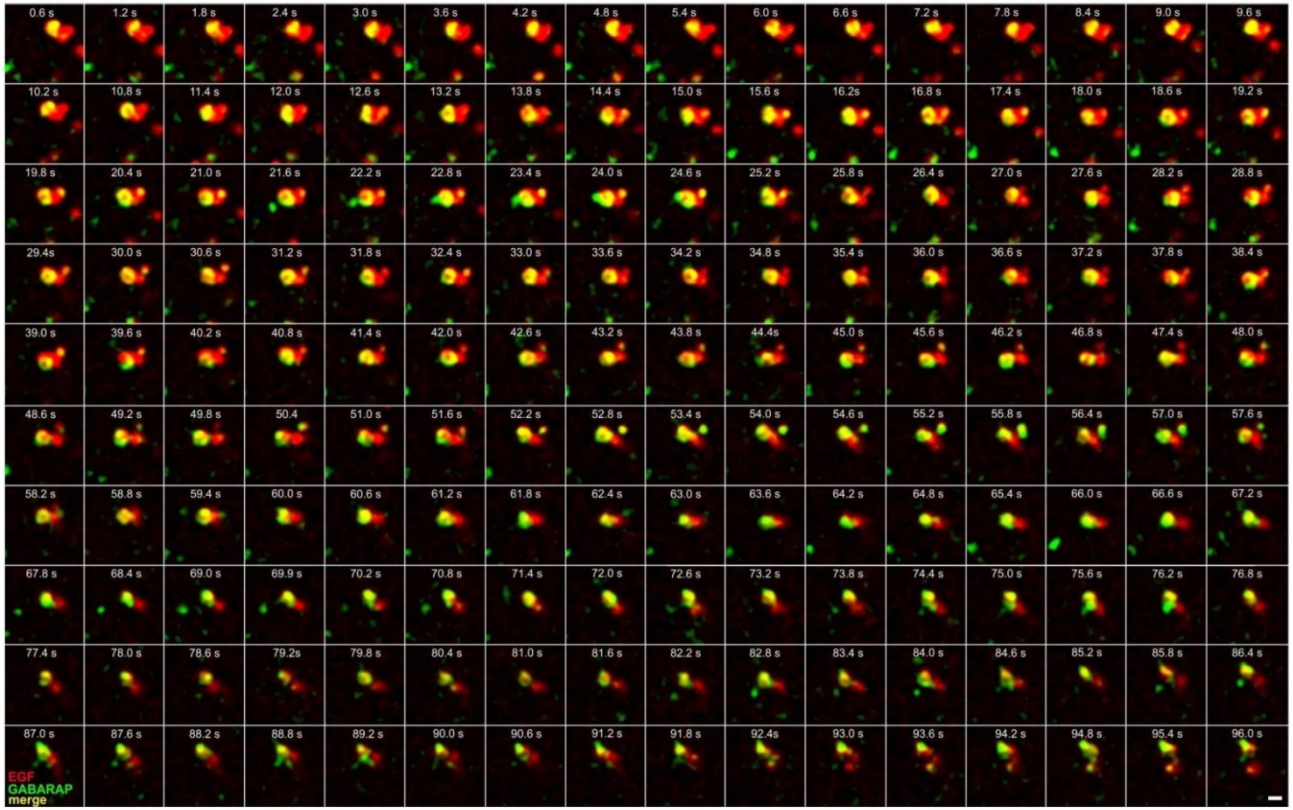

Figure S5: Live cell imaging of HEK293 KI cells expressing GFP-GABARAP under the endogenous *GABARAP* promoter and stimulated with EGF-Alexa647 by spinning disk confocal fluorescence microscopy.

HEK293 GFP-GABARAP KI cells were treated with 40 ng/ml EGF-Alexa647 for 60 min and imaged under live-cell conditions by spinning disk confocal fluorescence microscopy. The montage features selected time points for areas shown in figures 7 B to D. Dynamic vesicles which are GABARAP positive (green structures), EGF positive (red structures) or GABARAP/EGF double positive (yellow structures) are shown over a time course of 95.4 s with intervals of 0.6 s between images. GABARAP is shown in green and EGF in red. Video can be found under movie S2. Scale bar = 3μm.

A Source blots corresponding to figure 1

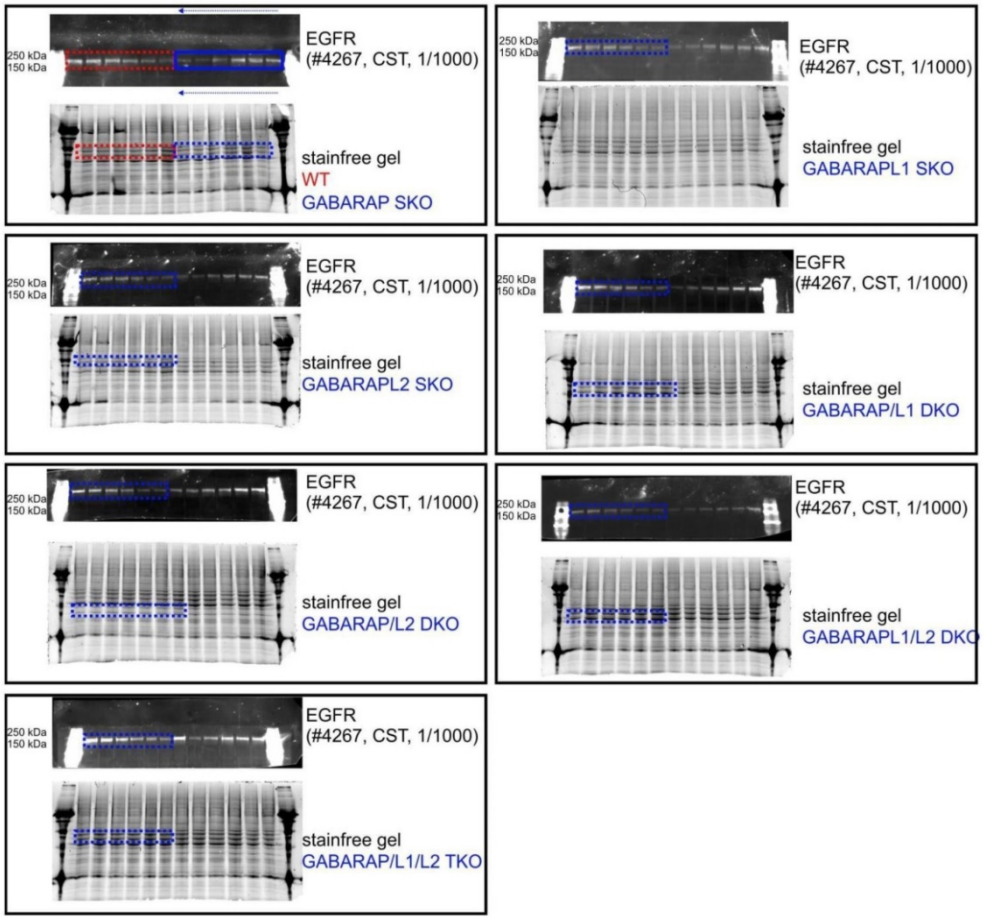

106

145

107

B Source blots corresponding to figure 2

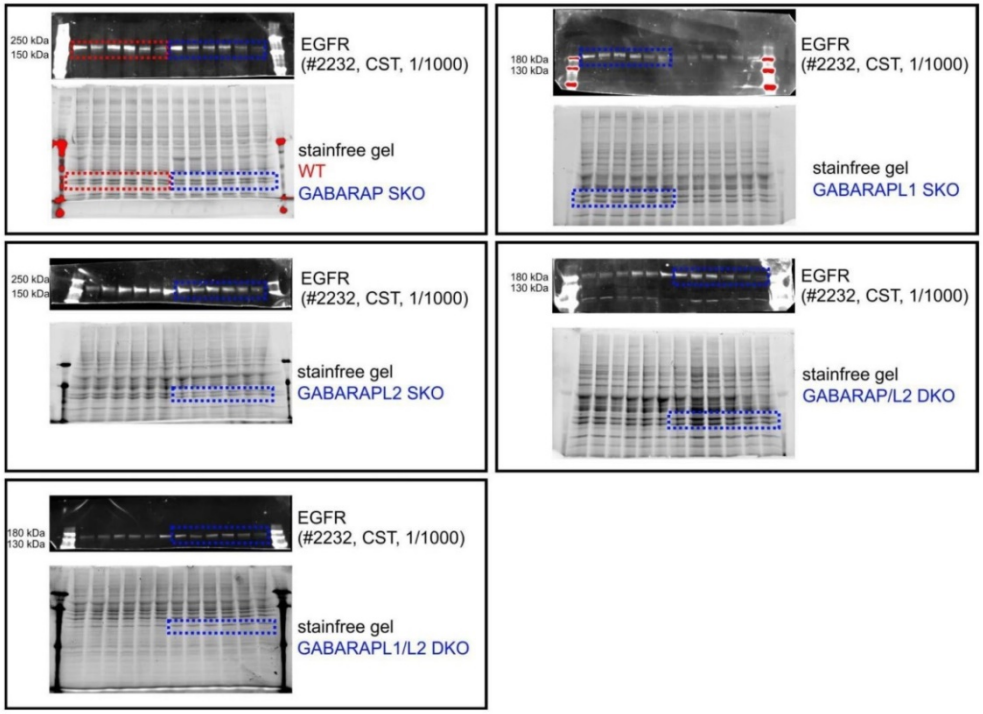

108

146

C Source blots corresponding to figure 3

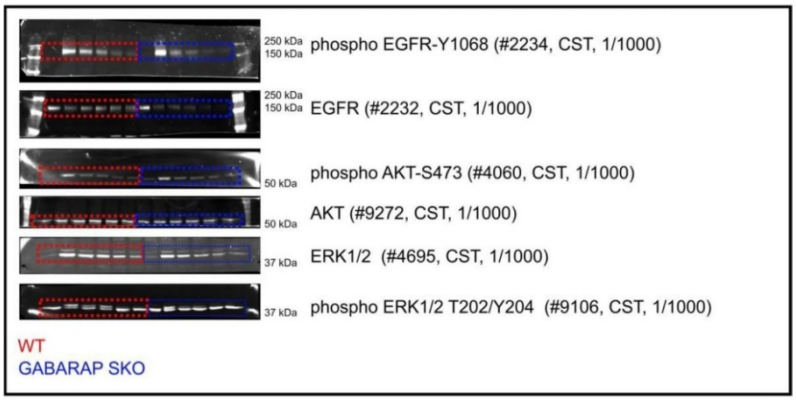

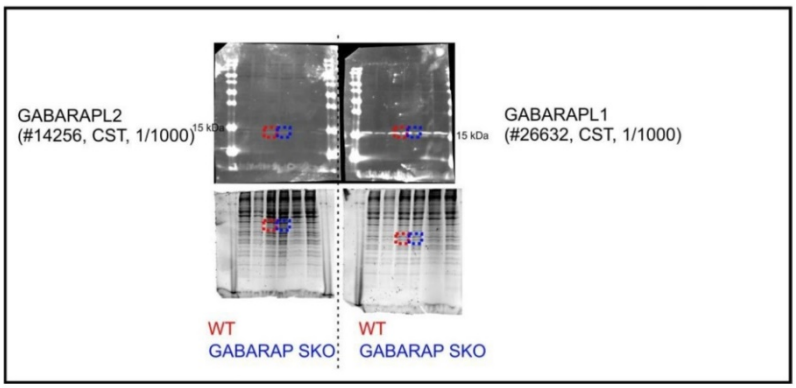

109

D Source blots corresponding to figure 4

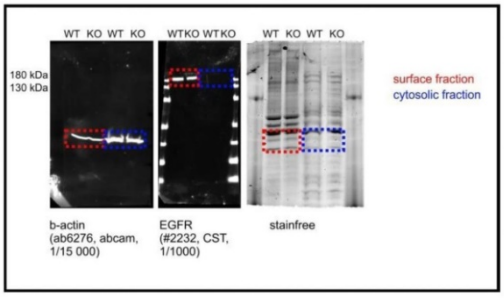

110

E Source blots corresponding to figure 6

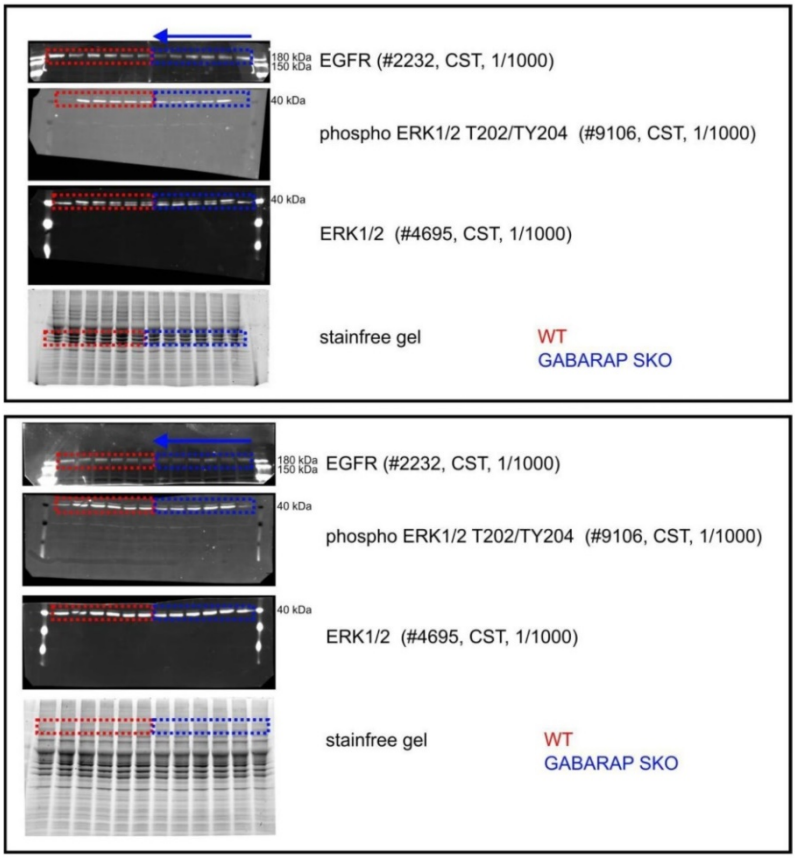

111

112

F Source blots corresponding to figure 8

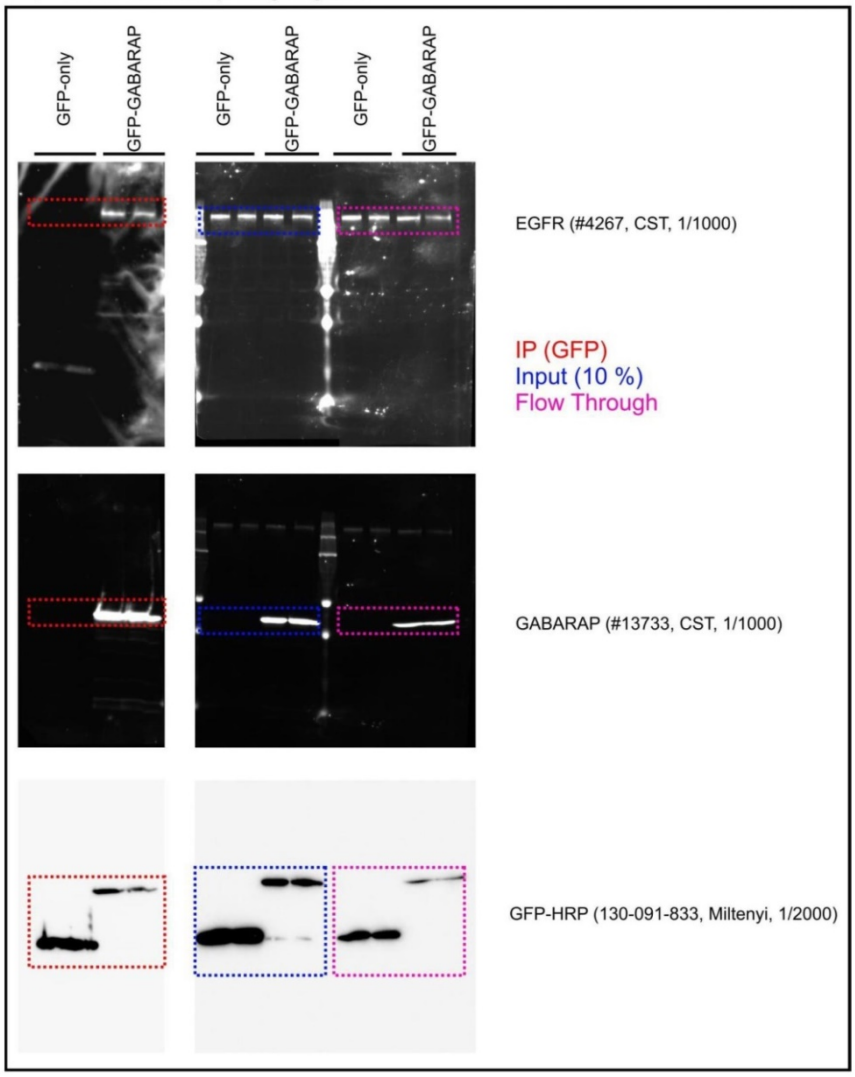

113

G Source blots corresponding to figure S1

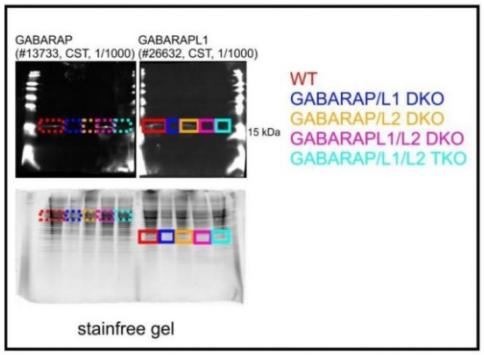

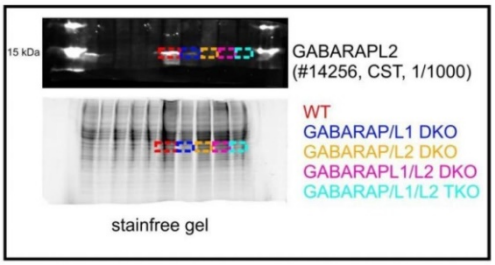

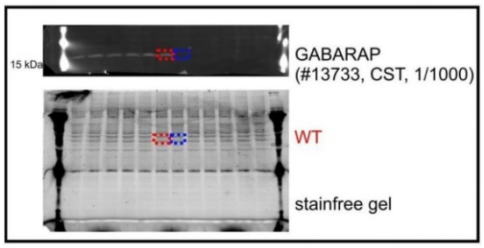

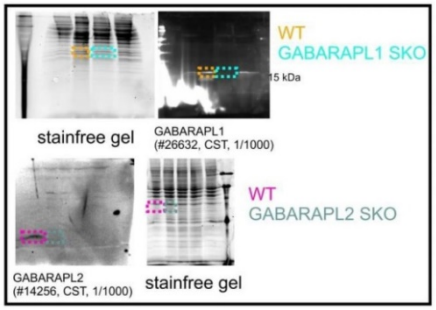

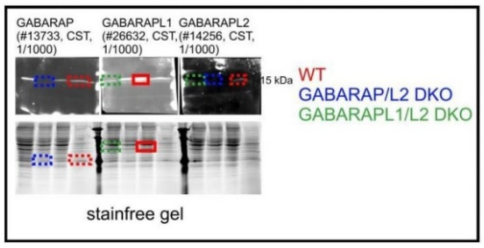

114

H Source blots corresponding to figure S2

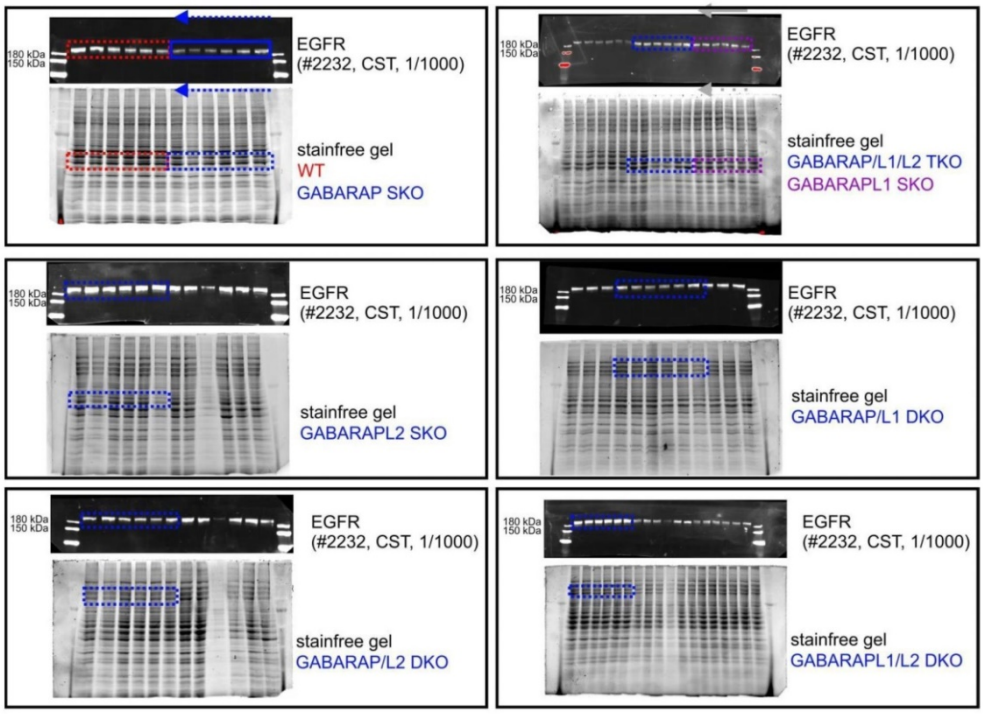

Figure S6: Uncropped source blots of immunoblotting experiments.

This figure contains the source blots corresponding to respective immunoblotting experiments as indicated. (A) Uncropped source blots corresponding to figure 1. (B) Uncropped source blots corresponding to figure 2. (C) Uncropped source blots corresponding to figure 3. (D) Uncropped source blots corresponding to figure 4. (E) Uncropped source blots corresponding to figure 6. (F) Uncropped source blots corresponding to figure 8. (G) Uncropped source blots corresponding to figure S1. (H) Uncropped source blots corresponding to figure S2. Used antibodies are indicated for each blot.

5. Summary and Conclusion

The involvement of the GABARAP subfamily has been suggested for numerous cellular processes. Among those, their role during autophagy is by far best described and detailed analyses thereof are steadily increasing. Although GABARAP subfamily proteins were originally identified to be involved in the trafficking of cell surface receptors, detailed analysis on that matter has been relatively scarce. In both cases, analysis is often restricted to the whole subfamily and a high degree of functional redundancy between individual subfamily members is assumed. However, comparative analysis between individual subfamily proteins is largely lacking. Such task is complicated by high sequence and structural similarity between GABARAP subfamily proteins which represents a major obstacle in deciphering unique and non-redundant functions of individual family proteins.

Therefore, the need for a toolbox enabling investigation of individual GABARAP subfamily proteins and combinations of them without interference from the others is obvious. CRISPR/Cas9-mediated genome editing allows for generation of each desired KO combination due to specific targeting of the endonuclease Cas9 to distinct genomic *loci*. It was applied during this PhD work to lay the groundwork of addressing scientific questions about GABARAP subfamily protein biology.

5.1 CRISPR/Cas9 genome-edited cell lines allow for systematic analysis of GABARAP subfamily specific functions

At the start of the present thesis, human KO cell lines of individual proteins or combinations of GABARAP subfamily members, mediated by genome editing via CRISPR/Cas9, had not been published and were not available within the “Atg8” scientific community.

Such KO cells provide an essential tool for evaluation of processes which are dependent on a specific GABARAP subfamily protein and thus impaired after loss of a certain paralog. Additionally, redundancy can also be assessed by analysis of double and triple deficient cell lines. The demand for such tools was consequently high. Importantly, the introduction of an efficient CRISPR/Cas9 workflow in our institute was successfully completed as an essential part of this PhD project and thus set the foundation for any subsequent analysis of autophagy-independent roles of the GABARAP subfamily and individual proteins thereof.

The successful generation of single KO (SKO) cell lines of individual family members, double KO (DKO) combinations thereof and triple KO (TKO) cells lacking the whole subfamily was achieved for HEK293 cells. These HEK293-based SKO clonal lines, first published in this work (4.1), were employed to validate specificity of commercially available anti-GABARAP, anti-GABARAPL1 and anti-GABARAPL2 antibodies for IB. Although these antibodies were

specifically and readily validated within this PhD project for IB, a related PhD project demonstrated that such validation is not directly applicable to other techniques such as IF imaging [273]. This is probably due to the fact that when experimental conditions differ, particularly considering native (IF) versus denatured (IB) antigens, antibodies may show cross-reactivity with other subfamily members or no reactivity at all.

This comprehensively illustrates the necessity to validate antibodies always in an application-specific manner to avoid false positive results. Use of antibodies also enables to check whether transient or stable artificial overexpression of proteins alters their native subcellular localization which is a major issue, e.g. during overexpression of GFP-tagged proteins of interest [274].

While the focus of this publication (4.1) was mainly on describing a novel GABARAP-specific antibody with the focus on staining autophagic structures as part of a related project within the institute, the successful implementation of CRISPR/Cas9-mediated genome engineering in our institute was a key step for this PhD project and laid the basis for the following analyses of autophagy-independent roles of the GABARAP subfamily (4.2) and individual members thereof (4.3).

5.2 GABARAP subfamily proteins are involved in maintenance of Golgi apparatus morphology and influence surfaceome composition

In contrast to autophagy research, there are comparatively few studies which investigate the role of GABARAP subfamily proteins during cell surface protein trafficking. Most of them describe association of individual GABARAP subfamily proteins with receptors [5, 134, 137, 146, 275] or only cover two GABARAP subfamily proteins [141]. Because systematic analyses of e.g. the proteome of autophagosomes [276] or the interactome of autophagy-related proteins [277] already existed, it was obvious that an equally systematic analysis of the impact of GABARAP subfamily proteins on general cell surface protein trafficking and biology was overdue.

Because a certain degree of functional redundancy within the GABARAP subfamily is likely, an unbiased analysis to identify potentially influenced proteins involving cells lacking the whole subfamily represents the optimal approach. Based on this notion, the within this PhD project generated HEK293 TKO cells were used as a model system to identify cell surface proteins which are potentially dependent on one, two or all three members of the GABARAP subfamily (4.2).

The comparative surfaceome analysis between TKO and WT cells as applied within this PhD project allows for a more general view on the involvement of GABARAP subfamily proteins on cell surface protein trafficking. Apart from analysis of the influence of individual

GABARAP subfamily proteins on the trafficking of specific surface receptors known from the literature, these results expand the landscape of cell surface proteins potentially influenced by GABARAP subfamily proteins. The unbiased identification and quantification of surfaceome composition has major advantages:

1.) Previously unknown potential GABARAP subfamily-interacting proteins might be identified and can be analyzed in detailed downstream analysis to decipher the involvement of individual subfamily members and the nature of such interactions.
2.) The nature and function of the differentially abundant surface-located proteins gives insight into which processes might be generally affected when the whole GABARAP subfamily is lacking. Because the proteins which were identified by this approach are rather diverse in terms of function, and include e.g. transporter/channel proteins, receptors, cell adhesion molecules and proteins involved in immunity, a widespread impact on intracellular homeostasis can be expected.
3.) It can intrinsically confirm previously described GABARAP subfamily-interacting proteins and may hint towards a mechanistic role. For example, the TFRC was among the proteins with higher surface abundance in TKO cells. While the association of GABARAP and TFRC is long known [5], mechanistic and functional insights are largely lacking. Its identification within this work could be used to develop new hypotheses regarding the mechanistic relevance of this interaction. For example, its degradation might depend on presence of any of the GABARAP proteins. Altered glycosylation patterns or reduced anterograde Golgi to PM trafficking are additional possibilities.

However, altered surface expression might be based on a variety of factors and not necessarily be a primary outcome due to lack of GABARAP subfamily protein interaction. Together with the data of a related PhD project which is included in the manuscript (4.2), it could be shown that lack of individual GABARAP proteins, especially GABARAP and GABARAPL2 significantly altered Golgi apparatus morphology. Analysis of the transport of fluorescently labelled ceramide could further show that lack of the GABARAP subfamily resulted in strongly decreased PM transport of this lipid. Conclusively, altered degradation and/or recycling of the respective proteins, Golgi bypass secretion, mislocalization or perturbation of general homeostasis, e.g. by influencing the autophagy pathway, potentially add with different strengths to the outcome of surface protein localization and abundance. Additionally, altered surface abundance cannot directly be pinned down to an individual member or combinations of the GABARAP subfamily, as one, two or all three members might be causative for the observed effects or even act antagonistically.

In summary, the identified alterations of surfaceome composition of TKO compared to WT cells provides a framework to identify cell surface proteins which might be influenced by each individual or all of the GABARAP subfamily proteins regarding their trafficking already under steady-state conditions.

5.3 GABARAP, but none of its paralogs, slows down EGF-induced EGFR degradation

As illustrated in the aims of the present thesis (3), to further address the scientific question of whether and how the GABARAP subfamily or an individual protein thereof may be involved in intracellular trafficking events required identification and employment of an ideal model system.

The EGFR fulfilled all of the defined requirements for such a model system: it is by far the most extensively studied RTK and thus a huge variety of materials and methods, including specific and sensitive antibodies, expression plasmids and qPCR primers, were available. It is activated by several extracellular ligands which include the eponymous EGFR-specific EGF. Effects of stimulation with EGF are well-studied (2.2.1 – 2.2.3) and the activation of downstream signaling pathways is well-defined which allows for a direct readout of EGFR activation and its degradation upon high ligand concentrations. EGF is also available conjugated to a fluorescent dye, allowing live-cell studies of EGF uptake and intracellular EGF/EGFR trafficking.

In addition, all of the desirable optional requirements were met: EGFR exhibits potential LIR motifs in its cytoplasmic tail, enabling analysis of a putative direct interaction with GABARAP subfamily proteins. Furthermore, it is ubiquitously expressed in most cell types and tissues and although expression levels vary greatly between cell types [278], this infers a certain degree of generalizability of observed phenotypes. Finally, several facts at the initiation of the project already hinted at GABARAP subfamily proteins taking part in intracellular trafficking and degradation of the EGFR. GABARAPL1 was described to be important in increased EGFR surface expression under hypoxic but not basal conditions [149]. This hinted at GABARAP subfamily proteins being involved during (stress)-induced trafficking of receptors. Further suggestions were given by the fact that PLEKHM1 was described to simultaneously bind to LC3/GABARAP proteins and the HOPS complex and to mediate EGF-induced lysosomal degradation of EGFR independent of autophagy [100]. These characteristics rendered the EGFR as an optimal model system for investigating every aspect of intracellular trafficking, recycling and degradation events. Taken together, EGFR was a promising candidate to analyze the involvement of individual GABARAP subfamily proteins during autophagy-independent intracellular trafficking (4.3).

Because endogenous EGFR expression levels are relatively low in HEK293 cells compared to other cell types [279], liver-derived Huh7.5 cells were additionally subjected to genome editing to generate clonal KO cell lines of GABARAP subfamily members. Systematic analysis of all available KO combinations in these two independent cell types consistently revealed that lack of GABARAP either alone or in combination with GABARAPL2 results in accelerated EGF-induced EGFR degradation.

On the basis of this observation, the implications of accelerated EGFR degradation and the underlying mechanisms were analyzed in Huh7.5 GABARAP SKO cells and revealed that EGFR downstream signaling and target gene expression were strongly reduced, although activation of the receptor was initially even enhanced in GABARAP SKO cells. Further analysis clarified that EGFR total and surface levels as well as gene expression levels were unaltered, indicating that GABARAP influences steps downstream of gene expression, protein translation and anterograde transport of the receptor to the PM. Consistently, EGF uptake was initially not influenced by GABARAP deficiency, but significantly reduced over time as measured in a FACS-based EGF uptake assay. Consequently, EGF uptake over time as analyzed by a pulse-based uptake assay in parallel within a related project was also reduced.

Within the present PhD project, a GFP-GABARAP KI cell line was generated enabling live-cell analysis of FP-tagged GABARAP under control of endogenous regulatory elements. This cell line was consequently used during live-cell imaging within the institute and it could be shown that GABARAP and EGF transiently comigrate in highly dynamic vesicular structures. These included large GABARAP-positive ring-like structures of up to 3 µm in diameter which exhibited dynamic changes in local GABARAP concentrations where EGF-containing vesicles fused and budded off.

Supporting a direct interaction, co-immunoprecipitation experiments performed within this PhD project revealed association of GABARAP and EGFR in living cells. Related to that, work within the institute could show that GABARAP binds to synthetic LIR-containing peptides derived from the EGFR cytoplasmic tail. However, the obtained binding affinities for both the phosphorylated and unphosphorylated peptide were up to 1930-fold lower compared to e.g. binding of GABARAP to an ULK1-derived LIR-containing peptide described by a recent study [280]. Increase in GABARAP and/or EGFR, e.g. by clustering of either protein, could nonetheless result in locally sufficient concentrations to allow interaction by the LIR analyzed in this work. Whether other determinants such as additional LIRs or an UIM within the receptor's cytoplasmic tail further contribute to, or even solely mediate, interaction of GABARAP and EGFR *in vivo* needs to be further investigated.

Taken together, the results obtained within this project under conditions not inducing autophagy, clearly demonstrate a direct influence of GABARAP during intracellular cell surface protein trafficking independent of autophagy (4.3).

5.4 Conclusion

Although autophagy-inhibiting peptides binding to LC3/GABARAP proteins exhibiting much higher affinity for the GABARAP compared to the LC3 subfamily have recently been described [281], binding to members of the LC3 subfamily cannot be excluded, possibly interfering with any function specifically assigned to GABARAP subfamily proteins. Therefore, specific deletion of individual GABARAP subfamily proteins by genome editing, as performed within this PhD project, is better suited to dissect individual protein functions. During the course of this PhD work, several other working groups applied CRISPR/Cas9-mediated genome editing in human cell lines to investigate functions of LC3 and GABARAP subfamily proteins.

Apart from LC3B2, the working group of Lazarou generated cells lacking the complete LC3 and GABARAP subfamily in Henrietta Lacks (HeLa) cells [80]. They analyzed TKO cells of both subfamilies and hexa KO cells lacking all six remaining LC3/GABARAP proteins and concentrated their analysis on mitophagy. Based on reconstitution experiments of hexa KO cells with individual proteins of both subfamilies, they identified the GABARAP subfamily as a main organizer of PINK1-mediated mitophagy and mediator of lysosomal fusion. Interestingly, they found autophagosome biogenesis in hexa KO cells to be delayed and resulting autophagosomes were much smaller in size compared to WT cells. Later, Harper *et al.* also analyzed HeLa-based LC3 and GABARAP TKO as well as hexa KO cells focusing on autophagy [282]. In accordance with Lazarou *et al.*, they found the lack of the GABARAP subfamily resulting in lysosomal fusion defects and reduced autophagic flux. They also used a proteomics approach to identify proteins with differential abundance in autophagosomes lacking the whole GABARAP subfamily after chloroquine treatment to enrich autophagosomal structures. Finally, Kim *et al.* also analyzed cells deficient for either one or both subfamilies and performed reconstitution experiments with individual LC3/GABARAP proteins to identify LC3B and LC3C as negative as well as GABARAP and GABARAPL1 as positive regulators of ULK1 activity and thus early steps of autophagy initiation [28].

Despite exhibiting a certain degree of overlap, especially in terms of methodology, major differences exist compared to this PhD thesis. Importantly, analysis conducted in this thesis was focused on individual GABARAP subfamily members, while all other three studies using KO cell lines published so far, focused analysis on the LC3 and GABARAP subfamily in comparison to each other. In contrast to the presented PhD thesis which focused analysis

strictly on conditions not inducing autophagy, all three described publications investigated the role of LC3 and GABARAP subfamily proteins on processes directly related to autophagy. In addition, the generation of cells expressing GFP-GABARAP under endogenous promoter and other regulatory elements is a major strength of this thesis and to date the only published use of GFP-GABARAP KI cells. Minor differences include use of different cell lines and/or different CRISPR/Cas9 targeting strategies.

Taken together, the present PhD thesis adds further complexity to the biological functions of GABARAP subfamily proteins by emphasizing on non-redundant and autophagy-independent roles of individual subfamily members for cell surface protein biology including anterograde transport, intracellular trafficking and degradation. Figure 8 summarizes the scientific significance of the novel aspects of GABARAP subfamily functions discovered within this PhD project.

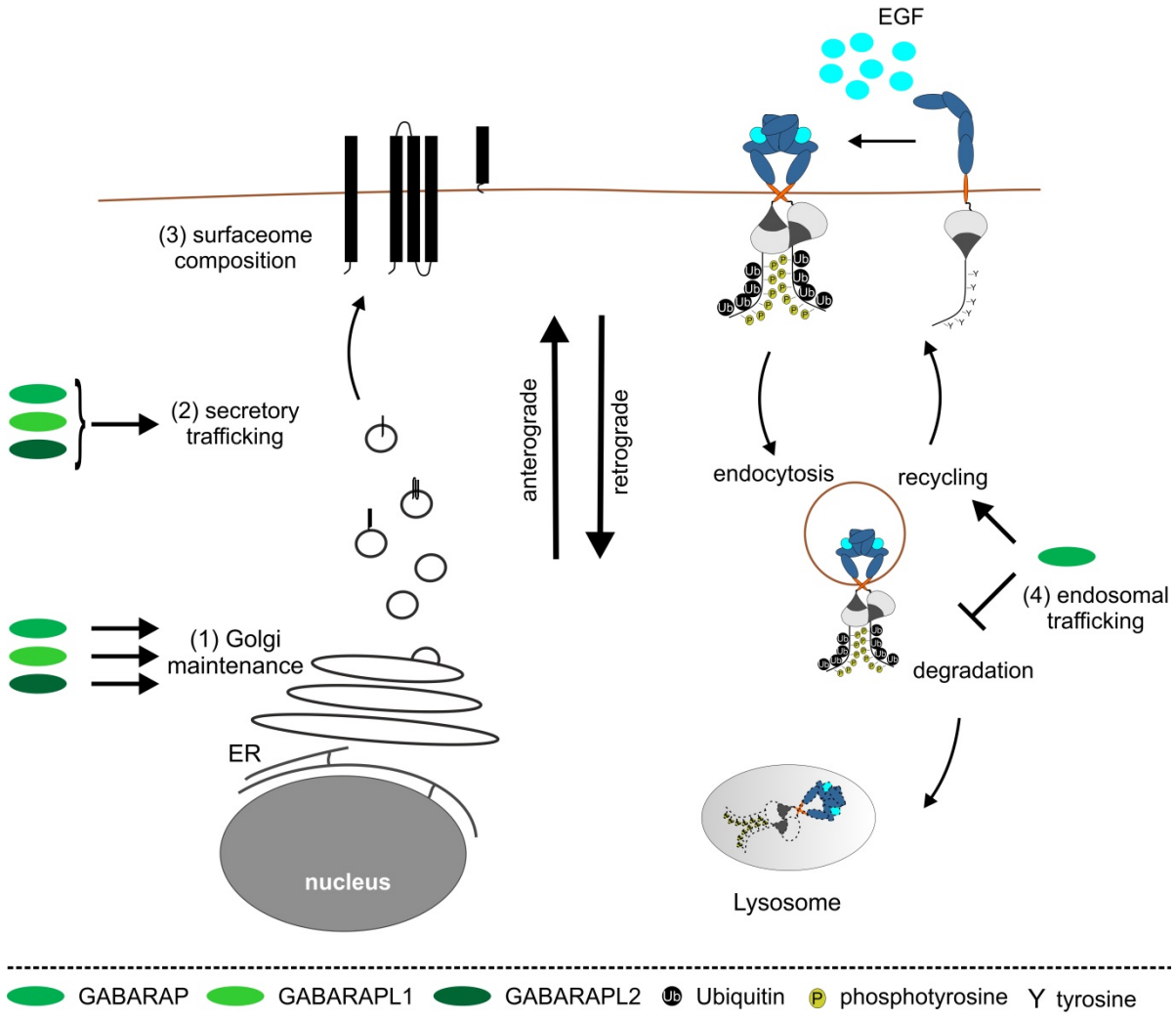

Figure 8: Summary of the novel aspects of autophagy-independent functions of GABARAP subfamily proteins identified within this PhD thesis. (1) Each GABARAP subfamily protein was identified to be involved in Golgi apparatus maintenance, while (2) the whole GABARAP subfamily was found to act in positive regulation

of anterograde secretory vesicle trafficking. (3) These novel aspects in concert may explain the observed influence of GABARAP subfamily proteins on surfaceome composition. (4) Deficiency of GABARAP but not its paralogs resulted in accelerated EGF-induced EGFR degradation. GABARAP thereby potentially acts as a positive regulator of endosomal recycling and/or a negative regulator of degradation.

6. Outlook

GABARAP and its paralogs seem to share most of their direct interaction partners, at least during *in vitro* interaction studies [277]. Nonetheless, a novel and potentially non-redundant role of GABARAP in EGFR trafficking was revealed during this work (4.3). How GABARAP subfamily proteins may achieve individual specificity thus needs to be addressed in the future. One possibility is that subcellular localization differs between GABARAP paralogs under different intracellular conditions. Endogenous intracellular levels of FP-tagged GABARAP subfamily proteins as enabled by CRISPR/Cas9-mediated genome editing (4.3) can help clarify this point in all of those cases where the applied tagging strategy does not influence the protein activity to be analyzed. Use of small tags such as e.g. hemagglutinin (HA)-tags should be considered, as e.g. during mitophagy GFP-tagged GABARAP did not localize to mitochondria [123], while HA-tagged GABARAP did [80]. However, for live-cell imaging experiments, FP-tagged GABARAP remains the optimal solution as it can be visualized without further staining and in living cells. To circumvent potential functional impairment by N-terminal FP-tagging, alternative constructs could be applied. Conjugation-deficient GABARAP [283] might be C-terminally FP-tagged and conjugated to WT GABARAP, thereby forming a dimer with each one free N- and C-terminus which would then be able to engage in endogenous interactions.

Another possibility to achieve individual specificity could be differential gene expression and/or protein levels of GABARAP subfamily proteins between different tissues and cell types or in response to different stimuli. This can be further addressed by promoter analyses in case of gene expression and quantitative proteomics in case of protein abundance. Interestingly, GABARAPL1 but not GABARAPL2 protein levels were found to be increased in GABARAP SKO cells (4.3), suggesting at least some degree of compensatory regulation which might additionally contribute to any observed SKO phenotype.

The dependence on GABARAP lipidation status is another important issue. Whether lipidation and thus covalent membrane association is necessary for GABARAP subfamily proteins to influence endosomal trafficking of the EGFR can be analyzed by using lipidation-deficient GABARAP mutants, ideally via KI to maintain endogenous regulation of expression levels.

LC3 subfamily proteins may also be important in understanding the interplay between, and the necessity of, both subfamilies. Interestingly, in cells deficient for the whole GABARAP subfamily, lipidation of LC3B was shown to be enhanced [80]. This was also shown for GABARAP knockdown in response to starvation [109], indicating either accumulation within autophagosomes due to reduced autophagic flux or compensatory upregulation of total LC3B levels.

As discussed in work published as part of this PhD thesis (4.3), a fairly large number of LC3/GABARAP-interacting proteins which were already described to be involved particularly in EGFR trafficking and degradation, exist. To clarify which of these interactions contribute to GABARAP-mediated EGFR trafficking remains to be elucidated in future studies.

The targeting of PI4KIIα by GABARAP to autophagosomes in response to nutrient starvation [109] could be an additional link between GABARAP, autophagy and endosomal trafficking. This kinase and its reaction product PI4P have already been described to regulate endosomal trafficking of receptors, in particular degradation of EGFR [284, 285]. Targeting of PI4KIIα to endosomes by GABARAP is therefore easily imaginable and could represent a switch to regulate local production of lipid messengers such as PI4P on distinct vesicles in response to starvation and/or other stimuli such as EGF binding to EGFR. Colocalization of GABARAP and PI4KIIα on cytosolic vesicles has also been reported to be independent of GABARAP lipidation [216]. Such membrane association would allow for a fast and transient local increase in GABARAP concentration, enabling rapid recruitment of effector molecules for vesicular fusion. It is thus conceivable that, e.g. dependent on cell type and cellular metabolic state, distinct GABARAP (and/or LC3) subfamily proteins may define vesicular identity by local protein gradients. In support with this idea, Leidal *et al.* could recently show a role for LC3B during cargo loading into EVs [286]. In parallel, work from a related PhD project performed within our institute demonstrated the secretion of GABARAP within EVs [287]. Interestingly, at least *in vitro*, LC3/GABARAP proteins were also described to be attached to phosphatidylserine [288] which would further increase the possibilities of LC3/GABARAP proteins to define membrane identity.

GABARAP might not only be involved in vesicle fusion, but also fission. The highly dynamic local increase in GFP-GABARAP observed at ring-like structures during live-cell imaging (4.3) with the associated EGF-containing vesicle budding events bears a striking resemblance to a certain recycling-associated process. The recently reported ER-associated endosomal fission mediated by transmembrane and coiled-coil domains protein 1 (TMCC1) positively regulates recycling of late endosomal cargo [289]. Interestingly, TMCC1 contains several xLIR motifs which might link GABARAP to such fission events. Following this line of thought, the GABARAP-positive ring-like structures might indeed be sorting endosomes. Clarification of their identity will thus be an exciting and important task.

Taken together, GABARAP subfamily proteins are involved in a steadily increasing number of different processes, some of which are described in this PhD project (4.2, 4.3). These add to their functions during autophagy-related processes and include e.g. disease [275] and killing of intracellular pathogens [290]. Together with different modes of their association to single or double lipid bilayer membranes, either dependent or independent of lipidation, this exhibits a striking resemblance to another small protein modifier, namely ubiquitin.

Attachment of ubiquitin to amino acid side chains of proteins (ubiquitination) was initially, and still is, mainly associated with tagging proteins intended for proteasomal degradation [291-293]. Actually, ubiquitination affects almost any cellular process, including e.g. cell cycle control [294], DNA DSB repair [295] targeting of proteins for endosomal sorting [296], regulation of immune response [297] and modification of kinase activity [298].
Whether the versatility of GABARAP subfamily proteins will indeed reach the level of ubiquitin will thus be, at least in my opinion, one of the most exciting aspects in the future.

7. References

1. Schaaf, M.B.E.; Keulers, T.G.; Vooijs, M.A.; Rouschop, K.M.A. LC3/GABARAP family proteins: autophagy-(un)related functions. *FASEB J.* **2016**, *30*, 3961–3978.

2. Coyle, J.E.; Qamar, S.; Rajashankar, K.R.; Nikolov, D.B. Structure of GABARAP in Two Conformations. *Neuron* **2002**, *33*, 63–74.

3. Knight, D.; Harris, R.; McAlister, M.S.B.; Phelan, J.P.; Geddes, S.; Moss, S.J.; Driscoll, P.C.; Keep, N.H. The X-ray Crystal Structure and Putative Ligand-derived Peptide Binding Properties of γ-Aminobutyric Acid Receptor Type A Receptor-associated Protein. *J. Biol. Chem.* **2002**, *277*, 5556–5561.

4. Paz, Y.; Elazar, Z.; Fass, D. Structure of GATE-16, Membrane Transport Modulator and Mammalian Ortholog of Autophagocytosis Factor Aut7p. *J. Biol. Chem.* **2000**, *275*, 25445–25450.

5. Green, F.; O'Hare, T.; Blackwell, A.; Enns, C.A. Association of human transferrin receptor with GABARAP. *FEBS Lett.* **2002**, *518*, 101–106.

6. Shpilka, T.; Weidberg, H.; Pietrokovski, S.; Elazar, Z. Atg8: An autophagy-related ubiquitin-like protein family. *Genome Biol.* **2011**, *12*.

7. Jatana, N.; Ascher, D.B.; Pires, D.E.V.; Gokhale, R.S.; Thukral, L. Human LC3 and GABARAP subfamily members achieve functional specificity via specific structural modulations. *Autophagy* **2020**, *16*, 239–255.

8. Pacheco, V.; Ma, P.; Thielmann, Y.; Hartmann, R.; Weiergräber, O.H.; Mohrlüder, J.; Willbold, D. Assessment of GABARAP self-association by its diffusion properties. *J. Biomol. NMR* **2010**, *48*, 49–58.

9. Wild, P.; McEwan, D.G.; Dikic, I. The LC3 interactome at a glance. *J. Cell Sci.* **2014**, *127*, 3–9.

10. Rogov, V. V; Stolz, A.; Ravichandran, A.C.; Rios-Szwed, D.O.; Suzuki, H.; Kniss, A.; Löhr, F.; Wakatsuki, S.; Dötsch, V.; Dikic, I.; et al. Structural and functional analysis of the GABARAP interaction motif (GIM). *EMBO Rep.* **2018**, *19*, e47268.

11. Noda, N.N.; Ohsumi, Y.; Inagaki, F. Atg8-family interacting motif crucial for selective autophagy. *FEBS Lett.* **2010**, *584*, 1379–1385.

12. Huber, J.; Obata, M.; Gruber, J.; Akutsu, M.; Löhr, F.; Rogova, N.; Güntert, P.; Dikic, I.; Kirkin, V.; Komatsu, M.; et al. An atypical LIR motif within UBA5 (ubiquitin like

modifier activating enzyme 5) interacts with GABARAP proteins and mediates membrane localization of UBA5. *Autophagy* **2019**, *0*, 1.

13. Jacomin, A.C.; Samavedam, S.; Promponas, V.; Nezis, I.P. iLIR database: A web resource for LIR motif-containing proteins in eukaryotes. *Autophagy* **2016**, *12*, 1945–1953.

14. Marshall, R.S.; Hua, Z.; Mali, S.; McLoughlin, F.; Vierstra, R.D. ATG8-Binding UIM Proteins Define a New Class of Autophagy Adaptors and Receptors. *Cell* **2019**, *177*, 766-781.e24.

15. Tsukada, M.; Ohsumi, Y. Isolation and characterization of autophagy-defective mutants of Saccharomyces cerevisiae. *FEBS Lett.* **1993**, *333*, 169–174.

16. Klionsky, D.J. Autophagy revisited: A conversation with Christian de Duve. *Autophagy* **2008**, *4*, 740–743.

17. Takeshige, K.; Baba, M.; Tsuboi, S.; Noda, T.; Ohsumi, Y. Autophagy in yeast demonstrated with proteinase-deficient mutants and conditions for its induction. *J. Cell Biol.* **1992**, *119*, 301–312.

18. Ravikumar, B.; Sarkar, S.; Davies, J.E.; Futter, M.; Garcia-Arencibia, M.; Green-Thompson, Z.W.; Jimenez-Sanchez, M.; Korolchuk, V.I.; Lichtenberg, M.; Luo, S.; et al. Regulation of Mammalian Autophagy in Physiology and Pathophysiology. *Physiol. Rev.* **2010**, *90*, 1383–1435.

19. Weidberg, H.; Shvets, E.; Shpilka, T.; Shimron, F.; Shinder, V.; Elazar, Z. LC3 and GATE-16/GABARAP subfamilies are both essential yet act differently in autophagosome biogenesis. *EMBO J.* **2010**, *29*, 1792–1802.

20. Lee, Y.-K.; Lee, J.-A. Role of the mammalian ATG8/LC3 family in autophagy: differential and compensatory roles in the spatiotemporal regulation of autophagy. *BMB Rep.* **2016**, *49*, 424–430.

21. Rabanal-Ruiz, Y.; Otten, E.G.; Korolchuk, V.I. mTORC1 as the main gateway to autophagy. *Essays Biochem.* **2017**, *61*, 565–584.

22. Hosokawa, N.; Hara, T.; Kaizuka, T.; Kishi, C.; Takamura, A.; Miura, Y.; Iemura, S.; Natsume, T.; Takehana, K.; Yamada, N.; et al. Nutrient-dependent mTORC1 Association with the ULK1–Atg13–FIP200 Complex Required for Autophagy. *Mol. Biol. Cell* **2009**, *20*, 1981–1991.

23. Ganley, I.G.; Lam, D.H.; Wang, J.; Ding, X.; Chen, S.; Jiang, X. ULK1·ATG13·FIP200 Complex Mediates mTOR Signaling and Is Essential for Autophagy. *J. Biol. Chem.* **2009**, *284*, 12297–12305.

24. Webster, C.P.; Smith, E.F.; Bauer, C.S.; Moller, A.; Hautbergue, G.M.; Ferraiuolo, L.; Myszczynska, M.A.; Higginbottom, A.; Walsh, M.J.; Whitworth, A.J.; et al. The C9orf72 protein interacts with Rab1a and the ULK1 complex to regulate initiation of autophagy. *EMBO J.* **2016**, *35*, 1656–1676.

25. Carlos Martín Zoppino, F.; Damián Militello, R.; Slavin, I.; Álvarez, C.; Colombo, M.I. Autophagosome Formation Depends on the Small GTPase Rab1 and Functional ER Exit Sites. *Traffic* **2010**, *11*, 1246–1261.

26. Axe, E.L.; Walker, S.A.; Manifava, M.; Chandra, P.; Roderick, H.L.; Habermann, A.; Griffiths, G.; Ktistakis, N.T. Autophagosome formation from membrane compartments enriched in phosphatidylinositol 3-phosphate and dynamically connected to the endoplasmic reticulum. *J. Cell Biol.* **2008**, *182*, 685–701.

27. Joachim, J.; Jefferies, H.B.J.; Razi, M.; Frith, D.; Snijders, A.P.; Chakravarty, P.; Judith, D.; Tooze, S.A. Activation of ULK Kinase and Autophagy by GABARAP Trafficking from the Centrosome Is Regulated by WAC and GM130. *Mol. Cell* **2015**, *60*, 899–913.

28. Grunwald, D.S.; Otto, N.M.; Park, J.-M.; Song, D.; Kim, D.-H. GABARAPs and LC3s have opposite roles in regulating ULK1 for autophagy induction. *Autophagy* **2020**, *16*, 600–614.

29. Zhong, Y.; Wang, Q.J.; Li, X.; Yan, Y.; Backer, J.M.; Chait, B.T.; Heintz, N.; Yue, Z. Distinct regulation of autophagic activity by Atg14L and Rubicon associated with Beclin 1-phosphatidylinositol-3-kinase complex. *Nat. Cell Biol.* **2009**, *11*, 468–476.

30. Kihara, A.; Kabeya, Y.; Ohsumi, Y.; Yoshimori, T. Beclin–phosphatidylinositol 3-kinase complex functions at the trans -Golgi network. *EMBO Rep.* **2001**, *2*, 330–335.

31. Sun, Q.; Fan, W.; Chen, K.; Ding, X.; Chen, S.; Zhong, Q. Identification of Barkor as a mammalian autophagy-specific factor for Beclin 1 and class III phosphatidylinositol 3-kinase. *Proc. Natl. Acad. Sci.* **2008**, *105*, 19211–19216.

32. Backer, J.M. The intricate regulation and complex functions of the Class III phosphoinositide 3-kinase Vps34. *Biochem. J.* **2016**, *473*, 2251–2271.

33. Menon, M.B.; Dhamija, S. Beclin 1 Phosphorylation – at the Center of Autophagy Regulation. *Front. Cell Dev. Biol.* **2018**, *6*, 1–9.

34. Pattingre, S.; Tassa, A.; Qu, X.; Garuti, R.; Liang, X.H.; Mizushima, N.; Packer, M.; Schneider, M.D.; Levine, B. Bcl-2 Antiapoptotic Proteins Inhibit Beclin 1-Dependent Autophagy. *Cell* **2005**, *122*, 927–939.

35. Wei, Y.; Zou, Z.; Becker, N.; Anderson, M.; Sumpter, R.; Xiao, G.; Kinch, L.; Koduru, P.; Christudass, C.S.; Veltri, R.W.; et al. EGFR-Mediated Beclin 1 Phosphorylation in Autophagy Suppression, Tumor Progression, and Tumor Chemoresistance. *Cell* **2013**, *154*, 1269–1284.

36. Tang, D.; Kang, R.; Livesey, K.M.; Cheh, C.-W.; Farkas, A.; Loughran, P.; Hoppe, G.; Bianchi, M.E.; Tracey, K.J.; Zeh, H.J.; et al. Endogenous HMGB1 regulates autophagy. *J. Cell Biol.* **2010**, *190*, 881–892.

37. Wei, Y.; Pattingre, S.; Sinha, S.; Bassik, M.; Levine, B. JNK1-Mediated Phosphorylation of Bcl-2 Regulates Starvation-Induced Autophagy. *Mol. Cell* **2008**, *30*, 678–688.

38. Park, J.-M.; Seo, M.; Jung, C.H.; Grunwald, D.; Stone, M.; Otto, N.M.; Toso, E.; Ahn, Y.; Kyba, M.; Griffin, T.J.; et al. ULK1 phosphorylates Ser30 of BECN1 in association with ATG14 to stimulate autophagy induction. *Autophagy* **2018**, *14*, 584–597.

39. Itakura, E.; Kishi, C.; Inoue, K.; Mizushima, N. Beclin 1 Forms Two Distinct Phosphatidylinositol 3-Kinase Complexes with Mammalian Atg14 and UVRAG. *Mol. Biol. Cell* **2008**, *19*, 5360–5372.

40. Fan, W.; Nassiri, A.; Zhong, Q. Autophagosome targeting and membrane curvature sensing by Barkor/Atg14(L). *Proc. Natl. Acad. Sci.* **2011**, *108*, 7769–7774.

41. Matsunaga, K.; Saitoh, T.; Tabata, K.; Omori, H.; Satoh, T.; Kurotori, N.; Maejima, I.; Shirahama-Noda, K.; Ichimura, T.; Isobe, T.; et al. Two Beclin 1-binding proteins, Atg14L and Rubicon, reciprocally regulate autophagy at different stages. *Nat. Cell Biol.* **2009**, *11*, 385–396.

42. Itakura, E.; Mizushima, N. Characterization of autophagosome formation site by a hierarchical analysis of mammalian Atg proteins. *Autophagy* **2010**, *6*, 764–776.

43. Matsunaga, K.; Morita, E.; Saitoh, T.; Akira, S.; Ktistakis, N.T.; Izumi, T.; Noda, T.; Yoshimori, T. Autophagy requires endoplasmic reticulum targeting of the PI3-kinase

complex via Atg14L. *J. Cell Biol.* **2010**, *190*, 511–521.

44. Russell, R.C.; Tian, Y.; Yuan, H.; Park, H.W.; Chang, Y.Y.; Kim, J.; Kim, H.; Neufeld, T.P.; Dillin, A.; Guan, K.L. ULK1 induces autophagy by phosphorylating Beclin-1 and activating VPS34 lipid kinase. *Nat. Cell Biol.* **2013**, *15*, 741–750.

45. Di Bartolomeo, S.; Corazzari, M.; Nazio, F.; Oliverio, S.; Lisi, G.; Antonioli, M.; Pagliarini, V.; Matteoni, S.; Fuoco, C.; Giunta, L.; et al. The dynamic interaction of AMBRA1 with the dynein motor complex regulates mammalian autophagy. *J. Cell Biol.* **2010**, *191*, 155–168.

46. Schu, P. V.; Takegawa, K.; Fry, M.J.; Stack, J.H.; Waterfield, M.D.; Emr, S.D. Phosphatidylinositol 3-kinase encoded by yeast VPS34 gene essential for protein sorting. *Science (80-.).* **1993**, *260*, 88–91.

47. Stack, J.H.; Emr, S.D. Vps34p is a phosphatidylinositol-specific PI 3-kinase required for vacuolar protein sorting in yeast and possesses both lipid and protein kinase activities. *J. Biol. Chem.* **1994**, *269*, 31552–31562.

48. Petiot, A.; Ogier-Denis, E.; Blommaart, E.F.C.; Meijer, A.J.; Codogno, P. Distinct Classes of Phosphatidylinositol 3'-Kinases Are Involved in Signaling Pathways That Control Macroautophagy in HT-29 Cells. *J. Biol. Chem.* **2000**, *275*, 992–998.

49. Birgisdottir, Å.B.; Mouilleron, S.; Bhujabal, Z.; Wirth, M.; Sjøttem, E.; Evjen, G.; Zhang, W.; Lee, R.; O'Reilly, N.; Tooze, S.A.; et al. Members of the autophagy class III phosphatidylinositol 3-kinase complex I interact with GABARAP and GABARAPL1 via LIR motifs. *Autophagy* **2019**, *15*, 1333–1355.

50. Mizushima, N.; Sugita, H.; Yoshimori, T.; Ohsumi, Y. A New Protein Conjugation System in Human. The Counterpart of the Yeast Apg12p Conjugation System Essential for Autophagy. **1998**, 33889–33893.

51. Tanida, I.; Tanida-Miyake, E.; Ueno, T.; Kominami, E. The human homolog of Saccharomyces cerevisiae Apg7p is a protein-activating enzyme for multiple substrates including human Apg12p, GATE-16, GABARAP, and MAP-LC3. *J. Biol. Chem.* **2001**, *276*, 1701–1706.

52. Nemoto, T.; Tanida, I.; Tanida-Miyake, E.; Minematsu-Ikeguchi, N.; Yokota, M.; Ohsumi, M.; Ueno, T.; Kominami, E. The mouse APG10 homologue, an E2-like enzyme for Apg12p conjugation, facilitates MAP-LC3 modification. *J. Biol. Chem.* **2003**, *278*, 39517–39526.

53. Mizushima, N.; Kuma, A.; Kobayashi, Y.; Yamamoto, A.; Matsubae, M.; Takao, T.; Natsume, T.; Ohsumi, Y.; Yoshimori, T. Mouse Apg16L, a novel WD-repeat protein, targets to the autophagic isolation membrane with the Apg12-Apg5 conjugate. *J. Cell Sci.* **2003**, *116*, 1679–1688.

54. Kabeya, Y. LC3, a mammalian homologue of yeast Apg8p, is localized in autophagosome membranes after processing. *EMBO J.* **2000**, *19*, 5720–5728.

55. Agrotis, A.; Pengo, N.; Burden, J.J.; Ketteler, R. Redundancy of human ATG4 protease isoforms in autophagy and LC3/GABARAP processing revealed in cells. *Autophagy* **2019**, *15*, 976–997.

56. Tanida, I.; Tanida-Miyake, E.; Komatsu, M.; Ueno, T.; Kominami, E. Human Apg3p/Aut1p homologue is an authentic E2 enzyme for multiple substrates, GATE-16, GABARAP, and MAP-LC3, and facilitates the conjugation of hApg12p to hApg5p. *J. Biol. Chem.* **2002**, *277*, 13739–13744.

57. Klionsky, D.J.; Abdelmohsen, K.; Abe, A.; Abedin, M.J.; Abeliovich, H.; Acevedo Arozena, A.; Adachi, H.; Adams, C.M.; Adams, P.D.; Adeli, K.; et al. Guidelines for the use and interpretation of assays for monitoring autophagy (3rd edition). *Autophagy* **2016**, *12*, 1–222.

58. Fujita, N.; Itoh, T.; Omori, H.; Fukuda, M.; Noda, T.; Yoshimori, T. The Atg16L Complex Specifies the Site of LC3 Lipidation for Membrane Biogenesis in Autophagy. *Mol. Biol. Cell* **2008**, *19*, 2092–2100.

59. Dooley, H.C.; Razi, M.; Polson, H.E.J.; Girardin, S.E.; Wilson, M.I.; Tooze, S.A. WIPI2 Links LC3 Conjugation with PI3P, Autophagosome Formation, and Pathogen Clearance by Recruiting Atg12–5-16L1. *Mol. Cell* **2014**, *55*, 238–252.

60. Kaufmann, A.; Beier, V.; Franquelim, H.G.; Wollert, T. Molecular Mechanism of Autophagic Membrane-Scaffold Assembly and Disassembly. *Cell* **2014**, *156*, 469–481.

61. Nath, S.; Dancourt, J.; Shteyn, V.; Puente, G.; Fong, W.M.; Nag, S.; Bewersdorf, J.; Yamamoto, A.; Antonny, B.; Melia, T.J. Lipidation of the LC3/GABARAP family of autophagy proteins relies on a membrane-curvature-sensing domain in Atg3. *Nat. Cell Biol.* **2014**, *16*, 415–424.

62. Knorr, R.L.; Nakatogawa, H.; Ohsumi, Y.; Lipowsky, R.; Baumgart, T.; Dimova, R. Membrane morphology is actively transformed by covalent binding of the protein Atg8

to PE-lipids. *PLoS One* **2014**, *9*, e115357.

63. Juhasz, G.; Neufeld, T.P. Autophagy: A forty-year search for a missing membrane source. *PLoS Biol.* **2006**, *4*, 161–164.

64. Yamamoto, A.; Masaki, R.; Tashiro, Y. Characterization of the isolation membranes and the limiting membranes of autophagosomes in rat hepatocytes by lectin cytochemistry. *J. Histochem. Cytochem.* **1990**, *38*, 573–580.

65. Yamamoto, A.; Masaki, R.; Fukui, Y.; Tashiro, Y. Absence of cytochrome P-450 and presence of autolysosomal membrane antigens on the isolation membranes and autophagosomal membranes in rat hepatocytes. *J. Histochem. Cytochem.* **1990**, *38*, 1571–1581.

66. Hailey, D.W.; Rambold, A.S.; Satpute-Krishnan, P.; Mitra, K.; Sougrat, R.; Kim, P.K.; Lippincott-Schwartz, J. Mitochondria Supply Membranes for Autophagosome Biogenesis during Starvation. *Cell* **2010**, *141*, 656–667.

67. Graef, M.; Friedman, J.R.; Graham, C.; Babu, M.; Nunnari, J. ER exit sites are physical and functional core autophagosome biogenesis components. *Mol. Biol. Cell* **2013**, *24*, 2918–2931.

68. Ge, L.; Melville, D.; Zhang, M.; Schekman, R. The ER–Golgi intermediate compartment is a key membrane source for the LC3 lipidation step of autophagosome biogenesis. *Elife* **2013**, *2*, 1–23.

69. Tan, D.; Cai, Y.; Wang, J.; Zhang, J.; Menon, S.; Chou, H.-T.; Ferro-Novick, S.; Reinisch, K.M.; Walz, T. The EM structure of the TRAPPIII complex leads to the identification of a requirement for COPII vesicles on the macroautophagy pathway. *Proc. Natl. Acad. Sci.* **2013**, *110*, 19432–19437.

70. Longatti, A.; Lamb, C.A.; Razi, M.; Yoshimura, S.I.; Barr, F.A.; Tooze, S.A. TBC1D14 regulates autophagosome formation via Rab11- and ULK1-positive recycling endosomes. *J. Cell Biol.* **2012**, *197*, 659–675.

71. Puri, C.; Renna, M.; Bento, C.F.; Moreau, K.; Rubinsztein, D.C. Diverse Autophagosome Membrane Sources Coalesce in Recycling Endosomes. *Cell* **2013**, *154*, 1285–1299.

72. Knævelsrud, H.; Søreng, K.; Raiborg, C.; Håberg, K.; Rasmuson, F.; Brech, A.; Liestøl, K.; Rusten, T.E.; Stenmark, H.; Neufeld, T.P.; et al. Membrane remodeling by

the PX-BAR protein SNX18 promotes autophagosome formation. *J. Cell Biol.* **2013**, *202*, 331–349.

73. Ravikumar, B.; Moreau, K.; Jahreiss, L.; Puri, C.; Rubinsztein, D.C. Plasma membrane contributes to the formation of pre-autophagosomal structures. *Nat. Cell Biol.* **2010**, *12*, 747–757.

74. Orsi, A.; Razi, M.; Dooley, H.C.; Robinson, D.; Weston, A.E.; Collinson, L.M.; Tooze, S.A. Dynamic and transient interactions of Atg9 with autophagosomes, but not membrane integration, are required for autophagy. *Mol. Biol. Cell* **2012**, *23*, 1860–1873.

75. Lamb, C.A.; Nühlen, S.; Judith, D.; Frith, D.; Snijders, A.P.; Behrends, C.; Tooze, S.A. TBC1D14 regulates autophagy via the TRAPP complex andATG 9 traffic. *EMBO J.* **2016**, *35*, 281–301.

76. Knorr, R.L.; Lipowsky, R.; Dimova, R. Autophagosome closure requires membrane scission. *Autophagy* **2015**, *11*, 2134–2137.

77. Reggiori, F.; Ungermann, C. Autophagosome Maturation and Fusion. *J. Mol. Biol.* **2017**, *429*, 486–496.

78. Vergne, I.; Roberts, E.; Elmaoued, R.A.; Tosch, V.; Delgado, M.A.; Proikas-Cezanne, T.; Laporte, J.; Deretic, V. Control of autophagy initiation by phosphoinositide 3-phosphatase jumpy. *EMBO J.* **2009**, *28*, 2244–2258.

79. Taguchi-Atarashi, N.; Hamasaki, M.; Matsunaga, K.; Omori, H.; Ktistakis, N.T.; Yoshimori, T.; Noda, T. Modulation of Local PtdIns3P Levels by the PI Phosphatase MTMR3 Regulates Constitutive Autophagy. *Traffic* **2010**, *11*, 468–478.

80. Nguyen, T.N.; Padman, B.S.; Usher, J.; Oorschot, V.; Ramm, G.; Lazarou, M. Atg8 family LC3/GABARAP proteins are crucial for autophagosome–lysosome fusion but not autophagosome formation during PINK1/Parkin mitophagy and starvation. *J. Cell Biol.* **2016**, *215*, 857–874.

81. Weidberg, H.; Shpilka, T.; Shvets, E.; Abada, A.; Shimron, F.; Elazar, Z. LC3 and GATE-16 N Termini Mediate Membrane Fusion Processes Required for Autophagosome Biogenesis. *Dev. Cell* **2011**, *20*, 444–454.

82. Bozic, M.; van den Bekerom, L.; Milne, B.A.; Goodman, N.; Roberston, L.; Prescott, A.R.; Macartney, T.J.; Dawe, N.; McEwan, D.G. A conserved ATG2-GABARAP family

interaction is critical for phagophore formation. *EMBO Rep.* **2020**, *21*, 1–17.

83. Zhao, Y.G.; Chen, Y.; Miao, G.; Zhao, H.; Qu, W.; Li, D.; Wang, Z.; Liu, N.; Li, L.; Chen, S.; et al. The ER-Localized Transmembrane Protein EPG-3/VMP1 Regulates SERCA Activity to Control ER-Isolation Membrane Contacts for Autophagosome Formation. *Mol. Cell* **2017**, *67*, 974-989.e6.

84. Kimura, S.; Noda, T.; Yoshimori, T. Dynein-dependent Movement of Autophagosomes Mediates Efficient Encounters with Lysosomes. *Cell Struct. Funct.* **2008**, *33*, 109–122.

85. Pu, J.; Guardia, C.M.; Keren-Kaplan, T.; Bonifacino, J.S. Mechanisms and functions of lysosome positioning. *J. Cell Sci.* **2016**, *129*, 4329–4339.

86. Kjos, I.; Vestre, K.; Guadagno, N.A.; Borg Distefano, M.; Progida, C. Rab and Arf proteins at the crossroad between membrane transport and cytoskeleton dynamics. *Biochim. Biophys. Acta - Mol. Cell Res.* **2018**, *1865*, 1397–1409.

87. Vale, R.D. The Molecular Motor Toolbox for Intracellular Transport. *Cell* **2003**, *112*, 467–480.

88. Raiborg, C.; Wenzel, E.M.; Pedersen, N.M.; Olsvik, H.; Schink, K.O.; Schultz, S.W.; Vietri, M.; Nisi, V.; Bucci, C.; Brech, A.; et al. Repeated ER–endosome contacts promote endosome translocation and neurite outgrowth. *Nature* **2015**, *520*, 234–238.

89. Jordens, I.; Fernandez-Borja, M.; Marsman, M.; Dusseljee, S.; Janssen, L.; Calafat, J.; Janssen, H.; Wubbolts, R.; Neefjes, J. The Rab7 effector protein RILP controls lysosomal transport by inducing the recruitment of dynein-dynactin motors. *Curr. Biol.* **2001**, *11*, 1680–1685.

90. Van Der Kant, R.; Fish, A.; Janssen, L.; Janssen, H.; Krom, S.; Ho, N.; Brummelkamp, T.; Carette, J.; Rocha, N.; Neefjes, J. Late endosomal transport and tethering are coupled processes controlled by RILP and the cholesterol sensor ORP1L. *J. Cell Sci.* **2013**, *126*, 3462–3474.

91. Pankiv, S.; Alemu, E.A.; Brech, A.; Bruun, J.-A.; Lamark, T.; Øvervatn, A.; Bjørkøy, G.; Johansen, T. FYCO1 is a Rab7 effector that binds to LC3 and PI3P to mediate microtubule plus end–directed vesicle transport. *J. Cell Biol.* **2010**, *188*, 253–269.

92. Olsvik, H.L.; Lamark, T.; Takagi, K.; Larsen, K.B.; Evjen, G.; Øvervatn, A.; Mizushima, T.; Johansen, T. FYCO1 Contains a C-terminally Extended, LC3A/B-preferring LC3-interacting Region (LIR) Motif Required for Efficient Maturation of Autophagosomes

during Basal Autophagy. *J. Biol. Chem.* **2015**, *290*, 29361–29374.

93. Cheng, X.; Wang, Y.; Gong, Y.; Li, F.; Guo, Y.; Hu, S.; Liu, J.; Pan, L. Structural basis of FYCO1 and MAP1LC3A interaction reveals a novel binding mode for Atg8-family proteins. *Autophagy* **2016**, *12*, 1330–1339.

94. Monastyrska, I.; Rieter, E.; Klionsky, D.J.; Reggiori, F. Multiple roles of the cytoskeleton in autophagy. *Biol. Rev.* **2009**, *84*, 431–448.

95. Eskelinen, E.-L.; Saftig, P. Autophagy: A lysosomal degradation pathway with a central role in health and disease. *Biochim. Biophys. Acta - Mol. Cell Res.* **2009**, *1793*, 664–673.

96. Tsuboyama, K.; Koyama-Honda, I.; Sakamaki, Y.; Koike, M.; Morishita, H.; Mizushima, N. The ATG conjugation systems are important for degradation of the inner autophagosomal membrane. *Science (80-.).* **2016**, *354*, 1036–1041.

97. Balderhaar, H.J. k.; Ungermann, C. CORVET and HOPS tethering complexes - coordinators of endosome and lysosome fusion. *J. Cell Sci.* **2013**, *126*, 1307–1316.

98. Zlatic, S.A.; Tornieri, K.; L'Hernault, S.W.; Faundez, V. Metazoan cell biology of the HOPS tethering complex. *Cell. Logist.* **2011**, *1*, 111–117.

99. Spang, A. Membrane Tethering Complexes in the Endosomal System. *Front. Cell Dev. Biol.* **2016**, *4*, 1–7.

100. McEwan, D.G.; Popovic, D.; Gubas, A.; Terawaki, S.; Suzuki, H.; Stadel, D.; Coxon, F.P.; MirandadeStegmann, D.; Bhogaraju, S.; Maddi, K.; et al. PLEKHM1 regulates autophagosome-lysosome fusion through HOPS complex and LC3/GABARAP proteins. *Mol. Cell* **2015**, *57*, 39–54.

101. Tabata, K.; Matsunaga, K.; Sakane, A.; Sasaki, T.; Noda, T.; Yoshimori, T. Rubicon and PLEKHM1 Negatively Regulate the Endocytic/Autophagic Pathway via a Novel Rab7-binding Domain. *Mol. Biol. Cell* **2010**, *21*, 4162–4172.

102. Itakura, E.; Kishi-Itakura, C.; Mizushima, N. The Hairpin-type Tail-Anchored SNARE Syntaxin 17 Targets to Autophagosomes for Fusion with Endosomes/Lysosomes. *Cell* **2012**, *151*, 1256–1269.

103. Jiang, P.; Nishimura, T.; Sakamaki, Y.; Itakura, E.; Hatta, T.; Natsume, T.; Mizushima, N. The HOPS complex mediates autophagosome–lysosome fusion through interaction with syntaxin 17. *Mol. Biol. Cell* **2014**, *25*, 1327–1337.

104. Diao, J.; Liu, R.; Rong, Y.; Zhao, M.; Zhang, J.; Lai, Y.; Zhou, Q.; Wilz, L.M.; Li, J.; Vivona, S.; et al. ATG14 promotes membrane tethering and fusion of autophagosomes to endolysosomes. *Nature* **2015**, *520*, 563–566.

105. Ebner, P.; Poetsch, I.; Deszcz, L.; Hoffmann, T.; Zuber, J.; Ikeda, F. The IAP family member BRUCE regulates autophagosome–lysosome fusion. *Nat. Commun.* **2018**, *9*, 1–15.

106. Wang, T.; Li, L.; Hong, W. SNARE proteins in membrane trafficking. *Traffic* **2017**, *18*, 767–775.

107. Chen, Y.A.; Scheller, R.H. Snare-mediated membrane fusion. *Nat. Rev. Mol. Cell Biol.* 2001, *2*, 98–106.

108. Liang, C.; Lee, J.; Inn, K.-S.; Gack, M.U.; Li, Q.; Roberts, E.A.; Vergne, I.; Deretic, V.; Feng, P.; Akazawa, C.; et al. Beclin1-binding UVRAG targets the class C Vps complex to coordinate autophagosome maturation and endocytic trafficking. *Nat. Cell Biol.* **2008**, *10*, 776–787.

109. Wang, H.; Sun, H.-Q.; Zhu, X.; Zhang, L.; Albanesi, J.; Levine, B.; Yin, H. GABARAPs regulate PI4P-dependent autophagosome:lysosome fusion. *Proc. Natl. Acad. Sci.* **2015**, *112*, 7015–7020.

110. Kolter, T.; Sandhoff, K. PRINCIPLES OF LYSOSOMAL MEMBRANE DIGESTION: Stimulation of Sphingolipid Degradation by Sphingolipid Activator Proteins and Anionic Lysosomal Lipids. *Annu. Rev. Cell Dev. Biol.* **2005**, *21*, 81–103.

111. Schulze, H.; Kolter, T.; Sandhoff, K. Principles of lysosomal membrane degradation. *Biochim. Biophys. Acta - Mol. Cell Res.* **2009**, *1793*, 674–683.

112. Müller, S.; Dennemärker, J.; Reinheckel, T. Specific functions of lysosomal proteases in endocytic and autophagic pathways. *Biochim. Biophys. Acta - Proteins Proteomics* **2012**, *1824*, 34–43.

113. Samie, M.A.; Xu, H. Lysosomal exocytosis and lipid storage disorders. *J. Lipid Res.* **2014**, *55*, 995–1009.

114. Kirkin, V. History of the Selective Autophagy Research: How Did It Begin and Where Does It Stand Today? *J. Mol. Biol.* **2020**, *432*, 3–27.

115. Beese, C.J.; Brynjólfsdóttir, S.H.; Frankel, L.B. Selective Autophagy of the Protein Homeostasis Machinery: Ribophagy, Proteaphagy and ER-Phagy. *Front. Cell Dev.*

Biol. **2020**, *7*, 1–12.

116. Vargas, J.N.S.; Wang, C.; Bunker, E.; Hao, L.; Maric, D.; Schiavo, G.; Randow, F.; Youle, R.J. Spatiotemporal Control of ULK1 Activation by NDP52 and TBK1 during Selective Autophagy. *Mol. Cell* **2019**, *74*, 347-362.e6.

117. Ravenhill, B.J.; Boyle, K.B.; von Muhlinen, N.; Ellison, C.J.; Masson, G.R.; Otten, E.G.; Foeglein, A.; Williams, R.; Randow, F. The Cargo Receptor NDP52 Initiates Selective Autophagy by Recruiting the ULK Complex to Cytosol-Invading Bacteria. *Mol. Cell* **2019**, *74*, 320-329.e6.

118. Turco, E.; Fracchiolla, D.; Martens, S. Recruitment and Activation of the ULK1/Atg1 Kinase Complex in Selective Autophagy. *J. Mol. Biol.* **2020**, *432*, 123–134.

119. Bjørkøy, G.; Lamark, T.; Brech, A.; Outzen, H.; Perander, M.; Øvervatn, A.; Stenmark, H.; Johansen, T. p62/SQSTM1 forms protein aggregates degraded by autophagy and has a protective effect on huntingtin-induced cell death. *J. Cell Biol.* **2005**, *171*, 603–614.

120. Pankiv, S.; Clausen, T.H.; Lamark, T.; Brech, A.; Bruun, J.-A.; Outzen, H.; Øvervatn, A.; Bjørkøy, G.; Johansen, T. p62/SQSTM1 Binds Directly to Atg8/LC3 to Facilitate Degradation of Ubiquitinated Protein Aggregates by Autophagy. *J. Biol. Chem.* **2007**, *282*, 24131–24145.

121. Kim, P.K.; Hailey, D.W.; Mullen, R.T.; Lippincott-Schwartz, J. Ubiquitin signals autophagic degradation of cytosolic proteins and peroxisomes. *Proc. Natl. Acad. Sci.* **2008**, *105*, 20567–20574.

122. Kim, I.; Lemasters, J.J. Mitochondrial degradation by autophagy (mitophagy) in GFP-LC3 transgenic hepatocytes during nutrient deprivation. *Am. J. Physiol. Physiol.* **2011**, *300*, C308–C317.

123. Lazarou, M.; Sliter, D.A.; Kane, L.A.; Sarraf, S.A.; Wang, C.; Burman, J.L.; Sideris, D.P.; Fogel, A.I.; Youle, R.J. The ubiquitin kinase PINK1 recruits autophagy receptors to induce mitophagy. *Nature* **2015**, *524*, 309–314.

124. Narendra, D.P.; Jin, S.M.; Tanaka, A.; Suen, D.-F.; Gautier, C.A.; Shen, J.; Cookson, M.R.; Youle, R.J. PINK1 Is Selectively Stabilized on Impaired Mitochondria to Activate Parkin. *PLoS Biol.* **2010**, *8*, e1000298.

125. Princely Abudu, Y.; Pankiv, S.; Mathai, B.J.; Håkon Lystad, A.; Bindesbøll, C.;

Brenne, H.B.; Yoke Wui Ng, M.; Thiede, B.; Yamamoto, A.; Mutugi Nthiga, T.; et al. NIPSNAP1 and NIPSNAP2 Act as “Eat Me” Signals for Mitophagy. *Dev. Cell* **2019**, *49*, 509-525.e12.

126. Novak, I.; Kirkin, V.; McEwan, D.G.; Zhang, J.; Wild, P.; Rozenknop, A.; Rogov, V.; Löhr, F.; Popovic, D.; Occhipinti, A.; et al. Nix is a selective autophagy receptor for mitochondrial clearance. *EMBO Rep.* **2010**, *11*, 45–51.

127. Park, S.Y.; Koh, H.C. FUNDC1 regulates receptor-mediated mitophagy independently of the PINK1/Parkin-dependent pathway in rotenone-treated SH-SY5Y cells. *Food Chem. Toxicol.* **2020**, *137*, 111163.

128. Bhujabal, Z.; Birgisdottir, Å.B.; Sjøttem, E.; Brenne, H.B.; Øvervatn, A.; Habisov, S.; Kirkin, V.; Lamark, T.; Johansen, T. FKBP8 recruits LC3A to mediate Parkin-independent mitophagy. *EMBO Rep.* **2017**, *18*, 947–961.

129. Strappazzon, F.; Nazio, F.; Corrado, M.; Cianfanelli, V.; Romagnoli, A.; Fimia, G.M.; Campello, S.; Nardacci, R.; Piacentini, M.; Campanella, M.; et al. AMBRA1 is able to induce mitophagy via LC3 binding, regardless of PARKIN and p62/SQSTM1. *Cell Death Differ.* **2015**, *22*, 419–432.

130. Di Rita, A.; Peschiaroli, A.; D'Acunzo, P.; Strobbe, D.; Hu, Z.; Gruber, J.; Nygaard, M.; Lambrughi, M.; Melino, G.; Papaleo, E.; et al. HUWE1 E3 ligase promotes PINK1/PARKIN-independent mitophagy by regulating AMBRA1 activation via IKKα. *Nat. Commun.* **2018**, *9*, 3755.

131. Grumati, P.; Morozzi, G.; Hölper, S.; Mari, M.; Harwardt, M.-L.I.; Yan, R.; Müller, S.; Reggiori, F.; Heilemann, M.; Dikic, I. Full length RTN3 regulates turnover of tubular endoplasmic reticulum via selective autophagy. *Elife* **2017**, *6*, 1–32.

132. Fumagalli, F.; Noack, J.; Bergmann, T.J.; Cebollero, E.; Pisoni, G.B.; Fasana, E.; Fregno, I.; Galli, C.; Loi, M.; Soldà, T.; et al. Translocon component Sec62 acts in endoplasmic reticulum turnover during stress recovery. *Nat. Cell Biol.* **2016**, *18*, 1173–1184.

133. Khaminets, A.; Heinrich, T.; Mari, M.; Grumati, P.; Huebner, A.K.; Akutsu, M.; Liebmann, L.; Stolz, A.; Nietzsche, S.; Koch, N.; et al. Regulation of endoplasmic reticulum turnover by selective autophagy. *Nature* **2015**, *522*, 354–358.

134. Chen, L.; Wang, H.; Vicini, S.; Olsen, R.W. The gamma -aminobutyric acid type A (GABAA) receptor-associated protein (GABARAP) promotes GABAA receptor

clustering and modulates the channel kinetics. *Proc. Natl. Acad. Sci.* **2000**, *97*, 11557–11562.

135. Wang, H.; Bedford, F.K.; Brandon, N.J.; Moss, S.J.; Olsen, R.W. GABA(A)-receptor-associated protein links GABA(A) receptors and the cytoskeleton. *Nature* **1999**, *397*, 69–72.

136. Leil, T.A. GABAA Receptor-Associated Protein Traffics GABAA Receptors to the Plasma Membrane in Neurons. *J. Neurosci.* **2004**, *24*, 11429–11438.

137. Mansuy, V.; Boireau, W.; Fraichard, A.; Schlick, J.-L.; Jouvenot, M.; Delage-Mourroux, R. GEC1, a protein related to GABARAP, interacts with tubulin and GABAA receptor. *Biochem. Biophys. Res. Commun.* **2004**, *325*, 639–648.

138. Nakajima, K.; Yin, X.; Takei, Y.; Seog, D.H.; Homma, N.; Hirokawa, N. Molecular Motor KIF5A Is Essential for GABAA Receptor Transport, and KIF5A Deletion Causes Epilepsy. *Neuron* **2012**, *76*, 945–961.

139. Kittler, J.T.; Rostaing, P.; Schiavo, G.; Fritschy, J.-M.; Olsen, R.; Triller, A.; Moss, S.J. The Subcellular Distribution of GABARAP and Its Ability to Interact with NSF Suggest a Role for This Protein in the Intracellular Transport of GABAA Receptors. *Mol. Cell. Neurosci.* **2001**, *18*, 13–25.

140. Sagiv, Y. GATE-16, a membrane transport modulator, interacts with NSF and the Golgi v-SNARE GOS-28. *EMBO J.* **2000**, *19*, 1494–1504.

141. Chen, C.; Li, J.G.; Chen, Y.; Huang, P.; Wang, Y.; Liu-Chen, L.Y. GEC1 interacts with the κ opioid receptor and enhances expression of the receptor. *J. Biol. Chem.* **2006**, *281*, 7983–7993.

142. Nakamura, T.; Hayashi, T.; Nasu-Nishimura, Y.; Sakaue, F.; Morishita, Y.; Okabe, T.; Ohwada, S.; Matsuura, K.; Akiyama, T. PX-RICS mediates ER-to-Golgi transport of the N-cadherin/β-catenin complex. *Genes Dev.* **2008**, *22*, 1244–1256.

143. Nakamura, T.; Sakaue, F.; Nasu-Nishimura, Y.; Takeda, Y.; Matsuura, K.; Akiyama, T. The Autism-Related Protein PX-RICS Mediates GABAergic Synaptic Plasticity in Hippocampal Neurons and Emotional Learning in Mice. *EBioMedicine* **2018**, *34*, 189–200.

144. Laínez, S.; Valente, P.; Ontoria-Oviedo, I.; Estévez-Herrera, J.; Camprubí-Robles, M.; Ferrer-Montiel, A.; Planells-Cases, R. GABAA receptor associated protein

(GABARAP) modulates TRPV1 expression and channel function and desensitization. *FASEB J.* **2010**, *24*, 1958–1970.

145. Cook, J.L.; Re, R.N.; DeHaro, D.L.; Abadie, J.M.; Peters, M.; Alam, J. The trafficking protein GABARAP binds to and enhances plasma membrane expression and function of the angiotensin II type 1 receptor. *Circ. Res.* **2008**, *102*, 1539–1547.

146. Reining, S.C.; Gisler, S.M.; Fuster, D.; Moe, O.W.; O'Sullivan, G.A.; Betz, H.; Biber, J.; Murer, H.; Hernando, N. GABARAP deficiency modulates expression of NaPi-IIa in renal brush-border membranes. *Am. J. Physiol. Physiol.* **2009**, *296*, F1118–F1128.

147. Reining, S.C.; Liesegang, A.; Betz, H.; Biber, J.; Murer, H.; Hernando, N. Expression of renal and intestinal Na/Pi cotransporters in the absence of GABARAP. *Pflugers Arch. Eur. J. Physiol.* **2010**, *460*, 207–217.

148. Chen, C.; Li, J.-G.; Chen, Y.; Huang, P.; Wang, Y.; Liu-Chen, L.-Y. GEC1 Interacts with the κ Opioid Receptor and Enhances Expression of the Receptor. *J. Biol. Chem.* **2006**, *281*, 7983–7993.

149. Keulers, T.G.; Schaaf, M.B.E.; Peeters, H.J.M.; Savelkouls, K.G.M.; Vooijs, M.A.; Bussink, J.; Jutten, B.; Rouschop, K.M.A. GABARAPL1 is required for increased EGFR membrane expression during hypoxia. *Radiother. Oncol.* **2015**, *116*, 417–422.

150. Dutta, P.; Dargahi, L.; O'Connell, K.E.; Bolia, A.; Ozkan, B.; Sailer, A.W.; Dev, K.K. A novel modelling mechanism of PAEL receptor and GABARAPL2 interaction involved in Parkinson's disease. *Neurosci. Lett.* **2018**, *673*, 12–18.

151. Winer, H.; Fraiberg, M.; Abada, A.; Dadosh, T.; Tamim-Yecheskel, B.-C.; Elazar, Z. Autophagy differentially regulates TNF receptor Fn14 by distinct mammalian Atg8 proteins. *Nat. Commun.* **2018**, *9*, 3744.

152. Mizushima, N.; Klionsky, D.J. Protein Turnover Via Autophagy: Implications for Metabolism. *Annu. Rev. Nutr.* **2007**, *27*, 19–40.

153. Wieduwilt, M.J.; Moasser, M.M. The epidermal growth factor receptor family: Biology driving targeted therapeutics. *Cell. Mol. Life Sci.* 2008, *65*, 1566–1584.

154. Roskoski, R. The ErbB/HER family of protein-tyrosine kinases and cancer. *Pharmacol. Res.* 2014, *79*, 34–74.

155. Lax, I.; Burgess, W.H.; Bellot, F.; Ullrich, A.; Schlessinger, J.; Givol, D. Localization of a major receptor-binding domain for epidermal growth factor by affinity labeling. *Mol.*

Cell. Biol. **1988**, *8*, 1831–1834.

156. Bajaj, M.; Waterfield, M.D.; Schlessinger, J.; Taylor, W.R.; Blundell, T. On the tertiary structure of the extracellular domains of the epidermal growth factor and insulin receptors. *Biochim. Biophys. Acta - Protein Struct. Mol. Enzymol.* **1987**, *916*, 220–226.

157. Zhang, X.; Gureasko, J.; Shen, K.; Cole, P.A.; Kuriyan, J. An Allosteric Mechanism for Activation of the Kinase Domain of Epidermal Growth Factor Receptor. *Cell* **2006**, *125*, 1137–1149.

158. Ceresa, B.P.; Peterson, J.L. Cell and Molecular Biology of Epidermal Growth Factor Receptor. In *International Review of Cell and Molecular Biology*; Elsevier Inc., 2014; Vol. 313, pp. 145–178 ISBN 9780128001776.

159. Cohen, S.; Carpenter, G.; King, L. Epidermal growth factor-receptor-protein kinase interactions. Co-purification of receptor and epidermal growth factor-enhanced phosphorylation activity. *J. Biol. Chem.* **1980**, *255*, 4834–4842.

160. Chen, J.; Zeng, F.; Forrester, S.J.; Eguchi, S.; Zhang, M.-Z.; Harris, R.C. Expression and Function of the Epidermal Growth Factor Receptor in Physiology and Disease. *Physiol. Rev.* **2016**, *96*, 1025–1069.

161. Yarden, Y.; Sliwkowski, M.X. Untangling the ErbB signalling network. *Nat. Rev. Mol. Cell Biol.* **2001**, *2*, 127–137.

162. Jones, J.T.; Akita, R.W.; Sliwkowski, M.X. Binding specificities and affinities of egf domains for ErbB receptors. *FEBS Lett.* **1999**, *447*, 227–231.

163. Zanetti-Domingues, L.C.; Korovesis, D.; Needham, S.R.; Tynan, C.J.; Sagawa, S.; Roberts, S.K.; Kuzmanic, A.; Ortiz-Zapater, E.; Jain, P.; Roovers, R.C.; et al. The architecture of EGFR's basal complexes reveals autoinhibition mechanisms in dimers and oligomers. *Nat. Commun.* **2018**, *9*, 4325.

164. Maruyama, I. Mechanisms of Activation of Receptor Tyrosine Kinases: Monomers or Dimers. *Cells* **2014**, *3*, 304–330.

165. Yu, X.; Sharma, K.D.; Takahashi, T.; Iwamoto, R.; Mekada, E. Ligand-independent Dimer Formation of Epidermal Growth Factor Receptor (EGFR) Is a Step Separable from Ligand-induced EGFR Signaling. *Mol. Biol. Cell* **2002**, *13*, 2547–2557.

166. Macdonald, J.L.; Pike, L.J. Heterogeneity in EGF-binding affinities arises from

negative cooperativity in an aggregating system. *Proc. Natl. Acad. Sci.* **2008**, *105*, 112–117.

167. Liu, P.; Cleveland, T.E.; Bouyain, S.; Byrne, P.O.; Longo, P.A.; Leahy, D.J. A single ligand is sufficient to activate EGFR dimers. *Proc. Natl. Acad. Sci.* **2012**, *109*, 10861–10866.

168. Moriki, T.; Maruyama, H.; Maruyama, I.N. Activation of preformed EGF receptor dimers by ligand-induced rotation of the transmembrane domain. *J. Mol. Biol.* **2001**, *311*, 1011–1026.

169. Dawson, J.P.; Berger, M.B.; Lin, C.-C.; Schlessinger, J.; Lemmon, M.A.; Ferguson, K.M. Epidermal Growth Factor Receptor Dimerization and Activation Require Ligand-Induced Conformational Changes in the Dimer Interface. *Mol. Cell. Biol.* **2005**, *25*, 7734–7742.

170. Macdonald-Obermann, J.L.; Pike, L.J. The Intracellular Juxtamembrane Domain of the Epidermal Growth Factor (EGF) Receptor Is Responsible for the Allosteric Regulation of EGF Binding. *J. Biol. Chem.* **2009**, *284*, 13570–13576.

171. Ruan, Z.; Kannan, N. Mechanistic Insights into R776H Mediated Activation of Epidermal Growth Factor Receptor Kinase. *Biochemistry* **2015**, *54*, 4216–4225.

172. Huang, Y.; Bharill, S.; Karandur, D.; Peterson, S.M.; Marita, M.; Shi, X.; Kaliszewski, M.J.; Smith, A.W.; Isacoff, E.Y.; Kuriyan, J. Molecular basis for multimerization in the activation of the epidermal growth factor receptor. *Elife* **2016**, *5*, 1–27.

173. Needham, S.R.; Roberts, S.K.; Arkhipov, A.; Mysore, V.P.; Tynan, C.J.; Zanetti-Domingues, L.C.; Kim, E.T.; Losasso, V.; Korovesis, D.; Hirsch, M.; et al. EGFR oligomerization organizes kinase-active dimers into competent signalling platforms. *Nat. Commun.* **2016**, *7*, 13307.

174. Macdonald-Obermann, J.L.; Pike, L.J. Different Epidermal Growth Factor (EGF) Receptor Ligands Show Distinct Kinetics and Biased or Partial Agonism for Homodimer and Heterodimer Formation. *J. Biol. Chem.* **2014**, *289*, 26178–26188.

175. Freed, D.M.; Bessman, N.J.; Kiyatkin, A.; Salazar-Cavazos, E.; Byrne, P.O.; Moore, J.O.; Valley, C.C.; Ferguson, K.M.; Leahy, D.J.; Lidke, D.S.; et al. EGFR Ligands Differentially Stabilize Receptor Dimers to Specify Signaling Kinetics. *Cell* **2017**, *171*, 683-695.e18.

176. Wee, P.; Wang, Z. Epidermal growth factor receptor cell proliferation signaling pathways. *Cancers (Basel).* **2017**, *9*, 1–45.

177. Xie, H.; Pallero, M.A.; Gupta, K.; Chang, P.; Ware, M.F.; Witke, W.; Kwiatkowski, D.J.; Lauffenburger, D.A.; Murphy-Ullrich, J.E.; Wells, A. EGF receptor regulation of cell motility: EGF induces disassembly of focal adhesions independently of the motility-associated PLCgamma signaling pathway. *J. Cell Sci.* **1998**, *111 (Pt 5*, 615–24.

178. Uemura, T.; Kametaka, S.; Waguri, S. GGA2 interacts with EGFR cytoplasmic domain to stabilize the receptor expression and promote cell growth. *Sci. Rep.* **2018**, *8*, 1–14.

179. Jones, S.; Rappoport, J.Z. Interdependent epidermal growth factor receptor signalling and trafficking. *Int. J. Biochem. Cell Biol.* **2014**, *51*, 23–28.

180. Mendoza, M.C.; Er, E.E.; Blenis, J. The Ras-ERK and PI3K-mTOR pathways: cross-talk and compensation. *Trends Biochem. Sci.* **2011**, *36*, 320–328.

181. Burke, P.; Schooler, K.; Wiley, H.S. Regulation of Epidermal Growth Factor Receptor Signaling by Endocytosis and Intracellular Trafficking. *Mol. Biol. Cell* **2001**, *12*, 1897–1910.

182. Hanover, J.A.; Willingham, M.C.; Pastan, I. Kinetics of transit of transferrin and epidermal growth factor through clathrin-coated membranes. *Cell* **1984**, *39*, 283–293.

183. Sigismund, S.; Woelk, T.; Puri, C.; Maspero, E.; Tacchetti, C.; Transidico, P.; Di Fiore, P.P.; Polo, S. Clathrin-independent endocytosis of ubiquitinated cargos. *Proc. Natl. Acad. Sci.* **2005**, *102*, 2760–2765.

184. Ozcan, F.; Klein, P.; Lemmon, M.A.; Lax, I.; Schlessinger, J. On the nature of low- and high-affinity EGF receptors on living cells. *Proc. Natl. Acad. Sci.* **2006**, *103*, 5735–5740.

185. Simonsen, A.; Lippe, R.; Christoforidis, S.; Gaullier, J.-M.; Brech, A.; Callaghan, J.; Toh, B.-H.; Murphy, C.; Zerial, M.; Stenmark, H. EEA1 links PI(3)K function to Rab5 regulation of endosome fusion. *Nature* **1998**, *394*, 494–498.

186. Balderhaar, H.J.K.; Lachmann, J.; Yavavli, E.; Bröcker, C.; Lürick, A.; Ungermann, C. The CORVET complex promotes tethering and fusion of Rab5/Vps21-positive membranes. *Proc. Natl. Acad. Sci. U. S. A.* **2013**, *110*, 3823–3828.

187. van der Kant, R.; Jonker, C.T.H.; Wijdeven, R.H.; Bakker, J.; Janssen, L.; Klumperman, J.; Neefjes, J. Characterization of the Mammalian CORVET and HOPS

Complexes and Their Modular Restructuring for Endosome Specificity. *J. Biol. Chem.* **2015**, *290*, 30280–30290.

188. Guo, X.; Farías, G.G.; Mattera, R.; Bonifacino, J.S. Rab5 and its effector FHF contribute to neuronal polarity through dynein-dependent retrieval of somatodendritic proteins from the axon. *Proc. Natl. Acad. Sci.* **2016**, *113*, E5318–E5327.

189. Yao, X.; Wang, X.; Xiang, X. FHIP and FTS proteins are critical for dynein-mediated transport of early endosomes in Aspergillus. *Mol. Biol. Cell* **2014**, *25*, 2181–2189.

190. Frangioni, J. V.; Beahm, P.H.; Shifrin, V.; Jost, C.A.; Neel, B.G. The nontransmembrane tyrosine phosphatase PTP-1B localizes to the endoplasmic reticulum via its 35 amino acid C-terminal sequence. *Cell* **1992**, *68*, 545–560.

191. Tiganis, T. Protein Tyrosine Phosphatases: Dephosphorylating the Epidermal Growth Factor Receptor. *IUBMB Life (International Union Biochem. Mol. Biol. Life)* **2002**, *53*, 3–14.

192. Haj, F.G.; Markova, B.; Klaman, L.D.; Bohmer, F.D.; Neel, B.G. Regulation of Receptor Tyrosine Kinase Signaling by Protein Tyrosine Phosphatase-1B. *J. Biol. Chem.* **2003**, *278*, 739–744.

193. Baumdick, M.; Brüggemann, Y.; Schmick, M.; Xouri, G.; Sabet, O.; Davis, L.; Chin, J.W.; Bastiaens, P.I.H. EGF-dependent re-routing of vesicular recycling switches spontaneous phosphorylation suppression to EGFR signaling. *Elife* **2015**, *4*, 1–28.

194. Chi, S.; Cao, H.; Wang, Y.; McNiven, M.A. Recycling of the Epidermal Growth Factor Receptor Is Mediated by a Novel Form of the Clathrin Adaptor Protein Eps15. *J. Biol. Chem.* **2011**, *286*, 35196–35208.

195. Welz, T.; Wellbourne-Wood, J.; Kerkhoff, E. Orchestration of cell surface proteins by Rab11. *Trends Cell Biol.* **2014**, *24*, 407–415.

196. Sigismund, S.; Argenzio, E.; Tosoni, D.; Cavallaro, E.; Polo, S.; Di Fiore, P.P. Clathrin-Mediated Internalization Is Essential for Sustained EGFR Signaling but Dispensable for Degradation. *Dev. Cell* **2008**, *15*, 209–219.

197. Watanabe, S.; Boucrot, E. Fast and ultrafast endocytosis. *Curr. Opin. Cell Biol.* **2017**, *47*, 64–71.

198. Huang, F.; Kirkpatrick, D.; Jiang, X.; Gygi, S.; Sorkin, A. Differential Regulation of EGF Receptor Internalization and Degradation by Multiubiquitination within the Kinase

Domain. *Mol. Cell* **2006**, *21*, 737–748.

199. Huang, F.; Zeng, X.; Kim, W.; Balasubramani, M.; Fortian, A.; Gygi, S.P.; Yates, N.A.; Sorkin, A. Lysine 63-linked polyubiquitination is required for EGF receptor degradation. *Proc. Natl. Acad. Sci.* **2013**, *110*, 15722–15727.

200. Haglund, K.; Sigismund, S.; Polo, S.; Szymkiewicz, I.; Di Fiore, P.P.; Dikic, I. Multiple monoubiquitination of RTKs is sufficient for their endocytosis and degradation. *Nat. Cell Biol.* **2003**, *5*, 461–466.

201. Rink, J.; Ghigo, E.; Kalaidzidis, Y.; Zerial, M. Rab Conversion as a Mechanism of Progression from Early to Late Endosomes. *Cell* **2005**, *122*, 735–749.

202. Shinde, S.R.; Maddika, S. PTEN modulates EGFR late endocytic trafficking and degradation by dephosphorylating Rab7. *Nat. Commun.* **2016**, *7*, 10689.

203. Wollert, T.; Hurley, J.H. Molecular mechanism of multivesicular body biogenesis by ESCRT complexes. *Nature* **2010**, *464*, 864–869.

204. Alwan, H.A.J.; Van Zoelen, E.J.J.; Van Leeuwen, J.E.M. Ligand-induced lysosomal epidermal growth factor receptor (EGFR) degradation is preceded by proteasome-dependent EGFR de-ubiquitination. *J. Biol. Chem.* **2003**, *278*, 35781–35790.

205. Johansson, M.; Rocha, N.; Zwart, W.; Jordens, I.; Janssen, L.; Kuijl, C.; Olkkonen, V.M.; Neefjes, J. Activation of endosomal dynein motors by stepwise assembly of Rab7–RILP–p150Glued, ORP1L, and the receptor βIII spectrin. *J. Cell Biol.* **2007**, *176*, 459–471.

206. Bright, N.A.; Davis, L.J.; Luzio, J.P. Endolysosomes Are the Principal Intracellular Sites of Acid Hydrolase Activity. *Curr. Biol.* **2016**, *26*, 2233–2245.

207. Futter, C.E.; Pearse, A.; Hewlett, L.J.; Hopkins, C.R. Multivesicular endosomes containing internalized EGF-EGF receptor complexes mature and then fuse directly with lysosomes. *J. Cell Biol.* **1996**, *132*, 1011–1023.

208. Ravikumar, B.; Imarisio, S.; Sarkar, S.; O'Kane, C.J.; Rubinsztein, D.C. Rab5 modulates aggregation and toxicity of mutant huntingtin through macroautophagy in cell and fly models of Huntington disease. *J. Cell Sci.* **2008**, *121*, 1649–1660.

209. Zhou, F.; Zou, S.; Chen, Y.; Lipatova, Z.; Sun, D.; Zhu, X.; Li, R.; Wu, Z.; You, W.; Cong, X.; et al. A Rab5 GTPase module is important for autophagosome closure. *PLOS Genet.* **2017**, *13*, e1007020.

210. Zhou, F.; Wu, Z.; Zhao, M.; Murtazina, R.; Cai, J.; Zhang, A.; Li, R.; Sun, D.; Li, W.; Zhao, L.; et al. Rab5-dependent autophagosome closure by ESCRT. *J. Cell Biol.* **2019**, *218*, 1908–1927.

211. Puri, C.; Vicinanza, M.; Ashkenazi, A.; Gratian, M.J.; Zhang, Q.; Bento, C.F.; Renna, M.; Menzies, F.M.; Rubinsztein, D.C. The RAB11A-Positive Compartment Is a Primary Platform for Autophagosome Assembly Mediated by WIPI2 Recognition of PI3P-RAB11A. *Dev. Cell* **2018**, *45*, 114-131.e8.

212. Gordon, P.B.; Seglen, P.O. Prelysosomal convergence of autophagic and endocytic pathways. *Biochem. Biophys. Res. Commun.* **1988**, *151*, 40–47.

213. Sanjuan, M.A.; Dillon, C.P.; Tait, S.W.G.; Moshiach, S.; Dorsey, F.; Connell, S.; Komatsu, M.; Tanaka, K.; Cleveland, J.L.; Withoff, S.; et al. Toll-like receptor signalling in macrophages links the autophagy pathway to phagocytosis. *Nature* **2007**, *450*, 1253–1257.

214. Sanjuan, M.A.; Milasta, S.; Green, D.R. Toll-like receptor signaling in the lysosomal pathways. *Immunol. Rev.* **2009**, *227*, 203–220.

215. Heckmann, B.L.; Teubner, B.J.W.; Tummers, B.; Boada-Romero, E.; Harris, L.; Yang, M.; Guy, C.S.; Zakharenko, S.S.; Green, D.R. LC3-Associated Endocytosis Facilitates β-Amyloid Clearance and Mitigates Neurodegeneration in Murine Alzheimer's Disease. *Cell* **2019**, *0*.

216. Chen, Y.; Sun, H.-Q.; Eichorst, J.P.; Albanesi, J.P.; Yin, H.; Mueller, J.D. Comobility of GABARAP and Phosphatidylinositol 4-Kinase 2A on Cytoplasmic Vesicles. *Biochemistry* **2018**, *57*, 3556–3559.

217. Szalai, P.; Hagen, L.K.; Sætre, F.; Luhr, M.; Sponheim, M.; Øverbye, A.; Mills, I.G.; Seglen, P.O.; Engedal, N. Autophagic bulk sequestration of cytosolic cargo is independent of LC3, but requires GABARAPs. *Exp. Cell Res.* **2015**, *333*, 21–38.

218. Chakrama, F.Z.; Seguin-Py, S.; Le Grand, J.N.; Fraichard, A.; Delage-Mourroux, R.; Despouy, G.; Perez, V.; Jouvenot, M.; Boyer-Guittaut, M. GABARAPL1 (GEC1) associates with autophagic vesicles. *Autophagy* **2010**, *6*, 495–505.

219. Le Grand, J.N.; Chakrama, F.Z.; Seguin-Py, S.; Fraichard, A.; Delage-Mourroux, R.; Jouvenot, M.; Risold, P.-Y.; Boyer-Guittaut, M. GABARAPL1 antibodies: Target one protein, get one free! *Autophagy* **2011**, *7*, 1302–1307.

220. Jacobsen, L.B.; Calvin, S.A.; Lobenhofer, E.K. Transcriptional effects of transfection: the potential for misinterpretation of gene expression data generated from transiently transfected cells. *Biotechniques* **2009**, *47*, 617–624.

221. Omidi, Y.; Hollins, A.J.; Benboubetra, M.; Drayton, R.; Benter, I.F.; Akhtari, S. Toxicogenomics of non-viral vectors for gene therapy: A microarray study of lipofectin- and oligofectamine-induced gene expression changes in human epithelial cells. *J. Drug Target.* **2003**, *11*, 311–323.

222. Omidi, Y.; Barar, J.; Heidari, H.R.; Ahmadian, S.; Yazdi, H.A.; Akhtar, S. Microarray analysis of the toxicogenomics and the genotoxic potential of a cationic lipid-based gene delivery nanosystem in human alveolar epithelial A549 cells. *Toxicol. Mech. Methods* **2008**, *18*, 369–378.

223. Hagen, L.; Sharma, A.; Aas, P.A.; Slupphaug, G. Off-target responses in the HeLa proteome subsequent to transient plasmid-mediated transfection. *Biochim. Biophys. Acta - Proteins Proteomics* **2015**, *1854*, 84–90.

224. Mo, R.H.; Zaro, J.L.; Ou, J.-H.J.; Shen, W.-C. Effects of Lipofectamine 2000/siRNA Complexes on Autophagy in Hepatoma Cells. *Mol. Biotechnol.* **2012**, *51*, 1–8.

225. Liu, H.S.; Jan, M.S.; Chou, C.K.; Chen, P.H.; Ke, N.J. Is green fluorescent protein toxic to the living cells? *Biochem. Biophys. Res. Commun.* **1999**, *260*, 712–717.

226. Endemann, G.; Schechtman, D.; Mochly-Rosen, D. Cytotoxicity of pEGFP vector is due to residues encoded by multiple cloning site. *Anal. Biochem.* **2003**, *313*, 345–347.

227. Mak, G.W.Y.; Wong, C.H.; Tsui, S.K.W. Green fluorescent protein induces the secretion of inflammatory cytokine interleukin-6 in muscle cells. *Anal. Biochem.* **2007**, *362*, 296–298.

228. Chen, D.; Murphy, B.; Sung, R.; Bromberg, J.S. Adaptive and innate immune responses to gene transfer vectors: Role of cytokines and chemokines in vector function. *Gene Ther.* **2003**, *10*, 991–998.

229. Stepanenko, A.A.; Heng, H.H. Transient and stable vector transfection: Pitfalls, off-target effects, artifacts. *Mutat. Res. - Rev. Mutat. Res.* **2017**, *773*, 91–103.

230. Gibson, T.J.; Seiler, M.; Veitia, R.A. The transience of transient overexpression. *Nat. Methods* **2013**, *10*, 715–721.

231. Brandt, C.R.; Buonaguro, F.M.; McDougall, J.K.; Galloway, D.A. Plasmid mediated

mutagenesis of a cellular gene in transfected eukaryotic cells. *Nucleic Acids Res.* **1987**, *15*, 561–573.

232. Weber, S.; Hofmann, A.; Herms, S.; Hoffmann, P.; Doerfler, W. Destabilization of the human epigenome: consequences of foreign DNA insertions. *Epigenomics* **2015**, *7*, 745–755.

233. Winnard, P.; Glackin, C.; Raman, V. Stable integration of an empty vector in MCF-7 cells greatly alters the karyotype. *Cancer Genet. Cytogenet.* **2006**, *164*, 174–176.

234. Bylund, L.; Kytölä, S.; Lui, W.-O.; Larsson, C.; Weber, G. Analysis of the cytogenetic stability of the human embryonal kidney cell line 293 by cytogenetic and STR profiling approaches. *Cytogenet. Genome Res.* **2004**, *106*, 28–32.

235. Dumont, J.E.; Dremier, S.; Pirson, I.; Maenhaut, C. Cross signaling, cell specificity, and physiology. *Am. J. Physiol. Physiol.* **2002**, *283*, C2–C28.

236. Grimm, D.; Streetz, K.L.; Jopling, C.L.; Storm, T.A.; Pandey, K.; Davis, C.R.; Marion, P.; Salazar, F.; Kay, M.A. Fatality in mice due to oversaturation of cellular microRNA/short hairpin RNA pathways. *Nature* **2006**, *441*, 537–541.

237. Castanotto, D.; Sakurai, K.; Lingeman, R.; Li, H.; Shively, L.; Aagaard, L.; Soifer, H.; Gatignol, A.; Riggs, A.; Rossi, J.J. Combinatorial delivery of small interfering RNAs reduces RNAi efficacy by selective incorporation into RISC. *Nucleic Acids Res.* **2007**, *35*, 5154–5164.

238. Böttger, J.; Arnold, K.; Thiel, C.; Rennert, C.; Aleithe, S.; Hofmann, U.; Vlaic, S.; Sales, S.; Shevchenko, A.; Matz-Soja, M. RNAi in murine hepatocytes: the agony of choice—a study of the influence of lipid-based transfection reagents on hepatocyte metabolism. *Arch. Toxicol.* **2015**, *89*, 1579–1588.

239. Danielli, M.; Marinelli, R.A. Lipid-based transfection reagents can interfere with cholesterol biosynthesis. *Anal. Biochem.* **2016**, *495*, 1–2.

240. Mojica, F.J.M.; Díez-Villaseñor, C.; García-Martínez, J.; Soria, E. Intervening Sequences of Regularly Spaced Prokaryotic Repeats Derive from Foreign Genetic Elements. *J. Mol. Evol.* **2005**, *60*, 174–182.

241. Pourcel, C.; Salvignol, G.; Vergnaud, G. CRISPR elements in Yersinia pestis acquire new repeats by preferential uptake of bacteriophage DNA, and provide additional tools for evolutionary studies. *Microbiology* **2005**, *151*, 653–663.

242. Bolotin, A.; Quinquis, B.; Sorokin, A.; Ehrlich, S.D. Clustered regularly interspaced short palindrome repeats (CRISPRs) have spacers of extrachromosomal origin. *Microbiology* **2005**, *151*, 2551–2561.

243. Makarova, K.S.; Grishin, N. V.; Shabalina, S.A.; Wolf, Y.I.; Koonin, E. V. A putative RNA-interference-based immune system in prokaryotes: Computational analysis of the predicted enzymatic machinery, functional analogies with eukaryotic RNAi, and hypothetical mechanisms of action. *Biol. Direct* **2006**, *1*, 1–26.

244. Barrangou, R.; Fremaux, C.; Deveau, H.; Richards, M.; Boyaval, P.; Moineau, S.; Romero, D. a; Horvath, P. CRISPR Provides Acquired Resistance Against Viruses in Prokaryotes. *Science (80-.).* **2007**, *315*, 1709–1712.

245. Deltcheva, E.; Chylinski, K.; Sharma, C.M.; Gonzales, K.; Chao, Y.; Pirzada, Z.A.; Eckert, M.R.; Vogel, J.; Charpentier, E. CRISPR RNA maturation by trans-encoded small RNA and host factor RNase III. *Nature* **2011**, *471*, 602–607.

246. Brouns, S.J.J.; Jore, M.M.; Lundgren, M.; Westra, E.R.; Slijkhuis, R.J.H.; Snijders, A.P.L.; Dickman, M.J.; Makarova, K.S.; Koonin, E. V.; van der Oost, J. Small CRISPR RNAs Guide Antiviral Defense in Prokaryotes. *Science (80-.).* **2008**, *321*, 960–964.

247. Garneau, J.E.; Dupuis, M.-È.; Villion, M.; Romero, D.A.; Barrangou, R.; Boyaval, P.; Fremaux, C.; Horvath, P.; Magadán, A.H.; Moineau, S. The CRISPR/Cas bacterial immune system cleaves bacteriophage and plasmid DNA. *Nature* **2010**, *468*, 67–71.

248. Gasiunas, G.; Barrangou, R.; Horvath, P.; Siksnys, V. Cas9-crRNA ribonucleoprotein complex mediates specific DNA cleavage for adaptive immunity in bacteria. *Proc. Natl. Acad. Sci.* **2012**, *109*, E2579–E2586.

249. Jinek, M.; Chylinski, K.; Fonfara, I.; Hauer, M.; Doudna, J.A.; Charpentier, E. A Programmable Dual-RNA-Guided DNA Endonuclease in Adaptive Bacterial Immunity. *Science (80-.).* **2012**, *337*, 816–821.

250. Cong, L.; Ran, F.A.; Cox, D.; Lin, S.; Barretto, R.; Habib, N.; Hsu, P.D.; Wu, X.; Jiang, W.; Marraffini, L.A.; et al. Multiplex genome engineering using CRISPR/Cas systems. *Science (80-.).* **2013**, *339*, 819–823.

251. Mali, P.; Yang, L.; Esvelt, K.M.; Aach, J.; Guell, M.; DiCarlo, J.E.; Norville, J.E.; Church, G.M. RNA-Guided Human Genome Engineering via Cas9. *Science (80-.).* **2013**, *339*, 823–826.

252. Cencic, R.; Miura, H.; Malina, A.; Robert, F.; Ethier, S.; Schmeing, T.M.; Dostie, J.; Pelletier, J. Protospacer Adjacent Motif (PAM)-Distal Sequences Engage CRISPR Cas9 DNA Target Cleavage. *PLoS One* **2014**, *9*, e109213.

253. Mitelman, F.; Johansson, B.; Mertens, F. The impact of translocations and gene fusions on cancer causation. *Nat. Rev. Cancer* **2007**, *7*, 233–245.

254. Negrini, S.; Gorgoulis, V.G.; Halazonetis, T.D. Genomic instability — an evolving hallmark of cancer. *Nat. Rev. Mol. Cell Biol.* **2010**, *11*, 220–228.

255. Zhivotovsky, B.; Kroemer, G. Apoptosis and genomic instability. *Nat. Rev. Mol. Cell Biol.* **2004**, *5*, 752–762.

256. Vijg, J.; Montagna, C. Genome instability and aging: Cause or effect? *Transl. Med. Aging* **2017**, *1*, 5–11.

257. Wilson, J.H.; Berget, P.B.; Pipas, J.M. Somatic cells efficiently join unrelated DNA segments end-to-end. *Mol. Cell. Biol.* **1982**, *2*, 1258–1269.

258. Chiruvella, K.K.; Liang, Z.; Wilson, T.E. Repair of Double-Strand Breaks by End Joining. *Cold Spring Harb. Perspect. Biol.* **2013**, *5*, a012757–a012757.

259. Mao, Z.; Bozzella, M.; Seluanov, A.; Gorbunova, V. Comparison of nonhomologous end joining and homologous recombination in human cells. *DNA Repair (Amst).* **2008**, *7*, 1765–1771.

260. Sfeir, A.; Symington, L.S. Microhomology-Mediated End Joining: A Back-up Survival Mechanism or Dedicated Pathway? *Trends Biochem. Sci.* **2015**, *40*, 701–714.

261. Brinkman, E.K.; Chen, T.; de Haas, M.; Holland, H.A.; Akhtar, W.; van Steensel, B. Kinetics and Fidelity of the Repair of Cas9-Induced Double-Strand DNA Breaks. *Mol. Cell* **2018**, *70*, 801-813.e6.

262. Zhang, X.H.; Tee, L.Y.; Wang, X.G.; Huang, Q.S.; Yang, S.H. Off-target effects in CRISPR/Cas9-mediated genome engineering. *Mol. Ther. - Nucleic Acids* **2015**, *4*, e264.

263. Leenay, R.T.; Beisel, C.L. Deciphering, Communicating, and Engineering the CRISPR PAM. *J. Mol. Biol.* **2017**, *429*, 177–191.

264. Ran, F.A.; Hsu, P.D.; Lin, C.; Gootenberg, J.S.; Konermann, S.; Trevino, A.E.; Scott, D.A.; Inoue, A.; Matoba, S.; Zhang, Y.; et al. Double Nicking by RNA-Guided CRISPR

Cas9 for Enhanced Genome Editing Specificity. *Cell* **2013**, *154*, 1380–1389.

265. Chen, S.-J. Minimizing off-target effects in CRISPR-Cas9 genome editing. *Cell Biol. Toxicol.* **2019**, *35*, 399–401.

266. Liang, F.; Han, M.; Romanienko, P.J.; Jasin, M. Homology-directed repair is a major double-strand break repair pathway in mammalian cells. *Proc. Natl. Acad. Sci.* **1998**, *95*, 5172–5177.

267. Lin, S.; Staahl, B.T.; Alla, R.K.; Doudna, J.A. Enhanced homology-directed human genome engineering by controlled timing of CRISPR/Cas9 delivery. *Elife* **2014**, *3*, e04766.

268. Jinek, M.; East, A.; Cheng, A.; Lin, S.; Ma, E.; Doudna, J. RNA-programmed genome editing in human cells. *Elife* **2013**, *2013*, 1–9.

269. Koch, B.; Nijmeijer, B.; Kueblbeck, M.; Cai, Y.; Walther, N.; Ellenberg, J. Generation and validation of homozygous fluorescent knock-in cells using CRISPR–Cas9 genome editing. *Nat. Protoc.* **2018**, *13*, 1465–1487.

270. Abe, S.; Kobayashi, K.; Oji, A.; Sakuma, T.; Kazuki, K.; Takehara, S.; Nakamura, K.; Okada, A.; Tsukazaki, Y.; Senda, N.; et al. Modification of single-nucleotide polymorphism in a fully humanized CYP3A mouse by genome editing technology. *Sci. Rep.* **2017**, *7*, 15189.

271. Chen, B.; Zou, W.; Xu, H.; Liang, Y.; Huang, B. Efficient labeling and imaging of protein-coding genes in living cells using CRISPR-Tag. *Nat. Commun.* **2018**, *9*, 5065.

272. Khan, A.O.; White, C.W.; Pike, J.A.; Yule, J.; Slater, A.; Hill, S.J.; Poulter, N.S.; Thomas, S.G.; Morgan, N. V. Optimised insert design for improved single-molecule imaging and quantification through CRISPR-Cas9 mediated knock-in. *Sci. Rep.* **2019**, *9*, 14219.

273. Simons, I.M.; Mohrlüder, J.; Feederle, R.; Kremmer, E.; Zobel, T.; Dobner, J.; Bleffert, N.; Hoffmann, S.; Willbold, D. The highly GABARAP specific rat monoclonal antibody 8H5 visualizes GABARAP in immunofluorescence imaging at endogenous levels. *Sci. Rep.* **2019**, *9*, 526.

274. Lisenbee, C.S.; Karnik, S.K.; Trelease, R.N. Overexpression and Mislocalization of a Tail-Anchored GFP Redefines the Identity of Peroxisomal ER. *Traffic* **2003**, *4*, 491–501.

275. Nelson, A.D.; Caballero-Florán, R.N.; Rodríguez Díaz, J.C.; Hull, J.M.; Yuan, Y.; Li, J.; Chen, K.; Walder, K.K.; Lopez-Santiago, L.F.; Bennett, V.; et al. Ankyrin-G regulates forebrain connectivity and network synchronization via interaction with GABARAP. *Mol. Psychiatry* **2018**.

276. Dengjel, J.; Høyer-Hansen, M.; Nielsen, M.O.; Eisenberg, T.; Harder, L.M.; Schandorff, S.; Farkas, T.; Kirkegaard, T.; Becker, A.C.; Schroeder, S.; et al. Identification of Autophagosome-associated Proteins and Regulators by Quantitative Proteomic Analysis and Genetic Screens. *Mol. Cell. Proteomics* **2012**, *11*, M111.014035.

277. Behrends, C.; Sowa, M.E.; Gygi, S.P.; Harper, J.W. Network organization of the human autophagy system. *Nature* **2010**, *466*, 68–76.

278. Real, F.X.; Rettig, W.J.; Chesa, P.G.; Melamed, M.R.; Old, L.J.; Mendelsohn, J. Expression of epidermal growth factor receptor in human cultured cells and tissues: relationship to cell lineage and stage of differentiation. *Cancer Res.* **1986**, *46*, 4726–31.

279. Yavas, S.; Macháň, R.; Wohland, T. The Epidermal Growth Factor Receptor Forms Location-Dependent Complexes in Resting Cells. *Biophys. J.* **2016**, *111*, 2241–2254.

280. Wirth, M.; Zhang, W.; Razi, M.; Nyoni, L.; Joshi, D.; O'Reilly, N.; Johansen, T.; Tooze, S.A.; Mouilleron, S. Molecular determinants regulating selective binding of autophagy adapters and receptors to ATG8 proteins. *Nat. Commun.* **2019**, *10*, 2055.

281. Li, J.; Zhu, R.; Chen, K.; Zheng, H.; Zhao, H.; Yuan, C.; Zhang, H.; Wang, C.; Zhang, M. Potent and specific Atg8-targeting autophagy inhibitory peptides from giant ankyrins. *Nat. Chem. Biol.* **2018**, *14*, 778–787.

282. Vaites, L.P.; Paulo, J.A.; Huttlin, E.L.; Harper, J.W. Systematic Analysis of Human Cells Lacking ATG8 Proteins Uncovers Roles for GABARAPs and the CCZ1/MON1 Regulator C18orf8/RMC1 in Macroautophagic and Selective Autophagic Flux. *Mol. Cell. Biol.* **2017**, *38*, e00392-17.

283. Kabeya, Y. LC3, GABARAP and GATE16 localize to autophagosomal membrane depending on form-II formation. *J. Cell Sci.* **2004**, *117*, 2805–2812.

284. Minogue, S.; Waugh, M.G.; De Matteis, M.A.; Stephens, D.J.; Berditchevski, F.; Hsuan, J.J. Phosphatidylinositol 4-kinase is required for endosomal trafficking and degradation of the EGF receptor. *J. Cell Sci.* **2006**, *119*, 571–581.

285. Henmi, Y.; Morikawa, Y.; Oe, N.; Ikeda, N.; Fujita, A.; Takei, K.; Minogue, S.; Tanabe, K. PtdIns4 KIIα generates endosomal PtdIns(4)P and is required for receptor sorting at early endosomes. *Mol. Biol. Cell* **2016**, *27*, 990–1001.

286. Leidal, A.M.; Huang, H.H.; Marsh, T.; Solvik, T.; Zhang, D.; Ye, J.; Kai, F.; Goldsmith, J.; Liu, J.Y.; Huang, Y.-H.; et al. The LC3-conjugation machinery specifies the loading of RNA-binding proteins into extracellular vesicles. *Nat. Cell Biol.* **2020**, *22*, 187–199.

287. Sanwald, J.L.; Poschmann, G.; Stühler, K.; Behrends, C.; Hoffmann, S.; Willbold, D. The GABARAP Co-Secretome Identified by APEX2-GABARAP Proximity Labelling of Extracellular Vesicles. *Cells* **2020**, *9*, 1468.

288. Sou, Y.; Tanida, I.; Komatsu, M.; Ueno, T.; Kominami, E. Phosphatidylserine in Addition to Phosphatidylethanolamine Is an in Vitro Target of the Mammalian Atg8 Modifiers, LC3, GABARAP, and GATE-16. *J. Biol. Chem.* **2006**, *281*, 3017–3024.

289. Hoyer, M.J.; Chitwood, P.J.; Ebmeier, C.C.; Striepen, J.F.; Qi, R.Z.; Old, W.M.; Voeltz, G.K. A Novel Class of ER Membrane Proteins Regulates ER-Associated Endosome Fission. *Cell* **2018**, *175*, 254-265.e14.

290. Sasai, M.; Sakaguchi, N.; Ma, J.S.; Nakamura, S.; Kawabata, T.; Bando, H.; Lee, Y.; Saitoh, T.; Akira, S.; Iwasaki, A.; et al. Essential role for GABARAP autophagy proteins in interferon-inducible GTPase-mediated host defense. *Nat. Immunol.* **2017**, *18*, 899–910.

291. Goldknopf, I.L.; Busch, H. Isopeptide linkage between nonhistone and histone 2A polypeptides of chromosomal conjugate-protein A24. *Proc. Natl. Acad. Sci.* **1977**, *74*, 864–868.

292. Ciechanover, A.; Heller, H.; Elias, S.; Haas, A.L.; Hershko, A. ATP-dependent conjugation of reticulocyte proteins with the polypeptide required for protein degradation. *Proc. Natl. Acad. Sci. U. S. A.* **1980**, *77*, 1365–1368.

293. Wilkinson, K.D. The discovery of ubiquitin-dependent proteolysis. *Proc. Natl. Acad. Sci. U. S. A.* **2005**, *102*, 15280–15282.

294. Nakayama, K.I.; Nakayama, K. Ubiquitin ligases: cell-cycle control and cancer. *Nat. Rev. Cancer* **2006**, *6*, 369–381.

295. Schwertman, P.; Bekker-Jensen, S.; Mailand, N. Regulation of DNA double-strand break repair by ubiquitin and ubiquitin-like modifiers. *Nat. Rev. Mol. Cell Biol.* **2016**,

17, 379–394.

296. Piper, R.C.; Dikic, I.; Lukacs, G.L. Ubiquitin-Dependent Sorting in Endocytosis. *Cold Spring Harb. Perspect. Biol.* **2014**, *6*, a016808–a016808.

297. Malynn, B.A.; Ma, A. Ubiquitin Makes Its Mark on Immune Regulation. *Immunity* **2010**, *33*, 843–852.

298. Ball, K.A.; Johnson, J.R.; Lewinski, M.K.; Guatelli, J.; Verschueren, E.; Krogan, N.J.; Jacobson, M.P. Non-degradative Ubiquitination of Protein Kinases. *PLOS Comput. Biol.* **2016**, *12*, e1004898.

8. Appendix

Additional Supplementary Data for manuscript 4.2:

➔ Supplementary Table S1 containing raw mass spectrometry data can be found online (https://www.mdpi.com/1422-0067/22/1/85/s1) or on the enclosed compact disc.

Additional Supplementary Data for manuscript 4.3:

➔ Movies S1 and S2 can be found online (https://www.mdpi.com/2073-4409/9/5/1296/s1) or on the enclosed compact disc.